ELICITORS, SECRET AGENTS AT THE SERVICE OF THE PLANT KINGDOM

EDITED BY: Essaid Ait Barka, Rachid Lahlali and Brigitte Mauch-Mani
PUBLISHED IN: Frontiers in Plant Science

frontiers Research Topics

frontiers

ISSN 1664-8714
ISBN 978-2-83250-668-4
DOI 10.3389/978-2-83250-668-4

About Frontiers

Frontiers is more than just an open-access publisher of scholarly articles: it is a pioneering approach to the world of academia, radically improving the way scholarly research is managed. The grand vision of Frontiers is a world where all people have an equal opportunity to seek, share and generate knowledge. Frontiers provides immediate and permanent online open access to all its publications, but this alone is not enough to realize our grand goals.

Frontiers Journal Series

The Frontiers Journal Series is a multi-tier and interdisciplinary set of open-access, online journals, promising a paradigm shift from the current review, selection and dissemination processes in academic publishing. All Frontiers journals are driven by researchers for researchers; therefore, they constitute a service to the scholarly community. At the same time, the Frontiers Journal Series operates on a revolutionary invention, the tiered publishing system, initially addressing specific communities of scholars, and gradually climbing up to broader public understanding, thus serving the interests of the lay society, too.

Dedication to Quality

Each Frontiers article is a landmark of the highest quality, thanks to genuinely collaborative interactions between authors and review editors, who include some of the world's best academicians. Research must be certified by peers before entering a stream of knowledge that may eventually reach the public - and shape society; therefore, Frontiers only applies the most rigorous and unbiased reviews.
Frontiers revolutionizes research publishing by freely delivering the most outstanding research, evaluated with no bias from both the academic and social point of view. By applying the most advanced information technologies, Frontiers is catapulting scholarly publishing into a new generation.

What are Frontiers Research Topics?

Frontiers Research Topics are very popular trademarks of the Frontiers Journals Series: they are collections of at least ten articles, all centered on a particular subject. With their unique mix of varied contributions from Original Research to Review Articles, Frontiers Research Topics unify the most influential researchers, the latest key findings and historical advances in a hot research area! Find out more on how to host your own Frontiers Research Topic or contribute to one as an author by contacting the Frontiers Editorial Office: frontiersin.org/about/contact

ELICITORS, SECRET AGENTS AT THE SERVICE OF THE PLANT KINGDOM

Topic Editors:
Essaid Ait Barka, Université de Reims Champagne-Ardenne, France
Rachid Lahlali, Ecole Nationale d'Agriculture de Meknès, Morocco
Brigitte Mauch-Mani, Université de Neuchâtel, Switzerland

Citation: Barka, E. A., Lahlali, R., Mauch-Mani, B., eds. (2022). Elicitors, Secret Agents at the Service of the Plant Kingdom. Lausanne: Frontiers Media SA. doi: 10.3389/978-2-83250-668-4

Table of Contents

frontiers | Frontiers in Plant Science

TYPE Editorial
PUBLISHED 18 October 2022
DOI 10.3389/fpls.2022.1060483

OPEN ACCESS

EDITED AND REVIEWED BY
Mario Serrano,
Center for Genomic Sciences,
National Autonomous University of
Mexico, Mexico

*CORRESPONDENCE
Essaid Ait Barka
ea.barka@univ-reims.fr

SPECIALTY SECTION
This article was submitted to
Plant Pathogen Interactions,
a section of the journal
Frontiers in Plant Science

RECEIVED 03 October 2022
ACCEPTED 12 October 2022
PUBLISHED 18 October 2022

CITATION
Barka EA, Lahlali R and Mauch-Mani B
(2022) Editorial: Elicitors, secret agents
at the service of the plant kingdom.
Front. Plant Sci. 13:1060483.
doi: 10.3389/fpls.2022.1060483

Editorial: Elicitors, secret agents at the service of the plant kingdom

Essaid Ait Barka[1]*, Rachid Lahlali[2] and Brigitte Mauch-Mani[3]

[1]Unité de Recherche Résistance Induite et Bio-Protection des Plantes-EA 4707-USC INRAE1488, Reims Champagne-Ardenne University, Reims, France, [2]Department of Plant Protection, Phytopathology Unit, Ecole Nationale d'Agriculture de Meknès, Meknès, Morocco, [3]Institute of Biology, University of Neuchâtel, Neuchâtel, Switzerland

KEYWORDS

effectors, pathogen-associated molecular pattern, pattern recognition receptors, plant defense, resistance

Editorial on the Research Topic
Elicitors, secret agents at the service of the plant kingdom

Due to their sessile lifestyle plants had to acquire skills enabling them to defend themselves against a wide range of various stresses. At the very beginning of a successful defense is the capability to perceive a given stressor that will lead to the mounting and activation of defense responses (Jones and Dangl, 2006). The self/nonself perception in plants in defence is tightly linked to the presence of the plants' own innate immune system (Sanabria et al., 2010). In this system, a first layer of immunity is based on the perception of pathogen-associated molecular patterns (PAMPs) or microbe-associated molecular patterns (MAMPs) and generally referred to as PAMP-triggered immunity (PTI) (Couto and Zipfel, 2016).

An additional layer of defense is based on the ability of plants to being primed (Mauch-Mani et al., 2017). In priming, elicitors derived from pathogens, beneficial microorganisms, or in the form of various synthetic and natural compounds sensitize the plant cells to react more rapidly or/and accurately to a future challenging infection. Most of such so-called exogenous elicitors of plant defense responses are nonspecific and fluctuate widely in their chemical nature including proteins, glycoproteins, oligosaccharides, and lipids (Abdul Malik et al., 2020).

Since elicitors help to protect plants from diseases by triggering their immune system, they also represent encouraging alternatives to pesticides and are in line with today's requirement for more sustainability in agriculture. Therefore, the current topic presents various suggestions for promising candidates that could be integrated into a future low-pesticide approaches to plant protection.

Until recently, the function of *VirE3* of Agrobacterium in the plant hormone signal transduction pathway for tumorigenesis was not known. In their contribution, Li et al. show that Agrobacterium VirE3 can interact with Arabidopsis JAZ8 in cells, leading to a repression of the transcription activity of *VirE3* by JAZ8. The authors suggest that *VirE3*

and *JAZ8* may antagonistically modulate the SA/JA mediated plant defense signaling response during Agrobacterium infection.

In the search for new elicitors, the sea might constitute a good source. In this context, de Borba et al. report for that foliar application of ulvan, a characterized water-soluble polysaccharide from the green seaweed *Ulva fasciata*, induces resistance in wheat against *Zymoseptoria tritici*, the causing agent of *Septoria tritici* blotch (STB), that leads to high economic losses. Ulvan treatment interestingly did not cause substantial changes in the wheat metabolome suggesting only low metabolic costs for this induced resistance.

Not only microbial pathogens but also nematodes are able to cause damage to plants. Singh et al. show in their contribution that ascorbate oxidation in rice, known to induce resistance (Singh et al., 2020), enhances the phenylpropanoid-based response to nematode infection and leads to a tolerance phenotype in treated rice plants.

In their contribution, Nakamura et al. showed that effectors can play different roles in host and non-host plants. The bacterial strains *Acidovorax avenae* N1141 and K1 produce an effector called protein rice HR cell death inducing-factor (RHIF). This novel effector RHIFs performs in both establishing infection in host plants and inducing ETI in non-host plants.

SOBIR1 (Suppressor Of BIR1) is a receptor-like kinase (Gao et al., 2009) that associates with a plethora of pattern-recognition receptors (PRRs) of the receptor-like protein (RLP) type at the plasma membrane. Based on bimolecular fluorescence complementation and affinity purification assays, Li et al. established that *Nb*RLP1 associates with *Nb*SOBIR1. The presented data support a model where *Nb*RLP1 acts as a positive regulator for plant PTI through its binding with *Nb*SOBIR1.

Pathogenic microbes release a body of effector proteins which manipulate host immunity to successfully colonize the plants. In this way, the *Valsa mali* effector VmEP1 is an essential virulence factor for the establishment of apple Valsa canker (Li et al.). Wang et al. present evidence for a mechanism by which a *V. mali* effector protein targets the host pathogenesis-related protein 10 to attenuate the host resistance.

The citrus disease Huanglongbing (HLB) caused by *Candidatus Liberibacter asiaticus* seriously threatens citrus production (Duan et al., 2009). Microbial Fermentation Application (MFA), an elicitor program, is formulated with a bacterial fermentation medium, yeast cell wall extract and a Cu component has been shown to reduce infection rates in other crops (Twamley et al.). Lally et al. show that MFA can stabilise HLB infection and increase the expression of important defence pathways in citrus under field conditions, including multiple PR genes, lignin formation genes, ROS-related genes, hormone synthases, and hormone regulators, providing therefore important evidence where MFA may play an pivotal role as a plant elicitor in the battle against HLB in citrus but also in other agronomically important crops.

Arabinogalactan proteins (AGPs) are cell wall resident glycosylated proteins found in land plants, and which are known to play a role in several plant biological functions. Přerovská et al. have isolated an arabinogalactan protein-like (AGP-like) enriched fraction from *Ulva lactuca* and assessed its ability to protect oilseed rape (*B. napus*) cotyledons against *Leptosphaeria maculans*, and to activate the host immune responses. Preventive application of the Ulva AGP-like enriched fraction on oilseed rape, followed by cotyledon inoculation with *L. maculans*, significantly reduces the progress of infection. The authors conclude that *U. lactuca* AGP-like glycoproteins exhibit promising elicitor activity and that plant eliciting properties of sea lettuce extract, might result not only from an ulvan-originated eliciting proprieties, but also be AGP-like originated.

Damage-associated molecular patterns (DAMPs) are danger signals released from the damaged host tissue or present on the surface of stressed cells (Bhat and Ryu, 2016). In their contribution, Kim et al. investigate self-extracellular RNA (eRNA) as a danger signal in plants. Their field experiments in pepper against viral and bacterial pathogens demonstrate, that self-eRNA can successfully trigger plant systemic immunity without any growth penalty, suggesting the potential of eRNA as a novel disease management agent against a wild range of pathogenic microbes.

Author contributions

All authors listed have made a substantial, direct, and intellectual contribution to the work and approved it for publication.

Conflict of interest

The authors declare that the research was conducted in the absence of any commercial or financial relationships that could be construed as a potential conflict of interest.

Publisher's note

References

Abdul Malik, N. A., Kumar, I. S., and Nadarajah, K. (2020). Elicitor and receptor molecules: Orchestrators of plant defense and immunity. *Int. J. Mol. Sci.* 21 (3), 963. doi: 10.3390/ijms21030963

Bhat, A., and Ryu, C.-M. (2016). Plant perceptions of extracellular DNA and RNA. *Mol. Plant* 9, 956–958. doi: 10.1016/j.molp.2016.05.014

Couto, D., and Zipfel, C. (2016). Regulation of pattern recognition receptor signalling in plants. *Nat. Rev. Immunol.* 16, 537–552.). doi: 10.1038/nri.2016.77

Gao, M., Wang, X., Wang, D., Xu, F., Ding, X., Zhang, Z., et al. (2009). Regulation of cell death and innate immunity by two receptor-like kinases in arabidopsis. *Cell Host Microbe* 6 (1), 34–44. doi: 10.1016/j.chom.2009.05.019

Duan, Y., Zhou, L., Hall, D.G., Li, W., Doddapaneni, H., Lin, H., et al. (2009). Complete genome sequence of citrus huanglongbing bacterium,'Candidatus Liberibacter asiaticus' obtained through metagenomics. *Mol. Plant-Microbe Interact* 22 (8), 1011–1020. doi: 10.1016/j.chom.2009.05.019

Jones, J. D., and Dangl, J. L. (2006). The plant immune system. *Nature* 444, 323–329. doi: 10.1038/nature05286

Mauch-Mani, B., Baccelli, I., Luna, E., and Flors, V. (2017). Defense priming: An adaptive part of induced resistance. *Annu. Rev. Plant Biol.* 68, 485–512. doi: 10.1146/annurev-arplant-042916-041132

Sanabria, N. M., Huang, J. C., and Dubery, I. A. (2010). Self/nonself perception in plants in innate immunity and defense. *Self Nonself.* 1 (1), 40–54. doi: 10.4161/self.1.1.10442

Singh, R. R., Verstraeten, B., Siddique, S., Tegene, A. M., Tenhaken, R., Frei, M., et al. (2020). Ascorbate oxidation activates systemic defence against root-knot nematode *Meloidogyne graminicola* in rice. *J. Exp. Bot.* 71 (14), 4271–4284. doi: 10.1093/jxb/eraa171

frontiers in Plant Science

ORIGINAL RESEARCH
published: 06 August 2021
doi: 10.3389/fpls.2021.716738

Novel Effector RHIFs Identified From *Acidovorax avenae* Strains N1141 and K1 Play Different Roles in Host and Non-host Plants

Minami Nakamura[1†], Machiko Kondo[2†], Aika Suzuki[1], Hiroyuki Hirai[2] and Fang-Sik Che[1,2,3]*

[1]*Graduate School of Biosciences, Nagahama Institute of Bio-Science and Technology, Nagahama, Japan,* [2]*Departmentof Bio-Science, Nagahama Institute of Bio-Science and Technology, Nagahama, Japan,* [3]*Genome Editing Research Institute, Nagahama Institute of Bio-Science and Technology, Nagahama, Japan*

Plant pathogenic bacteria inject effectors into plant cells using type III secretion systems (T3SS) to evade plant immune systems and facilitate infection. In contrast, plants have evolved defense systems called effector-triggered immunity (ETI) that can detect such effectors during co-evolution with pathogens. The rice-avirulent strain N1141 of the bacterial pathogen *Acidovorax avenae* causes rice ETI, including hypersensitive response (HR) cell death in a T3SS-dependent manner, suggesting that strain N1141 expresses an ETI-inducing effector. By screening 6,200 transposon-tagged N1141 mutants based on their ability to induce HR cell death, we identified 17 mutants lacking this ability. Sequence analysis and T3SS-mediated intracellular transport showed that a protein called rice HR cell death inducing factor (RHIF) is a candidate effector protein that causes HR cell death in rice. *RHIF*-disrupted N1141 lacks the ability to induce HR cell death, whereas *RHIF* expression in this mutant complemented this ability. In contrast, RHIF from rice-virulent strain K1 functions as an ETI inducer in the non-host plant finger millet. Furthermore, inoculation of rice and finger millet with either RHIF-deficient N1141 or K1 strains showed that a deficiency of *RHIF* genes in both strains results in decreased infectivity toward each the host plants. Collectively, novel effector RHIFs identified from *A. avenae* strains N1141 and K1 function in establishing infection in host plants and in ETI induction in non-host plants.

Keywords: pathogen effector, hypersensitive response cell death, effector-triggered immunity, symptom formation, p-loop NTPase, rice, finger millet

OPEN ACCESS

Edited by:
Essaid Ait Barka, Université de Reims Champagne-Ardenne, France

Reviewed by:
Haitao Cui, Fujian Agriculture and Forestry University, China
Christian Danve Marco Castroverde, Wilfrid Laurier University, Canada

***Correspondence:**
Fang-Sik Che
k_sai@nagahama-i-bio.ac.jp

†These authors have contributed equally to this work

Specialty section:
This article was submitted to Plant Pathogen Interactions, a section of the journal Frontiers in Plant Science

Received: *29 May 2021*
Accepted: *05 July 2021*
Published: *06 August 2021*

Citation:
Nakamura M, Kondo M, Suzuki A, Hirai H and Che F-S (2021) Novel Effector RHIFs Identified From Acidovorax avenae Strains N1141 and K1 Play Different Roles in Host and Non-host Plants. Front. Plant Sci. 12:716738. doi: 10.3389/fpls.2021.716738

INTRODUCTION

Plant pathogens employ sophisticated strategies to both evade plant immune systems and facilitate infection. In particular, plant pathogenic bacteria utilize effector proteins injected into plant cells using type III secretion systems (T3SS) as a means to circumvent plant defense mechanisms (Hueck, 1998; Buttner, 2016; Dey et al., 2019). When translocated into plant cells, these effectors alter various plant cell functions and promote successful infection by making the host more susceptible (Toruno et al., 2016). To combat such effectors, plants have evolved intracellular sensing systems to detect pathogen effectors either directly or indirectly while

co-evolving with plant pathogens (Jones et al., 2016; Saur et al., 2020). Plant recognition of bacterial effector proteins is the basis for effector-triggered immunity (ETI; Jones and Dangl, 2006; Cui et al., 2015; Laflamme et al., 2020). Effector-triggered immunity is generally associated with strong immune responses, including hypersensitive response (HR) cell death which is one of the programmed cell death (Mur et al., 2008; Balint-Kurti, 2019; Bi and Zhou, 2021). Effector-triggered immunity induction is a critical determinant of host specificity of pathogenic bacteria because ETI is triggered by detecting molecules that pathogenic bacteria use to infect plants.

Several bacterial pathogen effectors have been demonstrated to adversely affect various host cellular processes. For example, *Pseudomonas syringae* HopX1 disrupts the jasmonate (JA) signaling by degrading the protein jasmonate zim domain (JAZ) (Gimenez-Ibanez et al., 2014). Transcriptional activator-like effectors produced by the rice (*Oryza sativa*) pathogen *Xanthomonas oryzae,* namely, PthXo1 and AvrXa7, promote sugar efflux from host plant cells by inducing the expression of several genes that encode SWEET family sugar transporters (Streubel et al., 2013; Macho, 2016). AvrRpt2, HopQ1, and AvrPtoB from *P. syringae* can sensitize host plant cells to the auxin, cytokinin, and abscisic acid signaling pathways, respectively, while AvrBs3 and AvrXccC from *Xanthomonas campestris* can induce several plant hormone signaling (Marois et al., 2002; Torres-Zabala et al., 2007; Cui et al., 2013; Ho et al., 2013; Hann et al., 2014). The *P. syringae* T3SS effector HopZ1 promotes infection by suppressing the isoflavone biosynthetic pathway (Zhou et al., 2011) while the shikimate and phenylpropanoid pathways are upregulated by WtsE from *Pantoea stewartii* upregulates to promote pathogen virulence (Asselin et al., 2015).

Pathogen effectors are secreted by plant pathogenic bacteria as well as animal pathogenic bacteria. However, plant pathogenic bacteria secrete 20–40 effectors during infection compared with the handful of effectors that animal pathogenic bacteria inject into animal cells (Macho, 2016). Co-evolution between plants and plant pathogens over millions of years has resulted in plants expressing many immune receptors as well as toxins to defend against infection (Frantzeskakis et al., 2019; Vries et al., 2020). Hence, plant pathogens employ a wide range of effectors to disable plant defenses, such as by nullifying toxins and disabling ETI induction (Block et al., 2013; Hurley et al., 2014). Individual effectors may employ diverse functional mechanisms, including yet unknown ones, in host vs. non-host plants.

Plant pathogen effectors are, in general, injected into plant cells using T3SS (Buttner, 2016). Type III secretion systems components are encoded by genes located in *hrp* (hypersensitive response and pathogenicity) gene clusters, and these genes within *hrp* operons are activated by two regulatory genes that are members of the OmpR family of two-component response regulators (Noel et al., 2002). We previously reported that the plant pathogen *Acidovorax avenae* possesses a 35-kb *hrp* gene cluster containing genes encoding T3SS components (Kondo et al., 2012). *Acidovorax avenae* is a Gram-negative bacterium that causes brown striped symptoms on the leaf sheaths of infected plants (Kadota et al., 1991). *Acidovorax avenae* has a wide host range among monocotyledonous plants, but individual strains of this pathogen infect only one or a few host species (Kadota et al., 1996). For example, strains isolated from rice, including K1, can infect only rice plants (rice-virulent), while strain N1141 isolated from finger millet (*Eleusine coracana*) cannot infect rice, even after being inoculated into rice tissues (rice-avirulent; Kadota et al., 1996). We reported that inoculation of rice with the rice-avirulent strain N1141 of *A. avenae* caused ETI responses, including HR cell death, accompanied by loss of plasma membrane permeability, nuclear DNA fragmentation, and upregulation of ETI-related genes, including *OsNAC4*, which positively regulates HR cell death (Che et al., 1999; Kaneda et al., 2009). In contrast, the rice-virulent strain K1 can suppress PAMP-triggered immunity (PTI) caused by N1141 flagellin but cannot induce ETI responses in rice (Kawaguchi et al., 2021). Interestingly, a T3SS-deleted N1141 mutant (*NΔT3SS*) did not cause ETI responses, while the T3SS-deleted K1 mutant (*KΔT3SS*) was defective in PTI suppression (Kondo et al., 2012; Kawaguchi et al., 2021). These results indicate that strains N1141 and K1 have multiple effectors with different functions in rice.

To determine how *A. avenae* effectors manipulate plant cell processes, we began by identifying PTI-suppressing effectors expressed by strain K1. The screening of transposon-tagged mutants based on PTI suppression ability, sequence analysis, transcriptome analysis, and *in silico* prediction of T3SS-mediated secretion showed that *A. avenae* K1 suppression factor 1 (AKSF1) is a candidate PTI suppressor. AKSF1 protein translocation into rice cells is dependent on T3SS during infection; furthermore, an *AKSF1*-disruption mutant lost its ability to suppress PTI responses while AKSF1 expression in the *AKSF1*-disruption mutant rescues the loss of PTI suppression. When rice plants were inoculated with *AKSF1*-disruption mutants, disease symptom severity was reduced and bacterial growth was suppressed. These results indicate that AKSF1 is a novel effector that can suppress PTI in host rice plants (Kawaguchi et al., 2021). Interestingly, whole-genome sequencing of strain N1141 revealed that it lacks *AKSF1*. Since the strict host specificity between *A. avenae* strains N1141 and K1 involves the T3SS-secreted effectors, AKSF1 is not a determinant of host specificity. To elucidate the mechanism underlying host specificity, novel effector molecules involved in determining host specificity must be identified.

In this study, we found that HR cell death was accompanied by the loss of plasma membrane integrity and nuclear DNA fragmentation in cultured rice cells and rice leaf sections following inoculation with strain N1141 in a T3SS-dependent manner. We screened transposon-tagged N1141 mutants based on their ability to induce HR cell death. Sequence analysis revealed that RHIF is a candidate ETI effector. *RHIF* gene disruption caused the loss of HR cell death induction ability while introduction of RHIF into an RHIF-deleted N1141 mutant complemented the induction ability of HR cell death. RHIF transport into rice cells and localization studies using a CyaA–RHIF fusion showed that RHIF is secreted through T3SS and localizes to the cytoplasm of rice cells. Interestingly, K1 RHIF with 13 amino acid substitutions can induce ETI responses, including HR cell death, in the non-host plant

finger millet, but not in the host plant rice. Inoculation tests using RHIF-deficient strains N1141 and K1 on rice and finger millet showed that a deficiency of *RHIF* genes in strains N1141 and K1 results in decreased infectivity toward host plants. Our results therefore indicate that RHIFs isolated from strains N1141 and K1 are novel effectors that induce ETI in non-host plants and promote infection in host plants.

MATERIALS AND METHODS

Plants and Bacteria

Suspension cultures of rice cells (line Oc) were provided from NAIST. Cultures of rice cells were grown at 30°C under light irradiation (Baba et al., 1986). The cells were diluted in fresh R2S medium (39.6 mm KNO_3, 2.5 mm $(NH_4)_2SO_4$, 1.0 mm $MgSO_4$•$7H_2O$, 1.0 mm $CaCl_2$•$2H_2O$, 1.7 mm NaH_2PO_4•$2H_2O$, 20.1 μm EDTA•2Na, 19.8 μm $FeSO_4$•$7H_2O$, 6.6 μm $MnSO_4$•$4H_2O$, 7.7 μm $ZnSO_4$•$4H_2O$, 0.5 μm $CuSO_4$•$5H_2O$, 48.5 μm H_3BO_3, 0.6 μm $NaMoO_4$•$2H_2O$, 1% [w/v] Murashige and Skoog Vitamin powder (Sigma-Aldrich, St. Louis, United States), 18 μm 2,4-dichlorophenoxyacetic acid, and 87.6 mm Sucrose) every week, and all experiments were performed 4 days after transfer. *Acidovorax avenae* N1141 (MAFF 301141), T3SS-deficient N1141 strain (*NΔT3SS*), K1 (MAFF 301755), and T3SS-deficient K1 strain (*KΔT3SS*) were used as previously described (Kadota et al., 1996; Che et al., 2000; Kondo et al., 2017). Rice (*O. sativa L. subsp*. Kinmaze) was provided from NAIST. Finger millet (*E. coracana*) was purchased from TAKII & Co., Ltd. Rice and finger millet were grown for 3 weeks in a growth chamber with a 16 h day (200 μE m^{-2} s^{-1} at 30°C) and 8 h night (28°C) cycle.

Cell Death Detection in Cultured Rice Cells

Cell death in cultured rice cells was detected by previously described method (Che et al., 1999). Cultured rice cells were inoculated with each bacteria strain (10^8 cfu/ml), and incubated at 30°C for several periods. The cultured rice cells were transferred in 24-well tissue culture plates, the medium was removed, and then 0.05% Evans blue was added. 15 min later, cultured rice cells were washed three times with water, and the Evans blue dye in rice cells was extracted with extraction buffer (50% methanol and 1% SDS) for 12 h at room temperature. The amount of the extracted dye was estimated by measuring the absorbance at 595 nm.

Cell Death Detection in Leaf Sheath Sections

Leaf sheaths of the seedlings were cut into 100 μm section with a razor (FEATHER, Osaka, Japan). Plate stem sections were incubated at 30°C with each bacterial strain (10^9 cfu/ml). The stem sections were stained with 0.1% Evans blue for 15 min then washed extensively with distilled water to remove excess dye and observed by microscopy (Axioskop 2 plus, Carl Zeiss, Germany) used 40× objective lens.

TUNEL Staining

Terminal deoxynucleotidyl transferase-mediated dUTP nick-end labeling (TUNEL) staining was performed by a previously described method (Che et al., 1999) with several modifications. Cultured cells were washed three times with phosphate buffered salts (PBS) (pH 7.4) and fixed in 4% (v/v) paraformaldehyde in PBS at 25°C overnight. The cells were washed three times with PBS and digested with proteinase K (10 μg/ml) containing 10 mm Tris–HCl (pH 7.5) at 37°C for 30 min and washed three times with PBS. The cells were subjected to TUNEL for 1 h at 37°C using a DeadEnd™ Fluorometric TUNEL System (Promega, Madison, WI, United States). After washing with PBS, 4′,6-diamidino-2-phynylindole was added to the cells (1 μg/ml) in 50 mm NaCl, 5 mm EDTA, and 10 mm Tris–HCl (pH 7.4). Stained cells were observed by the confocal laser scanning microscope (FV1000, OLYMPUS, Tokyo, Japan; OLYMPUS UPlanSApo 40× lens, scan speed 20 us/pixel, laser intensity 5%, HV 600 V, Gain 1×, Offset 0%, and pinhole diameter 300 μm). The number of TUNEL-positive nuclei and DAPI staining nuclei was determined by counting nuclei within 20 individual fields. Each determination was done with at least 100 nuclei in each of three independent experiments.

Generation of the Transposon-Tagged N1141 Mutant and Sequence Analysis the Transposon Insertion Site

To generate the transposon-tagged N1141 mutant, EZ-Tn5™<KAN-2>Tnp Transposome™ (EPICENTER, Lucigen, United States) was electro-transformed into *A. avenae* N1141 strain. Electroporation was performed using a Gene Pulser (Bio-Rad) under the conditions of voltage 1.7 kV/cm, capacitance 25 μf, and cuvette resistance 200 Ω. In order to clarify the sequence of transposon – inserted site, DNA near the transposon was amplified by the Random Amplification of Transposon Ends (RATE) method using primer set (5′- CGAACTTTT GCTGAGTTGAAGGACT -3′ and 5′- GAGCAAGACGTTTCC CGTTGAATAT -3′).

RNA Isolation and qRT-PCR

Total RNA was isolated from cultured rice cells using the RNeasy plant mini kit (Qiagen, Hilden, Germany) with DNase digestion. qRT-PCR was performed on Opticon2 instrument (Bio-Rad, Hercules, CA, United States), using the GoTaq One-Step RT-qPCR kit (Promega) with the following *OsNAC4*-specific primers (F: 5′- TCCTGCCACCACCATTCTGAGATG -3′ and R: 5′- TTGCAGAATCATGCTTGCCAG -3′) and *PAL*-specific primers (F: 5′- ACATCGGCAAGCTCATGTTC -3′ and R: 5′- CCCTTGAACCCGTAGTCCAA -3′). The mRNA levels were normalized based on the reference gene, *actin1* (F: 5′- TCCATCTTGGCATCTCTCAG -3′ and R: 5′- TGGCTTAG -CATTCTTGGGTC -3′).

Generation of RHIF Mutants

DNA was isolated from each strain using a previously described protocol (Wilson, 1987). To generate RHIF-deletion mutants,

upstream and downstream regions of *RHIF* were PCR amplified using two sets of specific primers (F: 5′- CAGGTCGACTCTAG AGATCGCCATCACCGGAGCCT -3′ and R: 5′- GCTGTCATG CGGACATGATCCCCCGGAGCGTAC -3′ for the upstream region of *RHIF*; F: 5′- GATCATGTCCGCATGACAGCCCA CGGCGATG -3′ and R: 5′- CGGGGATCCTCTAGACGCTAT TACGGCGCCGTGGC -3′ for the downstream region of *RHIF*), respectively. Each amplified PCR products were diluted and mixed equally, and then, the mixed PCR products were re-amplified using the upstream region of *RHIF* F primer and the downstream region of *RHIF* R primer. The PCR product was cloned into *pK18mobsacBTET* linearized by *Xba*I using the In-fusion cloning kit (Takara Bio, Shiga, Japan), and the resulting plasmid was designated *NΔRHIF/pK18mobsacBTET*. The *NΔRHIF/pK18mobsacBTET* was electro-transformed into *A. avenae* N1141 strain. Electroporation was performed using a Gene Pulser (Bio-Rad; voltage 1.7 kV/cm, capacitance 25 μf, and cuvette resistance 200 Ω). The bacterial cells were plated on LB agar plates (containing 20 μg/ml of tetracycline) and incubated at 30°C for 48 h. For second crossing-over event, the provided bacterial strains were incubated in sucrose selection media (Pseudomonas F liquid medium containing 1% [w/v] Bacto Tryptone (Thermo Fisher Scientific, Waltham, United States), 1% [w/v] Proteose Peptone No. 3 (Thermo Fisher Scientific), 0.15% [w/v] K_2HPO_4, 0.15% [w/v] $MgSO_4$ and 26% sucrose) at 30°C for 72 h.

To generate *RHIF* complementary N1141 mutant (*NΔRHIFC*), *RHIF* was PCR amplified using the upstream region of RHIF F primer and the downstream region of *RHIF* R primer. The PCR product was cloned into *pK18mobsacBKm* linearized by *Spe*I using the In-fusion cloning kit (Takara Bio, Shiga, Japan), and the resulting plasmid was designated *NΔRHIFC/pK18mobsacBKm*. The *NΔRHIFC/pK18mobsacBKm* was electro-transformed into *NΔRHIF*. The bacterial cells were plated on LB agar plates (containing 50 μg/ml of kanamycin) and incubated at 30°C for 48 h. For second crossing-over event, the bacterial strain was incubated in sucrose selection media (Pseudomonas F liquid medium containing 27% sucrose) at 30°C for 72 h. *RHIF*-deletion K1 mutant (*KΔRHIF*) and *RHIF* complementary K1 mutant (*KΔRHIFC*) were generated in the same methods.

Adenylate Cyclase Translocation Assay

Promoter region of *flaA* (336 bp) containing additional 5′-terminal *XbaI* site and 3′-terminal *Hin*dIII site was PCR amplified from *A. avenae* N1141 genome using specific primer set (5′-TCTAGAGGCGGAACTCCTGCG-3′ and 5′-AAGCTTCAT TGCAAATCTCCTGAAAAGAAC-3′) and cloned into *pGEM-T*. The plasmid was digested by *Xba*I and *Hin*dIII and cloned into *pBBR1Tp*, and the generated plasmid was named *flapro/pBBR1Tp*. *CyaA* was amplified with PCR using primer set (5′-AAGCTTCAGCAATCGCATCAGGC-3′ and 5′-GGTACCT CAGCTGTCATAGCCGGA-3′) and cloned into *pGEM-T*. The plasmid was digested by *Hin*dIII and *Kpn*I and cloned into *flapro/pBBR1Tp*, and the generated plasmid was named *flapro-CyaA/pBBR1TP*. *RHIF* was PCR amplified from N1141 genome using specific primer set (5′- AAGCTTATGTCCACTCCCCCTT CCCTGC -3′ and 5′- AAGCTTTGCCCGCACCCCGAGC -3′). The PCR product was cloned into *flapro-CyaA/pBBR1TP* linearized by *Hin*dIII using the In-fusion HD cloning kit (Takara Bio), and the generated plasmid, *flapro-RHIF-CyaA/pBBR1TP,* was transformed into N1141 or *NΔT3SS* by electroporation. Cultured rice cells were inoculated with 1.0×10^8 cfu/ml of N1141 carrying *RHIF-CyaA* vector and incubated for 10 h at 30°C. After incubation, cultured rice cells were washed three times with distilled water and resuspended in 200 μl distilled water. The cells were boiled for 5 min, smashed with zirconia beads using the Bead Smash 12(WAKENYAKU, Kyoto, Japan) at 5,000 rpm for 5 min, and then centrifuged at 1,500 × *g* for 10 min at 4°C. Concentration of cAMP in the supernatant was measured using the Cyclic AMP EIA Kit (Cayman Chemical, Ann Arbor, MI, United States).

Protoplast Preparation and Gene Transformation

Protoplast preparation and gene transformation were performed as described by Takai et al. (2007).

Inoculation Test

Inoculation of *A. avenae* to rice or finger millet was performed by previously described method (Kondo et al., 2017), with the slightly modifications. The bacteria suspended in sterilized distilled water (1×10^6 cfu/μl) were drop on the end of a needle in an amount of one microliter (10^6 cfu), and then the sheath of 3 weeks old seedlings was pricked at a point 3 cm above the soil level. Inoculated seedlings were grown for 4 days in a growth chamber with a 16 h day (200 μE m^{-2} s^{-1} at 30°C) and 8 h night (28°C) cycle. The pathogenicity of each strain was estimated by assessing the brown stripe development around the inoculation site.

The growth of each bacterial strain was evaluated by measuring the number of bacterial cells in whole plants. Three sets of randomly selected rice plants were harvested, rinsed thoroughly in 1% HClO, 70% ethanol, and sterile water, and homogenized in distilled water. Dilutions of the homogenate were plated into Pseudomonas F agar. After incubation at 30°C for 48 h, the number of colony-forming units was determined.

RESULTS

Rice ETI Induction by the Rice-Avirulent *Acidovorax avenae* Strain N1141

To identify ETI effectors, we first attempted to characterize ETI responses induced by the rice-avirulent *A. avenae* strain N1141. The loss of plasma membrane integrity is an important feature of HR cell death. Evans blue staining, which is used to detect the loss of plasma membrane integrity, is typically used to quantify dead cells. Therefore, we first examined rice HR cell death induced by strain N1141 using Evans blue staining.

When strain N1141 (10^8 cfu/ml) was incubated with cultured rice cells, cell death was detected 6 h post-inoculation, and the number of dead cells gradually increased until 12 h

post-inoculation. In contrast, inoculation with the rice-virulent strain K1 did not cause cell death in cultured rice cells until 6 h post-inoculation (**Figure 1A**). Unlike wild-type strain K1, neither T3SS-deficient strain N1141 (*NΔT3SS*) nor T3SS-deficient strain K1 (*KΔT3SS*) could induce the death of cultured rice cells (**Figure 1A**).

Next, we determined whether HR cell death induced by strain N1141 is also observed in rice leaf sheath sections. Staining rice leaf sheath sections with Evans blue showed that many stained cells were interspersed with unstained cells 6 h post-inoculation with strain N1141. In contrast, no stained cells were observed after inoculation with the virulent K1, *KΔT3SS*, or *NΔT3SS* strains (**Figure 1B**). Stained cells were not detected in the mock-inoculated sheath section (data not shown), which suggests that the loss of plasma membrane integrity observed in both cultured rice cells and rice sheath sections is induced by strain N1141, but not strain K1. Moreover, this induction is dependent on the T3SS of strain N1141.

Another important feature of HR cell death is nuclear DNA cleavage at specific chromosomal sites by DNA endonucleases

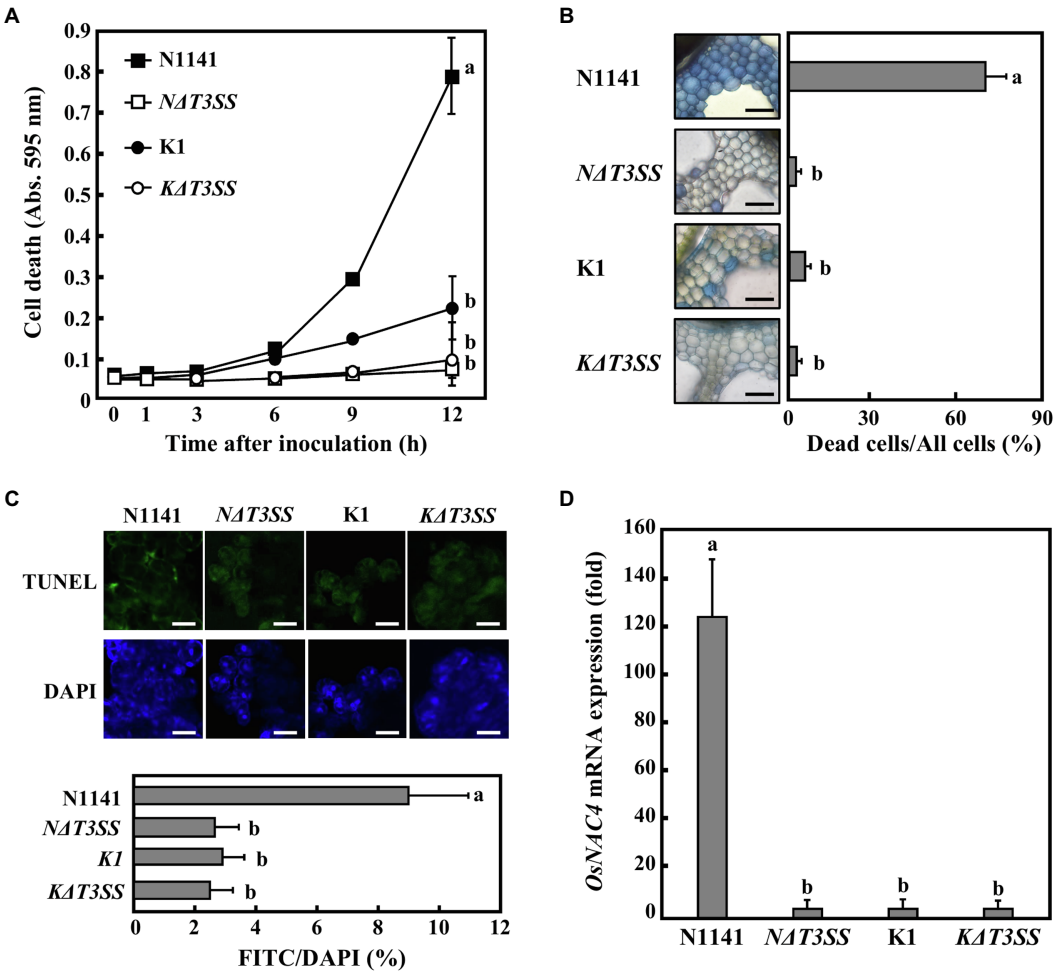

FIGURE 1 | Rice hypersensitive response (HR) cell death induced by each strain of *Acidovolax. avenae* **(A)** Time course of HR cell death in cultured rice cells inoculated with N1141 wild type (solid square), *NΔT3SS* (open square), K1 wild type (solid circle), or *KΔT3SS* (open circle). Hypersensitive response cell death was detected by Evans blue staining. That time point values without letters indicate no statistical significance. **(B)** Induction of HR cell death in leaf sheath sections. Rice sheath cross-sections were inoculated with N1141, *NΔT3SS*, K1, and *KΔT3SS*, and 6 h after inoculation, Evans blue staining was performed. Bar represents 100 μm. Left graph shows the percentage of dead cell in leaf sheath sections. Each determination was done with at least 100 cells in each experiment. **(C)** Terminal deoxynucleotidyl transferase-mediated dUTP nick-end labeling (TUNEL) staining of each strain-inoculated cultured rice cells. Upper photographs represent TUNEL staining cell images of cultured rice cells inoculated with N1141 wild type, *NΔT3SS*, K1 wild type, or *KΔT3SS*. Lower photographs represent DAPI staining cell images of cultured rice cells inoculated with N1141 wild type, *NΔT3SS*, K1 wild type, or *KΔT3SS*. Scale bar in photographs represents 10 μm. Lower graph represents percentage of TUNEL-positive nuclei in cultured rice cells inoculated with each strain. The percentage of TUNEL-positive nuclei was determined by counting nuclei within 10 individual fields. Each determination was done with at least 1,000 nuclei in each of three independent experiments. **(D)** *OsNAC4* mRNA levels in cultured rice cells inoculated with N1141, *NΔT3SS*, K1, or *KΔT3SS*. The x-axis represents the fold change in mRNA levels relative to those in cultured cells prior to treatment. Error bars in all figures represent standard deviation of three independent experiments. Values followed by a different letter in figures were significantly different according to Tukey-Kramer test ($p < 0.05$).

(Ryerson and Heath, 1996; Ootsubo et al., 2016). To determine whether DNA fragmentation is associated with the loss of plasma membrane integrity induced by strain N1141 and whether the T3SS of N1141 is involved in DNA fragmentation, TUNEL (McCabe et al., 1997) was performed on cultured rice cells inoculated with either N1141, K1, or a T3SS-deficient strain. Terminal deoxynucleotidyl transferase-mediated dUTP nick-end labeling staining of cultured rice cells 6 h post-inoculation revealed that many fluorescein-derived bright green fluorescence signals were observed in N1141-inoculated cultured rice cells. The positions of all bright green signals coincided with those of nuclei stained with 4′,6-diamidino-2-phenylindole (DAPI; **Figure 1C**). Terminal deoxynucleotidyl transferase-mediated dUTP nick-end labeling-positive nuclei were observed in 9% of N1141-inoculated cells. In contrast, the percentage of cultured rice cells inoculated with either K1, *KΔT3SS*, or *NΔT3SS* that showed TUNEL-positive nuclei was about 3%, lower than for N1141-inoculated cells (**Figure 1C**).

OsNAC4 is a plant-specific transcription factor that contains a consensus sequence called the NAC domain. We previously reported that OsNAC4 positively regulates HR cell death in rice. We therefore measured changes in OsNAC4 expression in cultured rice cells inoculated with either strain K1, *KΔT3SS*, or *NΔT3SS* using qRT-PCR. *OsNAC4* transcription was detected 6 h post-inoculation with N1141, but no induction of *OsNAC4* genes was observed in rice cells inoculated with either K1, *KΔT3SS*, or *NΔT3SS* (**Figure 1D**). Induction of *OsNAC4* expression during HR cell death indicates that *OsNAC4* expression can act as a marker for ETI induction. Taken together, our results suggest that the HR cell death specifically induced by strain N1141 is caused by effector proteins secreted through its T3SS.

Identification of ETI Effector Genes From Strain N1141

To identify effector proteins that positively regulate HR cell death, a tagged transposon library was constructed for strain N1141. The workflow for high-throughput screening of the HR-inducing effector-encoding genes is described in **Supplementary Figure S1**. By screening 6,200 mutants according to this workflow, we found that 17 transposon-tagged N1141 mutants lost their ETI induction ability. Sequence analysis of transposon flanking regions using RATE polymerase chain reaction (Ducey and Dyer, 2002) revealed that the transposons were inserted into five unique genes, namely, *NT1, NT2, NT3, NT4,* and *NT5*.

Among the five genes, *NT1, NT2,* and *NT3* are located within the *Hrp* cluster and encode HrpX, HrpD5, and HrcU, respectively. Additionally, *NT4* encodes a proton channel-related protein. Since the T3SS machinery includes these four proteins, *NT1–4* were not considered candidate effector genes because their deficiency would impair T3SS function. *NT5*, however, encodes an unrelated protein composed of 350 amino acids. A search of the GenBank/EMBL database for similar sequences identified a domain consisting of amino acid residues 22–198 within this protein that shows 43% identity to the P-loop NTPase domain of *O. sativa* (rice) isopentenyl transferase10 (**Figure 2A**).

If NT5 is an HR cell death inducible effector, then, it should be translocated into plant cells during infection. Adenylate cyclase (CyaA) requires calmodulin for its activity. Since calmodulin is only present in eukaryotic cells, CyaA is only active in eukaryotic cells (Sory and Cornelis, 1994). Thus, accumulation of the CyaA product, cAMP, in inoculated plant tissues can be used to measure type III effector delivery into plant cells (Casper-Lindley et al., 2002; Schechter et al., 2004). We monitored the intracellular transport of NT5 using an NT5-CyaA hybrid protein. In order to do this, we generated N1141 and *NΔT3SS* transformants that express NT5-CyaA. We extracted cAMP from cultured rice cells 9 h post-inoculation and measured its concentration using an enzyme immunoassay. High levels of cAMP (about 180 pmol/ml) were detected in cultured rice cells inoculated with N1141 expressing NT5-CyaA, whereas very small amounts of cAMP accumulation were observed in cells inoculated with *NΔT3SS* expressing NT5-CyaA (**Figure 2B**), suggesting that NT5 is transported into rice cells through the T3SS of strain N1141. Based on these data, we concluded that NT5 is a candidate effector protein that causes HR cell death in rice. We therefore named NT5 rice HR cell death inducing factor (RHIF).

Identification of RHIF as an ETI Effector in Rice

To determine whether RHIF functions as an effector that causes HR cell death in rice, we generated an *RHIF*-deletion N1141

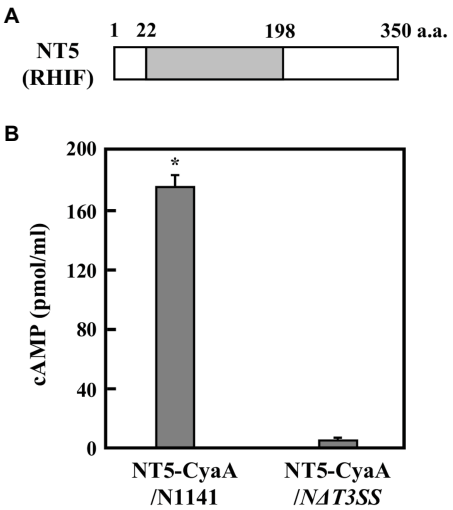

FIGURE 2 | ETI effector candidate protein NT5 (RHIF). **(A)** Schematic drawing of NT5 (RHIF) structure. Gray box indicates the region that is homologous to the p-loop NTPase domain within rice isopentenyl transferase10. **(B)** Transport of NT5 (RHIF) from N1141 into rice cells. Cultured rice cells were inoculated with *A. avenae* N1141 strain and *NΔT3SS* carrying pBBR1Tp plasmid expressing the NT5 (RHIF)-CyaA fusion protein, and 12 h after inoculation, cAMP concentration was measured. Bars indicate the standard deviation of three independent experiments. Asterisk indicates significant difference (*t*-test, $p < 0.05$).

mutant (*NΔRHIF*). We also generated an RHIF-complement *NΔRHIF* mutant (reintroduction of *RHIF* into the genome of *NΔRHIF: NΔRHIFC* mutant) using homologous recombination. Cultured rice cells were inoculated with either strain N1141, *NΔRHIF, NΔRHIFC*, or *NΔT3SS*. Plasma membrane integrity was monitored by Evans blue staining. Clear cell death was induced in N1141-inoculated cultured cells 6 h post-inoculation, while no cell death was observed in cultured rice cells inoculated with *NΔRHIF* (**Figure 3A**). When cultured rice cells were inoculated with *NΔRHIFC*, which is the RHIF-complement *NΔRHIF*, cell death was induced to the same extent as that observed in N1141-inoculated cultured rice cells (**Figure 3A**). Similarly, Evans blue staining showed that cell death in rice leaf sheaths was induced by inoculation with *NΔRHIFC*, but not by *NΔRHIF* (**Figure 3B**).

We used a TUNEL assay to determine whether the DNA fragmentation observed during HR cell death was also induced by RHIF. Cultured rice cells were inoculated with N1141, *NΔRHIF*, *NΔRHIFC*, and *NΔT3SS*. Six hours post-inoculation, TUNEL was performed. The percentage of TUNEL-positive nuclei observed in N1141- and *NΔRHIFC*-inoculated cultured rice cells reached about 8%, while the percentage of TUNEL-positive nuclei in the cultured rice cells inoculated with *NΔRHIF* and *NΔT3SS* was only about 3% (**Figure 3C**).

To clarify the involvement of RHIF in the induction of *OsNAC4*, which is an indicator of ETI induction, *OsNAC4* mRNAs were quantified in N1141-, *NΔRHIF*-, *NΔRHIFC*-, and *NΔT3SS*-inoculated cultured rice cells. The *OsNAC4* expression level was about 100 times higher in cultured rice cells inoculated with either N1141 or *NΔRHIFC* than in cells inoculated with either *NΔRHIF* or *NΔT3SS* (**Figure 3D**).

It was reported that ETI and HR can sometimes be uncoupled (Chiang and Coaker 2015; Menna et al. 2015). We previously reported that *OsPAL* which is involved in plant secondary metabolism is T3SS-dependently induced by N1141 of *A. avenae* (Kondo et al., 2012). To determine whether RHIF positively regulates ETI as well as HR cell death, *OsPAL* mRNA were quantified in N1141-, *NΔRHIF*-, *NΔRHIFC*-, and *NΔT3SS*-inoculated cultured rice cells (**Figure 3E**). 6 h after inoculation, the expression level of *OsPAL* was about 30 times higher in cultured rice cells inoculated with either N1141 or *NΔRHIFC* than in cells before inoculation. In contrast, *OsPAL* expression level in *NΔRHIF*-inoculated cultured rice cells was lower than that in N1141-ioculated cultured rice cells, and no increase of *OsPAL* expression was observed in *NΔT3SS*-inoculated cultured rice cells. These results indicate that RHIF from N1141 induces not only HR cell death but also ETI.

To determine whether HR cell death is triggered by RHIF transported into rice cells, we constructed three plasmids, one of which contains the *RHIF* gene while the others contain either *GUS* as a negative control or *OsNAC4* as a positive control. The individual plasmids were used to transform rice protoplasts. As shown in **Figure 4A**, approximately 80% of RHIF- and OsNAC4-expressing rice protoplasts were stained with Evans blue, while the proportion of dead cells in GUS-expressing rice protoplasts was significantly reduced. Because another important feature of rice HR cell death induced

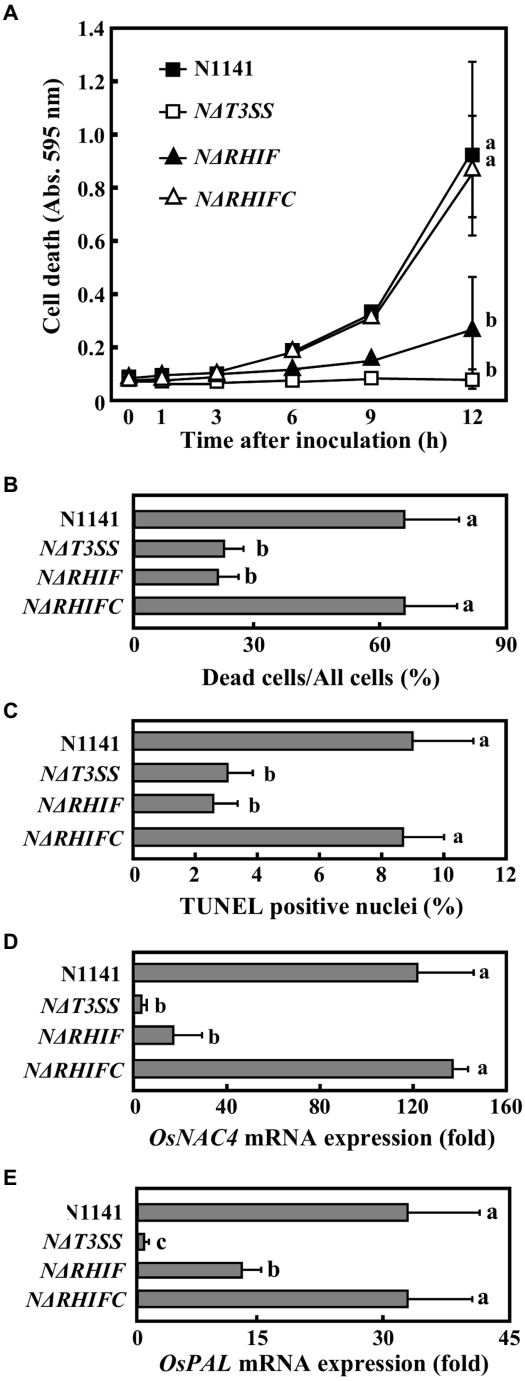

FIGURE 3 | Role of RHIF in induction of rice ETI. **(A)** Time course of HR cell death in cultured rice cells inoculated with N1141 (solid square), *NΔT3SS* (open square), *NΔRHIF* (solid triangle), or *NΔRHIFC* (open triangle). That time point values without letters indicate no statistical significance. **(B)** Percentage of dead cell in leaf sheath sections. Rice sheath cross-sections 6 h after treatment with N1141, *NΔT3SS*, *NΔRHIF*, and *NΔRHIFC* were monitored for dead cells using Evans blue staining. Each determination was done with at least 100 cells in each experiment. **(C)** Percentage of TUNEL-positive nuclei in cultured rice cells inoculated with N1141, *NΔT3SS*, *NΔRHIF*, and *NΔRHIFC*. The percentage of TUNEL-positive nuclei was determined by counting nuclei within 10 individual fields. Each determination was done with

(*Continued*)

FIGURE 3 | at least 1,000 nuclei in each of three independent experiments. **(D)** *OsNAC4* mRNA levels in cultured rice cells inoculated with N1141, *NΔT3SS*, *NΔRHIF*, and *NΔRHIFC*. The x-axis represents the fold change in mRNA levels relative to those in cultured cells prior to treatment. **(E)** *PAL* mRNA levels in cultured rice cells inoculated with N1141, *NΔT3SS*, *NΔRHIF*, and *NΔRHIFC*. The x-axis represents the fold change in mRNA levels relative to those in cultured cells prior to treatment. Error bars in figures represent standard deviation of three independent experiments. Values followed by a different letter in figures were significantly different according to Tukey-Kramer test ($p < 0.05$).

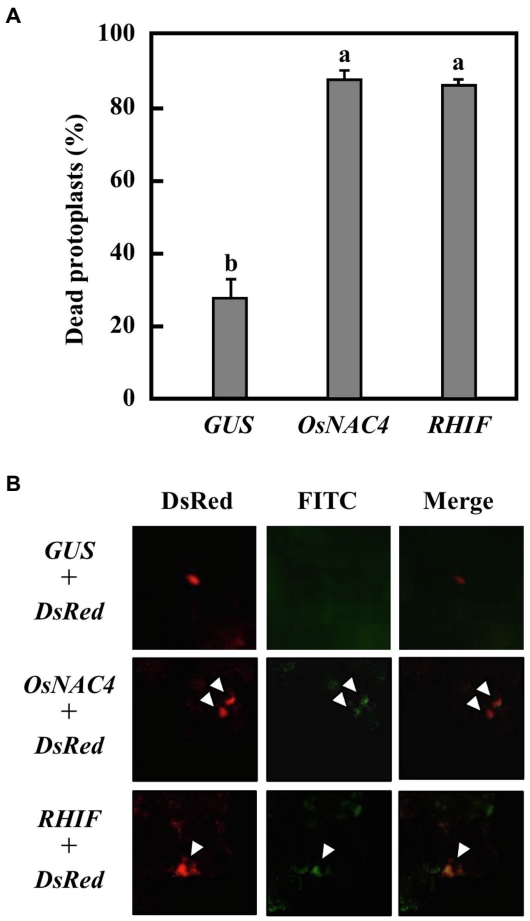

FIGURE 4 | HR cell death induction by *RHIF*. **(A)** Percentage of dead protoplasts induced by expression *GUS*, *OsNAC4*, and *RHIF*. HR cell death was detected by Evans blue staining. Error bars represent standard deviation of three independent experiments. Values followed by a different letter were significantly different according to Tukey-Kramer test ($p < 0.05$). **(B)** DNA fragmentation detected by TUNEL staining. *GUS* and *DsRed* (upper panels), *NRHIF* and *DsRed* (middle panels), and *KRHIF* and *DsRed* (lower panels) were co-expressed. The arrow indicates the TUNEL-positive nucleus.

by strain N1141 is nuclear DNA fragmentation (Che et al., 1999), TUNEL staining was attempted on rice cells expressing RHIF. Gold particles for bombardment were coated with a mixture of *RHIF*-expressing vector and *DsRed*-expressing vector before being bombarded into cultured rice cells. Six hours post-inoculation, the *RHIF*-expressing cultured rice cells (DsRed-positive cells) exhibited fluorescein-derived bright green fluorescence of their nuclei, as detected by TUNEL (**Figure 4B**). Similar nuclear DNA fragmentation was also observed in OsNAC4-expressing cultured rice cells, while no fluorescein-derived bright green fluorescence was found in GUS-expressing cultured rice cells, suggesting that ectopic expression of RHIF in rice cells causes nuclear DNA fragmentation. Based on the above results, we concluded that HR cell death in rice is induced by RHIF transported from N1141 into rice cells.

Role of RHIF Derived From Strain K1 in ETI Induction

As mentioned above, strain N1141 causes rice ETI responses, but strain K1 does not. If strain K1 expresses RHIF, what role does K1-derived RHIF play in inducing ETI responses? Therefore, we next attempted to identify the *RHIF* gene of strain K1. *RHIF* gene derived from strain K1 was amplified by PCR using strain K1 genomic DNA as a template, and the sequence of the amplified DNA fragment was determined. We found that the putative *RHIF* gene contains an open reading frame of 1,050 bp, located at the same chromosomal locus as the N1141-derived *RHIF* gene. The translated amino acid sequence revealed that the RHIF derived from strain K1 is also composed of 350 amino acids, with a difference of only 13 residues compared with the N1141 ortholog (**Figure 5A**). Interestingly, all residues that differ between both RHIFs are present outside the P-loop NTPase domain (**Figure 5A**). Since strain K1 carries a different *RHIF* allele from that of strain N1141, we named the N1141 allele *NRHIF* and the K1 allele *KRHIF*.

To determine the role of KRHIF in ETI induction, we generated a *KRHIF*-deletion K1 mutant (*NΔRHIF*) and a *KRHIF* complementation *KΔRHIF* mutant (reintroduction of KRHIF into the genome of *KΔRHIF: KΔRHIFC*). Cultured rice cells were inoculated with either strain K1, *KΔRHIF*, or *KΔRHIFC*, and cell death was monitored by Evans blue staining. Cell death in cultured rice cells was not induced not only by K1 but also by *KΔRHIF* or *KΔRHIFC* until 12 h post-inoculation (**Figure 5B**). When rice leaf sheaths were inoculated with either K1, *KΔRHIF*, or *KΔRHIFC*, we did not detect cell death (**Figure 5C**). Moreover, we could not detect nuclear DNA fragmentation in cultured rice cells inoculated with either K1, *KΔRHIF*, or *KΔRHIFC* (**Figure 5D**). Similarly, the expression level of *OsNAC4* in cultured rice cells was not increased by inoculation with either *KΔRHIF* or *KΔRHIFC* (**Figure 5E**). Furthermore, when KRHIF was expressed in cultured rice cells, neither cell death nor nuclear DNA fragmentation was observed (**Supplementary Figure S2**). These results indicate that KRHIF does not function as an ETI-inducible effector in rice.

The host plants of strains K1 and N1141 are rice and finger millet, respectively. Therefore, we next evaluated the effect of KRHIF on the non-host finger millet. Evans blue staining of finger millet leaf sheath sections inoculated with strain K1 showed that cell death was induced in more than 60% of cells 12 h post-inoculation. A reduction in dead cells was observed in sheath sections inoculated with either *KΔT3SS* or *KΔRHIF* (**Figure 6**). Cell death was induced to the same extent in finger millet leaf sheath sections at the same level by strain

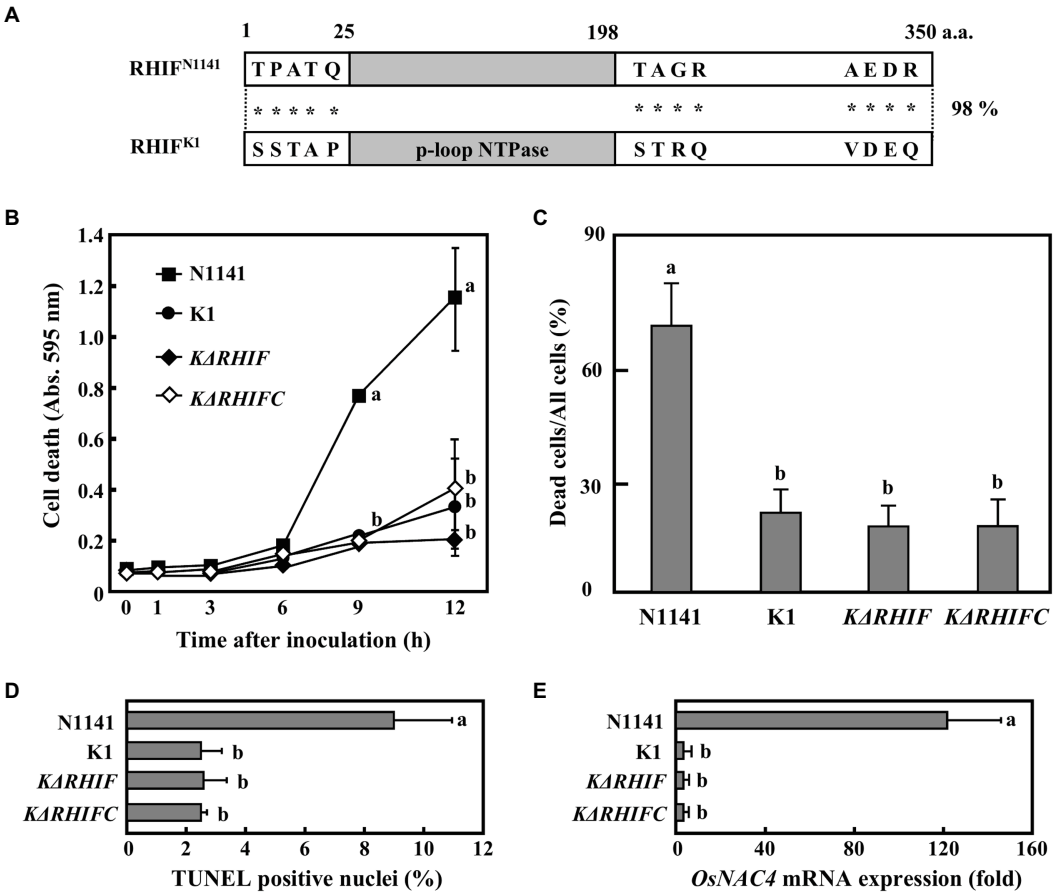

FIGURE 5 | Role of KRHIF in induction of rice ETI. **(A)** Schematic drawing of RHIFs. Gray box indicates the p-loop NTPase domain. Asterisks indicate non-conserved amino acid residues. **(B)** Time course of HR cell death in cultured rice cells inoculated with N1141 (solid square), K1 (solid circle), *KΔRHIF* (solid rhomb), or *KΔRHIFC* (open rhomb). That time point values without letters indicate no statistical significance. **(C)** Percentage of dead cell in leaf sheath sections. Rice sheath cross-sections 6 h after treatment with N1141, K1, *KΔRHIF* and *KΔRHIFC* were monitored for dead cells by Evans blue staining. Each determination was done with at least 100 cells in each experiment. **(D)** Percentage of TUNEL-positive nuclei in cultured rice cells inoculated with N1141, K1, *KΔRHIF*, and *KΔRHIFC*. The percentage of TUNEL-positive nuclei was determined by counting nuclei within 10 individual fields. Each determination was done with at least 1,000 nuclei in each of three independent experiments. **(E)** *OsNAC4* mRNA levels in cultured rice cells inoculated with N1141, K1, *KΔRHIF*, and *KΔRHIFC*. The x-axis represents the fold change in mRNA levels relative to those in cultured cells prior to treatment. Error bars in figures represent standard deviation of three independent experiments. Values followed by a different letter in figures were significantly different according to Tukey-Kramer test ($p < 0.05$).

K1 and the KRHIF complementation mutant, *KΔRHIFC* (**Figure 6**), which suggests that *KRHIF* functions as an effector that induces cell death in finger millet.

Roles of NRHIF and KRHIF in Disease Formation in Rice and Finger Millet

To clarify the roles of NRHIF and KRHIF on disease formation in rice, rice plants were inoculated with either N1141, K1, *NΔT3SS*, *KΔT3SS*, *NΔRHIF*, *KΔRHIF*, *NΔRHIFC*, or *KΔRHIFC* using the needle injection method. Brown stripe symptoms in K1-inoculated rice appeared 2 days post-inoculation and gradually spread 4 days post-inoculation (**Figures 7A**,**B**). In contrast, when rice was inoculated with either N1141, *NΔRHIF*, *NΔRHIFC*, *NΔT3SS*, or *KΔT3SS*, no brown stripe symptoms appeared within 4 days post-inoculation (**Figures 7A**,**B**). Interestingly, inoculation with *KΔRHIF* reduced the severity of symptoms by about 50%; this reduction was restored by RHIF complementation (**Figures 7A**,**B**). The presence of inoculated bacteria was determined by measuring internal bacterial load. When wild-type K1 (1×10^6 cfu) was inoculated into rice, the number of K1 cells reached 3×10^7 cfu/plant 4 days post-inoculation (**Figure 7C**). No remarkable increase in the numbers of *KΔRHIF*, *KΔT3SS*, and *NΔRHIF* cells was observed 4 days post-inoculation (**Figure 7C**). In contrast, the numbers of N1141, *NΔT3SS*, and *NΔRHIFC* in rice 4 days post-inoculation was lower than the number of inoculated bacterial cells. These observations, together with the lesion formation data, indicate that the absence of *NRHIF* genes increases the infectivity of strain N1141, and the absence of the *KRHIF* gene decreases the infectivity of strain K1 toward rice.

To determine the role of NRHIF and KRHIF in disease formation in finger millet, we conducted a similar inoculation test on finger millet with N1141, K1, *NΔT3SS*, *KΔT3SS*, *NΔRHIF*,

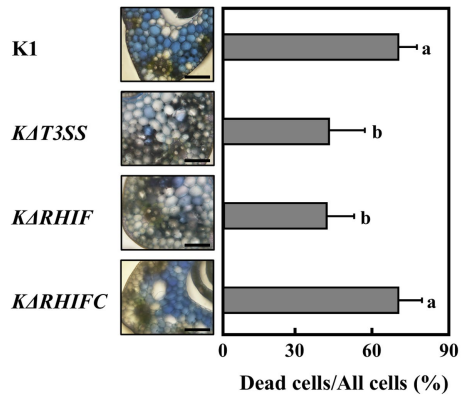

FIGURE 6 | Role of KRHIF in induction of finger millet cell death. Finger millet sheath cross-sections were inoculated with K1, *KΔT3SS*, *KΔRHIF*, and *KΔRHIFC*, and 12 h after inoculation, Evans blue staining was performed. Scale bar represents 100 μm. Light graphs show the percentage of dead cell in leaf sheath sections of finger millet. Each determination was done with at least 100 cells in each experiment. Error bars represent standard deviation of three independent experiments. Values followed by a different letter were significantly different according to Tukey-Kramer test ($p < 0.05$).

KΔRHIF, NΔRHIFC, and *KΔRHIF*. The brown stripe symptom in finger millet appeared 4 days post-inoculation with finger millet-virulent strain N1141. We observed a 30% reduction in symptoms in finger millet inoculated with *NΔRHIF* while the symptoms observed in finger millet inoculated with the RHIF complementation strain, *NΔRHIFC*, were similar to those inoculated with wild-type strain N1141 (**Figures 7D**,**E**). When the number of each bacterial strain in plants was measured 4 days post-inoculation, we found that the number of N1141 cells increased by about three times compared with the number of inoculated cells. In contrast, the number of bacteria decreased in finger millet inoculated with *NΔRHIF*, and *NΔRHIFC* proliferated in finger millet to the same level as wild-type N1141. Unexpectedly, RHIF-deficient strain K1 did not appear to proliferate in finger millet (**Figure 7F**). These results indicated that *NRHIF* deficiency decreases strain N1141's infectivity toward finger millet.

DISCUSSION

In this study, we demonstrate that NRHIF identified from the rice-avirulent strain N1141 of *A. avenae* is novel effector that induces ETI including HR cell death in rice. In contrast, KRHIF from rice-virulent strain K1 functions as an ETI inducer in the non-host plant finger millet. Finally, we show that inoculation of rice and finger millet with either RHIF-deficient N1141 or K1 strains showed that a deficiency of *RHIF* genes in both strains results in decreased infectivity toward each host plants. To clarify that NRHIF and KRHIF play different roles for each host plant, the *NRHIF* and *KRHIF* genes-swapping mutants are useful. Therefore, we generate two swapping mutants; *KRHIF*/*NΔRHIF* strain in which *KRHIF* was introduced into *NΔRHIF* genome, *NRHIF*/*KΔRHIF* strain in which *NRHIF* was introduced into *KΔRHIF* genome. However, ETI induction ability and infectivity of each swapping mutant could not be evaluated because poor growth of the mutants, decreased expression and instability of RHIFs were observed in each swapping mutants. We conclude that NRHIF and KRHIF play different roles for each host or non-host plant from the collective of these experimental data.

The P-loop NTPase domain is common to both NRHIF and KRHIF. The P-loop NTPase domain is the most prevalent domain among bacterial and eukaryotic proteins (Leipe et al., 2003). While there is some variety in the enzyme-catalyzed reaction of the P-loop NTPase, the most common one is the hydrolysis of the β–γ phosphate bond of a bound nucleoside triphosphate (Arya and Acharya, 2018). The P-loop NTPase domain of NRHIF and KRHIF has high sequence homology with the P-loop NTPase domain of tRNA isopentenyltransferase that catalyzes the addition of the 5-carbon isopentenyl moiety to the exocyclic amine of adenine 37 located outside the anticodon using dimethylallyl pyrophosphate (DMAPP; Sakamoto et al., 2006). Detailed studies have been conducted on the structure–activity relationship of the *MiaA* encoded tRNA isopentenyltransferase. Gln166, which is present in the P-loop of MiaA, is conservatively replaced by bulky charged residues, while Arg167 is strictly conserved between species (Soderberg and Poulter, 2001). Substitution of Arg167 with Ala resulted in a significant reduction in catalytic efficiency, with K_m increased by 20 times for RNA and nearly 10 times for DMAPP compared to wild-type (Chimnaronk et al., 2009). The conservation of Glu187 and Arg188 within the P-loop NTPase domain of RHIFs indicates that the P-loop NTPase domain of RHIF retains its enzymatic activity. The P-loop NTPase domain is involved in a variety of complex biological processes, including programmed cell death, disease, and immune responses in plants and animals through its own enzymatic activity (Leipe et al., 2004). NRHIF and KRHIF caused ETI responses, including HR cell death in non-host plants. The 13 amino acid differences between NRHIF and KRHIF are also located outside the P-loop NTPase. Therefore, it is highly likely that the pleiotropic effects, including ETI responses and the development of symptoms triggered by KRHIF and NRHIF in host and non-host plants, are caused by the enzymatic activity of their P-loop NTPase domain.

The functional dualities of KRHIF and NRHIF may be due to the presence of specific *R*-like genes corresponding to KRHIF and NRHIF. Since there is an R-like protein corresponding to NRHIF in rice and a different R-like protein corresponding to KRHIF in finger millet, KRHIF and NRHIF induce different biological reactions in rice and finger millet. The specific correspondence between each RHIF and an appropriate R-like protein is likely defined by a 13 amino acid difference between the both RHIFs. Furthermore, these different amino acids also need to abolish the development of symptoms mediated by the P-loop NTPase activity of RHIF isolated from avirulent strains.

Recognition of its corresponding effector by an R protein initiates a defense signaling cascade that results in ETI, including HR cell death (Arya and Acharya, 2018). Many R proteins expressed by plants belong to the nucleotide-binding and leucine-rich repeat protein family (NB-LRR). The NB-LRR class of R proteins can be further divided into two groups based on whether

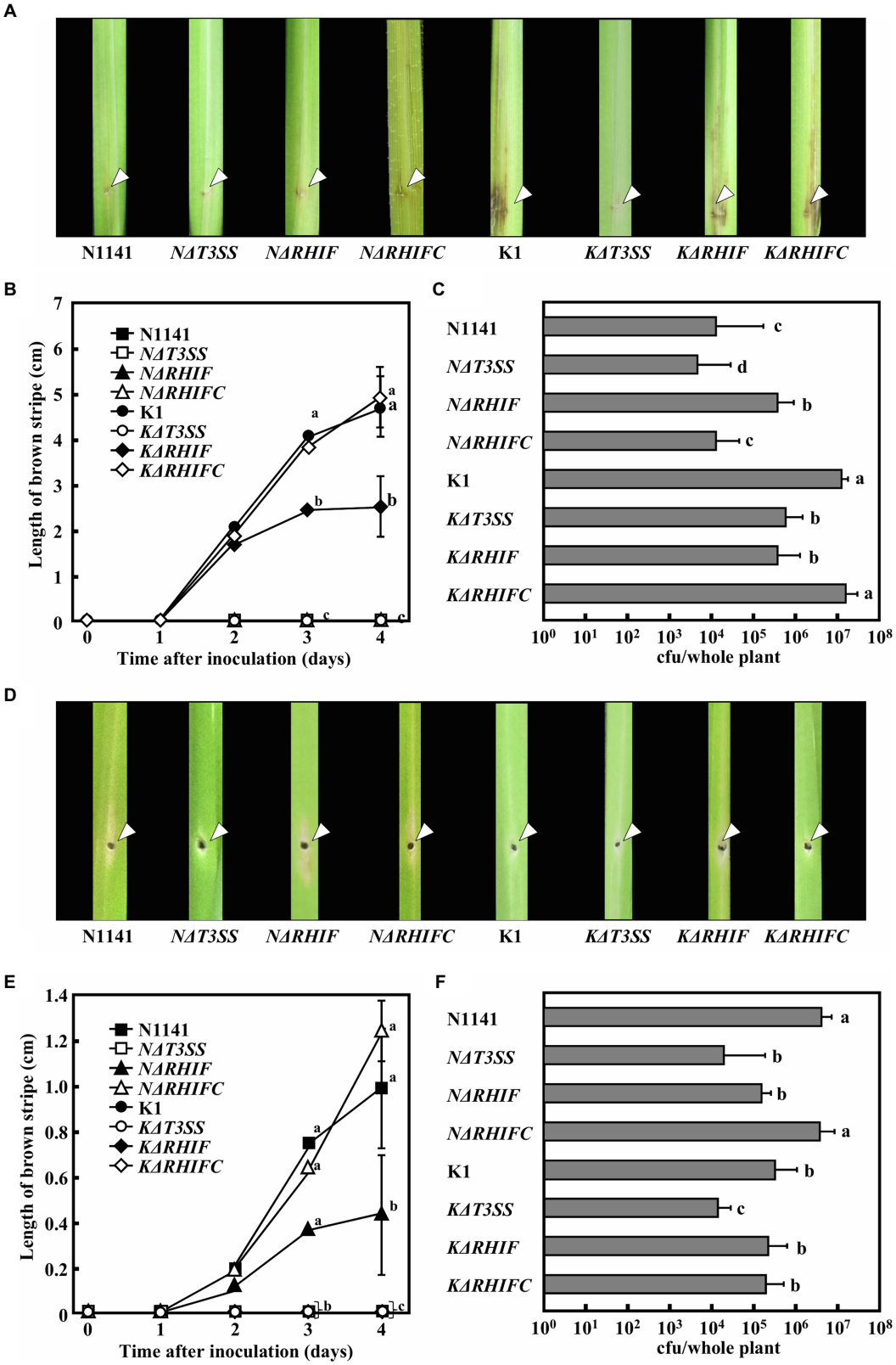

FIGURE 7 | Inoculation tests of N1141, *NΔT3SS*, *NΔRHIF*, *NΔRHIFC*, K1, *KΔT3SS*, *KΔRHIF*, and *KΔRHIFC*. **(A)** Photographs of rice inoculated with each strain. Each strain was inoculated into rice using the single-needle method, and symptoms were observed 4 days later. The arrow indicates the inoculation points.

(*Continued*)

FIGURE 7 | (B) Length of brown stripe symptoms in N1141 (solid square)-, *NΔT3SS* (open square)-, *NΔRHIF* (solid triangle)-, *NΔRHIFC* (open triangle)-, K1 (solid circle)-, *KΔT3SS* (open circle)-, *KΔRHIF* (solid diamond)-, and *KΔRHIFC* (open diamond)-inoculated rices. That time point values without letters indicate no statistical significance. **(C)** Number of bacterial cells in whole rice plants 4 days after inoculation. Error bars indicate the standard deviation of three independent experiments. **(D)** Photographs of finger millet inoculated with each strain. Bacterial strains were inoculated into finger millet using the single-needle method, and symptoms were observed 4 days later. The arrow indicates the inoculation points. **(E)** Length of brown stripe symptoms in N1141 (solid square)-, *NΔT3SS* (open square)-, *NΔRHIF* (solid triangle)-, *NΔRHIFC* (open triangle)-, K1 (solid circle)-, *KΔT3SS* (open circle)-, *KΔRHIF* (solid diamond)-, and *KΔRHIFC* (open diamond)-inoculated finger millets. That time point values without letters indicate no statistical significance. **(F)** Number of bacterial cells in whole finger millet plants 4 days after inoculation. Bars indicate standard deviation of three independent experiments. Error bars in figures represent standard deviation of three independent experiments. Values followed by a different letter in figures were significantly different according to Tukey-Kramer test ($p < 0.05$).

they have a Toll/interleukin-1 receptor domain or a coiled-coil (CC) domain at their N-terminus (Collier and Moffett, 2009). Analysis of various plant genomes, including those of *A. thaliana*, *O. sativa*, *Solanum tuberosum* (potato), *Brassica rapa* (field mustard), and *Brachypodium distachyon* (purple false brome), has demonstrated that the NBS-LRR class of R proteins is among the largest gene families in Kingdom Plantae (Marone et al., 2013; Baggs et al., 2017). The majority of R protein NBS-LRRs, such as *A. thaliana* RPS4 and tobacco N., belong to the apoptotic ATPase family of P-loop NTPases. The accumulation of RHIFs possessing a P-loop NTPase domain in plant cells perturbs signal transduction mediated by the R protein. Such perturbance mediated by the P-loop NTPase likely results in ETI induction and symptom development caused by RHIFs.

Motif analysis using PSORT and cNLS Mapper showed that NRHIF localizes mainly to the cytosol. When NRHIF-Venus was expressed in rice cells, Venus-derived yellow fluorescence was observed in both nucleus and cytosol. Since the predicted molecular mass of NRHIF-Venus is 65 kDa, it can diffuse to a limited extent into the nucleus without a nuclear localization signal (NLS). Since NRHIF lacks an NLS, these results suggest that NRHIF localizes mainly to the cytosol in rice cells. The presence of RHIFs in the cytoplasm is reasonable if the enzymatic addition of the 5-carbon isopentenyl moiety to the extracellular amine of adenine 37 by the RHIF P-loop NTPase domain is responsible for inducing HR cell death and the development of symptoms.

Pathogenic bacteria are known to secrete multiple effectors into plant cells during infection. These effectors are involved in inducing ETI, suppressing PTI, and establishing infection. We previously reported that screening a library of transposon-tagged *A. avenae* K1 strains based on suppression of flagellin-triggered H_2O_2 generation showed that the suppression activity of 156 transposon-tagged K1 mutants was reduced to the same level as that of *KΔT3SS*. Moreover, sequence analysis of regions flanking the transposons revealed that they were inserted into 68 different genes. In addition, multiple proteins were secreted by strains N1141 and K1 using their T3SS (Kondo et al., 2017; Kawaguchi et al., 2021). The presence of multiple effectors in *A. avenae* strains N1141 and K1 raises the question of whether NRHIF and KRHIF are the only ETI-inducible effectors for rice and finger millet, respectively. ETI responses including HR cell death induction and OsNAC4 expression in *NΔRHIF*-inoculated rice cells were reduced to almost the same extent as that in *NΔT3SS*-inoculated rice cells (**Figures 3, 4**). Similar results were observed in finger millet inoculated with either *KΔRHIF* or *KΔT3SS* (**Figure 6**). In addition, our screen employing 6,200 transposon-tagged N1141 mutants covered almost all genes in the genome because the whole-genome sequence of strain N1141 indicates the presence of 4,787 open reading frames. Only RHIF has been identified as an ETI-inducible effector by our transposon-tagged N1141 mutant screen. Taken together, our results suggest that NRHIF is the major effector that causes the ETI responses in rice.

Inoculation tests on rice showed that the growth of strain N1141 was increased by NRHIF deficiency, and that growth was reduced by complementation of *NRHIF* in the *NRHIF*-deficient strain, to the same level as wild-type N1141. Such changes in bacterial growth indicate that NRHIF also functions as an ETI-inducible effector when infecting non-host plants. In contrast, KRHIF-deficient strain K1 did not affect bacterial growth in non-host finger millet. This may be due to differences in the contribution of KRHIF and NRHIF to ETI induction in non-host plants. NRHIF was identified by comprehensive screening of transposon-tagged N1141 mutants while KRHIF was identified based on sequence homology with NRHIF. Therefore, it is unclear whether KRHIF expressed by strain K1 is the only effector involved in ETI induction of finger millet. Multiple effectors apart from KRHIF may be involved in recognizing strain K1 and ETI induction by finger millet. Identification of ETI inducers apart from KRHIF in strain K1 is important for elucidating the molecular mechanism underlying the narrow host range of *A. avenae*.

DATA AVAILABILITY STATEMENT

The original contributions presented in the study are included in the article/**Supplementary Material**, further inquiries can be directed to the corresponding author.

AUTHOR CONTRIBUTIONS

MN, MK, AS, and F-SC conceived, performed, and designed the experiments. MN, MK, and HH analyzed the data and performed the computational analysis. MN, MK, and F-SC wrote the paper. All authors read and approved the final manuscript.

FUNDING

This work was supported by JSPS KAKENHI grant numbers 19K15843 and 19K15844 and the Private University Research Branding Project, Ministry of Education, Culture, Sports, Science and Technology, Japan.

ACKNOWLEDGMENTS

We are grateful to Yukihiko Nakagawa, Takamasa Kawaguchi Katsuki Yagyu, Tomohiro Norikyo, Hiyori Ueda, and Honoka Oomori for excellent technical support.

SUPPLEMENTARY MATERIAL

The Supplementary Material for this article can be found online at: https://www.frontiersin.org/articles/10.3389/fpls.2021.716738/full#supplementary-material

REFERENCES

Arya, P., and Acharya, V. (2018). Plant STAND P-loop NTPases: a current perspective of genpme distribution, evolution, and function. *Mol. Gen. Genomics* 293, 17–31. doi: 10.1007/s00438-017-1368-3

Asselin, J. A. E., Lin, J., Perez-Quintero, A. L., Gentzel, I., Majerczak, D., Opiyo, S. O., et al. (2015). Perturbation of maize phenylpropanoid metabolism by an AvrE family type III effector from *Pantoea stewartia*. *Plant Physiol.* 167, 1117–1135. doi: 10.1104/pp.114.253120

Baba, A., Hasezawa, S., and Syono, K. (1986). Cultivation of rice protoplasts and their transformation mediated by *Agrobacterium* spheroplasts. *Plant Cell Physiol.* 27, 463–471. doi: 10.1093/oxfordjournals.pcp.a077122

Baggs, E., Dagdas, G., and Krasileva, K. V. (2017). NLR diversity, helpers and integrated domains: making sense of the NLR IDentity. *Curr. Opin. Plant Biol.* 38, 59–67. doi: 10.1016/j.pbi.2017.04.012

Balint-Kurti, P. (2019). The plant hypersensitive response: concepts, control and consequences. *Mol. Plant Pathol.* 20, 1163–1178. doi: 10.1111/mpp.12821

Bi, G., and Zhou, J. M. (2021). Regulation of cell death and signaling by pore-forming resistosomes. *Annu. Rev. Phytopathol.* 59. doi:10.1146/annurev-phyto-020620-095952 [Epub ahead of print]

Block, A., Toruno, T. Y., Elowsky, C. G., Zhang, C., Steinbrenner, J., Beynon, J., et al. (2013). The *Pseudomonas syringae* type III effector HopD1 suppresses effector-triggered immunity, localizes to the endoplasmic reticulum, and targets the Arabidopsis transcription factor NTL9. *New Phytol.* 201, 1358–1370. doi: 10.1111/nph.12626

Buttner, D. (2016). Behind the lines–actions of bacterial type III effector proteins in plant cells. *FEMS Microbiol. Rev.* 40, 894–937. doi: 10.1093/femsre/fuw026

Casper-Lindley, C., Dahlbeck, D., Clark, E. T., and Staskawicz, B. J. (2002). Direct biochemical evidence for type III secretion-dependent translocation of the AvrBs2 effector protein into plant cells. *PNAS* 99, 8336–8341. doi: 10.1073/pnas.122220299

Che, F. S., Iwano, M., Tanaka, N., Takayama, S., Minami, E., Shibuya, N., et al. (1999). Biochemical and morphological features of rice cell death induced by *Pseudomonas avenae*. *Plant Cell Physiol.* 40, 1036–1045. doi: 10.1093/oxfordjournals.pcp.a029485

Che, F. S., Nakajima, Y., Tanaka, N., Iwano, M., Yoshida, T., Takayama, S., et al. (2000). Flagellin from an incompatible strain of *Pseudomonas avenae* induces a resistance response in cultured rice cells. *J. Biol. Chem.* 275, 32347–32356. doi: 10.1074/jbc.M004796200

Chiang, Y. H., and Coaker, G. (2015). Effector triggered immunity: NLR immune perception and downstream defense responses. *BioOne COMPLETE*, e0183. doi: 10.1199/tab.0183

Chimnaronk, S., Forouhar, F., Sakai, J., Yao, M., Tron, C. M., Atta, M., et al. (2009). Snapshots of dynamics in synthesizing N^6-Isopentenyladenosine at the tRNA anticodon. *Biochemistry* 48, 5057–5065. doi: 10.1021/bi900337d

Collier, S. M., and Moffett, P. (2009). NB-LRRs work a "bait and switch" on pathogens. *Trends Plant Sci.* 14, 1360–1383. doi: 10.1016/j.tplants

Cui, H., Tsuda, K., and Parker, J. E. (2015). Effector-triggered immunity: from pathogen perception to robust defense. *Annu. Rev. Plant Biol.* 66, 487–511. doi: 10.1146/annurev-arplant-050213-040012

Cui, F., Wu, S., Sun, W., Coaker, G., Kunkel, B., He, P., et al. (2013). The *Pseudomonas syringae* type III effector AvrRpt2 promotes pathogen virulence via stimulating Arabidopsis auxin/indole acetic acid protein turnover. *Plant Physiol.* 162, 1018–1029. doi: 10.1104/pp.113.219659

Dey, S., Chakravarty, A., Biswas, P. G., and Guzman, R. N. D. (2019). The type III secretion system needle, tip, and translocon. *Protein Sci.* 28, 1582–1593. doi: 10.1002/pro.3682

Ducey, T. F., and Dyer, D. W. (2002). Rapid identification of EZ:TN™ transposon insertion sites in the genome of *Neisseria gonorrhoeae*. *Epicentre Forum* 9, 6–7.

Frantzeskakis, L., Pietro, A. D., Rep, M., Schirawski, J., Wu, C. H., and Panstruga, R. (2019). Rapid evolution in plant–microbe interactions – a molecular genomics perspective. *New Phytol.* 225, 1134–1142. doi: 10.1111/nph.15966

Gimenez-Ibanez, S., Boter, M., Fernandez-Barbero, G., Chini, A., Rathjen, J. P., and Solano, R. (2014). The bacterial effector HopX1 targets JAZ transcriptional repressors to activate jasmonate signaling and promote infection in Arabidopsis. *PLoS Biol.* 12:e1001792. doi: 10.1371/journal.pbio.1001792

Hann, D. R., Dominguez-Ferreras, A., Motyka, V., Dobrev, P. I., Schornack, S., Jehle, A., et al. (2014). The pseudomonas type III effector HopQ1 activates cytokinin signaling and interferes with plant innate immunity. *New Phytol.* 201, 585–598. doi: 10.1111/nph.12544

Ho, F. P., Tan, C. M., Li, M. Y., Lin, H., Deng, W. L., and Yang, J. Y. (2013). The AvrB_AvrC domain of AvrXccC of *Xanthomonas campestris* pv. *Campestris* is required to elicit plant defense responses and manipulate ABA homeostasis. *Mol. Plant-Microbe Interact.* 26, 419–430. doi: 10.1094/MPMI-06-12-0164-R

Hueck, C. G. (1998). Type III protein secretion systems in bacterial pathogens of animals and plants. *Microbiol. Mol. Biol. Rev.* 62, 379–433. doi: 10.1128/MMBR.62.2.379-433.1998

Hurley, B., Lee, D., Mott, A., Wilton, M., Liu, J., Liu, Y. C., et al. (2014). The *Pseudomonas syringae* type III effector HopF2 suppresses Arabidopsis stomatal immunity. *PLoS One* 9:e114921. doi: 10.1371/journal.pone.0114921

Jones, J. D., and Dangl, J. L. (2006). The plant immune system. *Nature* 444, 323–329. doi: 10.1038/nature05286

Jones, J. D., Vance, R. E., and Dangl, J. L. (2016). Intracellular innate immune surveillance devices in plants and animals. *Science* 345:aaf6395. doi: 10.1126/science.aaf6395

Kadota, I., Mizuno, A., and Nishiyama, K. (1996). Detection of a protein specific to the strain of *Pseudomonas avenae* Manns 1909 pathogenic to Rice. *Ann. Phytopathol. Soc. Jpn.* 62, 425–428. doi: 10.3186/jjphytopath.62.425

Kadota, I., Ohuchi, A., and Nishiyama, K. (1991). Serological properties and specificitu of *Pseudomonas avenae* Manns 1909, the causal agent of bacterial brown stripe of rice. *Jpn. J. Phytopathol.* 57, 268–273. doi: 10.3186/jjphytopath.57.268

Kaneda, T., Yaga, Y., Takai, R., Iwano, M., Matsui, H., Takayama, S., et al. (2009). The transcription factor OsNAC4 is a key positive regulator of plant hypersensitive cell death. *EMBO J.* 28, 926–936. doi: 10.1038/emboj.2009.39

Kawaguchi, T., Nakamura, M., Hirai, H., Furukawa, T., Kondo, M., and Che, F. S. (2021). AKSF1 isolated from the rice-virulent strain *Acidovorax avenae* K1 is a novel effector that suppresses PAMP-triggered immunity in rice. *MPMI* 34, 186–197. doi: 10.1094/MPMI-10-20-0271-R

Kondo, M., Hirai, H., Furukawa, T., Yoshida, Y., Suzuki, A., Kawaguchi, T., et al. (2017). Frameshift mutation confers function as virulence factor to leucine-rich repeat protein from *Acidovorax avenae*. *Front. Plant Sci.* 7:1988. doi: 10.3389/fpls.2016.01988

Kondo, M., Yoshida, Y., Miyata, C., Fujiwara, S., Nakajima, Y., Hirai, H., et al. (2012). Genetic organization of the *hrp* gene cluster in *Acidovorax avenae* strain N1141 and a novel effector protein that elicits immune responses in rice (*Oryza sativa* L.). *Biosci. Biotechnol. Biochem.* 76, 129–138. doi: 10.1271/bbb.110597

Laflamme, B., Dillon, M. M., Martel, A., Almeida, R. N. D., Desveaux, D., and Guttman, D. S. (2020). The pan-genome effector-triggered immunity landscape of a host-pathogen interaction. *Science* 367, 763–768. doi: 10.1126/science.aax4079

Leipe, D. D., Koonin, E. V., and Aravind, L. (2003). Evolution and classification of P-loop kinases and related proteins. *J. Mol. Biol.* 333, 781–515. doi: 10.1016/j.jmb.2003.08.040

Leipe, D. D., Koonin, E. V., and Aravind, L. (2004). STAND, a class of p-loop NTPases including animal and plant regulators of programmed cell death: multiple, complex domain architectures, unusual phyletic patterns, and

evolution by horizontal gene transfer. *J. Mol. Biol.* 343, 1–28. doi: 10.1016/j.jmb.2004.08.023

Macho, A. P. (2016). Subversion of plant cellular functions by bacterial type-III effectors: beyond suppression of immunity. *New Phytol.* 210, 51–57. doi: 10.1111/nph.13605

Marois, E., Ackerveken, G. W. D., and Bonas, U. (2002). The xanthomonas type III effector protein AvrBs3 modulates plant gene expression and induces cell hypertrophy in the susceptible host. *Mol. Plant-Microbe Interact.* 15, 637–646. doi: 10.1094/MPMI.2002.15.7.637

Marone, D., Russo, M. A., Laidò, G., De Leonardis, A. M., and Mastrangelo, A. M. (2013). Plant nucleotide binding site-leucine-rich repeat (NBS-LRR) genes: active guardians in host defense responses. *Int. J. Mol. Sci.* 14, 7302–7326. doi: 10.3390/ijms14047302

McCabe, P. F., Levine, A., Meijer, P. J., Tapon, N. A., and Pennell, R. I. (1997). A programmed cell death pathway activated in carrot cells cultured at low cell density. *Plant J.* 12, 267–280. doi: 10.1046/j.1365-313X.1997.12020267.x

Menna, A., Nguyen, D., Guttman, D. S., and Desveaux, D. (2015). Elevated Temperature Differentially Influences Effector-Triggered Immunity Outputs in Arabidopsis. *Front. Plant Sci.* 6:995. doi: 10.3389/fpls.2015.00995

Mur, L. A. L., Kenton, P., Lloyd, A. J., Ougham, H., and Prats, E. (2008). The hypersensitive response; the centenary is upon us but how much do we know? *J. Exp. Bot.* 59, 501–520. doi: 10.1093/jxb/erm239

Noel, L., Thieme, F., Nennstiel, D., and Bonas, U. (2002). Two novel type III-secreted proteins of *Xanthomonas campestris* pv. *Vesicatoria* are encoded within the *hrp* pathogenicity island. *J. Bacteriol.* 184, 1340–1348. doi: 10.1128/JB.184.5.1340-1348.2002

Ootsubo, Y., Hibino, T., Wakazono, T., Mukai, Y., and Che, F. S. (2016). IREN, a novel EF-hand motif-containing nuclease, functions in the degradation of nuclear DNA during the hypersensitive response cell death in rice. *Biosci. Biotechnol. Biochem.* 80, 748–760. doi: 10.1080/09168451.2015.1123610

Ryerson, D. E., and Heath, M. C. (1996). Cleavage of nuclear DNA into oligonuculeosomal fragments during cell death induced by fungal onfection or by abiotic treatments. *Plant Cell* 8, 393–402. doi: 10.2307/3870320

Sakamoto, T., Sakakibara, H., Kojima, M., Yamamoto, Y., Nagasaki, H., Inuki, Y., et al. (2006). Ectopic expression of KNOTTED1-like homeobox protein induces expression of cytokinin biosynthesis genes in rice. *Plant Physiol.* 142, 54–62. doi: 10.1104/pp.106.085811

Saur, I. M. L., Panstruga, R., and Schulze-Lefert, P. (2020). NOD-like receptor-mediated plant immunity: from structure to cell death. *Nat. Rev. Immunol.* 21, 305–318. doi: 10.1038/s41577-020-00473-z

Schechter, L. M., Roberts, K. A., Jamir, Y., Alfano, L. R., and Collmer, A. (2004). *Pseudomonas syringae* type III secretion system targeting signals and novel effectors studied with a Cya translocation reporter. *J. Bacteriol.* 186, 543–555. doi: 10.1128/JB.186.2.543-555.2004

Soderberg, T., and Poulter, C. D. (2001). *Escherichia coli* dimethylallyl diphosphate:tRNA dimethylallyltransferase: site-directed mutagenesis of highly conserved residues. *Biochemistry* 40, 1734–1740. doi: 10.1021/bi002149t

Sory, M. P., and Cornelis, G. R. (1994). Translocation of a hybrid YopE-adenylate cyclase from *Yersinia enterocolitica* into HeLa cells. *Mol. Microbiol.* 14, 583–594. doi: 10.1111/j.1365-2958.1994.tb02191.x

Streubel, J., Pesce, C., Hutin, M., Koebnik, R., Boch, J., and Szurel, B. (2013). Five phylogenetically close rice SWEET genes confer TAL effector-mediated susceptibility to Xanthomonas oryzae pv. oryzae. *New Phytologist.* 200, 808–819. doi: 10.1111/nph.12411

Takai, R., Kaneda, T., Isogai, A., Takayama, S., and Che, F. S. (2007). A new method of defense response analysis using a transient expression system in rice protoplasts. *Biosci. Biotechnol. Biochem.* 71, 590–593. doi: 10.1271/bbb.60526

Torres-Zabala, M. D., Truman, W., Bennett, M., Lafforgue, G., Mansfield, J. W., and Egea, et al., (2007). *Pseudomonas syringae* pv. tomato hijacks the Arabidopsis abscisic acid signalling pathway to cause disease. *EMBO J.* 26, 1434–1443. doi: 10.1038/sj.emboj.7601575

Toruno, T. Y., Stergiopoulos, I., and Coaker, G. (2016). Plant-pathogen effectors: cellular probes interfering with plant defenses in spatial and temporal manners. *Annu. Rev. Phytopathol.* 54, 419–441. doi: 10.1146/annurev-phyto-080615-100204

Vries, S. D., Stukenbrock, E. H., and Rose, L. E. (2020). Rapid evolution in plant–microbe interactions – an evolutionary genomics perspective. *New Phytol.* 226, 1256–1262. doi: 10.1111/nph.16458

Wilson, K. (1987). Preparation of genomic DNA from bacteria. *Curr. Protoc. Mol. Biol.*, 241–245. doi: 10.1002/0471142727.mb0204s56

Zhou, H., Lin, J., Johnson, A., Morgan, R. L., Zhong, W., and Ma, W. (2011). *Pseudomonas syringae* type III effector HopZ1 targets a host enzyme to suppress isoflavone biosynthesis and promote infection in soybean. *Cell Host Microbe* 9, 177–186. doi: 10.1016/j.chom.2011.02.007

Conflict of Interest: The authors declare that the research was conducted in the absence of any commercial or financial relationships that could be construed as a potential conflict of interest.

Publisher's Note: All claims expressed in this article are solely those of the authors and do not necessarily represent those of their affiliated organizations, or those of the publisher, the editors and the reviewers. Any product that may be evaluated in this article, or claim that may be made by its manufacturer, is not guaranteed or endorsed by the publisher.

frontiers in Plant Science

ORIGINAL RESEARCH
published: 11 August 2021
doi: 10.3389/fpls.2021.713870

Induced Resistance by Ascorbate Oxidation Involves Potentiating of the Phenylpropanoid Pathway and Improved Rice Tolerance to Parasitic Nematodes

*Richard Raj Singh[1], Jessil Ann Pajar[1†], Kris Audenaert[2] and Tina Kyndt[1]**

[1]Department of Biotechnology, Faculty of Bioscience Engineering, Ghent University, Ghent, Belgium, [2]Department of Plants and Crops, Ghent University, Ghent, Belgium

OPEN ACCESS

Edited by:
Rachid Lahlali,
Ecole Nationale d'Agriculture de Meknès, Morocco

Reviewed by:
Paola Leonetti,
National Research Council (CNR), Italy
Fouad Mokrini,
National Institute for Agricultural Research, Morocco

***Correspondence:**
Tina Kyndt
tina.kyndt@ugent.be

†Present address:
Jessil Ann Pajar,
International Max Planck Research School,
Max Planck Institute for Chemical Ecology, Jena, Germany

Specialty section:
This article was submitted to Plant Pathogen Interactions, a section of the journal Frontiers in Plant Science

Received: 24 May 2021
Accepted: 08 July 2021
Published: 11 August 2021

Citation:
Singh RR, Pajar JA, Audenaert K and Kyndt T (2021) Induced Resistance by Ascorbate Oxidation Involves Potentiating of the Phenylpropanoid Pathway and Improved Rice Tolerance to Parasitic Nematodes. Front. Plant Sci. 12:713870. doi: 10.3389/fpls.2021.713870

Anticipating an increased ecological awareness, scientists have been exploring new strategies to reduce the use of chemical pesticides to control pests and diseases. Triggering the intrinsic plant defense system is one of the promising strategies to reduce yield loss by pathogenic organisms, such as nematodes. Ascorbate oxidase (AO) enzyme plays an important role in plant defense by regulating the apoplastic ascorbate/dehydroascorbate (DHA) ratio *via* the ascorbate oxidation process. Ascorbate oxidation is known to induce systemic resistance in rice against parasitic root-knot nematodes (RKN). Here, we sought to evaluate if AO- or DHA-induced resistance (IR) against RKN *M. graminicola* involves activation of the phenylpropanoid pathway and whether this IR phenotype has potential effects on growth of rice seedlings under stressed and unstressed conditions. Our results show that AO/DHA-IR against these parasitic nematodes is dependent on activation of phenylalanine ammonia lyase (PAL). However, application of reduced ascorbic acid (AA) did not induce this response. Gene expression analysis *via* qRT-PCR showed that *OsPAL2* and *OsPAL4* are highly expressed in AO/DHA-sprayed nematode-infected roots and PAL-activity measurements confirmed that AO/DHA spraying triggers the plants for primed activation of this enzyme upon nematode infection. AO/DHA-IR is not effective in plants sprayed with a chemical PAL inhibitor confirming that AO/DHA-induced resistance is dependent on PAL activity. Improved plant growth and low nematode infection in AO/DHA-sprayed plants was found to be correlated with an increase in shoot chlorophyll fluorescence (Fv/Fm), chlorophyll index (CHlIdx), and modified anthocyanin reflection index which were proven to be good above-ground parameters for nematode infestation. A detailed growth analysis confirmed the improved growth of AO/DHA-treated plants under nematode-infected conditions. Taken together, our results indicate that ascorbate oxidation enhances the phenylpropanoid-based response to nematode infection and leads to a tolerance phenotype in treated rice plants.

Keywords: tolerance, priming, phenotyping, *Oryza sativa*, *Meloidogyne graminicola*, phenylalanine ammonia lyase

INTRODUCTION

Rice (*Oryza sativa* L.) is one of the world's most valuable agricultural commodities, a staple food for half of the global population, and an important model plant for the study of the interaction between a monocotyledonous plant and plant parasitic nematodes at molecular and physiological level (De Waele and Elsen, 2007; Kyndt et al., 2014). Root-knot nematode (RKN) *Meloidogyne graminicola* is an obligate endo-parasitic root pathogen (Mantelin et al., 2017), with significant detrimental effects on rice (Bridge et al., 2005; De Waele and Elsen, 2007). *M. graminicola* is dominant in rainfed and lowland (irrigated) rice, as well as in deep-water ecosystems (Prot and Rahman, 1994). It is known to cause substantial yield losses in all the rice growing belts of southeast Asia (Rao and Biswas, 1973; Kumari et al., 2016). An estimated yield loss caused by this nematode can be up to 87% of production (Plowright and Bridge, 1990; Netscher, 1993). *M. graminicola* has a short life cycle when compared with other RKN species: 19–27 days at temperatures of 22–29°C (Bridge and Page, 1982). Its short life cycle and wide host range make this species difficult to control (De Waele and Elsen, 2007). The infective second-stage juvenile (J2) penetrates the rice root in the elongation zone, migrates to the vascular tissue, and forms a feeding site, consisting of 3–8 giant cells (Kyndt et al., 2014). These giant cells function as a specialized sink, supplying nutrients to the nematode for its development and reproduction (Caillaud et al., 2008). Female nematodes will develop within 14 days after infection, after which they start to lay eggs (Kyndt et al., 2014). The females lay hundreds of eggs in a protective gelatinous matrix, forming an egg mass. *M. graminicola* females lay eggs in the root cortex embedded in galls while in other RKN species egg masses are found on the root surface (Kyndt et al., 2014; Escobar et al., 2015). Hyperplasia and hypertrophy of the surrounding cells lead to the development of root knots (galls) and hooked root tips, typical root symptoms induced by *M. graminicola* infection (Bridge et al., 2005; Karssen et al., 2006; Karssen and Moens, 2006; Kyndt et al., 2014). This gall formation disturbs normal root physiological functions, such as water and nutrient transport, ultimately causing chlorosis and stunted growth and observable patchy growth in rice fields (Bridge and Page, 1982).

Induced resistance (IR) is an enhanced plant disease resistance phenotype in response to stimulation by a pathogen, insect herbivory, wounding, a beneficial microbe, or by exogenous application of natural or synthetic compounds (Conrath, 2006; Bektas and Eulgem, 2015; Conrath et al., 2015). IR can work through direct activation of plant defense even without pathogen challenge and/or it can work *via* defense priming whereby some genes, enzymes, or pathways are only activated when the plant is challenged by a pathogen (De Kesel et al., 2021). Upon this challenge, the plant effectively mounts a faster and/or stronger defense response resulting in reduced disease and/or stress tolerance (Mauch-Mani et al., 2017). However, potential changes in plant development and plant growth should be monitored upon IR activation, as excessive activation of plant defense can have fitness costs (van Hulten et al., 2006; Wu et al., 2010; Koen et al., 2014; Luna et al., 2014, 2020; Cohen et al., 2016; Yassin et al., 2021).

Compounds, such as beta-aminobutyric acid (BABA; Ji et al., 2015), thiamine (Huang et al., 2016), silicon (Zhan et al., 2018), methyl jasmonate (MeJA), ethephon (Eth), the salicylic acid (SA) analogue benzothiadiazole BTH (Nahar et al., 2011), COS-OGA (Singh et al., 2019), and ascorbic acid (AA, vitamin C; Arrigoni et al., 1979; Al-Sayed and Thomason, 1988; Osman, 1993; Hamada et al., 2000; Osman et al., 2013), are known to induce resistance against RKN. AA is a water-soluble compound and the most abundant antioxidant in plants (Smirnoff, 2018; Foyer et al., 2020). The redox status of total AA in the apoplast, regulated by ascorbate oxidase (AO; Pignocchi and Foyer, 2003; Foyer and Noctor, 2005; Fotopoulos and Kanellis, 2013), is known to influence plant growth. This is mediated by effect on hormone pathways, antioxidant enzyme activities, mitogen-activated protein kinase (MAPK) activity, and calcium channels (Pignocchi and Foyer, 2003). AO catalyzes oxidation of AA to the unstable radical monodehydroascorbate (MDHA) and subsequently to DHA in the apoplast. DHA is then transported to the symplast and reduced back to AA through the symplastic AA–glutathione (AA–GSH) cycle (Horemans et al., 2000), which includes among others dehydroascorbate reductases (Smirnoff, 2000; Smirnoff and Wheeler, 2000).

Secondary metabolites play an important role in plant defense against parasitic nematodes (Desmedt et al., 2020). One of the best-known secondary metabolic pathways in plants is the phenylpropanoid pathway. Phenylpropanoids are derived from cinnamic acid, which is formed from phenylalanine (Vogt, 2010). The phenylpropanoid pathway is constituted of a complex series of branching biochemical pathways. This plant-specific pathway produces a variety of compounds, including structural cell wall components (lignin, suberin, and other cell wall-associated phenolics), antioxidants (flavonoids and anthocyanins), immunity signals (SA), and toxins (coumarins and furanocoumarins; Dixon et al., 2002; Vogt, 2010; Lefevere et al., 2020). The first step in the phenylpropanoid pathway, where phenylalanine ammonia lyase (PAL) catalyzes the conversion of phenylalanine to trans-cinnamate, is important in the transition between primary and secondary metabolism (Hahlbrock and Scheel, 1989; Dixon and Paiva, 1995; Huang et al., 2010; Vogt, 2010). The expression of the *PAL* gene responds to biotic and abiotic stresses, such as pathogens, UV irradiation, and low temperature (Dixon and Paiva, 1995; MacDonald and D'Cunha, 2007). PAL can be induced by wounding and insect herbivory, pathogen infection, and abiotic stresses (Hahlbrock and Scheel, 1989; Dixon and Paiva, 1995), as well as by jasmonate (Taheri and Tarighi, 2010, 2011).

In previous research (Singh et al., 2020b), we have shown that ascorbate oxidation by exogenous application of AO induces rice defense against *M. graminicola*. The process involves systemic activation of the ethylene/jasmonate pathway coupled with high H_2O_2 accumulation upon nematode infection. We also confirmed that exogenous application of the product of AO, namely, DHA, gives a similar IR phenotype. This uncovered a previously unknown role for ascorbate oxidation in activation of systemic resistance pathways against nematodes. In this research, we sought

to evaluate whether IR induced by ascorbate oxidation involves activation of the phenylpropanoid pathway and whether this IR phenotype has plant growth effects. After confirmation of the DHA and AO-IR phenotype against RKN in rice, we analyzed the expression of *OsPAL2* and *OsPAL4* and quantified PAL activity in the shoots and roots of DHA/AO-treated plants, both under uninfected and nematode-infected conditions. Then, we manipulated PAL levels by treating plants with the PAL inhibitor, L-2-aminooxy-3-phenylpropanoic acid (AOPP) and analyzed the susceptibility of rice plants to nematodes. To study the morphological and physiological consequences of the AO/DHA application, a state-of-the-art high-throughput sensor-to-plant phenotyping platform (automated phenotyping platform, APP) was used. We used image analysis to quantify the changes in plant physiology of rice upon AO/DHA application, with and without nematode infection. Finally, the growth of AO- or DHA-treated rice plants was monitored to evaluate potential trade-off effects of the IR phenotype.

MATERIALS AND METHODS

Plant Material and Growth Conditions

Rice (*Oryza sativa* subsp. *japonica*) seeds of cultivar Nipponbare were provided by the US Department of Agriculture (GSOR-100). Germination was set by placing seeds on wet filter paper in a petri dish, which was then incubated at 30°C for 4 days. Thereafter, the seedlings were transplanted in polyvinyl-chloride tubes (one seedling per tube) containing a mixture of sterilized fine sand and synthetic absorbent polymer (SAP) substrate (Nahar et al., 2011; Huang et al., 2016). Rice seedlings were further kept in a growth room at 26°C, 12 h/12 h light regime (150 μmol/m^{2}s) and relative humidity of 70–75%. The plants were fertilized by giving 10 ml of Hoagland solution three times a week.

Plant Treatments

The following chemicals with respective concentrations were used as: reduced ascorbic acid (AA; Sigma-Aldrich, Missouri, United States) at 20 mM (Singh et al., 2020b), ascorbate oxidase (AO; Sigma-Aldrich, Missouri, United States) at 20 U/ml (Singh et al., 2020b), dehydroascorbic acid (DHA, Sigma-Aldrich, Missouri, United States) at 20 mM (Singh et al., 2020b), methyl jasmonate (MeJA, Sigma-Aldrich) at 100 μM (Nahar et al., 2011), and AOPP, an inhibitor of PAL activity, at 100 μM (Ji et al., 2015; Khanam et al., 2018). These concentrations have been optimized in the previous publications with chemical concentrations tested for bio-efficacy and lack of phytotoxicity. AOPP was dissolved in 1 ml of EtOH before diluting further in water. All other chemicals were dissolved in water. To allow efficient uptake, all solutions were supplemented with 0.02% (v/v) of Tween20 (Nahar et al., 2011) and were then administered *via* foliar spraying using Fantasea spray bottles (Jojoli, Netherlands). This allows spraying a fine mist without clogging. In each experiment, 14-day-old plants were sprayed with 6.25 ml of solution until runoff. Foliar spraying was done 24 h prior to nematode or mock inoculation. Plants in the control group were mock sprayed with distilled water containing 0.02% (v/v) of Tween20.

Nematode Inoculation and Analysis of Nematode Infection

A pure culture of *M. graminicola* originating from the Philippines (kindly provided by Prof. D. De Waele, Catholic University, Leuven, Belgium) was maintained on *O. sativa* cv. Nipponbare plants grown in potting soil under conditions similar to the experimental plants, as described earlier. After 3 months of infection, second-stage juveniles (J2) were extracted following the modified Baermann funnel method (Bridge et al., 2005) and were used as inoculum. The roots of rice host plants were washed thoroughly under running water. The roots consisting of galls were finely chopped (5 mm). The *M. graminicola* J2 suspension was collected 48 h after the extraction and was concentrated using centrifugation for 10 min at 1,500 rpm at room temperature. One day after treatment, 15-day-old plants were inoculated with approximately (≈)250 J2 of *M. graminicola* or mock inoculated with water. Plant susceptibility was evaluated at 14 days after inoculation (dai) by counting the number of galls. In addition, nematode reproduction was assessed by counting the number of egg-laying females (ELFs) per plant. To count the number of galls and ELFs, the plant roots were soaked in a boiling acid fuchsin solution for 3 min (0.8% acetic acid and 0.013% acid fuchsin; Nahar et al., 2011). Roots were then rinsed with running tap water to remove excess acid fuchsin and destained in acid glycerol. Galls and ELFs were counted using a stereomicroscope. All nematode infection experiments were repeated at least twice, each time including eight plants per treatment. The experimental timeline for spraying, nematode inoculation, and evaluating nematode susceptibility is shown in **Supplementary Figure 1A**.

Evaluation of Physiological Effects of DHA- and AO-Induced Resistance

To evaluate direct activation and/or a primed defense response, we set up a multifactorial experiment including eight groups of plants: (1) naïve plants uninfected (Ctrl), (2) naïve infected plants, (3) AA-sprayed uninfected, (4) AA-sprayed infected, (5) AO-sprayed uninfected, (6) AO-sprayed infected, (7) DHA-sprayed uninfected, and (8) DHA-sprayed infected plants. In all cases, 14-day-old plants were sprayed with chemicals or mock sprayed with water including 0.02% Tween20. Twenty-four hours later, plants were either mock inoculated or inoculated with ≈250 J2 nematodes. Evaluation of different parameters (see below) was done at 3 dai. The experimental timeline for spraying, nematode inoculation, and evaluation of different parameters (sampling) is shown in **Supplementary Figure 1B**.

PAL-Activity Measurement

Four biological replicates per treatment were sampled, with each biological replicate containing samples/tissues from 4–5

plants. Samples included galls, root tips (of uninfected plants), and complete shoots of infected or uninfected plants. After immediate freezing in liquid nitrogen (N_2) and grinding PAL activity was measured according to Camacho-Cristóbal et al. (2002). One hundred mg of each sample was dissolved in 800 µl of 50 mm sodium phosphate buffer containing 2% (w/v) poly-vinylpolypyrrolidone, 2 mm EDTA, 18 mm-mercaptoethanol, and 0.1% (v/v) Triton X-100. The homogenate was centrifuged at 8,000 rpm, at 4°C for 10 min. One hundred and thirty-five µl of reaction buffer was mixed with 50 µl of 5 mm of L-phenylalanine, and 20 µl of supernatant in separate tubes, after which absorbance was measured at 290 nm. Subsequently, the sample was incubated for 30 min at 40°C in a water bath, after which 10 µl of hydrochloric acid was added and mixed for 10 min. PAL activity was assayed by measuring the formation of trans-cinnamic acid at 290 nm, where 1 unit (U) of PAL activity is the amount of enzyme that produced 1 nmol trans-cinnamic acid per hour. Negative control reactions had no L-phenylalanine as substrate.

qRT-PCR

RNA was extracted using the Plant RNeasy Plant Mini kit (Qiagen) following the manufacturer's instructions. For each treatment, three biological replicates were sampled and analyzed, each consisting of a pool of root or shoot tissue of at least 4–5 plants per treatment. qRT-PCR was performed and analyzed as described in Huang et al. (2015), using normalization based on three reference genes, *OsEIF5C* (LOC_Os11g21990), *OsEXP* (LOC_Os03g27010), and *OsEXPNarcai* (LOC_Os07g02340). Primer pairs for *OsPAL2* and *OsPAL4* are described in Tonnessen et al. (2015) and for the reference genes in Huang et al. (2015).

Spectral Phenotyping and Image Analysis

The morphological and physiological changes in rice leaves were monitored using an APP, which visualizes diverse physiological traits in real time, based on specific absorption, reflection, and fluorescence patterns in visible and near-infrared (NIR) wavelengths. The platform consists of a 3CCD 6 Mp—16 bit camera mounted on a Cartesian coordinate robot, equipped with 12 optical interference filters (CropReporter, PhenoVation B.V., Wageningen, Netherlands). A total of five plants per treatment were monitored. The camera captured following images: RGB (red green blue) images, reflectance spectra to calculate the anthocyanin index and chlorophyll index (ChlIdx) and the minimal fluorescence, F_0, and the maximum fluorescence, F_m. Images were processed *via* the "Data Analysis Software" program (PhenoVation B.V., Wageningen, Netherlands).

The modified anthocyanin reflectance index (mARI) was calculated using following formula (Gitelson et al., 2009):

$$\mathrm{mARI} = \left(\frac{1}{\rho_{550\mathrm{nm}}} - \frac{1}{\rho_{710\mathrm{nm}}} \right) \rho_{770nm}$$

The ChlIdx was determined using following formula (Gitelson et al., 2009):

$$\mathrm{ChlIdx} = \left(\frac{\rho_{770nm}}{\rho_{710\mathrm{nm}}} - 1 \right)$$

where ρ_{550} is the reflectance in the first spectral band, which is maximally sensitive to anthocyanin content; ρ_{710} the reflectance in the second spectral band, which is maximally sensitive to chlorophyll content but not sensitive to anthocyanin content; and ρ_{770} the reflectance of the third spectral band, which compensates for leaf thickness and density.

The maximum quantum efficiency of photosystem II (F_v/F_m) was calculated using the formula of Baker (2008):

$$F_v / F_m = \left(F_m - F_0\right) / F_m$$

Before measurement, the plants were placed in the dark for 30 min to allow for dark adaptation of the leaves to maximally oxidize primary quinone acceptor QA. The minimal (F0) and maximal fluorescence (Fm) were quantified based on the OJIP induction curve according to the manufacturers specifications (Björkman and Demmig, 1987).

Evaluation of Growth Parameters of Treated Plants Under Nematode-Infected and Uninfected Conditions

The assessment of plant growth rate upon application of a plant protection product is an essential element in its efficacy evaluation (Kalamarakis and Markellou, 2007). To evaluate the plant growth rate in response to AA, AO, or DHA treatment and this under unstressed or nematode-uninfected conditions, a multifactorial experiment with eight groups of plants (see above) was set up and evaluation was done at different time points. Seed germination and growth in SAP were performed as described above. The shoot height of the 14-days old plants was recorded, after which rice plants were sprayed with the respective chemicals or mock sprayed with water as explained above. One day (24 h) after the treatment, the rice plants were inoculated with *M. graminicola* J2s (Mg^+) or mock inoculated with water (Mg^-). To evaluate the shoot growth rate, shoot height was measured at three time points 18, 22, and 26 days old on the same group of plants. To assess root growth, however, three independent groups of plants had to be set-up for end-point evaluation of root length, each at another time point (18, 22, or 26 days old). This was required because the trauma by uprooting from the substrate causes plant damage, potentially preventing re-establishment and affecting the plant growth rate. For all experiments, eight plants were used per treatment and all experiments were three times independently repeated. The shoot height and root length was measured with a ruler, taking the distance between the soil surface and the root apical meristem or the longest leaf of the plant.

RESULTS

Foliar Spraying With AO and DHA Induces Systemic Resistance in Rice Roots Against *M. graminicola* Infection and Promotes Growth

Previously, we evaluated the effect of the compounds (AA, AO, and DHA) on the number of galls and number of

nematodes and a significantly lower number of galls and nematodes was observed in rice plants sprayed with AO or with DHA, but not with AA (Singh et al., 2020b). Here, the effect of foliar AA, AO, or DHA treatment on rice plants was independently confirmed by counting the number of galls and extended by counting the total number of egg-laying females (ELFs). Reproduction capacity of a nematode is indicated by the number of ELFs and resistant plants support low or no nematode reproduction (Cook, 1987; Roberts, 2002). Foliar application of AO and DHA on rice plants significantly reduced the number of galls recorded at 14 days after inoculation (dai; 76 and 74% reduction, respectively; **Figure 1A, Supplementary Figure 1C**) when compared with mock-sprayed plants, confirming our previous results (Singh et al., 2020b). Furthermore, spraying with AO and DHA also reduced the number of ELFs (87 and 80% reduction, respectively; **Figure 1B, Supplementary Figure 1C**). Spraying with AA did not cause any significant changes in the number of galls (**Figure 1A**) or ELFs (**Figure 1B**). Application of positive control methyl jasmonate (MeJA) also significantly reduced gall and ELF development, consistent with the data shown before (Nahar et al., 2011; Verbeek et al., 2019).

To evaluate potential fitness costs of this IR phenotype, different plant growth parameters were compared between AA/AO/DHA-sprayed and mock-sprayed plants at the end of this experiment (14 dai). Foliar application of AO and DHA resulted in a significant increase (19 and 20%, respectively) in shoot height and root length (25 and 44%) and fresh root weight (34 and 49%) in comparison with that of mock-sprayed plants (**Supplementary Figures 2A–D**). No effect of AA on plant growth (shoot height, root length, and root weight) was observed (**Supplementary Figure 2**). These results reveal that AA, AO, and DHA pose no negative effects on plant growth and apparent morphology at 15 days after treatment. In fact, pre-treatment with 20 U/ml AO or 20 mm of DHA seemed to improve the shoot and root growth of plants compared to that of mock-sprayed and AA-sprayed plants.

AO/DHA-Induced Resistance Against Nematodes Is Dependent on Activation of PAL

To investigate whether the low *M. graminicola* susceptibility in AO- and DHA-sprayed rice plants was due to alterations in the phenylpropanoid pathway, 14-day-old rice plants were sprayed with AO or DHA or mock-sprayed. After 24 h, a subset of plants was inoculated with nematodes (Mg^{+}) while another subset was mock inoculated with water (Mg^{-}). We quantified the expression of Os*PAL2* and *OsPAL4* and measured the PAL activity at 3 days after inoculation, which corresponds with 4 days after spraying. Analyses were done on shoots of infected and non-infected plants as well as on galls versus root tips for uninfected plants. Our qRT-PCR analyses show that both *OsPAL2* and *OsPAL4* are significantly downregulated in the shoots of DHA-sprayed uninfected plants when compared with uninfected untreated plants (**Figure 1C**). However, in the root tissues, the expression of the *OsPAL4* gene was significantly induced upon DHA spraying (**Figure 1D**). Interestingly in the nematode-induced galls, significantly higher expression levels of *OsPAL2* and *OsPAL4* genes were observed in both AO as well as DHA-sprayed plants when compared with mock-sprayed uninfected or infected plants (**Figure 1D**).

PAL-activity measurements confirmed its enzymatic activation. Data show significant increase (~32%) in PAL activity in the shoots of AO/DHA-sprayed plants when compared with mock-sprayed plants, regardless of the infection (**Figure 1E**). Moreover, in galls of AO/DHA-sprayed plants, a significant increase in PAL activity was observed when compared with uninfected root tips of AO/DHA-sprayed plants (**Figure 1F**), suggesting that AO/DHA spraying triggers the plants for primed PAL activity in galls upon nematode infection.

To confirm the involvement of PAL activity in AO/DHA-induced resistance, an independent infection experiment was carried out using foliar application of a chemical PAL inhibitor AOPP. When chemically blocking this enzyme, no significant differences were observed in number of galls (**Figure 1G**) or number of ELFs (**Figure 1H**), confirming previous observations (Ji et al., 2015). Our data again show a significantly reduced number of galls (**Figure 1G**) and ELFs (**Figure 1H**) in AO/DHA-sprayed plants (reduction of 50–70%) when compared with mock-sprayed (Ctrl) plants. Plants sprayed with AO or DHA combined with AOPP, however, show enhanced *M. graminicola* susceptibility, to a level of severity observed in mock-sprayed (Ctrl) plants, suggesting that AO/DHA-induced resistance is dependent on PAL activity.

Improved Growth and Low Nematode Infection in AO/DHA-Sprayed Plants Is Correlated With Increases in Shoot Fv/Fm, Chlidx, and mARI

A positive effect of AO/DHA on growth of rice shoots and roots, amid low nematode susceptibility was observed in **Supplementary Figure 2**. Therefore, in the next experiment, the physiological response of treated plants with or without nematode infection was monitored in detail. Using image-based assessments, we investigated the potential changes in chlorophyll fluorescence imaging (Fv/Fm), ChlIdx, and modified anthocyanin index (mARI). As done before, 14-day-old plants were sprayed and 1 day later, plants were either inoculated with nematodes or mock inoculated. Three days after inoculation, corresponding to 4 days after spraying, the leaves of the plants were monitored using APP. A significantly higher mARI value was generally observed in the shoots of nematode-infected plants when compared with uninfected plants, regardless of the treatment (**Figure 2A**). Our data further reveal significantly increased mARI values in DHA-sprayed plants upon nematode challenge, when compared with all other treatments (**Figure 2A**). Looking at the Fv/Fm, the values significantly decreased in shoots of nematode-infected plants when compared with shoots of uninfected plants, but only when plants were mock sprayed or sprayed with AA (**Figure 2B**). In contrary, the Fv/Fm values

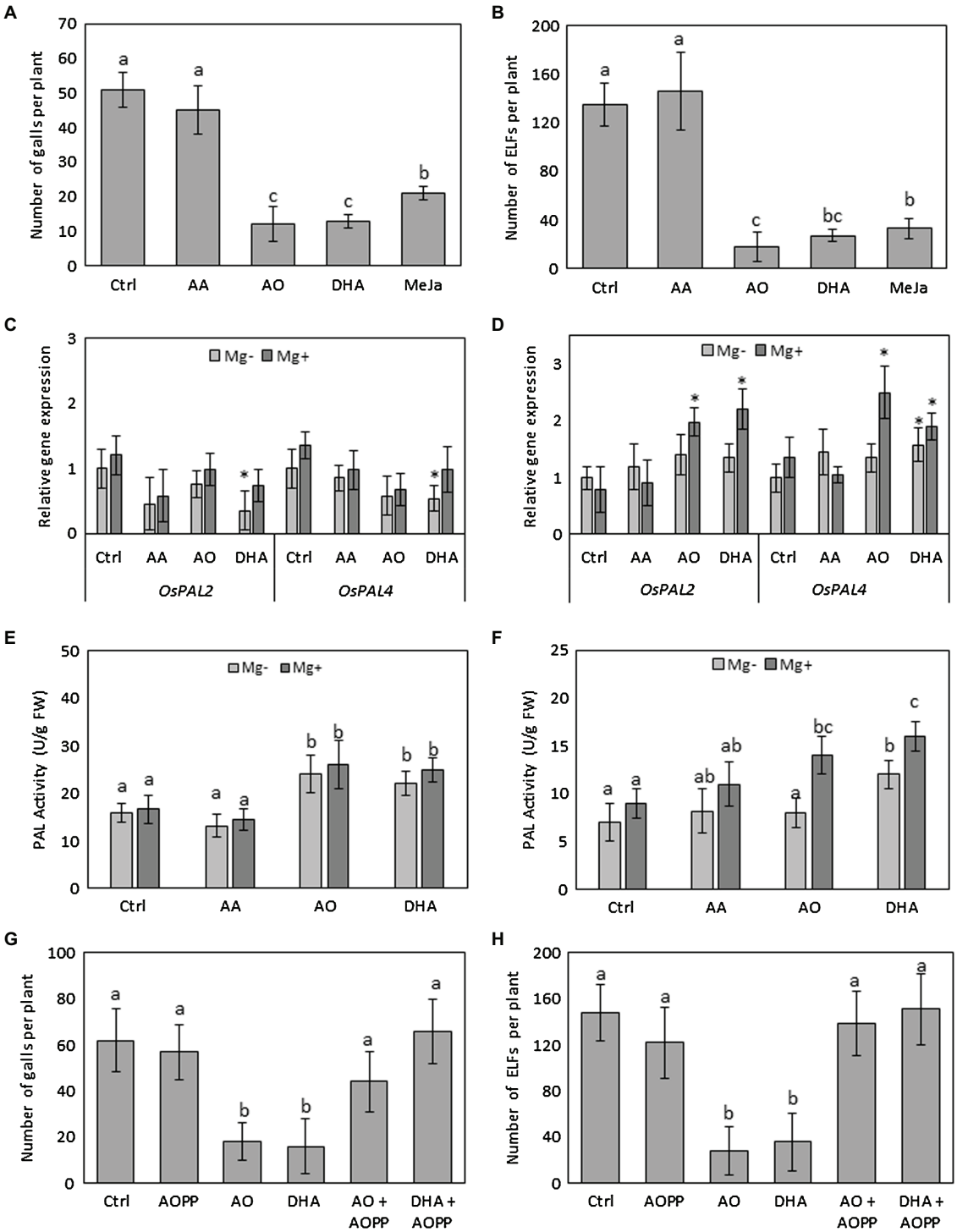

FIGURE 1 | Foliar spraying with AO and DHA induces systemic resistance in rice roots against *M. graminicola* through activation of PAL. Fourteen-day-old wild-type Nipponbare rice plants were sprayed with 20 mm of AA, 20 ml/unit of AO, and 20 mm of DHA or mock sprayed (Ctrl). After 24 h, plants from each treatment were inoculated with ≈250 s-stage juveniles of *M. graminicola* per plant. Total number of **(A)** galls and **(B)** egg-laying females (ELF) at 14 dai. **(C,D)** relative expression levels of phenylalanine ammonia lyase genes in shoot and root tissue at 3dai ($n = 3$). **(E,F)** PAL enzyme activity in shoots or nematode-induced galls of infected and uninfected plants at 3 dai ($n = 4$). **(G,H)** total numbers of galls and ELFs in L-2-aminooxy-3-phenylpropanoic acid (AOPP)-sprayed plants with and without DHA or AO treatment. For nematode infection experiments **(A,B, G,H)**, data represent mean ±SD ($n = 8$) and data were analyzed by student *t-test* at $p \leq 0.05$. For **C,D**, gene expression levels were normalized using three internal reference genes *OsEIF5C*, *OsEXP*, and *OsEXPNarcai*. Data are shown as relative transcript levels in comparison with the control plants (expression level set at 1). In c and d asterisks indicate significant differential expression between AO-treated and control plants (REST-analysis; $\alpha = 0.05$). For **E,F**, data were analyzed by one-way ANOVA followed by Tukey's *post-hoc* test. Different letters indicate statistically different means at $p \leq 0.05$.

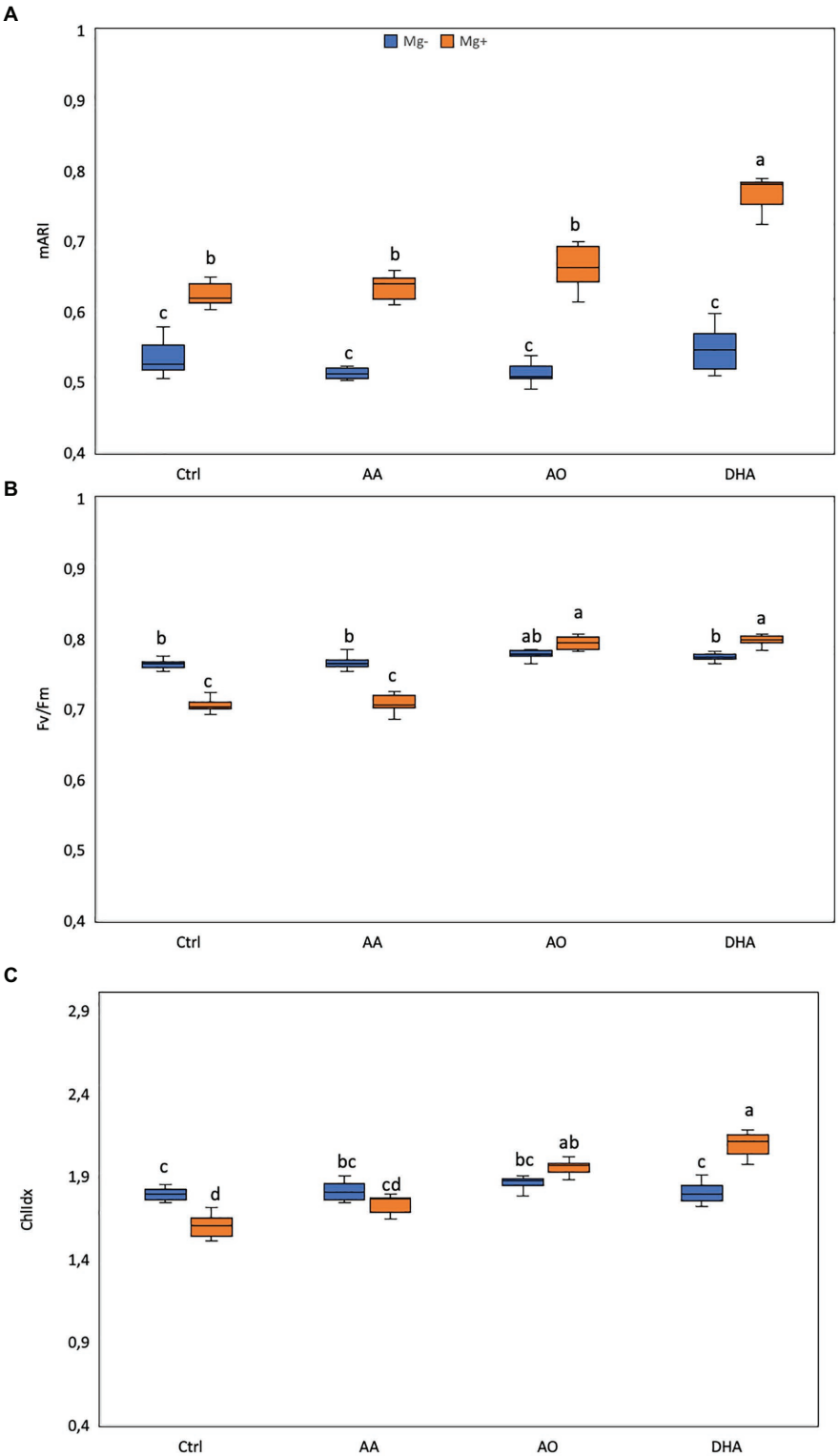

FIGURE 2 | Improved growth and reduced nematode infection in AO/DHA-sprayed plants is correlated with increases in shoot Fv mARI, Fv/Fm, and ChlIdx. The effect of AA (20 mm), AO (20 U/ml), and DHA (20 mm) on **(A)** modified anthocyanin reflectance index (mARI), **(B)** Fv/Fm, and **(C)** ChlIdx in rice leaves. Fourteen-day-old wild-type Nipponbare rice plants were sprayed with 20 mm of AA, 20 ml/unit of AO, and 20 mm of DHA or mock sprayed (Ctrl). After 24 h, plants from each treatment were inoculated with ≈250 s-stage juveniles of *M. graminicola* per plant. Shoots of un/infected plants were monitored for their mARI, Fv/Fm, and ChlIdx values using an automated phenotyping platform (APP) at 3dai (n = 5). One-way ANOVA was applied for the statistical analysis (Tukey test, $\alpha = 0.05$), and data are shown by box plots with median. Different letters indicate significant differences among the treatments.

in the shoots of AO- or DHA-sprayed infected plants significantly increased when compared with the shoots of mock-sprayed or AA-sprayed plants (**Figure 2B**).

Confirming the lowered Fv/Fm, the data also show significantly lower values of ChlIdx in shoots of mock-sprayed infected plants when compared with uninfected plants (**Figure 2C**). Moreover, the ChlIdx values increased significantly in the shoots of AO/DHA-sprayed infected plants when compared to shoots of mock-sprayed uninfected plants. The strongest increase in ChlIdx and Fv/Fm values was observed in DHA-sprayed infected plants. Taken together, nematode infection in untreated plants is correlated with decreases in Fv/Fm and ChlIdx in rice shoot tissue. However, the low nematode infection in AO/DHA-sprayed plants is correlated with increases in Fv/Fm, ChlIdx, and mARI.

AO/DHA Enhances Root Growth and Induces Tolerance to Nematode Stress

Because an increased growth and reduced nematode susceptibility were observed in AO/DHA-sprayed plants, a possible induced tolerance phenomenon could also be part of this mechanism. Accurate assessment of plant tolerance to nematodes requires comparative plant growth measurements on plants challenged with nematodes versus control plants (Roberts, 2002) and that is, why we investigated the effect of exogenous applications of AA, AO, or DHA on rice growth under nematode-uninfected and infected conditions. Plants were measured just before spraying (14-days old) and then again measured at 18, 22, and 26 days old with (Mg^+) or without (Mg^-) to monitor their growth. A slight decrease (30%, not significant) in shoot height was observed in untreated infected (Mg^+) plants compared with Ctrl (Mg^-) at 18 days and 26 days (**Figure 3A**), which illustrates the mild negative effect of nematode infection on above-ground rice growth. However, this effect was negated when the plants were pre-sprayed with AO or DHA. Interestingly, under nematode infection (Mg^+), significant increases in shoot height were observed in AO- or DHA-sprayed plants, when compared with untreated infected plants (Mg^+) at 26 days (**Figure 3A**). The positive effect of AO/DHA on shoot height was observed as early as 4 days after spraying but was much stronger in nematode-infected plants (Mg^+) than in uninoculated (Mg^-) plants. The AO/DHA-treated plants had a significant increase in root length at 22 and 26 days, when compared with untreated or AA-sprayed plants, and this effect seemed magnified mainly under nematode-infected conditions (**Figure 3B**).

DISCUSSION

In our previous work, we elucidated the role of ascorbate oxidation in rice defense against *M. graminicola*. In this study, we show that AO/DHA-induced resistance in rice against Mg is correlated with activation of the phenylpropanoid pathway and leads to a tolerant plant phenotype. Apoplastic AO is a blue-copper oxidase that oxidizes AA to DHA (Pignocchi and Foyer, 2003; Foyer and Noctor, 2005; Fotopoulos and Kanellis, 2013; Venkatesh and Park, 2014). AO is involved in a number of signaling cascades (De Tullio et al., 2013), where it influences both symplastic and apoplastic AA/DHA ratios, leading to effects on cell expansion and on the plant growth rate (Esaka et al., 1992; Li et al., 2017) as well as on stress tolerance (Miret and Müller, 2017). Although DHA and AO had clear effects on IR against nematodes, AA application did not activate such phenotype. This could be related to the fact that AA preferentially crosses cellular membranes in the oxidized form – as previously described by (Horemans et al. 1997). However, our previous research confirmed that foliar AA application, at the same concentration and with the same application method as used in the current study, is taken up by the shoots (Singh et al., 2020b). Noteworthy, this previous study also revealed that AA was not accumulating in the roots upon exogenous AA supply, while exogenous AO or DHA application did affect systemic changes in the AA levels as well as its redox state. These observations suggest that the oxidation state of AA would affect its transport in the plant. However, further research is needed to investigate this hypothesis.

An upregulation of *PAL* gene expression and increase in PAL activity was revealed upon application of AO or DHA, with a primed PAL activation in nematode-induced galls of AO/DHA-treated plants. While PAL-activity measurements confirmed enzymatic activation in the shoots of DHA-sprayed plants, its gene expression was negatively affected in this tissue. PAL is known to be metabolically regulated through negative feedback on PAL transcription and enzyme activity by cinnamic acid (Blount et al., 2000). This could indicate that the DHA-induced PAL activity leads to negative feedback control of PAL gene expression in shoot tissue. The phenylpropanoid pathway serves the production of an array of stress-responsive secondary metabolites, which includes SA, flavonoids – among which anthocyanins –, lignin, and hydroxycinnamic acids (Dixon et al., 2002; Desmedt et al., 2020; Yadav et al., 2020). The significance of this pathway in plant defense and induced resistance was previously shown in other crops and against different pathogens. For example, defense priming with BABA was shown to improve soybean resistance against aphids through activation of the phenylpropanoid metabolism and callose deposition (Yao et al., 2020). Similarly, PAL was shown to contribute to the resistance of black rice against *Xanthomonas oryzae* (Solekha et al., 2020).

Induced resistance against nematodes seems generally correlated with activation of the phenylpropanoid pathway. For example in Singh et al. (2019, 2020a), systemic activation of the phenylpropanoid pathway in response to application of COS-OGA in rice or AO in sugar beet was observed to be correlated with induced resistance to parasitic root-knot and cyst nematodes. Similarly, Huang et al. (2016) showed that thiamine-induced resistance against *M. graminicola* in rice involved lignin deposition in plant roots, and this correlated with enhanced transcription of *OsPAL1* and *OsC4H*, two genes involved in the phenylpropanoid pathway. In addition, *OsPAL4* is induced upon infection in the *M. graminicola*-resistant rice cultivar Vandana, while no differential expression was observed in susceptible cultivar Pusa (Kumari et al., 2016).

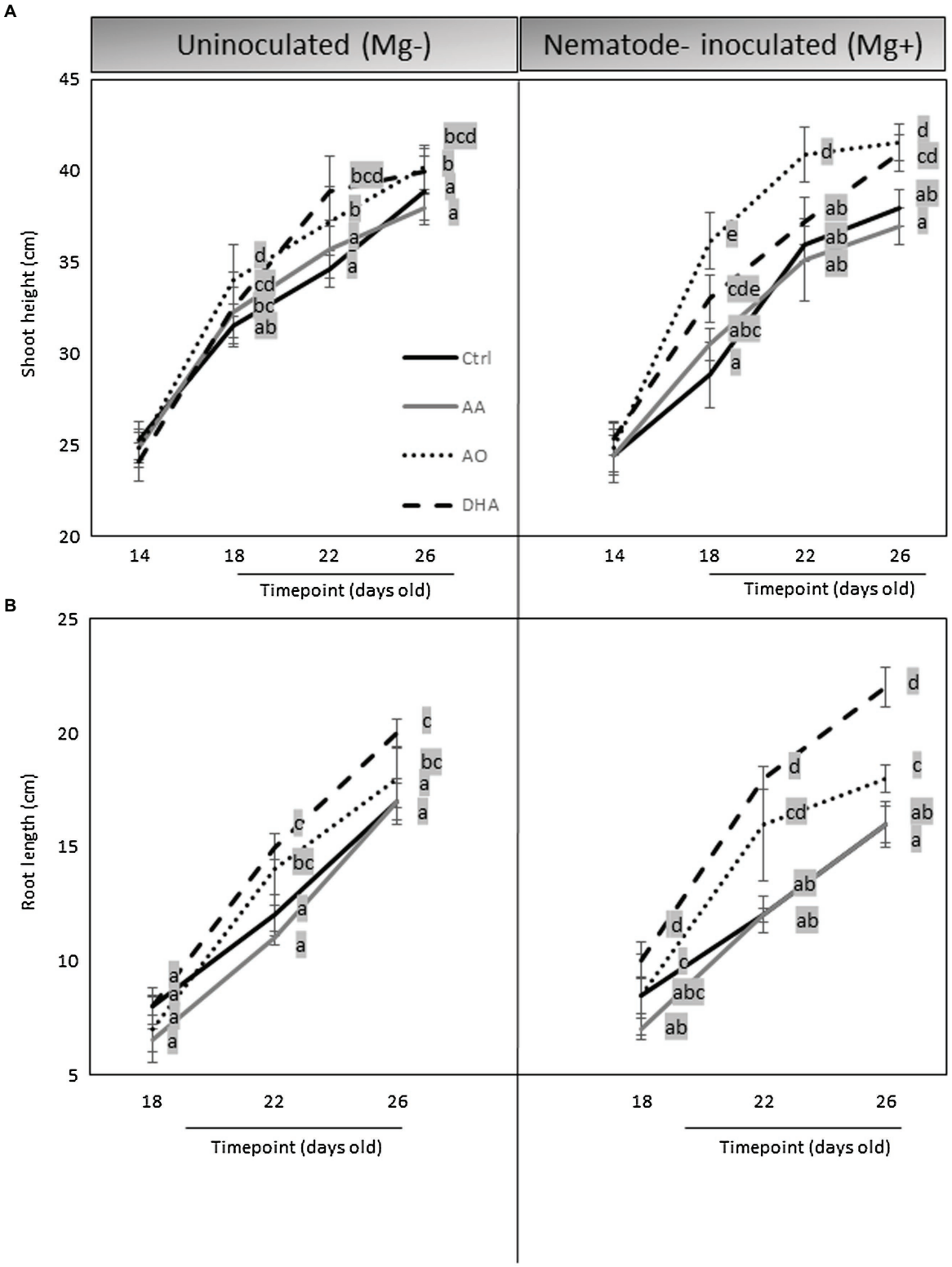

FIGURE 3 | AO/DHA enhances root growth and induces tolerance to nematode stress. Effect of AA, AO/DHA on Nipponbare **(A)** shoots **(B)** root at three time points under uninfected and nematode-infected conditions. Fourteen-days-old rice plants were first measured for their shoot height and then foliar sprayed with AA, AO/DHA, and water as a negative control (Ctrl). One day later, a subset of the plants was inoculated with 250 nematodes per plant (Mg^{+}) while a subset was mock inoculated (Mg^{-}). Shoots and roots were measured at 18, 22, and 26 days. Data were analyzed by one-way ANOVA followed by Tukey's *post-hoc* test. Different letters indicate statistically different means at each time point, $p \leq 0.05$.

Moreover, Khanam et al. (2018) showed induction of *OsPAL1* and increased PAL activity in the resistant rice cultivar Manikpukha against rice stem nematode *Ditylenchus angustus*. Meta-analysis of transcriptome studies showed increased expression of *OsPAL4* and several other family members during plant resistance to multiple pathogens (Tonnessen et al., 2015). However, chemically blocking PAL by AOPP does not lead to differences in number of galls or number of females in untreated plants, confirming previous observations of Ji et al. (2015). When chemically blocking this enzyme AO and DHA were no longer effective in IR and the plants were equally susceptible as the untreated control plants, showing that the phenylpropanoid pathway is involved in induced resistance against *M. graminicola*. Transcriptome analyses have shown that the phenylpropanoid pathway is generally suppressed in RKN-induced feeding sites in rice (Kyndt et al., 2012). Taken together, these data highlight the role of this pathway in nematode resistance. However, the complexity of the pathway makes it difficult to pinpoint which specific metabolite(s) is/are involved in nematode resistance. Based on the observation that blocking PAL does not enhance susceptibility, it is likely that different metabolites could even play opposite roles in plant susceptibility or defense. Our recent research revealed that temporary perturbation of the phenylpropanoid pathway leads to a general reprogramming of the plant defense metabolome, and broad-spectrum-induced resistance in tomato (Desmedt et al., 2021). Which metabolite(s) is/are responsible for this IR remains to be elucidated.

In addition to directly activating the plant's immune system, some IR stimuli can trigger priming of specific defense genes or pathways, a phenomenon which was also observed here in our research. Defense priming is an adaptive part of induced resistance, that is, marked by an enhanced activation of defense mechanisms upon pathogen attack. Upon initial stimulus perception – e.g., ascorbate oxidation – changes may occur in the plant at the physiological, transcriptional, metabolic, and epigenetic levels. This phase is called the priming phase and upon subsequent challenge, the plant effectively mounts a faster and/or stronger defense response, resulting in increased resistance and/or improved stress tolerance (Mauch-Mani et al., 2017; De Kesel et al., 2021). Some IR stimuli have been shown to lead to fitness costs, and as argued by Martinez-Medina et al. (2016), this should be evaluated for every stimulus. Our data rather revealed a positive effect of AO and DHA on rice growth, with increased rice shoot and root growth. These results clearly illustrate how IR is not generally accompanied with fitness costs.

Flavonoids constitute a large class of phenylpropanoid-derived carbon-based metabolites present in all land plants. There are several flavonoid subgroups based on their structural properties, including the chalcones, flavones, flavonols, flavandiols, condensed tannins, isoflavonoids, and anthocyanins (Winkel-Shirley, 2001; Erb and Kliebenstein, 2020). The spectral parameter mARI was found to be a good proxy for anthocyanin content in monocots and dicots (Gitelson et al., 2009). The mARI data suggest that anthocyanins are accumulating in leaves of AO/DHA-stimulated rice plants. A defense response in plants is often characterized by accumulation of foliar anthocyanins, which are produced as antioxidants (Steyn et al., 2002; Gould and Lister, 2006) to cope with the plant's reactive oxygen species ROS burst (Xu et al., 2017). Anthocyanins are known to have ROS scavenging properties and hence protect the cells from oxidative damage (Landi et al., 2015; Xu et al., 2017). Our image-based mARI data showed that nematode infection causes accumulation of anthocyanins in the shoots, correlating with the reported above-ground oxidative response upon RKN infection (Kyndt et al., 2017). Increased H_2O_2 levels were also previously reported upon AO treatment (Singh et al., 2020b). DHA/AO-sprayed plants showed a primed defense response against nematodes correlated with potentiated mARI values. Next to that, our image-based data show that low nematode infection in AO/DHA-sprayed plants is correlated with increases in Fv/Fm and ChlIdx. Similarly, Fan et al. (2020) showed that COS derivatives chitosan-thiadiazole-trifluorobutene (COSSZFB) activate induced resistance against *M. incognita* in cucumber and simultaneously improved plant growth through accumulation of photosynthetic pigments. Fv/Fm values are known to decrease along with the increasing effect of stresses (Rolfe and Scholes, 2010; Gorbe and Calatayud, 2012). For example, Meng et al. (2020) showed stronger reduction in Fv/Fm values in strawberry leaves with high infection of *Botrytis cinerea* similar to what we observe in leaves of untreated, nematode-infected plants.

DHA/AO-IR against RKN in rice was previously shown to result in a primed jasmonate response, the major pathway involved in rice defense against RKN (Nahar et al., 2011). Most likely, a systemic signaling cascade based on redox signals and/or DHA is activated upon foliar AO treatment. Likewise, a shoot-root signaling pathway, integrating ROS, and JA were shown to be involved in tomato defense against RKN (Wang et al., 2019). Noteworthy, it is known that the phenylpropanoid pathway is positively regulated by JA (Pauwels et al., 2008; Taheri and Tarighi, 2010).

The significant increases in chlorophyll fluorescence and growth of nematode-infected rice plants pre-sprayed with AO/DHA implies that ascorbate oxidation induces a tolerance mechanism. Plant tolerance is a phenotype where the negative effect of pathogens is low, and plant growth and yield are not negatively affected (Koch et al., 2016). Tolerance to nematode stress involves compensation *via* the growth of new tissues, increased number of roots, and enhanced water and nutrient uptake (Franco and Evans, 1979; Trudgill and Cotes, 1983; Fatemy and Evans, 1986a,b; Miltner et al., 1991). For example, Trudgill and Cotes (1983) showed that potato cultivars that are tolerant to cyst nematodes *G. rostochiensis* have a higher number of roots and increased root weight when under attack by nematodes. Similarly, Swain and Prasad (1988) showed increased chlorophyll content as a mechanism of tolerance of rice to *M. graminícola*. To confirm that these plants are really tolerant to nematode infestation, field trials in natural nematode-infested soils will be required.

Enhancing the natural tolerance/defense of plants toward different stress factors provides a durable approach for enhanced and sustainable crop production. Tolerance combined with resistance is preferred over tolerance alone because large healthy roots of tolerant, susceptible plants allow the nematode

population to increase (Roberts, 2002). Our research unveils that next to inducing resistance, ascorbate oxidation also positively affects plant tolerance to nematodes in rice. AO and DHA are therefore promising compounds to be used in sustainable crop protection.

DATA AVAILABILITY STATEMENT

The original contributions presented in the study are included in the article/**Supplementary Material**, and further inquiries can be directed to the corresponding author.

AUTHOR CONTRIBUTIONS

TK and RS planned and designed the research and wrote the manuscript. RS, KA, and JP conducted phenotyping and infection experiments. RS conducted biochemical analysis. All authors read and approved the manuscript.

FUNDING

This work was financially supported by the Special Research Fund (Bijzonder Onderzoeksfonds) of Ghent University through a BOF starting grant to TK. We acknowledge the Hercules initiative for the multispectral imaging platform that was granted (grant number: AUGE/15/17).

SUPPLEMENTARY MATERIAL

The Supplementary Material for this article can be found online at https://www.frontiersin.org/articles/10.3389/fpls.2021.713870/full#supplementary-material

REFERENCES

Al-Sayed, A., and Thomason, I. (1988). *Meloidogyne incognita* and tomato response to thiamine, ascorbic acid, L-arginine, and L-glutamic acid. *J. Nematol.* 20, 451–456.

Arrigoni, O., Zacheo, G., Arrigoni-Liso, R., Bleve-Zacheo, T., and Lamberti, F. (1979). Relationship between ascorbic acid and resistance in tomato plants to *Meloidogyne incognita*. *Phytopathology* 69, 579–581. doi: 10.1094/Phyto-69-579

Baker, N. R. (2008). Chlorophyll fluorescence: a probe of photosynthesis in vivo. *Annu. Rev. Plant Biol.* 59, 89–113. doi: 10.1146/annurev.arplant.59.032607.092759

Bektas, Y., and Eulgem, T. (2015). Synthetic plant defense elicitors. *Front. Plant Sci.* 5:804. doi: 10.3389/fpls.2014.00804

Björkman, O., and Demmig, B. (1987). Photon yield of O_2 evolution and chlorophyll fluorescence characteristics at 77 K among vascular plants of diverse origins. *Planta* 170, 489–504. doi: 10.1007/BF00402983

Blount, J. W., Korth, K. L., Masoud, S. A., Rasmussen, S., Lamb, C., and Dixon, R. A. (2000). Altering expression of cinnamic acid 4-hydroxylase in transgenic plants provides evidence for a feedback loop at the entry point into the phenylpropanoid pathway. *Plant Physiol.* 122, 107–116. doi: 10.1104/pp.122.1.107

Bridge, J., and Page, S. L. (1982). The rice root-knot nematode, *Meloidogyne graminicola*, on deep water rice (*Oryza sativa* subsp. *indica*). *Revue de Nematologie* 5, 225–232.

Bridge, J., Plowright, R., and Peng, D. (2005). "Nematode parasites of rice," in *Plant Parasitic Nematodes in Subtropical and Tropical Agricun lture. 2nd Edn.* eds. M. Luc, R. A. Sikora and J. Bridge (Wallingford, UK: CABI Publishing), 87–130.

Caillaud, M.-C., Dubreuil, G., Quentin, M., Perfus-Barbeoch, L., Lecomte, P., de Almeida Engler, J., et al. (2008). Root-knot nematodes manipulate plant cell functions during a compatible interaction. *J. Plant Physiol.* 165, 104–113. doi: 10.1016/j.jplph.2007.05.007

Camacho-Cristóbal, J. J., Anzellotti, D., and González-Fontes, A. (2002). Changes in phenolic metabolism of tobacco plants during short-term boron deficiency. *Plant Physiol. Biochem.* 40, 997–1002. doi: 10.1016/S0981-9428(02)01463-8

Cohen, Y., Vaknin, M., and Mauch-Mani, B. (2016). BABA-induced resistance: milestones along a 55-year journey. *Phytoparasitica* 44, 513–538. doi: 10.1007/s12600-016-0546-x

Conrath, U. (2006). Systemic acquired resistance. *Plant Signal. Behav.* 1, 179–184. doi: 10.4161/psb.1.4.3221

Conrath, U., Beckers, G. J., Langenbach, C. J., and Jaskiewicz, M. R. (2015). Priming for enhanced defense. *Annu. Rev. Phytopathol.* 53, 97–119. doi: 10.1146/annurev-phyto-080614-120132

Cook, R. (1987). "Resistance and tolerance," in *Principal and Practice of Nematode Control in Crops*. eds. R. H. Brown and B. R. Kerry (Sydney, N.S.W: Academic Press), 179–232.

De Kesel, J., Conrath, U., Flors, V., Luna, E., Mageroy, M. H., Mauch-Mani, B., et al. (2021). The induced resistance lexicon: Do's and Don'ts. *Trends Plant Sci.* 26, 685–691. doi: 10.1016/j.tplants.2021.01.001

De Tullio, M., Guether, M., and Balestrini, R. (2013). Ascorbate oxidase is the potential conductor of a symphony of signaling pathways. *Plant Signal. Behav.* 8:e23213. doi: 10.4161/psb.23213

De Waele, D., and Elsen, A. (2007). Challenges in tropical plant nematology. *Annu. Rev. Phytopathol.* 45, 457–485. doi: 10.1146/annurev.phyto.45.062806.094438

Desmedt, W., Jonckheere, W., Nguyen, V. H., Ameye, M., De Zutter, N., De Kock, K., et al. (2021). The phenylpropanoid pathway inhibitor piperonylic acid induces broad-spectrum pest and disease resistance in plants. *Plant Cell Environ.* doi: 10.1111/pce.14119 [Epub ahead of print].

Desmedt, W., Mangelinckx, S., Kyndt, T., and Vanholme, B. (2020). A phytochemical perspective on plant defense against nematodes. *Front. Plant Sci.* 11:602079. doi: 10.3389/fpls.2020.602079

Dixon, R. A., Achnine, L., Kota, P., Liu, C. J., Reddy, M. S., and Wang, L. (2002). The phenylpropanoid pathway and plant defence—a genomics perspective. *Mol. Plant Pathol.* 3, 371–390. doi: 10.1046/j.1364-3703.2002.00131.x

Dixon, R. A., and Paiva, N. L. (1995). Stress-induced phenylpropanoid metabolism. *Plant Cell* 7, 1085–1097. doi: 10.2307/3870059

Erb, M., and Kliebenstein, D. J. (2020). Plant secondary metabolites as defenses, regulators, and primary metabolites: the blurred functional trichotomy. *Plant Physiol.* 184, 39–52. doi: 10.1104/pp.20.00433

Esaka, M., Fujisawa, K., Goto, M., and Kisu, Y. (1992). Regulation of ascorbate oxidase expression in pumpkin by auxin and copper. *Plant Physiol.* 100, 231–237. doi: 10.1104/pp.100.1.231

Escobar, C., Barcala, M., Cabrera, J., and Fenoll, C. (2015). "Overview of root-knot nematodes and giant cells," in *Advances in Botanical Research*. eds. C. Escobar and C. Fenoll (Oxford, UK: Elsevier), 1–32.

Fan, Z., Qin, Y., Liu, S., Xing, R., Yu, H., and Li, P. (2020). Chitosan oligosaccharide fluorinated derivative control root-knot nematode (*Meloidogyne incognita*) disease based on the multi-efficacy strategy. *Mar. Drugs* 18:273. doi: 10.3390/md18050273

Fatemy, F., and Evans, K. (1986a). Effects of *Globodera rostochiensis* and water stress on shoot and root growth and nutrient uptake of potatoes. *Revue de Nematologie* 9, 181–184.

Fatemy, F., and Evans, K. (1986b). Growth, water uptake and calcium content of potato cultivars in relation to tolerance of cyst nematodes. *Revue de Nématologie* 9, 171–179.

Fotopoulos, V., and Kanellis, A. K. (2013). Altered apoplastic ascorbate redox state in tobacco plants via ascorbate oxidase overexpression results in delayed dark-induced senescence in detached leaves. *Plant Physiol. Biochem.* 73, 154–160. doi: 10.1016/j.plaphy.2013.09.002

Foyer, C. H., Kyndt, T., and Hancock, R. D. (2020). Vitamin C in plants: novel concepts, new perspectives, and outstanding issues. *Antioxid. Redox Signal.* 32, 463–485. doi: 10.1089/ars.2019.7819

Foyer, C. H., and Noctor, G. (2005). Redox homeostasis and antioxidant signaling: a metabolic interface between stress perception and physiological responses. *Plant Cell* 17, 1866–1875. doi: 10.1105/tpc.105.033589

Franco, J., and Evans, K. (1979). Tolerance to cyst-nematode attack in commercial potato cultivars and some possible mechanisms for its operation. *Nematologica* 25, 153–162. doi: 10.1163/187529279X00172

Gitelson, A. A., Chivkunova, O. B., and Merzlyak, M. N. (2009). Nondestructive estimation of anthocyanins and chlorophylls in anthocyanic leaves. *Am. J. Bot.* 96, 1861–1868. doi: 10.3732/ajb.0800395

Gorbe, E., and Calatayud, A. (2012). Applications of chlorophyll fluorescence imaging technique in horticultural research: a review. *Sci. Hortic.* 138, 24–35. doi: 10.1016/j.scienta.2012.02.002

Gould, K. S., and Lister, C. (2006). "Flavonoid functions in plants," in *Flavonoids: Chemistry, Biochemistry and Applications*. eds. Ø. M. Andersen and K. R. Markham (Boca Raton, FL, USA: CRC Press LLC), 397–441.

Hahlbrock, K., and Scheel, D. (1989). Physiology and molecular biology of phenylpropanoid metabolism. *Annu. Rev. Plant Biol.* 40, 347–369. doi: 10.1146/annurev.pp.40.060189.002023

Hamada, A., El-Zawahry, A., and Al-Hakimi, A. (2000). Soaking of egg plant seeds in ascorbic acid, pyridoxine or thiamine for control of *Meloidogyne javanica* infection. *Assiut. J. Agric. Sci.* 31, 227–241.

Horemans, N., Asard, H., and Caubergs, R. J. (1997). The ascorbate carrier of higher plant plasma membranes preferentially translocates the fully oxidized (dehydroascorbate) molecule. *Plant Physiol.* 114, 1247–1253. doi: 10.1104/pp.114.4.1247

Horemans, N., Foyer, C. H., and Asard, H. (2000). Transport and action of ascorbate at the plant plasma membrane. *Trends Plant Sci.* 5, 263–267. doi: 10.1016/S1360-1385(00)01649-6

Huang, J., Gu, M., Lai, Z., Fan, B., Shi, K., Zhou, Y.-H., et al. (2010). Functional analysis of the Arabidopsis PAL gene family in plant growth, development, and response to environmental stress. *Plant Physiol.* 153, 1526–1538. doi: 10.1104/pp.110.157370

Huang, W. K., Ji, H. I., Gheysen, G., Debode, J., and Kyndt, T. (2015). Biochar-amended potting medium reduces the susceptibility of rice to root-knot nematode infections. *BMC Plant Biol.* 15, 1–15. doi: 10.1186/s12870-015-0654-7

Huang, W. K., Ji, H. L., Gheysen, G., and Kyndt, T. (2016). Thiamine-induced priming against root-knot nematode infection in rice involves lignification and hydrogen peroxide generation. *Mol. Plant Pathol.* 17, 614–624. doi: 10.1111/mpp.12316

Ji, H., Kyndt, T., He, W., Vanholme, B., and Gheysen, G. (2015). β-Aminobutyric acid–induced resistance against root-knot nematodes in rice is based on increased basal defense. *Mol. Plant-Microbe Interact.* 28, 519–533. doi: 10.1094/MPMI-09-14-0260-R

Kalamarakis, A. E., and Markellou, E. (2007). Efficacy evaluation of plant protection products at EU level: data requirements and evaluation principles. *J. Pestic. Sci.* 32, 1–9. doi: 10.1584/jpestics.K06-13

Karssen, G., and Moens, M. (2006). "Taxonomy and principal general root-knot nematodes," in *Plant Nematology*. eds. R. Perry and M. Moens (Wallingford, UK: CAB International), 60–90.

Karssen, G., Moens, M., and Perry, R. (2006). *Plant Nematology*. Oxfordshire: CABI, 59–90.

Khanam, S., Bauters, L., Singh, R. R., Verbeek, R., Haeck, A., Sultan, S. M., et al. (2018). Mechanisms of resistance in the rice cultivar Manikpukha to the rice stem nematode *Ditylenchus angustus*. *Mol. Plant Pathol.* 19, 1391–1402. doi: 10.1111/mpp.12622

Koch, K. G., Chapman, K., Louis, J., Heng-Moss, T., and Sarath, G. (2016). Plant tolerance: a unique approach to control hemipteran pests. *Front. Plant Sci.* 7:1363. doi: 10.3389/fpls.2016.01363

Koen, E., Trapet, P., Brulé, D., Kulik, A., Klinguer, A., Atauri-Miranda, L., et al. (2014). β-Aminobutyric acid (BABA)-induced resistance in *Arabidopsis thaliana*: link with iron homeostasis. *Mol. Plant-Microbe Interact.* 27, 1226–1240. doi: 10.1094/MPMI-05-14-0142-R

Kumari, C., Dutta, T. K., Banakar, P., and Rao, U. (2016). Comparing the defence-related gene expression changes upon root-knot nematode attack in susceptible versus resistant cultivars of rice. *Sci. Rep.* 6:22846. doi: 10.1038/srep22846

Kyndt, T., Denil, S., Haegeman, A., Trooskens, G., Bauters, L., Van Criekinge, W., et al. (2012). Transcriptional reprogramming by root knot and migratory nematode infection in rice. *New Phytol.* 196, 887–900. doi: 10.1111/j.1469-8137.2012.04311.x

Kyndt, T., Fernandez, D., and Gheysen, G. (2014). Plant-parasitic nematode infections in rice: molecular and cellular insights. *Annu. Rev. Phytopathol.* 52, 135–153. doi: 10.1146/annurev-phyto-102313-050111

Kyndt, T., Zemene, H. Y., Haeck, A., Singh, R., De Vleesschauwer, D., Denil, S., et al. (2017). Below-ground attack by the root knot nematode Meloidogyne graminicola predisposes rice to blast disease. *Mol. Plant Microbe. Interact* 30, 255–266. doi: 10.1094/MPMI-11-16-0225-R

Landi, M., Tattini, M., and Gould, K. S. (2015). Multiple functional roles of anthocyanins in plant-environment interactions. *Environ. Exp. Bot.* 119, 4–17. doi: 10.1016/j.envexpbot.2015.05.012

Lefevere, H., Bauters, L., and Gheysen, G. (2020). Salicylic acid biosynthesis in plants. *Front. Plant Sci.* 11:338. doi: 10.3389/fpls.2020.00338

Li, R., Xin, S., Tao, C., Jin, X., and Li, H. (2017). Cotton ascorbate oxidase promotes cell growth in cultured tobacco bright yellow-2 cells through generation of apoplast oxidation. *Int. J. Mol. Sci.* 18:1346. doi: 10.3390/ijms18071346

Luna, E., Flandin, A., Cassan, C., Prigent, S., Chevanne, C., Kadiri, C. F., et al. (2020). Metabolomics to exploit the primed immune system of tomato fruit. *Meta* 10:96. doi: 10.3390/metabo10030096

Luna, E., Van Hulten, M., Zhang, Y., Berkowitz, O., López, A., Pétriacq, P., et al. (2014). Plant perception of β-aminobutyric acid is mediated by an aspartyl-tRNA synthetase. *Nat. Chem. Biol.* 10, 450–456. doi: 10.1038/nchembio.1520

MacDonald, M. J., and D'Cunha, G. B. (2007). A modern view of phenylalanine ammonia lyase. *Biochem. Cell Biol.* 85, 273–282. doi: 10.1139/O07-018

Mantelin, S., Bellafiore, S., and Kyndt, T. (2017). *Meloidogyne graminicola*: a major threat to rice agriculture. *Mol. Plant Pathol.* 18, 3–15. doi: 10.1111/mpp.12394

Martinez-Medina, A., Flors, V., Heil, M., Mauch-Mani, B., Pieterse, C. M., Pozo, M. J., et al. (2016). Recognizing plant defense priming. *Trends Plant Sci.* 21, 818–822. doi: 10.1016/j.tplants.2016.07.009

Mauch-Mani, B., Baccelli, I., Luna, E., and Flors, V. (2017). Defense priming: an adaptive part of induced resistance. *Annu. Rev. Plant Biol.* 68, 485–512. doi: 10.1146/annurev-arplant-042916-041132

Meng, L., Mestdagh, H., Ameye, M., Audenaert, K., Höfte, M., and Van Labeke, M.-C. (2020). Phenotypic variation of *Botrytis cinerea* isolates is influenced by spectral light quality. *Front. Plant Sci.* 11:1233. doi: 10.3389/fpls.2020.01233

Miltner, E., Karnok, K., and Hussey, R. (1991). Root response of tolerant and intolerant soybean cultivars to soybean cyst nematode. *Agron. J.* 83, 571–576. doi: 10.2134/agronj1991.00021962008300030014x

Miret, J. A., and Müller, M. (2017). "AsA/DHA redox pair influencing plant growth and stress tolerance," in *Ascorbic Acid in Plant Growth, Development and Stress Tolerance*. eds. M. ossain, S. Munné-Bosch, D. Burritt, P. Diaz-Vivancos, M. Fujita and A. Lorence (Cham, Switzerland: Springer), 297–319.

Nahar, K., Kyndt, T., De Vleesschauwer, D., Höfte, M., and Gheysen, G. (2011). The jasmonate pathway is a key player in systemically induced defense against root knot nematodes in rice. *Plant Physiol.* 157, 305–316. doi: 10.1104/pp.111.177576

Netscher, C. (1993). A root-knot nematode, Meloidogyne cf graminicola, parasitic on rice in Indonesia. *J. Nematology.* 3, 90–95.

Osman, G. (1993). Effect of amino acids and ascorbic acid on *Meloidogyne javanica* Chitw. (Tylenchidae, Nematoda). *Anzeiger Für Schädlingskunde, Pflanzenschutz, Umweltschutz* 66, 140–142. doi: 10.1007/BF01906844

Osman, H., Youssef, M., El-Gindi, A., Ameen, F., Abd-Elbary, N., and Lashein, A. (2013). Effect of abiotic resistance inducers, γ-amino-n-butyric acid (GABA), ascorbic acid and chitosan on certain enzyme activities of eggplant inoculated with root-knot nematode, Meloidogyne incognita. *Arch. Phytopathol. Plant Prot.* 46, 1857–1863. doi: 10.1080/03235408.2013.779427

Pauwels, L., Morreel, K., De Witte, E., Lammertyn, F., Van Montagu, M., Boerjan, W., et al. (2008). Mapping methyl jasmonate-mediated transcriptional

reprogramming of metabolism and cell cycle progression in cultured Arabidopsis cells. *Proc. Natl. Acad. Sci.* 105, 1380–1385. doi: 10.1073/pnas.0711203105

Pignocchi, C., and Foyer, C. H. (2003). Apoplastic ascorbate metabolism and its role in the regulation of cell signalling. *Curr. Opin. Plant Biol.* 6, 379–389. doi: 10.1016/S1369-5266(03)00069-4

Plowright, R., and Bridge, J. (1990). Effect of *Meloidogyne Graminicola* (Nematoda) on the establishment, growth and yield of rice cv IR36. *Nematologica* 36, 81–89. doi: 10.1163/002925990X00059

Prot, J.-C., and Rahman, M. (1994). "Nematode ecology, economic importance, and management in rice ecosystems in South and Southeast Asia," in *Rice Pest Science and Management*. eds. P. S. Teng, K.L. Heong and K. Moody (Los-Banos, Philippines: International Rice Research Institute, IRRI), 129–144.

Rao, Y., and Biswas, H. (1973). Evaluation of yield losses in rice due to the root-knot nematode *Meloidogyne incognita*. *Indian. J. Ematol.* 3:74.

Roberts, P. (2002). "Concepts and consequences of resistance," in *Plant Resistance to Parasitic Nematodes*. eds. J. L. Starr, R. Cook and J. Bridge (Wallingford, UK: CABI Publishing), 23–41.

Rolfe, S. A., and Scholes, J. D. (2010). Chlorophyll fluorescence imaging of plant–pathogen interactions. *Protoplasma* 247, 163–175. doi: 10.1007/s00709-010-0203-z

Singh, R. R., Chinnasri, B., De Smet, L., Haeck, A., Demeestere, K., Van Cutsem, P., et al. (2019). Systemic defense activation by COS-OGA in rice against root-knot nematodes depends on stimulation of the phenylpropanoid pathway. *Plant Physiol. Biochem.* 142, 202–210. doi: 10.1016/j.plaphy.2019.07.003

Singh, R. R., Nobleza, N., Demeestere, K., and Kyndt, T. (2020a). Ascorbate oxidase induces systemic resistance in sugar beet against cyst nematode *Heterodera schachtii*. *Front. Plant Sci.* 11:591715. doi: 10.3389/fpls.2020.591715

Singh, R. R., Verstraeten, B., Siddique, S., Tegene, A. M., Tenhaken, R., Frei, M., et al. (2020b). Ascorbate oxidation activates systemic defence against root-knot nematode *Meloidogyne graminicola* in rice. *J. Exp. Bot.* 71, 4271–4284. doi: 10.1093/jxb/eraa171

Smirnoff, N. (2000). Ascorbic acid: metabolism and functions of a multi-facetted molecule. *Curr. Opin. Plant Biol.* 3, 229–235. doi: 10.1016/S1369-5266(00)00069-8

Smirnoff, N. (2018). Ascorbic acid metabolism and functions: a comparison of plants and mammals. *Free Radic. Biol. Med.* 122, 116–129. doi: 10.1016/j.freeradbiomed.2018.03.033

Smirnoff, N., and Wheeler, G. L. (2000). Ascorbic acid in plants: biosynthesis and function. *Crit. Rev. Plant Sci.* 19, 267–290. doi: 10.1080/07352680091139231

Solekha, R., Susanto, F. A., Joko, T., Nuringtyas, T. R., and Purwestri, Y. A. (2020). Phenylalanine ammonia lyase (PAL) contributes to the resistance of black rice against *Xanthomonas oryzae* pv. *oryzae*. *J. Plant Pathol.* 102, 359–365. doi: 10.1007/s42161-019-00426-z

Steyn, W. J., Wand, S., Holcroft, D., and Jacobs, G. (2002). Anthocyanins in vegetative tissues: a proposed unified function in photoprotection. *New Phytol.* 155, 349–361. doi: 10.1046/j.1469-8137.2002.00482.x

Swain, B., and Prasad, J. (1988). Chlorophyll content in rice as influenced by the root-knot nematode, *Meloidogyne graminicola* infection. *Curr. Sci.* 57, 895–896.

Taheri, P., and Tarighi, S. (2010). Riboflavin induces resistance in rice against *Rhizoctonia solani* via jasmonate-mediated priming of phenylpropanoid pathway. *J. Plant Physiol.* 167, 201–208. doi: 10.1016/j.jplph.2009.08.003

Taheri, P., and Tarighi, S. (2011). A survey on basal resistance and riboflavin-induced defense responses of sugar beet against *Rhizoctonia solani*. *J. Plant Physiol.* 168, 1114–1122. doi: 10.1016/j.jplph.2011.01.001

Tonnessen, B. W., Manosalva, P., Lang, J. M., Baraoidan, M., Bordeos, A., Mauleon, R., et al. (2015). Rice phenylalanine ammonia-lyase gene OsPAL4 is associated with broad spectrum disease resistance. *Plant Mol. Biol.* 87, 273–286. doi: 10.1007/s11103-014-0275-9

Trudgill, D., and Cotes, L. (1983). Tolerance of potato to potato cyst nematodes (*Globodera rostochiensis* and *G. pallida*) in relation to the growth and efficiency of the root system. *Ann. Appl. Biol.* 102, 385–397. doi: 10.1111/j.1744-7348.1983.tb02708.x

van Hulten, M., Pelser, M., Van Loon, L., Pieterse, C. M., and Ton, J. (2006). Costs and benefits of priming for defense in Arabidopsis. *Proc. Natl. Acad. Sci.* 103, 5602–5607. doi: 10.1073/pnas.0510213103

Venkatesh, J., and Park, S. W. (2014). Role of L-ascorbate in alleviating abiotic stresses in crop plants. *Bot. Stud.* 55:38. doi: 10.1186/1999-3110-55-38

Verbeek, R. E., Van Buyten, E., Alam, Z., De Vleesschauwer, D., Van Bockhaven, J., Asano, T., et al. (2019). JA induced defence mechanisms in the belowground antagonistic interaction between *Pythium arrhenomanes* and *Meloidogyne graminicola* in rice. *Front. Plant Sci.* 10:1515. doi: 10.3389/fpls.2019.01515

Vogt, T. (2010). Phenylpropanoid biosynthesis. *Mol. Plant* 3, 2–20. doi: 10.1093/mp/ssp106

Wang, G., Hu, C., Zhou, J., Liu, Y., Cai, J., Pan, C., et al. (2019). Systemic root-shoot signaling drives jasmonate-based root defense against nematodes. *Curr. Biol.* 29, 3430–3438. doi: 10.1016/j.cub.2019.08.049

Winkel-Shirley, B. (2001). Flavonoid biosynthesis. a colorful model for genetics, biochemistry, cell biology, and biotechnology. *Plant Physiol.* 126, 485–493. doi: 10.1104/pp.126.2.485

Wu, C.-C., Singh, P., Chen, M.-C., and Zimmerli, L. (2010). L-glutamine inhibits beta-aminobutyric acid-induced stress resistance and priming in Arabidopsis. *J. Exp. Bot.* 61, 995–1002. doi: 10.1093/jxb/erp363

Xu, Z., Mahmood, K., and Rothstein, S. J. (2017). ROS induces anthocyanin production via late biosynthetic genes and anthocyanin deficiency confers the hypersensitivity to ROS-generating stresses in Arabidopsis. *Plant Cell Physiol.* 58, 1364–1377. doi: 10.1093/pcp/pcx073

Yadav, V., Wang, Z., Wei, C., Amo, A., Ahmed, B., Yang, X., et al. (2020). Phenylpropanoid pathway engineering: an emerging approach towards plant defense. *Pathogens* 9:312. doi: 10.3390/pathogens9040312

Yao, L., Zhong, Y., Wang, B., Yan, J., and Wu, T. (2020). BABA application improves soybean resistance to aphid through activation of phenylpropanoid metabolism and callose deposition. *Pest Manag. Sci.* 76, 384–394. doi: 10.1002/ps.5526

Yassin, M., Ton, J., Rolfe, S. A., Valentine, T. A., Cromey, M., Holden, N., et al. (2021). The rise, fall and resurrection of chemical-induced resistance agents. *Pest Manag. Sci.* doi: 10.1002/ps.6370 [Epub ahead of print].

Zhan, L.-P., Peng, D.-L., Wang, X.-L., Kong, L.-A., Peng, H., Liu, S.-M., et al. (2018). Priming effect of root-applied silicon on the enhancement of induced resistance to the root-knot nematode *Meloidogyne graminicola* in rice. *BMC Plant Biol.* 18, 1–12. doi: 10.1186/s12870-018-1266-9

Conflict of Interest: A patent about the use of DHA to protect plants from nematode infection has been submitted by Ghent University. The inventors are authors RS and TK.

The remaining authors declare that the research was conducted in the absence of any commercial or financial relationships that could be construed as a potential conflict of interest.

Publisher's Note: All claims expressed in this article are solely those of the authors and do not necessarily represent those of their affiliated organizations, or those of the publisher, the editors and the reviewers. Any product that may be evaluated in this article, or claim that may be made by its manufacturer, is not guaranteed or endorsed by the publisher.

frontiers in Plant Science

ORIGINAL RESEARCH
published: 01 September 2021
doi: 10.3389/fpls.2021.721548

NbSOBIR1 Partitions Into Plasma Membrane Microdomains and Binds ER-Localized *Nb*RLP1

Yi-Hua Li[1,2], Tai-Yu Ke[1], Wei-Che Shih[1], Ruey-Fen Liou[1] and Chao-Wen Wang[2]**

[1] Department of Plant Pathology and Microbiology, National Taiwan University, Taipei, Taiwan, [2] Institute of Plant and Microbial Biology, Academia Sinica, Taipei, Taiwan

The receptor-like kinase Suppressor of BIR1 (SOBIR1) binds various receptor-like proteins (RLPs) that perceive microbe-associated molecular patterns (MAMPs) at the plasma membrane, which is thought to activate plant pattern-triggered immunity (PTI) against pathogen invasion. Despite its potentially crucial role, how SOBIR1 transmits immune signaling to ultimately elicit PTI remains largely unresolved. Herein, we report that a *Nicotiana benthamiana* gene *Nb*RLP1, like *Nb*SOBIR1, was highly induced upon *Phytophthora parasitica* infection. Intriguingly, *Nb*RLP1 is characterized as a receptor-like protein localizing to the endoplasmic reticulum (ER) membrane rather than the plasma membrane. Using bimolecular fluorescence complementation and affinity purification assays, we established that *Nb*RLP1 is likely to associate with *Nb*SOBIR1 through the contact between the ER and plasma membrane. We further found that *Nb*SOBIR1 at the plasma membrane partitions into mobile microdomains that undergo frequent lateral movement and internalization. Remarkably, the dynamics of *Nb*SOBIR1 microdomain is coupled to the remodeling of the cortical ER network. When *Nb*SOBIR1 microdomains were induced by the *P. parasitica* MAMP ParA1, tobacco cells overexpressing *Nb*RLP1 accelerated *Nb*SOBIR1 internalization. Overexpressing *Nb*RLP1 in tobacco further exaggerated the ParA1-induced necrosis. Together, these findings have prompted us to propose that ER and the ER-localized *Nb*RLP1 may play a role in transmitting plant immune signals by regulating *Nb*SOBIR1 internalization.

Keywords: ER, plasma membrane, microdomain, SOBIR1, pattern-triggered immunity, receptor-like protein, microbe-associated molecular pattern, *Phytophthora parasitica*

OPEN ACCESS

Edited by:
Rachid Lahlali, Ecole Nationale d'Agriculture de Meknès, Morocco

Reviewed by:
Pengwei Wang, Huazhong Agricultural University, China
Dan Zhang, Temasek Life Sciences Laboratory, Singapore

****Correspondence:***
Ruey-Fen Liou
rfliou@ntu.edu.tw
Chao-Wen Wang
cwwang02@gate.sinica.edu.tw

Specialty section:
This article was submitted to Plant Pathogen Interactions, a section of the journal Frontiers in Plant Science

Received: *07 June 2021*
Accepted: *02 August 2021*
Published: *01 September 2021*

Citation:
Li Y-H, Ke T-Y, Shih W-C, Liou R-F and Wang C-W (2021) NbSOBIR1 Partitions Into Plasma Membrane Microdomains and Binds ER-Localized NbRLP1. Front. Plant Sci. 12:721548. doi: 10.3389/fpls.2021.721548

INTRODUCTION

As a sessile organism, plants have evolved a series of defense mechanisms to protect themselves against pathogens. Plant cells sense potential pathogens through the function of pattern recognition receptors (PRRs) that recognize a wide range of microbe-associated molecular patterns (MAMPs) to ultimately elicit pattern-triggered immunity (PTI) (Jones and Dangl, 2006; Dodds and Rathjen, 2010). The onset of PTI can rapidly activate a series of downstream plant defense responses, including callose deposition, generation of reactive oxygen species (ROS), activation of mitogen-activated protein kinase cascade, induction of defense genes, and in some cases cell death (Boller and Felix, 2009; Yu et al., 2017).

Plant PRRs are plasma membrane-localized transmembrane protein receptors belonging to the family of receptor-like kinases (RLKs) or receptor-like proteins (RLPs), which differ in the presence or absence of intracellular kinase domains (Zipfel, 2014). The emerging evidence suggests that plant immune response is triggered upon the perception of MAMPs, accompanied by the association of selected PRRs with additional factors, such as BRI1-associated receptor kinase 1 (BAK1), also known as somatic embryogenesis receptor-like kinase 3 (SERK3), and other members of the SERK family to form multimeric kinase complex on the cell surface (Roux et al., 2011; Albert et al., 2020). Moreover, PRRs of the RLP type are known to constitutively form complexes with Suppressor of BIR1 (SOBIR1), an RLK containing a short leucine-rich repeat (LRR) ectodomain (Liebrand et al., 2013).

SOBIR1 was originally identified in *Arabidopsis thaliana* as a counterplayer of BAK1-interacting receptor-like kinase1 (BIR1) (Gao et al., 2009). When overexpressed, SOBIR1 constitutively activates cell death and plant immune responses. Recent studies further demonstrated that SOBIR1 is indispensable for PTI elicited by various MAMPs, including sclerotinia culture filtrate elicitor 1 (SCFE1) from *Sclerotinia sclerotiorum*, *Botrytis cinerea* endopolygalacturonase 1, *Phytophthora* elicitins, and *Phytophthora sojae* XEG1, all of which are perceived by PRRs of the LRR-RLP type (Zhang et al., 2013, 2014; Du et al., 2015; Wang et al., 2018). Thus, SOBIR1 appears to function as a common adaptor protein for various LRR-RLP PRRs and thus is thought to play a central role in plant immunity.

Recent studies based on high-resolution microscopy indicate that the immune and growth receptors form distinct nanodomains on the plasma membrane and these organized units potentially provide specificity for the downstream signaling events in plants (Bücherl et al., 2017). Nonetheless, how exactly the upstream perception event communicates with intracellular components during plant immune signaling remains largely unknown. Notably, a variety of organelles are found in close proximity with the plasma membrane in plant cells, such as the endoplasmic reticulum (ER). This organelle occupies a large volume in the cell and exerts multiple functions, including protein and lipid synthesis, calcium storage, vesicular trafficking, as well as biogenesis of other organelles (Phillips and Voeltz, 2016). Moreover, it is known to further compartmentalize into sheets and tubules, along with a variety of microdomains, to enable its versatile functions (English et al., 2009). In *Arabidopsis*, the ER makes contact with the plasma membrane through the ER–PM contact site (EPCS), with synaptotagmin 1 (SYT1) and vesicle-associated protein 27 (VAP27) as tethers that mediate EPCS formation (Perez-Sancho et al., 2016). The presence of membrane contact site (MCS) defines a unique feature of eukaryotes. More and more pieces of evidence have shown that MCS form transiently between two membrane compartments, creating a bridge for interorganelle communication, such as exchanges of metabolite, cellular stress response, membrane dynamics, and signaling (Prinz et al., 2020). However, to date, not much is known about the association of cellular organelles with the PRRs and their role in plant immune responses.

Previously, we demonstrated that tomato (*Solanum lycopersicum*) *Sl*SOBIR1 and *Sl*SOBIR1-like are required for the perception of the elicitin ParA1, a MAMP from the oomycete pathogen *Phytophthora parasitica*, and for plant defense against this pathogen (Peng et al., 2015). We documented that *Sl*SOBIR1 is translocated from the plasma membrane to endosomes in response to ParA1 treatment, which suggests that *Sl*SOBIR1 endocytosis is coupled to the plant immune signaling. To further tackle the function and regulation of SOBIR1, we took the biochemical approach to look for SOBIR1-interacting proteins. In this study, we report a novel RLP from *Nicotiana benthamiana,* named *Nb*RLP1 that encodes an unconventional RLP protein residing within the ER membrane, but not the plasma membrane. By using bimolecular fluorescence complementation and tandem-affinity purification, we validated the interaction between *Nb*RLP1 and *Nb*SOBIR1. In addition, we observed that *Nb*SOBIR1 formed microdomains on the plasma membrane whose dynamics is coupled to the remodeling of the ER. Further evidence supports that *Nb*RLP1 downregulates the number of *Nb*SOBIR1 microdomains and promotes *Nb*SOBIR1 internalization in the presence of ParA1 that triggers partitioning of *Nb*SOBIR1 into the microdomains. As overexpressing *Nb*RLP1 exaggerated the ParA1-induced necrosis in plants, we propose that ER and unconventional RLPs in the ER, such as *Nb*RLP1, are engaged in SOBIR1-mediated plant immunity through mediating MAMP-induced SOBIR1 internalization.

RESULTS

Like *NbSOBIR1*, *NbRLP1* Is Highly Induced Upon *Phytophthora parasitica* Infection

*Sl*SOBIR1 is involved in PTI response to the *P. parasitica* MAMP termed ParA1 (Peng et al., 2015). To identify proteins associated with *Sl*SOBIR1 during the process, we treated *Nicotiana benthamiana* harboring *Sl*SOBIR1-GFP with ParA1, followed by immunoprecipitation with anti-GFP antibody. Among a collection of putative *Sl*SOBIR1-interacting proteins, we selected one of the major candidates, NbS0003586g0006.1 [Niben.0.4.4., Sol genetic network (SGN[1])] for further analysis. In contrast to no signal in the control without reverse transcriptase, two major transcripts were detected by reverse transcriptase-PCR reaction (**Figure 1A**). One is a 2.91 Kb cDNA (GenBank Accession number MW924093), which corresponds to the exact genomic DNA sequence of *NbRLP1*, and the other shorter cDNA of 1.41 Kb lacks the putative intron sequence (MW924094), reflecting a spliced form of *NbRLP1* (**Supplementary Table 1**). We focused on the 2.91-Kb gene, named NbRLP1 hereafter, that encodes a 969-amino acid protein with a characteristic of RLPs (**Figure 1A**).

Phylogenetic analysis of *NbRLP1* and its homologs from Solanaceae retrieved from the NCBI databases indicates that XP_009784945 of *Nicotiana sylvestris* and XP_019244125 of *Nicotiana attenuata* are close homologs of *NbRLP1* (**Figure 1B**). These genes along with AAC78592 (Hcr2-0A) and AAC78593

[1]http://solgenomics.net/

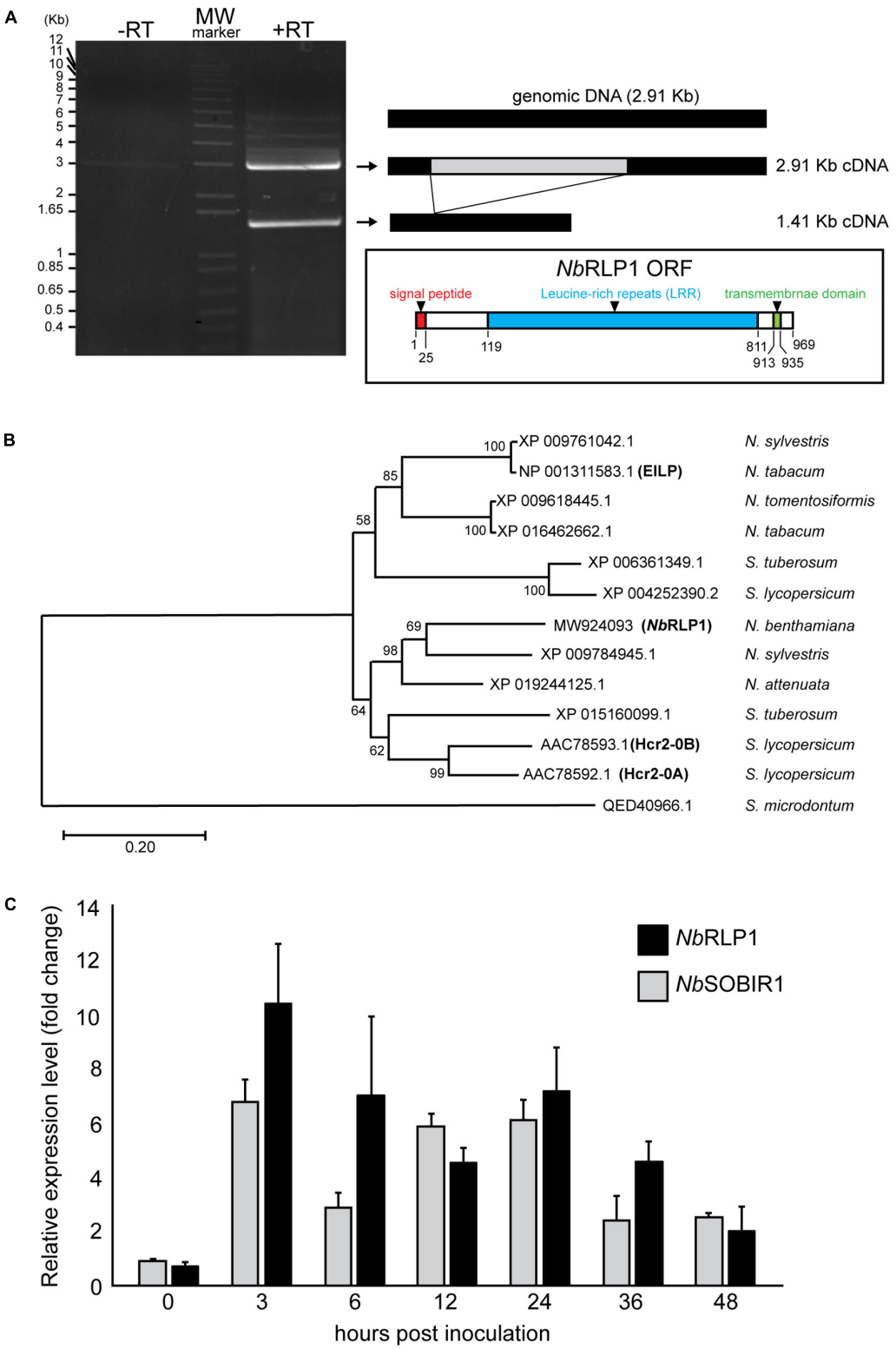

FIGURE 1 | The expression of *Nb*RLP1 is induced in response to infection by *Phytophthora parasitica*. **(A)** *Nb*RLP1 is alternatively spliced. Reverse transcriptase-polymerase chain reaction (RT-PCR) gave rise to two amplified products with respective length of 1.41 and 2.91 Kb (+ RT), which were not detected in the absence of reverse transcriptase (-RT). The 2.91-Kb gene, named *NbRLP1* (MW924093) encodes a 969-amino acid protein containing a signal peptide (predicted by SignalP), an LRR domain (predicted by InterPro), and a transmembrane domain (predicted by TMHMM) as illustrated in the inset. **(B)** Phylogenetic

(Continued)

FIGURE 1 | Continued
analysis of *Nb*RLP1. Multiple sequence alignment of *Nb*RLP1 and its homologs from *Nicotiana* and *Solanum* retrieved from the protein database of the National Center for Biological information (NCBI) was performed by using ClustalX. The phylogenetic tree was constructed by employing the maximum likelihood method, followed by bootstrap analysis with 1,000 pseudo-replicates. **(C)** The expression of the *Nb*RLP1 and *Nb*SOBIR1 is upregulated in response to *P. parasitica* infection. At the indicated hours post *P. parasitica* zoospore inoculation of *Nicotiana benthamiana,* total RNAs were isolated and analyzed by quantitative reverse transcription PCR (RT-PCR). Data are presented as fold-change relative to mock treatment of the same time point. Values are means (±SE) from three independent experiments.

(Hcr2-0B), two homologs of tomato disease resistance gene, Cf-5 (Dixon et al., 1998), form a clade distinct from that encompassing elicitor-inducible EILP of *Nicotiana tabacum* (Takemoto et al., 2000). As well, these two clades are distinguished from ELR of *Solanum microdontum* (QED40966), an RLP involved in the recognition of *Phytophthora* elicitins (Du et al., 2015).

To know whether *NbRLP1* is induced by pathogen infection, we infected *N. benthamiana* with *P. parasitica* zoospores and performed quantitative RT-PCR, with the expression level of elongation factor 1 alpha (*NbEF1a*) serving as an internal control. The results showed that the expression of *NbRLP1*, like *NbSOBIR1*, was largely induced 3 h post-inoculation (hpi) and persists high expression through later infection stage to at least 36 hpi (**Figure 1C**). Collectively, these data imply a potential role of *Nb*RLP1 for plant defense responses.

*Nb*RLP1 Is a Transmembrane Protein Localized to the ER

To protect against pathogens, plant cells possess a variety of transmembrane RLKs and RLPs on the plasma membranes, many of which contain extracellular LRR domains to enable ligand recognition. Intriguingly, when we analyzed *Nb*RLP1 localization by the use of GFP fused to either amino- or carboxyl-terminus of *Nb*RLP1 for fluorescence microscopy, we observed a distribution pattern of network and/or multiple puncta near the cell cortex (**Figure 2A**). As it resembles the plant ER network, we next examined cells coexpressing *Nb*RLP1-GFP with the plasma membrane marker *At*ACA8-mCherry (**Figure 2B**) or the ER marker mCherry-KDEL (**Figure 2C**). The results showed that *Nb*RLP1-GFP localization is in large agreement with the luminal ER protein mCherry-KDEL but not with the evenly distributed *At*ACA8-mCherry signal of the plasma membrane. Thus, we conclude that *Nb*RLP1 is an unconventional RLP localizing to the ER rather than the plasma membrane. Based on sequence prediction results, *Nb*RLP1 is likely to adapt the standard type I transmembrane protein topology in the ER as depicted in **Figure 2D**. The main moiety of this protein, containing LRR, is in the ER lumen, and the protein also contains a single spanning transmembrane helix and a short cytoplasmic tail.

*Nb*RLP1 Interacts With *Nb*SOBIR1

To consolidate the potential relationship between *Nb*RLP1 and *Nb*SOBIR1, we first employed the bimolecular fluorescence complementation (BiFC) assay, known to provide *in situ* interacting information *in planta*. Our results indicate that *Nb*RLP1-Vn, but not Vn-*Nb*RLP1, interacts with *Nb*SOBIR1-Vc in plants, thus showing Venus YFP fluorescence, in contrast to no or dim signals of various negative controls (**Figure 3A**). The fact that only Vn fused to *Nb*RLP1 at the C-terminus but not to N-terminus gave a positive BiFC signal, which is consistent with the topological prediction of *Nb*RLP1 in the ER (**Figure 2D**). Since *Nb*RLP1 is an ER protein and *Nb*SOBIR1 is a plasma membrane protein, we hypothesize that their interaction most likely is achieved through close proximity between the ER and plasma membrane. To know whether *Nb*RLP1 may partition into the previously characterized EPCS, *Nb*RLP1-GFP was coexpressed with the EPCS tether *At*SYT1-mCherry. Indeed, we observed that signals of the two proteins colocalized at the cell periphery (**Supplementary Figure 1**). Thus, these results imply that the ER-localized *Nb*RLP1 might interact with the plasma membrane-localized *Nb*SOBIR1 protein *in vivo*, likely at a position where cortical ER and the plasma membrane join in physical proximity, such as the EPCS tethered by *At*SYT1-mCherry.

We next performed biochemical studies to further strengthen the notion that *Nb*RLP1 interacts with *Nb*SOBIR1. To achieve this, we generated an *Nb*RLP1 harboring a TAP tag (an S-tag followed by a protein A tag) at its C-terminus and asked whether the fusion protein (termed *Nb*RLP1-TAP) binds *Nb*SOBIR1-mCherry in detergent-solubilized plant extracts. To unambiguously judge the interaction, we also tested whether *Nb*RLP1-TAP binds another plasma membrane protein *At*ACA8-mCherry. Our results showed that *Nb*SOBIR1-mCherry, but not *At*ACA8-mCherry, was pulled down by *Nb*RLP1-TAP, examined by Western blotting using an antibody against mCherry (**Figure 3B**) as well as mass spectrometry (not shown). In contrast, *Nb*SOBIR1 signal has never been detected in the pulled-down fractions derived from TAP-alone expressing samples, indicative of specificity. Intriguingly, Western blotting data revealed two major forms of *Nb*SOBIR1-mCherry with a size difference of ∼8.5 kD in the inputs; however, only *Nb*SOBIR1-mCherry with the higher molecular weight was pulled down by *Nb*RLP1-TAP (**Figure 3B**). Notably, the expression of *Nb*RLP1-TAP but not TAP alone in plants reduced the proportion of the larger molecular weight form of *Nb*SOBIR1 in the steady state (**Figure 3C**), implying that *Nb*RLP1-TAP not only binds to this unique form of *Nb*SOBIR1 but may further reduce its expression or accelerate its turnover.

The BiFC data supports that the short tail of *Nb*RLP1 fused with Vn interacts with the cytoplasmic domain of *Nb*SOBIR1 fused with Vc. To know the contribution of the N-terminal LRR domain and the short C-terminal cytoplasmic tail of *Nb*RLP1 to its interaction with *Nb*SOBIR1, we also prepared

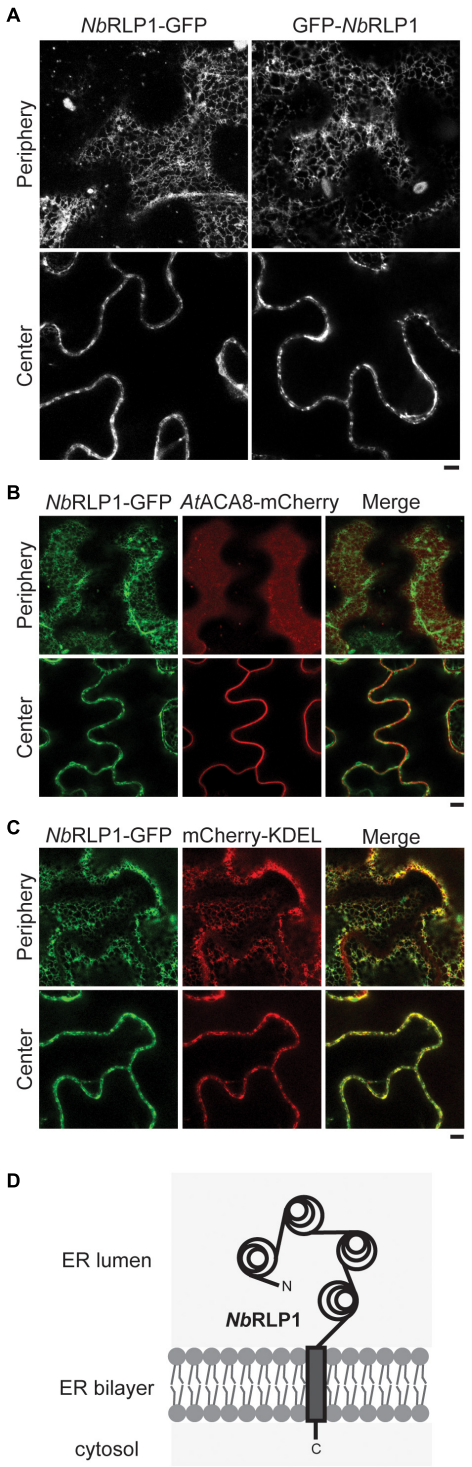

FIGURE 2 | *Nb*RLP1-GFP resides in the endoplasmic reticulum (ER) membrane. **(A)** Still images of *Nb*RLP1-GFP or GFP-*Nb*RLP1 taken from the periphery or the center of the same *Nicotiana benthamiana* leaves by Zeiss LSM880 confocal microscope. Scale bar, 5 μm. **(B)** Same as A, except that *Nb*RLP1-GFP and *At*ACA8-mCherry are coexpressed in plants and imaged. Also shown are the corresponding merged images. **(C)** Same as B, except that *Nb*RLP1-GFP and mCherry-KDEL are coexpressed in plants and imaged. **(D)** A scheme depicting *Nb*RLP1 topology in the ER based on TMHMM.

different truncated versions of *Nb*RLP1. Analysis by using the biochemical pulled-down assay indicates *Nb*RLP1-ΔC-TAP with the short cytoplasmic tail removed still bound with *Nb*SOBIR1 (**Supplementary Figure 2A**). In contrast, *Nb*RLP1-ΔN-TAP, having signal peptide but lacking the large LRR domain, is bound to *Nb*SOBIR1 with reduced affinity (**Supplementary Figure 2A**). Although the *Nb*RLP1 with cytoplasmic tail and a transmembrane anchor seems to be sufficient for binding with *Nb*SOBIR1, the result implies that other proteins in the ER or the plasma membrane may bridge or stabilize the interaction between *Nb*RLP1 and *Nb*SOBIR1 (**Supplementary Figure 2B**). Collectively, both *in vivo* and *in vitro* data support the notion that the ER-localized *Nb*RLP1 interacts with the plasma membrane-localized *Nb*SOBIR1.

*Nb*SOBIR1 Is Partitioned Into a Dynamic Microdomain on the Plasma Membrane

Having established that *Nb*RLP1 interacts with *Nb*SOBIR1, we next explored the potential regulatory mechanism underlying their interplay *in planta*. The observation of two major forms of *Nb*SOBIR1-mCherry, while only one form is capable of binding with and being regulated by *Nb*RLP1, prompted us to investigate whether *Nb*SOBIR1 may associate with distinct structures on the plasma membrane. We thus performed confocal microscopy with Airyscan to gain insights into *Nb*SOBIR1-mCherry localization on the plasma membrane. Interestingly, in addition to the dispersed signal along the plasma membrane, *Nb*SOBIR1-mCherry was identified in several punctate structures, which was not observed when another plasma membrane protein, *At*ACA8-mCherry, was subjected to imaging by the Airyscan microscopy (**Figure 4A**). Thereby, we suggest that a portion of *Nb*SOBIR1 is likely partitioned into microdomains on the plasma membrane.

To further understand the nature of *Nb*SOBIR1-mCherry microdomains on the plasma membrane, we imaged these fine structures using time-lapse microscopy with a time interval of 5 s. The results clearly showed that these plasma membrane microdomains of *Nb*SOBIR1 are mobile structures, although a small portion of them appeared relatively more static (**Figure 4B** and **Supplementary Movie 1**). Particle tracking analysis data indicated that the *Nb*SOBIR1-mCherry microdomains can move laterally, showing an irregular pattern (**Figure 4B**). During the course of our analysis, we also observed the disappearance (**Figure 4B**, green circle) and emergence (**Figure 4B**, yellow circle) of these microdomains on the plasma membrane. In either case, it appears to involve a quick biogenesis and turnover process, detected within the time interval of 5 s. Considering SOBIR1 functions as an adaptor protein that assembled together with various LRR-RLPs into a receptor complex on the plasma membrane awaiting ligand binding, partitioning of SOBIR1 into microdomains may serve as a platform to facilitate such a process. Overall, these observations have led us to hypothesize that the dynamics of these microdomains of *Nb*SOBIR1 is a regulated process and that the microdomain structure may represent one of the functional forms of *Nb*SOBIR1.

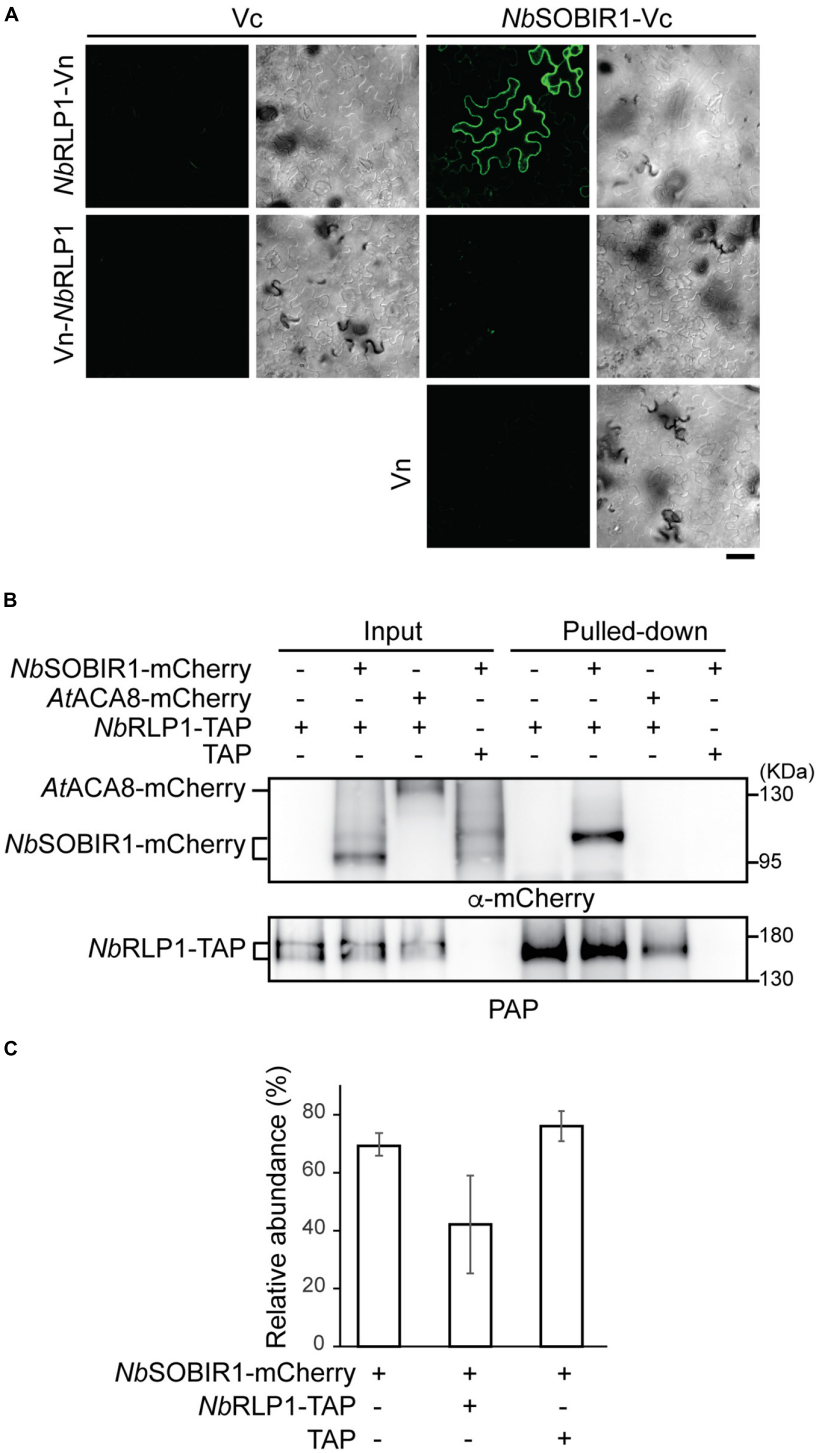

FIGURE 3 | *Nb*RLP1 interacts with *Nb*SOBIR1. **(A)** The carboxyl half of Venus protein (Vc) alone or fused to *Nb*SOBIR1 was coexpressed with the amino half of Venus (Vn) alone or fused to *Nb*RLP1 as indicated on the *Nicotiana benthamiana* leaves. Images were taken by Zeiss LSM880 confocal microscope. Complemented Venus fluorescence and differential interference contrast (DIC) images of the same area are shown. Scale bar, 40 μm. **(B)** *N. benthamiana* leaves expressing *Nb*SOBIR1-mCherry, *At*ACA8-mCherry, *Nb*RLP1-TAP, or TAP as indicated were harvested and lyzed. The lysate (input) was subjected to pull-down by IgG Sepharose as described in the Materials and Methods section. The input and the bound (pulled-down) fractions were subjected to SDS-PAGE followed by the Western blot analysis with the use of anti-mCherry and PAP antibodies. **(C)** *N. benthamiana* leaves expressing *Nb*SOBIR1-mCherry, *Nb*RLP1-TAP, or TAP as indicated were lyzed and *Nb*SOBIR1-mCherry proteins in the lysate were subjected to SDS-PAGE followed by Western blot analysis with anti-mCherry antibody. The ratio of the upper *Nb*SOBIR1 band (with higher molecular mass) relative to the total *Nb*SOBIR1 (combining both the upper and lower bands of *Nb*SOBIR1) was plotted and compared. Data from three experimental repeats are shown as means (± SD).

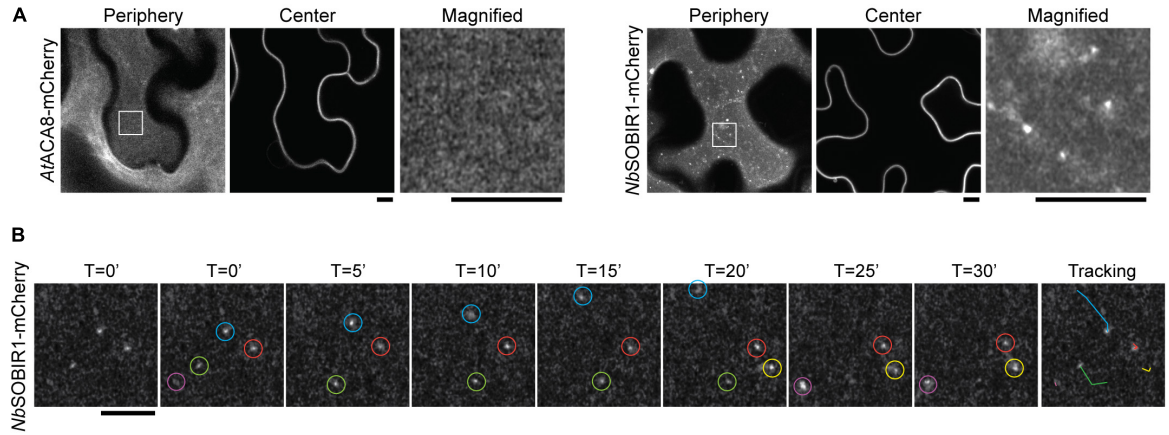

FIGURE 4 | *Nb*SOBIR1-mCherry forms microdomains in the plant plasma membrane. **(A)** *Nicotiana benthamiana* leaves expressing *At*ACA8-mCherry or *Nb*SOBIR1-mCherry were imaged at the periphery or center sections using Zeiss LSM880 confocal microscope with Airyscan. The box area in the image of the periphery section was enlarged and displayed to show the microdomains of *Nb*SOBIR1 that were not detectable on *At*ACA8-mCherry images. Scale bar, 5 μm. **(B)** *N. benthamiana* leaves expressing *Nb*SOBIR1-mCherry was subjected to time-lapse microscopy by Zeiss LSM880 confocal microscope with the Airyscan. The total image acquisition length was 16 min with a time interval of 5 s (**Supplementary Movie 1**). Representative area was selected for particle tracking analysis using the ImageJ, and the image of each time point is shown. Five microdomains, each circled by different colors were identified in the displayed image and their tracks are shown in the right-most image.

ER Remodeling Is Coupled to the Dynamics of *Nb*SOBIR1 Microdomains

Given that the aforementioned *Nb*SOBIR1-*Nb*RLP1 interaction depends on close proximity between the ER and the plasma membrane, we further asked whether these *Nb*SOBIR1 microdomains may have an association with the ER. The eukaryotic ER is organized into a complicated network containing various degrees of sheets and tubules (Shibata et al., 2006; English et al., 2009). The highly dynamic ER disperses throughout the entire cytoplasm and is thought to fine-tune cell physiology to cope with environmental cues. When the localization of *Nb*RLP1-GFP was compared with *Nb*SOBIR1-mCherry, we noticed that *Nb*SOBIR1-mCherry was either associated with the edge of the ER sheets or surrounded by the three-way junction of the ER tubules labeled with *Nb*RLP1 at the cell periphery (**Figure 5A**).

Employing time-lapse microscopy, we observed that ER labeled by *Nb*RLP1-GFP constantly undergoes morphological remodeling (**Figure 5B** and **Supplementary Movie 2**). Most importantly, the lateral movement of *Nb*SOBIR1 microdomains was correlated with the dynamic changes of the ER, as the ER labeled with *Nb*RLP1 always associated with the movement of the *Nb*SOBIR1 microdomains (**Figure 5B**, blue and white circles, and **Supplementary Movie 2**). The correlation of the *Nb*SOBIR1 microdomains with the cortical ER suggests that these microdomain structures are likely where *Nb*SOBIR1 makes contact with *Nb*RLP1 at the first place in their native state. Intriguingly, we observed that *Nb*SOBIR1-mCherry microdomains diminished in the condition when a wave of ER sheets transit through the cell cortex during ER remodeling (**Figure 5B**, white box). In addition, we observed *Nb*SOBIR1 microdomains originally surrounded by ER tubules disappeared in the next time point with the same area being replaced with ER sheets (**Figure 5B**, white and blue arrowheads). Collectively, the evidence in which *Nb*SOBIR1 microdomain dynamics is correlated with ER remodeling raises an interesting possibility that ER may contribute to *Nb*SOBIR1-mediated endocytosis and/or plant immunity.

*Nb*RLP1 Overexpression Promotes *Nb*SOBIR1 Endocytosis Upon ParA1 Elicitin Treatment

In our previous paper, we have established that *Sl*SOBIR1 endocytosis is triggered by the perception of an oomycete MAMP termed, ParA1. If the *Nb*SOBIR1 microdomain defines a functional unit for the protein, we suspect that this structure is likely responsive to ParA1. Accordingly, we treated the *Nb*SOBIR1-overexpressing plants with ParA1 to compare with the treatment with MES buffer, followed by Airyscan confocal microscopy to monitor the extent of *Nb*SOBIR1 microdomain formation on the plasma membrane. Our results clearly showed that the number of *Nb*SOBIR1 microdomain formed on the plasma membrane increased significantly in the ParA1-treated condition compared to the MES control, and the quantification results based on a number of cells examined further support the notion (**Figure 6A**). Remarkably, ParA1 treatment resulted in the formation of more *Nb*SOBIR1-mCherry microdomains of a larger size which appeared more static (**Figure 6A** and **Supplementary Movie 3**). Time-lapse microscopy experiments performed with *N. benthamiana* plants coexpressing *Nb*RLP1 identified that these larger *Nb*SOBIR1-mCherry puncta though relatively more static can become diminished and/or disappear quickly (**Figure 6B**, blue and yellow circles, and **Supplementary Movie 4**), representing the occurrence of either endocytosis or diffusion upon ParA1 perception. While focusing on the focal plane containing

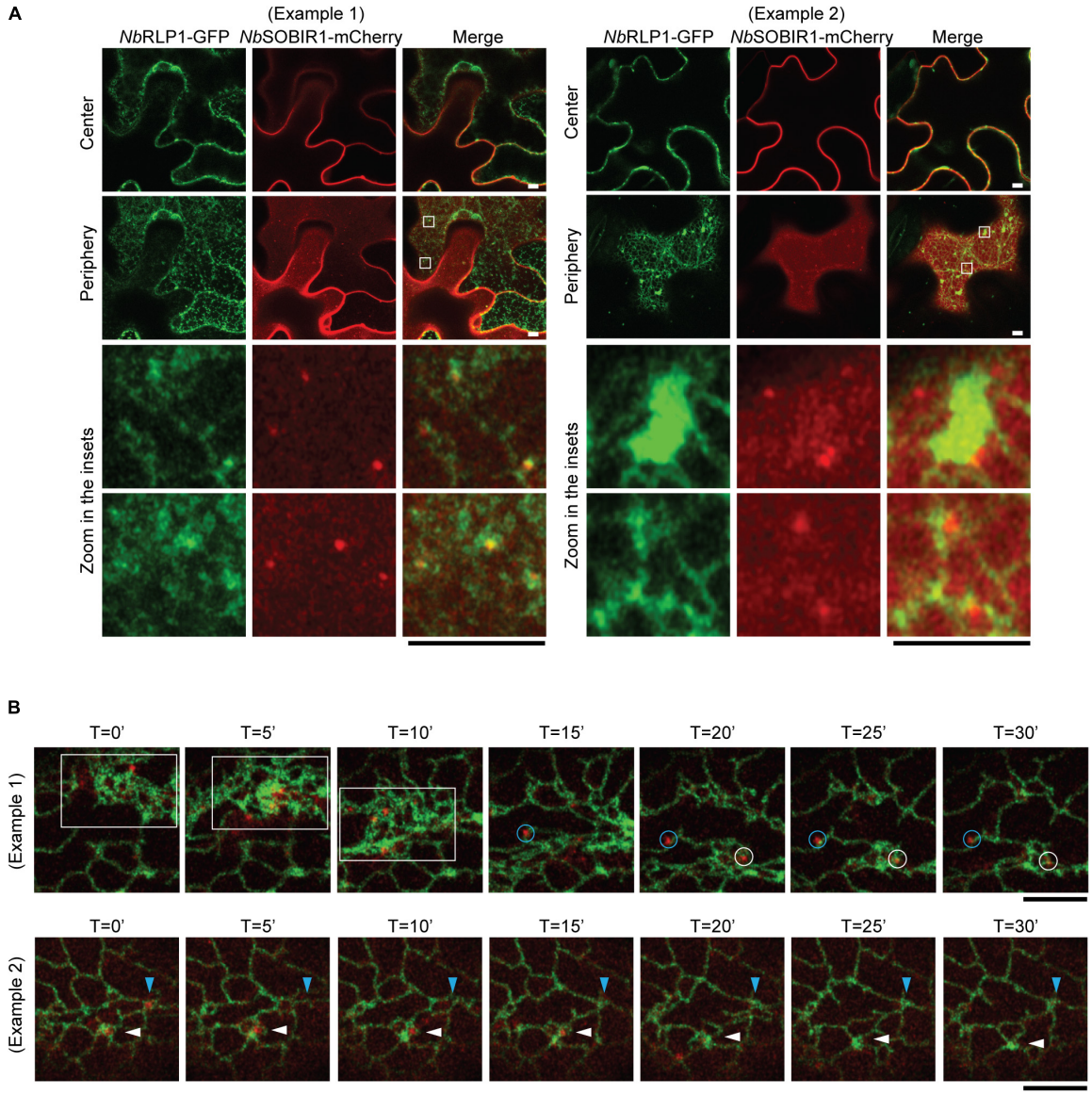

FIGURE 5 | The *Nb*SOBIR1 microdomains in the plasma membrane move as the cortical ER changes the morphology**. (A)** *Nicotiana benthamiana* leaves expressing *Nb*SOBIR1-mCherry and *Nb*RLP1-GFP were subjected to confocal microscopy by Zeiss LSM880 with use of Airyscan. The periphery and center sections of the epidermal cell of the same leaf were imaged, and the insets were enlarged to reveal the association between *Nb*SOBIR1-mCherry and *Nb*RLP1-GFP. Examples 1 and 2 show different degrees of ER tubules and sheets marked by *Nb*RLP1-GFP to reveal how *Nb*SOBIR1 microdomains are associated with the ER.
(B) *N. benthamiana* leaves expressing *Nb*SOBIR1-mCherry and *Nb*RLP1-GFP were subjected to time-lapse microscopy by Zeiss LSM880 confocal microscope with use of Airyscan. The total image acquisition length was 16 min with a time interval of 5 s (**Supplementary Movie 2**). Representative area was selected for display by time course. (Example 1) White box area, containing several *Nb*SOBIR1 microdomains, represents movement of these structures after a quick remodeling of the ER harboring high degree of sheets. Blue and white circles denote two *Nb*SOBIR1 microdomains associated with ER tubules. (Example 2) Blue and white arrowheads denote two *Nb*SOBIR1 microdomains that are internalized from the cell surface as the ER transformed from tubules to sheets. Scale bar, 5 μm.

the ParA1-induced static *Nb*SOBIR1 microdomains, time-lapse microscopy revealed that these structures move inward from the cell cortex, which supports that endocytosis of *Nb*SOBIR1 occurs directly through the microdomain structures upon ParA1 perception (**Supplementary Figure 3**).

We further investigated the potential role of *Nb*RLP1 for *Nb*SOBIR1 endocytosis under ParA1 treatment based on a condition we reported previously (Peng et al., 2015). First, we asked whether coexpressing *Nb*RLP1 and *Nb*SOBIR1 affect *Nb*SOBIR1 endocytosis in response to ParA1 treatment. Compared to the control coexpressing GFP and *Nb*SOBIR1-mCherry, more intracellular vesicles harboring *Nb*SOBIR1-mCherry were observed on tobacco leaves coexpressing *Nb*RLP1-GFP and *Nb*SOBIR1-mCherry in response to ParA1 treatment (**Figure 6C**). Given that ParA1 treatment induced the formation of *Nb*SOBIR1 microdomains and that *Nb*RLP1 overexpression

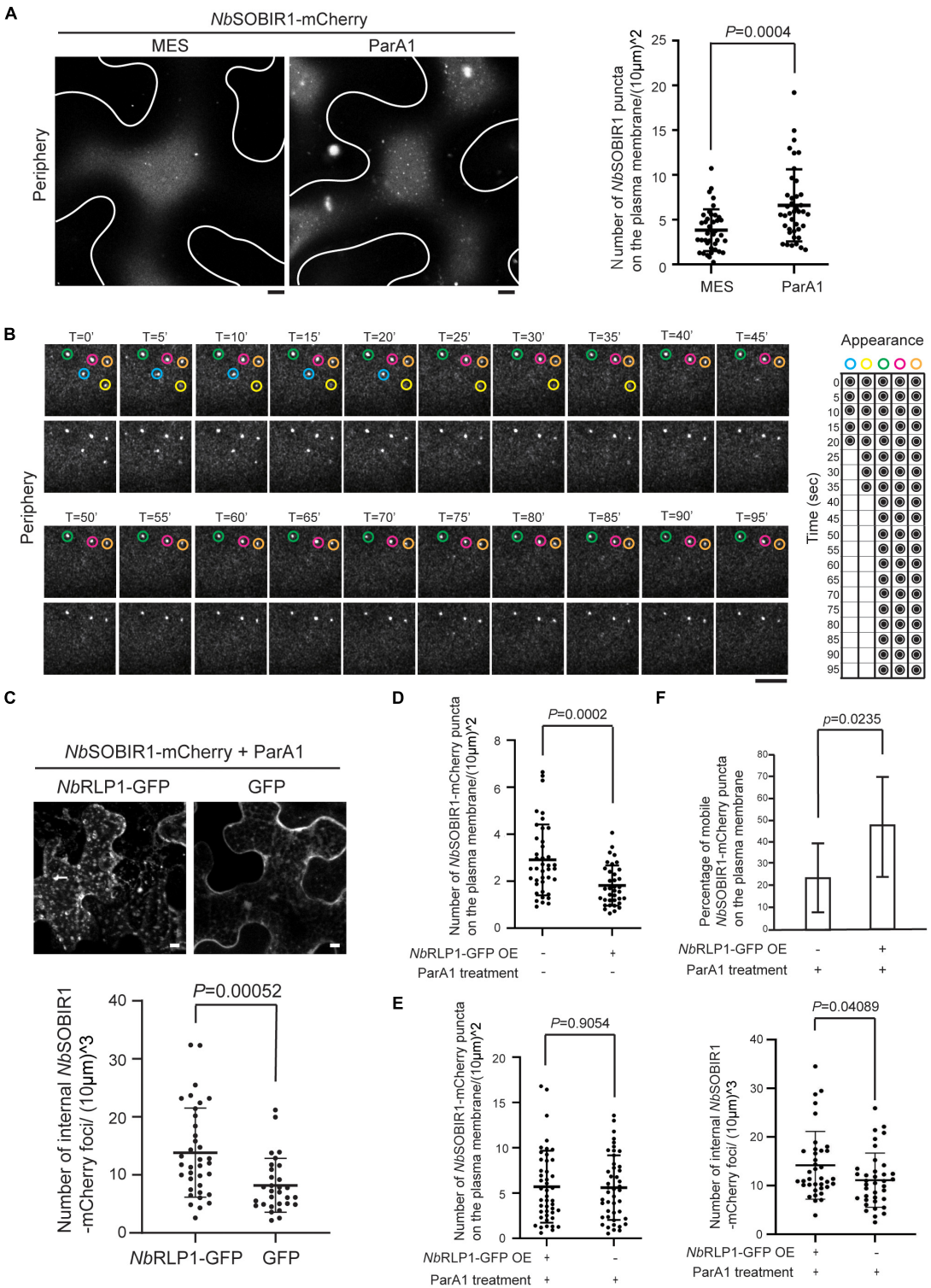

FIGURE 6 | *Nb*RLP1-GFP overexpression promotes *Nb*SOBIR1-mCherry endocytosis upon ParA1 elicitin treatment. **(A)** *Nicotiana benthamiana* leaves expressing *Nb*SOBIR1-mCherry were infiltrated with MES buffer alone (control) or 0.3 μMParA1 in MES buffer. After 30 min, the leaves were subjected to microscopy, focusing only on the periphery of the leaf epidermal cell, using the Zeiss LSM880 confocal microscope with an Airyscan. Representative images are shown on the left panel with an outline of the cell, and the quantification data using the scatter plot is shown on the right. Statistics is carried out by the two-tailed student's *t*-test and the.

(Continued)

FIGURE 6 | Continued
p-value is displayed. **(B)** *N. benthamiana* leaves expressing *Nb*SOBIR1-mCherry and *Nb*RLP1-GFP were infiltrated with 0.3 μM ParA1 in MES buffer. After 30 min, leaves were subjected to time-lapse microscopy using Zeiss LSM880 confocal microscope with Airyscan. The total image acquisition length was 16 min with a time interval of 5 s (**Supplementary Movie 4**). Representative area was selected for display by time course, and the appearance and absence of each microdomain at each displayed time point was summarized on the right. Blue and yellow circles mark two *Nb*SOBIR1 microdomains with a larger size undergoing endocytosis during the imaging time frame. Green, pink, and orange circles mark *Nb*SOBIR1 microdomains with a larger size that remain static during the imaging time frame. **(C)** *N. benthamiana* leaves expressing *Nb*SOBIR1-mCherry and *Nb*RLP1-GFP or GFP alone were infiltrated with 0.3 μM ParA1 in MES buffer. After 30 min, leaves were subjected to microscopy with five Z stack for a total of 8.20 mm stack size using Zeiss LSM 510 confocal microscope. The maximal projection images are shown. The number of internal *Nb*SOBIR1-mCherry puncta was quantified as described in the Materials and Methods section and displayed using a scatter plot. Statistical analysis was carried out with the two-tailed student's *t*-test and the *p*-value is shown. **(D)** *N. benthamiana* leaves expressing *Nb*SOBIR1-mCherry alone or coexpressed with *Nb*RLP1-GFP were subjected to microscopy using the Zeiss LSM880 confocal microscope with an Airyscan. Microdomain number was quantified as described in the Materials and Methods section and shown as scatter plots. Statistics is carried out with the two-tailed student's *t*-test and the *p*-value is displayed. **(E)** *N. benthamiana* leaves expressing NbSOBIR1-mCherry alone or coexpressing with NbRLP1-GFP were treated with 0.3 μM ParA1. After 30 min, leaves were subjected to microscopy by Zeiss LSM880 confocal microscope with the use of Airyscan. Microdomain number (left) was quantified as in **(D)**. The same leaves were subjected to Zeiss LSM880 confocal imaging and quantified for internal NbSOBIR1-mCherry foci number (right) as in **(C)**. Statistics is carried out with the two-tailed student's *t*-test and the *p*-values are displayed. **(F)** *N. benthamiana* leaves expressing NbSOBIR1-mCherry alone or coexpressing with NbRLP1-GFP were infiltrated with 0.3 μM ParA1. After 30 min, leaves were subjected to time-lapse microscopy by Zeiss LSM880 confocal microscope with the use of Airyscan. The ParA1-induced microdomains were quantified if their size was bigger than 0.4 mm in diameter. A total of 10 cells for each treatment was quantified within an imaging timeframe of 60 s and data are shown as percentage (number of mobile puncta/number of total puncta). Statistics is carried out with the two-tailed student's *t*-test and the *p*-value is displayed.

promoted ParA1-induced *Nb*SOBIR1 endocytosis, it seems plausible to predict that *Nb*RLP1 overexpression may facilitate *Nb*SOBIR1 endocytosis, thereby reducing the number of *Nb*SOBIR1 microdomains on the plasma membrane. As shown in **Figure 6D**, in the absence of ParA1, a condition when fewer *Nb*SOBIR1 microdomains were visualized, *Nb*RLP1 overexpression caused a significant reduction in the number of *Nb*SOBIR1 microdomains present on the plasma membrane. In the presence of ParA1, although overexpressing *Nb*RLP1 did not significantly reduce the number of *Nb*SOBIR1 microdomains on the plasma membrane (**Figure 6E**, left panel), it appears to accelerate the mobility of *Nb*SOBIR1 microdomains as reflected by the higher percentage of mobile *Nb*SOBIR1 puncta detected on the plasma membrane (**Figure 6F**). Moreover, overexpressing *Nb*RLP1 led to the detection of more *Nb*SOBIR1-mCherry-labeled structures inside the plant cells, indicative of more active *Nb*SOBIR1 endocytosis (**Figure 6E**, right panel). Collectively, these data have led us to propose that the ParA1 elicitin-inducible *Nb*SOBIR1 microdomain formed on the plasma membrane likely represents an active unit of *Nb*SOBIR1 for subsequent receptor-mediated endocytosis and that *Nb*RLP1 might act as a positive regulator for *Nb*SOBIR1 internalization.

Overexpressing *Nb*RLP1 Exaggerated the ParA1-Induced Necrosis in Plants

Our data have supported that the unconventional *Nb*RLP1 in ER underlies part of the regulatory network for *Nb*SOBIR1, the essential adaptor for various LRR-RLPs, and thus it seems likely that *Nb*RLP1 might contribute to the *Nb*SOBIR1-associated PTI. To explore this possibility, we analyzed the effect of *Nb*RLP1 overexpression on ParA1-induced necrosis, a downstream output of plant immune response. Consistent with our previous findings, ParA1 induced the formation of necrotic lesions on *N. benthamiana* leaves at 24 h post-treatment (**Figure 7**). *Nb*RLP1 silencing under either *Nb*RLP1 endogenous or overexpressing conditions did not cause a significant change for the ParA1-induced necrosis on *N. benthamiana* leaves when compared to the control group. However, when ParA1 treatment was carried out in the *N. benthamiana* plants overexpressing *Nb*RLP1-GFP, a condition when more *Nb*SOBIR1 endocytic vesicles were observed (**Figure 6C**), we observed that necrotic lesions on *N. benthamiana* leaves were more exaggerated as evaluated by ANOVA. Altogether, these results support that *Nb*RLP1 acting as a regulator lies within the repertoire of *Nb*SOBIR1-mediated PTI.

DISCUSSION

To combat pathogen infection, plants have evolved PRRs, which detect MAMPs at the cell surface to elicit PTI. Studies in various plant systems demonstrated that SOBIR1 plays a central role in PTI involving various PRRs of the LRR-RLP type (Tang et al., 2017; Domazakis et al., 2018). SOBIR1 moves from the plasma membrane to endocytic vesicles *via* endocytosis in response to MAMP treatment (Liebrand et al., 2013; Peng et al., 2015). However, how exactly SOBIR1 functions in plant immune response remains largely elusive.

Located at the outermost boundary of the cell as to communicate with the environment, the plasma membrane is known to be compartmentalized into subdomains, where immune complexes may be formed even in the absence of matching ligand, enabling rapid transmission and activation of diverse immune responses (Jarsch et al., 2014; Somssich et al., 2015; Bücherl et al., 2017). In this study, we report the identification of dynamic microdomains of *Nb*SOBIR1 on the plasma membrane, which reinforces the important concept of nano- and micro-domains in plant immune response.

We document in this study that the ParA1 elicitin treatment induced both in the number and size of *Nb*SOBIR1-labeled microdomaind, formed on the plasma membrane (**Figure 6A**), concomitant with the induction of *Nb*SOBIR1 internalization, reflecting that the protein forms clusters in response to elicitin perception in *N. benthamiana*. The importance of nano- and micro-domains for plant innate immunity has been

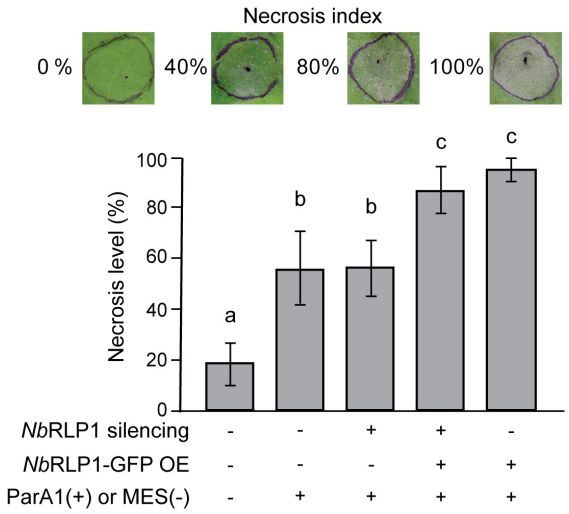

FIGURE 7 | *Nb*RLP1 overexpression exaggerated the ParA1-induced necrosis on *Nicotiana benthamiana* leaves. *N. benthamiana* leaves that are either silenced for *Nb*RLP1 expression or overexpressing *Nb*RLP1 are infiltrated with 0.3 μM ParA1 or 10 mM MES (control) as indicated. After 24 h, the development of cell death was analyzed based on the representative necrosis index, defined by the percentage of necrosis area over the infiltrated area. The experiment has been repeated four times with similar results, and only one set of the experimental result is shown. Values are means (± SD) of 18 biological repeats. Different letters indicate significant differences based on LSD ($p < 0.01$).

demonstrated in a number of recent studies. In the response of rice (*Oryza sativa*) to chitin elicitor, microdomains are required for the dynamics of the plasma membrane-anchored Rac/ROP small GTPase Rac1 (a molecular switch in defense signaling) and NADPH oxidase-encoding respiratory burst oxidase homologs (RBOHs) (Nagano et al., 2016). As well, the immune receptor FLS2 required for the perception of flg22 also localizes to the plasma membrane nanodomains of *Arabidopsis* (Bücherl et al., 2017). Consistently, *Nb*SOBIR1 microdomain we discovered here plays a crucial role in the PTI regulated through PRRs of the RLP type.

Our findings uncovered *Nb*RLP1 as a novel player in underlying the network of *Nb*SOBIR1-mediated PTI response, which led to a yet unexplored area regarding the engagement of ER during *Nb*SOBIR1 endocytosis and/or plant immunity. Using the *in vivo* BiFC assay and the *in vitro* pulled-down assay, we document in this study that the plasma membrane-localized *Nb*SOBIR1 interacts with the ER-localized transmembrane protein *Nb*RLP1, whose LRR domain resides within the ER lumen (**Figure 3**). This result also predicts that *Nb*RLP1 and *Nb*SOBIR1 might interact *via* a close association between the ER and the plasma membrane, such as EPCS or the ER-endosomes interface (Dong et al., 2016). However, BiFC fluorescence may emit artificially due to close proximity of target proteins, and the assay results in the irreversible formation of fluorescent proteins, thus limiting its applications to further explore the dynamics and transient interactions between *Nb*RLP1 and *Nb*SOBIR1 (Shyu and Hu, 2008). In addition, as reported by Tao et al. (2019), the BiFC assay in plants has the tendency to artificially induce membrane contact especially when involving the overexpression of two proteins which might interact with ER and plasma membrane interfaces. Thus, where exactly does the interaction between *Nb*RLP1 and *Nb*SOBIR1 occur awaits further investigation.

To compensate for this limitation, we studied the localization and dynamics of *Nb*RLP1 and *Nb*SOBIR1 in plants by transient overexpression followed by confocal microscopy. Remarkably, our findings clearly uncovered that the dynamics of *Nb*SOBIR1 microdomains on the plasma membrane, including its lateral movement and downregulation *via* endocytosis, is regulated through the remodeling of cortical ER underneath the plasma membrane (**Figures 4**, **5**). We suspect that the *Nb*RLP1 and *Nb*SOBIR1 interaction may contribute to binding the two compartments together to enable the coupled motility. However, when we performed biochemical studies to learn about the contribution of *Nb*RLP1 domains to the *Nb*RLP1-*Nb*SOBIR1 complex formation, the data suggested that the interaction between *Nb*RLP1 and *Nb*SOBIR1 might be bridged by other yet undiscovered factors (**Supplementary Figure 2**). Further evidence indicated that *Nb*RLP1, devoid of its cytoplasmic tail, showed slightly compromised activity to downregulate the number of *Nb*SOBIR1 microdomains on the plasma membrane (**Supplementary Figure 2C**), despite its binding with *Nb*SOBIR1. These observations have prompted us to hypothesize that the interaction between *Nb*RLP1 and *Nb*SOBIR1 is achieved transiently and/or involves remodeling of a complicated protein complex in order to regulate *Nb*SOBIR1 endocytosis. Along this line, understanding the exact composition of the *Nb*RLP1 and *Nb*SOBIR1-associated complex would be necessary to know how the ER contributes to *Nb*SOBIR1-mediated PTI response and *Nb*SOBIR1 endocytosis.

The *Nb*SOBIR1 microdomains in our studies showed an interesting pattern of either abutting or surrounded by the ER (**Figure 5**). In contrast to the flat ER sheets, the ER tubules are highly curved structures, shaped by the evolutionarily conserved reticulon family proteins that adopt a wedge-like topology in the ER. The reticulons localized to the border of the ER sheets, the ER tubules, and the three-way junction, all of which define the areas of the ER membrane that are highly curved (Nziengui et al., 2007). Intriguingly, these areas appear to be preferred by the *Nb*SOBIR1 microdomains on the plasma membrane to associate with the ER. Recently, EPCSs marked by SYT1-mCherry are identified at static ER tubules in plant (Ishikawa et al., 2018). In *Arabidopsis thaliana*, *At*SYT1 plays an essential role in maintaining cell integrity and virus movement (Uchiyama et al., 2014; Perez-Sancho et al., 2015). Notably, another plant EPCS tether *At*VAP27-1 has recently been shown to bind clathrin and phosphoinositides in *Arabidopsis* and *vap27-1/-3* mutant showed endocytosis defects, thus raising the possibility that endocytosis may occur at EPCS sites in plants (Stefano et al., 2018). In non-plant systems, EPCSs have been reported to get involved in diverse functions including lipid homeostasis, calcium influx, signaling, and endocytosis (Wakana et al., 2015; van der Burgh et al., 2019). Although the relationship between EPCSs and plant PRRs has not been established, the changes

of EPCS in space and time in response to pathogen infection are definitely of great interest to be explored as a missing link in plant immunity.

Given that *Nb*SOBIR1 moves from the plasma membrane to endocytic vesicles in response to the ParA1 elicitin (Peng et al., 2015), it seems most likely that *Nb*RLP1 might regulate *Nb*SOBIR1 endocytosis. Indeed, overexpressing of *Nb*RLP1 in the absence of ParA1 treatment significantly reduced the number of *Nb*SOBIR1 microdomains on the plasma membrane (**Figure 6D**). In the presence of ParA1, *Nb*RLP1 overexpression though showed no effect on the total number of *Nb*SOBIR1 microdomains on the plasma membrane (**Figure 6E**, left) significantly accelerated the mobility of the ParA1-induced microdomains (**Figure 6F**) and ParA1-triggered *Nb*SOBIR1 endocytosis (**Figure 6E**, right). The SOBIR1 is involved in PTI elicited by various proteinaceous MAMPs. Whether *Nb*RLP1 similarly regulates *Nb*SOBIR1 endocytosis that is triggered by other elicitors await further investigation. It would also be interesting to know whether endocytosis of the corresponding RLP-PRRs is regulated by *Nb*RLP1 and exactly how endocytosis regulation is accomplished in this scenario.

In this study, we detected on the immune blot, two forms of *Nb*SOBIR1 which differ in molecular weight of around ∼8.5 kD (**Figure 3B**), implying post-translational protein modification on *Nb*SOBIR1. Interestingly, overexpression of *Nb*RLP1 resulted in the reduction of the higher molecular weight form of *Nb*SOBIR1 that is also the form that binds *Nb*RLP1 (**Figure 3C**). Our hunch is that the *Nb*SOBIR1 of greater molecular weight may reside in the microdomains to mediate *Nb*RLP1 interaction. Since *Nb*RLP1 overexpression reduced the *Nb*SOBIR1 microdomain on the plasma membrane (**Figure 6D**), through facilitating its endocytosis, it seems plausible to predict that the reduction in protein abundance is due to its endocytic turnover. It has been reported that SOBIR1 when overexpressed constitutively activates immune responses and is highly phosphorylated in *A. thaliana*, likely through the kinase activity of SOBIR1 itself and BAK1 (van der Burgh et al., 2019). However, using an antibody specifically against phosphoserine failed to recognize the *Nb*SOBIR1 pulled down by *Nb*RLP1-TAP (our unpublished data). In addition, the larger *Nb*SOBIR1 that binds *Nb*RLP1 also showed resistance to phosphatase treatment (our unpublished data). Thus, this unique form of *Nb*SOBIR1 does not seem to represent a phosphorylated and activated form of this protein kinase at least in *N. benthamiana*. It would be of great interest to further identify the PTM and know whether it plays an important regulatory role for MAMP perception and PTI response in plants.

As shown by phylogenetic analysis, *Nb*RLP1 clustered with two genes from *N. sylvestris* and *N. attenuata*, respectively. This clade is distinct from that encompassing EILP from *N. tabacum* (Takemoto et al., 2000) but closer to that containing two Cf-5 homologs (Hcr2-0A and Hcr2-0B) from *S. lycopersicum* (Dixon et al., 1998). Therefore, *Nb*RLP1 appears not as an ortholog of EILP. Regarding the plant defense response, we document that *Nb*RLP1 overexpression enhanced ParA1-induced necrosis (**Figure 7**). Although its silencing did not show a profound effect on ParA1-induced necrosis, SOBIR1 endocytosis, and plant resistance against *P. parasitica* (**Supplementary Figure 3**), a previous report showed overexpressing a fragment of *Nb*RLP1 (termed *Nb*EILP previously) in plants enhanced the accumulation of *Bamboo mosaic virus*, whereas gene silencing reduced its accumulation (Chen et al., 2017). Collectively, it seems likely that this ER RLP actively participates in a variety of host–pathogen interactions. It would be necessary to further investigate the exact molecular function of *Nb*RLP1 in the ER *in planta*.

Overall, our studies on *Nb*RLP1 and *Nb*SOBIR1 have provided many new insights into the tale of *Nb*SOBIR1-mediated PTI. The discovery of the *Nb*SOBIR1 microdomain at the plasma membrane and the control of its dynamics through the contact with the ER not only advance our current knowledge on this important adaptor protein but also reinforce the concept of microdomain formation as an important platform during MAMP perception. Though more needs to be learned from how SOBIR1 works in concert with various RLPs to achieve plant immunity, it seems equally important to think beyond the plasma membrane toward a potential role of ER either in transmitting plant immunity signals or even in the organization of immune receptor complex upon MAMP perception.

MATERIALS AND METHODS

Plant Growth and Pathogen Culture Conditions

Nicotiana benthamiana was grown in a mixture of peat moss, perlite, and vermiculite (4:1:1) at 28°C under 12-h light/dark. *Phytophthora parasitica* (isolate 94069) was cultured on 10% V8 juice agar [10% V8 juice (Campbell, NJ, United States), 0.02% $CaCO_3$, and 1.5% select agar (Thermo Fisher Scientific, Waltham, MA, United States)] at 25°C.

Cloning and Sequence Analysis of *Nb*RLP1

Total RNAs were isolated from *N. benthamiana* leaves using the Plant Total RNA extraction kit (Viogene, New Taipei City, Taiwan) followed by using Turbo-DNA-free kit (Thermo Fisher Scientific, Waltham, MA, United States) to remove the residual DNA. *N. benthamiana* complementary DNA (cDNA) was prepared by using SuperScript III reverse transcriptase (Thermo Fisher Scientific, Waltham, MA, United States). The *NbRLP1* was amplified by using NbRLP1_F1-3 and NbRLP1_R1-2 primers (**Supplementary Table 1**), followed by cloning into the pENTR^{TM}/D-TOPO^{TM} vector (Thermo Fisher Scientific, Waltham, MA, United States) for sequencing and subsequent subcloning. The signal peptide of *Nb*RLP1 was predicted by using Signal P-5.0[2]. Positions of leucine-rich repeat and transmembrane domain of *Nb*RLP1 were predicted by InterPro[3] and TMHMM Server v.2.0[4], respectively. Multiple sequence alignment involved the use of Clustal X. Phylogenetic tree was generated by the maximum likelihood algorithm implemented

[2]http://www.cbs.dtu.dk/services/SignalP/

[3]http://www.ebi.ac.uk/interpro/

[4]http://www.cbs.dtu.dk/services/TMHMM/

in MEGA (v.10.0.5) with the default parameters. Nodal support of the tree was estimated by bootstrapping with 1,000 pseudoreplicate data sets.

Gene Expression Levels in the Infected Plants Quantified by qRT-PCR

At 0, 3, 6, 12, 24, 36, and 48 h after inoculation of *P. parasitica* zoospores, total RNAs from the 7th and 8th leaves of *N. benthamiana* were isolated and cDNA was synthesized as described in the previous section. Quantitative PCR (qPCR) was performed using the Power SYBR Green PCR Master Mix (Thermo Fisher Scientific, Waltham, MA, United States) with the primers listed in **Supplementary Table 1** by using the StepOnePlus real-time PCR system (Applied Biosystems, Foster City, CA, United States). Raw data were normalized to the level of *NbEF1α* (as an internal control) and displayed as a fold-change relative to the transcript level of mock-treated plants of the same time points.

Virus-Induced Gene Silencing

Virus-induced gene silencing (VIGS) experiments were performed as described by Peng et al. (2015). Briefly, a fragment of *Nb*RLP1 amplified by PCR with primers listed in **Supplementary Table 1** was cloned into pTRV2 (pYL279) by Gateway cloning (Thermo Fisher Scientific, Waltham, MA, United States) to generate TRV2:*Nb*RLP1, which was transformed into *Agrobacterium tumefaciens* GV3101 strain. After growth in Luria-Bertani (LB) broth amended with rifampicin and kanamycin at 28°C for 18 h, the bacteria were diluted with induction medium (10 mM MES, pH 5.6, 10 mM $MgCl_2$, and 200 μM acetosyringone) to OD_{600} of 0.6, which was then mixed with an equal volume of GV3101 bacteria harboring TRV1 (pYL192). The mixture was infiltrated onto leaves of 18-day-old *N. benthamiana* seedlings by the use of 1-mL syringes. Downregulation of gene expression was verified by qRT-PCR at 21 days post-agroinfection.

ParA1 Purification and Assays of ParA1-Induced Necrosis

Expression of His-tagged ParA1 in *Escherichia coli* and the subsequent protein purification were performed as described by Peng et al. (2015) and Hofzumahaus and Schallmey (2013) with some modifications. *Escherichia coli* strain C43 (DE) harboring pET-20b(+):ParA1 was grown in terrific broth (TB) [1.2% tryptone, 2.4% yeast extract, 0.5% glycerol, and 1 M TB salts (0.17 M KH_2PO_4 and 0.72 M K_2HPO_4)] at 37°C. When OD_{600} reached 1.0, 0.4 mM isopropyl β- d-1-thiogalactopyranoside (IPTG) was added and the bacteria culture was grown at 30°C with constant shaking at 150 rpm. After 24 h, bacteria were harvested and disrupted in a solution [50 mM potassium phosphate buffer (pH 6.5), 500 mM NaCl, and 10 mM imidazole] by the use of a high-pressure homogenizer (Avestin EF-C3, Ottawa, ON, Canada) and His-tagged ParA1 recombinant protein was purified with the use of Ni-NTA agarose according to the protocol of the manufacturer (Qiagen, Hilden, Düsseldorf, Germany). For the ParA1-induced necrosis assay, 0.3 μM recombinant protein in 10 mM MES (pH 5.6) was infiltrated onto leaves of 4.5-week-old *N. benthamiana*. After 24 h, the respective areas of infiltration and necrotic lesion for each leaf were measured by using the ImageJ software, and necrosis index was calculated accordingly by dividing the necrosis area with the infiltrated area.

Plasmid Construction

All plasmid constructs used in this study were made by using the Gateway cloning system (Thermo Fisher Scientific, Waltham, MA, United States). To generate the *GFP-NbRLP1* construct, the nucleotide sequence of *NbRLP1*ORF in the pENTR plasmid was first changed from $T^{79}C^{80}C^{81}A^{84}$ to $A^{79}G^{80}T^{81}T^{84}$, which introduced a *Sca*I site, whereas maintaining the same amino acid sequence. Then, a GFP-encoding DNA sequence was inserted into the *Sca*I site, followed by amplification and subcloning of the *GFP-NbRLP1* fragment into the pK7WG2 vector (Karimi et al., 2002) by Gateway cloning to get *pK7WG2:GFP-NbRLP1*. To generate the *Nb*RLP1-ΔN construct, a DNA fragment encompassing nucleotides 2,737–2,910 of *NbRLP1* ORF was amplified by PCR, which was then used to replace *NbRLP1* devoid of the signal peptide in *pENTR:NbRLP1* and then to get *pK7FWG2:NbRLP1-ΔN* by Gateway cloning. To generate the *NbRLP1-GFP* and *NbRLP1-ΔC* constructs, DNA fragments corresponding to the full-length *NbRLP1* ORF or *NbRLP1* lacking its cytoplasmic tail (with nucleotides 1–2805) were amplified by PCR and cloned into *pK7FWG2* to get *pK7FWG2:NbRLP1* and *pK7FWG2:NbRLP1-ΔC*, respectively. To prepare the constructs for the BiFC experiments, fragments of Venus N-terminal half (Vn) and Venus C-terminal half (Vc) were amplified (Sung and Huh, 2007) using primers listed in **Supplementary Table 1** and cloned into *pENTR-NbRLP1* and *pENTR-NbSOBIR1* to get *pK7WG2:NbRLP1-Vn* and *pK7WG2:NbSOBIR1-Vc*, respectively. To get *pK7WG2:Vn-NbRLP1*, Vn fragment was amplified to replace GFP in *pENTR:GFP-NbRLP1* followed by Gateway cloning. To get TAP-tagged expression constructs, TAP sequence (Puig et al., 2001) synthesized by Genomics (Xizhi, New Taipei City, Taiwan) was first cloned to *pENTR:NbRLP1*, *pENTR:NbRLP1-ΔN*, and *pENTR:NbRLP1-ΔC*, respectively, followed by Gateway cloning. To prepare the *AtSYT1-mCherry* construct, the *AtSYT1* amplified from the cDNA of *A. thaliana* was cloned into *p35S-C-mCherry* (Wu et al., 2011), followed by PCR amplification of the *AtSYT1-mCherry* fragment and subcloned into *pK7WG2*. The sequences for all primers are listed in **Supplementary Table 1**.

Confocal Imaging

For transient gene expression on *N. benthamiana*, the plasmid constructs described in the section above were transformed into *Agrobacterium tumefaciens* C58C1 for agroinfiltration as described by Peng et al. (2015). In brief, *A. tumefaciens* strains carrying constructs were cultured in LB broth amended with corresponding antibiotic at 28°C. After 18 h, the bacteria cells were harvested by centrifugation, resuspended with MMA (10 mM MES, pH 5.6, 10 mM $MgCl_2$, 200 μM acetosyringone) to OD_{600} of 0.2 for *Nb*RLP1-GFP, 0.05 for *Nb*SOBIR1-mCherry, and 0.2 for *At*SYT1-mCherry, respectively. Bacteria were infiltrated

onto the newly expanding leaves of 4-week-old *N. benthamiana* seedlings by the use of 1-mL needleless syringes. To suppress the silencing response, all treatments were coinfiltrated with *A. tumefaciens* C58C1 harboring P19-expressing construct ($OD_{600}$of 0.1). For the BiFC experiments, *A. tumefaciens* C58C1 carrying *pK7WG2:NbSOBIR1-Vc* or *pK7WG2:Vc* was adjusted to OD_{600} of 0.05 and those carrying *pK7WG2:Vn-NbRLP1*, *pK7WG2:NbRLP1-Vn*, or *pK7WG2:Vn* were adjusted to OD_{600} of 0.2. Fluorescence signals were visualized using the Zeiss LSM 510 Meta confocal microscope, Zeiss LSM 880 confocal microscope, or Leica Stellaris 8 confocal microscopy. The Zeiss LSM 880 confocal microscope with the Airyscan super resolution mode was used for imaging microdomains on the plasma membrane. GFP: excitation of 488 nm and emission from 500 to 550 nm; mCherry: excitation of 543 nm and emission from 565 to 615 nm; YFP: excitation of 514 nm and emission from 510 to 560 nm.

Quantification of *Nb*SOBIR1 Microdomains and Endocytic Structures

To quantify *Nb*SOBIR1 microdomains, we took still images specifically focused on the plasma membrane section using the Zeiss LSM880 with Airyscan mode. We used the ImageJ freehand selection tool followed by the ROI manager tool to define and calculate the area of the focused plasma membrane region. We manually counted the number of microdomains (usually ∼0.4–0.8 μm) using the multi-points tool of ImageJ. The number of *Nb*SOBIR1 puncta on plasma membrane was calculated using the number of microdomains divided by the area of the plasma membrane. To analyze the dynamics of *Nb*SOBIR1 microdomains, we performed particle tracking analysis using the ImageJ plugin Trackmate. We selected LoG detector tool to analyze particle diameter and intensity with estimated blob diameter of 0.8 μm and a threshold of 6.0. For analyses, we selected HyperStack displayer as a viewer and the simple lack tracker tool with the setting of linking max distance of 8 μm, gap-closing max distance of 8 μm, and gap-closing frame gap 2. To quantify endocytic structures, five z-stack images beneath the plasma membrane, each with 2.05 μm overlapped, were maximally projected to a final stack size of 8.20 μm. We used ImageJ to define and calculate the selected ROI area, followed by manually counting the number of endocytic structures. The number of *Nb*SOBIR1 endocytic vesicles was calculated using the number of endocytic structures divided by the volume of the stack.

TAP Purification

Agrobacterium tumefaciens C58C1 carrying *pK7WG2:NbRLP1-TAP*, *pK7WG2:NbRLP1-ΔN-TAP*, or *pK7WG2:NbRLP1-ΔC-TAP* (at a final OD_{600} of 0.2) was mixed with C58C1 harboring *pK7WG2:NbSOBIR1-mCherry* (at a final OD_{600} of 0.05) and infiltrated onto young expanding leaves of 4-week-old *N. benthamiana*. After 46 h, 1.5 g leaves were ground into fine powder in the presence of liquid nitrogen, followed by resuspension in 3 mL GTEN buffer (10% glycerol, 25 mM Tris–HCl, pH 7.5, 1 mM EDTA, 150 mM NaCl, 10 mM DTT, and 1.5% triton-X100) (Sacco et al., 2007) supplemented with protease inhibitors cocktail (Roche Molecular Systems, NJ, United States). After thawed, debris present in the mixture was removed by a quick spin of 1,000 rpm for 1 min, followed by another spin of 12,000 g for 10 min, both at 4°C. The resulting supernatant was collected and incubated with 100 μL IgG Sepharose^{TM} 6 FF at 4°C with gentle rotation for 3 h. After washing the beads four times with 10 ml GTEN buffer containing 1.25 mM PMSF, the bound proteins were eluted with 80 μL MURB (50 mM sodium phosphate, 25 mM MES, pH 7.0, 1% SDS, 3 M urea, and 5% β-mercaptoethanol) and boiled for 5 min. Samples were subjected to SDS-PAGE followed by the Western blot analysis with the use of PAP antibody (Jackson immune research, PA, United States) or our homemade anti-mCherry antibody (Wu et al., 2011). Signals on the blots were detected by using the UVP ChemiDoc-It imager (Upland, CA, United States).

Inoculation of *P. parasitica*

For inoculation, zoospore suspension ($2*10^4$ spores/mL) prepared as described by Yan and Liou (2006), or water as controls, was sprayed evenly on 5.5-week-old *N. benthamiana* till run-off, and the inoculated plants were maintained at 28°C in the dark in a moisture chamber for the indicated periods of time. Disease severity was scored, as follows, on a scale from 0 to 4, according to symptoms developed on the plants: 0, healthy, no water-soaking lesions; 1, slight water-soaking, with less than 50% wilting leaves; 2, obvious water-soaking lesions, with more than 50% wilting leaves; 3, severe water-soaking and wilting; 4, complete wilting along with the appearance of mycelia. The disease severity index was calculated as [sum (number of plants × disease index)])/[(total number of plants) × (maximal disease index)] × 100.

Statistical Analysis

All experiments were repeated at least three times. The two-tail student's *t*-test was used for two-paired comparison, and the *p*-value was displayed. Multiple comparison analysis testing was carried out with ANOVA and LSD ($p < 0.05$).

DATA AVAILABILITY STATEMENT

The original contributions presented in the study are publicly available. This data can be found here: The 2.91- and 1.41-kb NbRLP1 sequences can be found in the GenBank under the following accession numbers: MW924093 and MW924094, respectively.

AUTHOR CONTRIBUTIONS

R-FL and C-WW planned, designed the research, and wrote the manuscript. Y-HL, W-CS, and T-YK executed the experiments and analyzed the data. All authors contributed to the article and approved the submitted version.

FUNDING

This study was supported by the Academia Sinica Intramural Funds and Career Development Award (AS-CDA-104-L11) (to C-WW) and by a grant (MOST 102-2628-B-002-021-MY3) from the Ministry of Science and Technology, Taiwan (to R-FL).

ACKNOWLEDGMENTS

We are grateful to Ji-Ying Huang and Mei-Jane Fang at the Cell Biology Core Lab (IPMB, Academia Sinica) for the microscopy advice. We thank Rey-Huei Chen (IMB, Academia Sinica) for sharing lab resources and providing suggestions for our investigations. We also thank Tsung-Luo Jinn (Institute of Plant Biology, NTU) for providing the plasmid construct mCherry-KDEL.

SUPPLEMENTARY MATERIAL

The Supplementary Material for this article can be found online at: https://www.frontiersin.org/articles/10.3389/fpls.2021.721548/full#supplementary-material

Supplementary Figure 1 | Colocalization of *Nb*RLP1-GFP and *At*SYT1-mCherry. *Nicotiana benthamiana* leaves expressing *Nb*RLP1-GFP and *At*SYT1-mCherry were imaged at the periphery sections using Leica Stellaris 8 confocal microscope. Scale bar, 10 μm. The box area in the image of the periphery section is enlarged to show the colocalization of *Nb*RLP1-GFP and *At*SYT1-mCherry signals.

Supplementary Figure 2 | C-terminus of *Nb*RLP1 is sufficient for binding with *Nb*SOBIR1. **(A)** *Nicotiana benthamiana* leaves expressing *Nb*SOBIR1-mCherry and *Nb*RLP1-TAP, *Nb*RLP1-ΔN-TAP, *Nb*RLP1-ΔC-TAP, or TAP as indicated were harvested and lyzed. The lysate (input) was subjected to pull-down by IgG Sepharose as described in the Materials and Methods section. The input and the bound (pulled-down) fractions were subjected to SDS-PAGE followed by the Western blot analysis with use of anti-mCherry or PAP antibodies. **(B)** A scheme depicting the current model of how *Nb*RLP1-Vn in the ER might interact with *Nb*SOBIR1-Vc on the plasma membrane. X, Y, and Z indicate putative proteins that might bridge the *Nb*SOBIR1–*Nb*RLP1 interaction. **(C)** Deletion of the C-terminus but not N-terminus of *Nb*RLP1 showed slightly compromised activity to downregulate the number of *Nb*SOBIR1 microdomains on the plasma membrane. *N. benthamiana* leaves expressing *Nb*SOBIR1-mCherry alone or coexpressing with *Nb*RLP1-GFP, *Nb*RLP1-ΔN-GFP or *Nb*RLP1-ΔC-GFP were subjected to microscopy by using the Zeiss LSM880 confocal microscope with use of Airyscan. Microdomain number was quantified as described in the Materials and Methods section and shown as scatter plots. Different letters indicate significant differences based on LSD ($p < 0.01$).

Supplementary Figure 3 | Endocytosis occurs directly *via* the translocation of *Nb*SOBIR1 microdomains on the plasma membrane. *Nicotiana benthamiana* leaves expressing *Nb*SOBIR1-mCherry were infiltrated with 0.3 μM ParA1 in MES buffer. After 30 min, leaves were subjected to time-lapse microscopy by focusing on a few microdomains at the center of the cell using the Zeiss LSM880 confocal microscope with an Airyscan. The total image acquisition length was 16 min with a time interval of 5 s. Representative area was selected for display by time course.

Supplementary Figure 4 | *Nb*RLP1 silencing did not show a profound effect on *Sl*SOBIR1 endocytosis or plant resistance against *Phytophthora parasitica*. **(A)** *Sl*SOBIR1-GFP was expressed on *Nicotiana benthamiana* leaves pre-silenced for *Nb*RLP1 expression (TRV-*Nb*RLP1) or infected with TRV-GFP as the control. Around 44 h post-agroinfiltration, the leaves were treated with 0.3 μM ParA1 in MES buffer for 30 min, followed by microscopy with five Z stack for a total of 8.20 stack size using Zeiss LSM 510 confocal microscope. The maximal projection images are shown. The number of internal *Nb*SOBIR1-mCherry puncta was quantified as described in the Materials and Methods section and displayed using a scatter plot. Statistical analysis was carried out with the two-tailed student's *t*-test and the *p*-value is shown. **(B)** *N. benthamiana* silenced for *Nb*RLP1 expression (TRV-NbRLP1) or treated as the control carrying TRV-GFP were inoculated with zoospores of *P. parasitica*. At indicated hours post-inoculation (hpi), the development of disease symptoms was examined and the disease severity index was calculated as detailed in the Materials and methods section. The experiment has been repeated three times with similar results, and only one set of the experimental data is shown.

Supplementary Table 1 | A list of primers used in this study and the sequence of 1.41- and 2.91-Kb *Nb*RLP1.

Supplementary Movie 1 | *Nicotiana benthamiana* leaves expressing *Nb*SOBIR1-mCherry were subjected to time-lapse microscopy, focusing only on the periphery of the leaf epidermal cell, using Zeiss LSM880 confocal microscope with Airyscan. The total image acquisition length was 16 min with a time interval of 5 s.

Supplementary Movie 2 | *Nicotiana benthamiana* leaves expressing *Nb*SOBIR1-mCherry and *Nb*RLP1-GFP were subjected to time-lapse microscopy, focusing only on the periphery of the leaf epidermal cell, using Zeiss LSM880 confocal microscope with Airyscan. The total image acquisition length was 16 min with a time interval of 5 s.

Supplementary Movie 3 | *Nicotiana benthamiana* leaves expressing *Nb*SOBIR1-mCherry were treated with 0.3 μM ParA1 in MES buffer. After 30 min, the leaves were subjected to microscopy, focusing only on the periphery of the leaf epidermal cell, by Zeiss LSM880 confocal microscope with use of Airyscan. The total image acquisition length was 16 min with a time interval of 5 s.

Supplementary Movie 4 | *Nicotiana benthamiana* leaves expressing *Nb*SOBIR1-mCherry and *Nb*RLP1-GFP were treated with 0.3 μM ParA1 in MES buffer. After 30 min, the leaves were subjected to microscopy, focusing only on the periphery of the leaf epidermal cell, by using Zeiss LSM880 confocal microscope with Airyscan. The total image acquisition length was 16 min with a time interval of 5 s.

REFERENCES

Albert, I., Hua, C., Nurnberger, T., Pruitt, R. N., and Zhang, L. (2020). Surface sensor systems in plant immunity. *Plant Physiol.* 182, 1582–1596. doi: 10.1104/pp.19.01299

Boller, T., and Felix, G. (2009). A renaissance of elicitors: perception of microbe-associated molecular patterns and danger signals by pattern-recognition receptors. *Annu. Rev. Plant Biol.* 60, 379–406. doi: 10.1146/annurev.arplant.57.032905.105346

Bücherl, C. A., Jarsch, I. K., Schudoma, C., Segonzac, C., Mbengue, M., Robatzek, S., et al. (2017). Plant immune and growth receptors share common signalling components but localise to distinct plasma membrane nanodomains. *eLife* 6:e25114.

Chen, I. H., Huang, Y. P., Tseng, C. H., Ni, J. T., Tsai, C. H., Hsu, Y. H., et al. (2017). *Nicotiana benthamiana* elicitor-inducible leucine-rich repeat receptor-like protein assists bamboo mosaic virus cell-to-cell movement. *Front. Plant Sci.* 8:1736. doi: 10.3389/fpls.2017.01736

Dixon, M. S., Hatzixanthis, K., Jones, D. A., Harrison, K., and Jones, J. D. (1998). The tomato Cf-5 disease resistance gene and six homologs show pronounced allelic variation in leucine-rich repeat copy number. *Plant Cell* 10, 1915–1925. doi: 10.2307/3870913

Dodds, P. N., and Rathjen, J. P. (2010). Plant immunity: towards an integrated view of plant-pathogen interactions. *Nat. Rev. Genet.* 11, 539–548.

Domazakis, E., Wouters, D., Visser, R. G. F., Kamoun, S., Joosten, M., and Vleeshouwers, V. (2018). The ELR-SOBIR1 complex functions as a two-component receptor-like kinase to mount defense against *Phytophthora infestans*. *Mol. Plant Microbe Interact.* 31, 795–802. doi: 10.1094/mpmi-09-17-0217-r

Dong, R., Saheki, Y., Swarup, S., Lucast, L., Harper, J. W., and De Camilli, P. (2016). Endosome-ER contacts control actin nucleation and retromer function through

VAP-dependent regulation of PI4P. *Cell* 166, 408–423. doi: 10.1016/j.cell.2016.06.037

Du, J., Verzaux, E., Chaparro-Garcia, A., Bijsterbosch, G., Keizer, L. C., Zhou, J., et al. (2015). Elicitin recognition confers enhanced resistance to *Phytophthora infestans* in potato. *Nat. Plants* 1:15034.

English, A. R., Zurek, N., and Voeltz, G. K. (2009). Peripheral ER structure and function. *Curr. Opin. Cell Biol.* 21, 596–602. doi: 10.1016/j.ceb.2009.04.004

Gao, M., Wang, X., Wang, D., Xu, F., Ding, X., Zhang, Z., et al. (2009). Regulation of cell death and innate immunity by two receptor-like kinases in Arabidopsis. *Cell Host Microbe* 6, 34–44. doi: 10.1016/j.chom.2009.05.019

Hofzumahaus, S., and Schallmey, A. (2013). *Escherichia coli*-based expression system for the heterologous expression and purification of the elicitin beta-cinnamomin from *Phytophthora cinnamomi*. *Protein Expr. Purif.* 90, 117–123. doi: 10.1016/j.pep.2013.05.010

Ishikawa, K., Tamura, K., Ueda, H., Ito, Y., Nakano, A., Hara-Nishimura, I., et al. (2018). Synaptotagmin-associated endoplasmic reticulum-plasma membrane contact sites are localized to immobile ER Tubules. *Plant Physiol.* 178, 641–653. doi: 10.1104/pp.18.00498

Jarsch, I. K., Konrad, S. S., Stratil, T. F., Urbanus, S. L., Szymanski, W., Braun, P., et al. (2014). Plasma membranes are subcompartmentalized into a plethora of coexisting and diverse microdomains in Arabidopsis and Nicotiana benthamiana. *Plant Cell* 26, 1698–1711.

Jones, J. D., and Dangl, J. L. (2006). The plant immune system. *Nature* 444, 323–329.

Karimi, M., Inze, D., and Depicker, A. (2002). GATEWAY vectors for *Agrobacterium*-mediated plant transformation. *Trends Plant Sci.* 7, 193–195. doi: 10.1016/s1360-1385(02)02251-3

Liebrand, T. W., van den Berg, G. C., Zhang, Z., Smit, P., Cordewener, J. H., America, A. H., et al. (2013). Receptor-like kinase SOBIR1/EVR interacts with receptor-like proteins in plant immunity against fungal infection. *Proc. Natl. Acad. Sci. U.S.A.* 110, 10010–10015. doi: 10.1073/pnas.1220015110

Nagano, M., Ishikawa, T., Fujiwara, M., Fukao, Y., Kawano, Y., Kawai-Yamada, M., et al. (2016). Plasma membrane microdomains are essential for Rac1-RbohB/H-mediated immunity in rice. *Plant Cell* 28, 1966–1983. doi: 10.1105/tpc.16.00201

Nziengui, H., Bouhidel, K., Pillon, D., Der, C., Marty, F., and Schoefs, B. (2007). Reticulon-like proteins in *Arabidopsis thaliana*: structural organization and ER localization. *FEBS Lett.* 581, 3356–3362. doi: 10.1016/j.febslet.2007.06.032

Peng, K. C., Wang, C. W., Wu, C. H., Huang, C. T., and Liou, R. F. (2015). Tomato SOBIR1/EVR Homologs are involved in Elicitin perception and plant defense against the oomycete pathogen *Phytophthora parasitica*. *Mol. Plant Microbe Interact.* 28, 913–926. doi: 10.1094/mpmi-12-14-0405-r

Perez-Sancho, J., Tilsner, J., Samuels, A. L., Botella, M. A., Bayer, E. M., and Rosado, A. (2016). Stitching Organelles: organization and function of specialized membrane contact sites in plants. *Trends Cell Biol.* 26, 705–717. doi: 10.1016/j.tcb.2016.05.007

Perez-Sancho, J., Vanneste, S., Lee, E., McFarlane, H. E., Esteban Del Valle, A., Valpuesta, V., et al. (2015). The Arabidopsis synaptotagmin1 is enriched in endoplasmic reticulum-plasma membrane contact sites and confers cellular resistance to mechanical stresses. *Plant Physiol.* 168, 132–143. doi: 10.1104/pp.15.00260

Phillips, M. J., and Voeltz, G. K. (2016). Structure and function of ER membrane contact sites with other organelles. *Nat. Rev. Mol. Cell Biol.* 17, 69–82. doi: 10.1038/nrm.2015.8

Prinz, W. A., Toulmay, A., and Balla, T. (2020). The functional universe of membrane contact sites. *Nat. Rev. Mol. Cell Biol.* 21, 7–24. doi: 10.1038/s41580-019-0180-9

Puig, O., Caspary, F., Rigaut, G., Rutz, B., Bouveret, E., Bragado-Nilsson, E., et al. (2001). The tandem affinity purification (TAP) method: a general procedure of protein complex purification. *Methods* 24, 218–229. doi: 10.1006/meth.2001.1183

Roux, M., Schwessinger, B., Albrecht, C., Chinchilla, D., Jones, A., Holton, N., et al. (2011). The Arabidopsis leucine-rich repeat receptor-like kinases BAK1/SERK3 and BKK1/SERK4 are required for innate immunity to hemibiotrophic and biotrophic pathogens. *Plant Cell* 23, 2440–2455. doi: 10.1105/tpc.111.084301

Sacco, M. A., Mansoor, S., and Moffett, P. (2007). A RanGAP protein physically interacts with the NB-LRR protein Rx, and is required for Rx-mediated viral resistance. *Plant J.* 52, 82–93. doi: 10.1111/j.1365-313x.2007.03213.x

Shibata, Y., Voeltz, G. K., and Rapoport, T. A. (2006). Rough sheets and smooth tubules. *Cell* 126, 435–439. doi: 10.1016/j.cell.2006.07.019

Shyu, Y. J., and Hu, C. D. (2008). Fluorescence complementation: an emerging tool for biological research. *Trends Biotechnol.* 26, 622–630. doi: 10.1016/j.tibtech.2008.07.006

Somssich, M., Ma, Q., Weidtkamp-Peters, S., Stahl, Y., Felekyan, S., Bleckmann, A., et al. (2015). Real-time dynamics of peptide ligand-dependent receptor complex formation in planta. *Sci. Signal* 8:ra76.

Stefano, G., Renna, L., Wormsbaecher, C., Gamble, J., Zienkiewicz, K., and Brandizzi, F. (2018). Plant endocytosis requires the ER membrane-anchored proteins VAP27-1 and VAP27-3. *Cell Rep.* 23, 2299–2307. doi: 10.1016/j.celrep.2018.04.091

Sung, M. K., and Huh, W. K. (2007). Bimolecular fluorescence complementation analysis system for *in vivo* detection of protein-protein interaction in *Saccharomyces cerevisiae*. *Yeast* 24, 767–775. doi: 10.1002/yea.1504

Takemoto, D., Hayashi, M., Doke, N., Mishimura, M., and Kawakita, K. (2000). Isolation of the gene for EILP, an elicitor-inducible LRR receptor-like protein, from tobacco by differential display. *Plant Cell Physiol.* 41, 458–464. doi: 10.1093/pcp/41.4.458

Tang, D., Wang, G., and Zhou, J. M. (2017). Receptor Kinases in Plant-pathogen interactions: more than pattern recognition. *Plant Cell* 29, 618–637. doi: 10.1105/tpc.16.00891

Tao, K., Waletich, J. R., Arredondo, F., and Tyler, B. M. (2019). Manipulating endoplasmic reticulum-plasma membrane tethering in plants through fluorescent protein complementation. *Front. Plant Sci.* 10:635. doi: 10.3389/fpls.2019.00635

Uchiyama, A., Shimada-Beltran, H., Levy, A., Zheng, J. Y., Javia, P. A., and Lazarowitz, S. G. (2014). The Arabidopsis synaptotagmin SYTA regulates the cell-to-cell movement of diverse plant viruses. *Front. Plant Sci.* 5:584. doi: 10.3389/fpls.2014.00584

van der Burgh, A. M., Postma, J., Robatzek, S., and Joosten, M. (2019). Kinase activity of SOBIR1 and BAK1 is required for immune signalling. *Mol. Plant Pathol.* 20, 410–422. doi: 10.1111/mpp.12767

Wakana, Y., Kotake, R., Oyama, N., Murate, M., Kobayashi, T., Arasaki, K., et al. (2015). CARTS biogenesis requires VAP-lipid transfer protein complexes functioning at the endoplasmic reticulum-Golgi interface. *Mol. Biol. Cell* 26, 4686–4699. doi: 10.1091/mbc.e15-08-0599

Wang, Y., Xu, Y., Sun, Y., Wang, H., Qi, J., Wan, B., et al. (2018). Leucine-rich repeat receptor-like gene screen reveals that Nicotiana RXEG1 regulates glycoside hydrolase 12 MAMP detection. *Nat. Commun.* 9:594.

Wu, C. H., Lee, S. C., and Wang, C. W. (2011). Viral protein targeting to the cortical endoplasmic reticulum is required for cell-cell spreading in plants. *J. Cell Biol.* 193, 521–535. doi: 10.1083/jcb.201006023

Yan, H. Z., and Liou, R. F. (2006). Selection of internal control genes for real-time quantitative RT-PCR assays in the oomycete plant pathogen Phytophthora parasitica. Fungal Genet. *Biol.* 43, 430–438.

Yu, X., Feng, B., He, P., and Shan, L. (2017). From Chaos to harmony: responses and signaling upon microbial pattern recognition. *Annu. Rev. Phytopathol.* 55, 109–137. doi: 10.1146/annurev-phyto-080516-035649

Zhang, L., Kars, I., Essenstam, B., Liebrand, T. W., Wagemakers, L., Elberse, J., et al. (2014). Fungal endopolygalacturonases are recognized as microbe-associated molecular patterns by the arabidopsis receptor-like protein RESPONSIVENESS TO BOTRYTIS POLYGALACTURONASES1. *Plant Physiol.* 164, 352–364. doi: 10.1104/pp.113.230698

Zhang, W., Fraiture, M., Kolb, D., Loffelhardt, B., Desaki, Y., Boutrot, F. F., et al. (2013). Arabidopsis receptor-like protein30 and receptor-like kinase suppressor of BIR1-1/EVERSHED mediate innate immunity to necrotrophic fungi. *Plant Cell* 25, 4227–4241. doi: 10.1105/tpc.113.117010

Zipfel, C. (2014). Plant pattern-recognition receptors. *Trends Immunol.* 35, 345–351. doi: 10.1016/j.it.2014.05.004

Conflict of Interest: The authors declare that the research was conducted in the absence of any commercial or financial relationships that could be construed as a potential conflict of interest.

Publisher's Note: All claims expressed in this article are solely those of the authors and do not necessarily represent those of their affiliated organizations, or those of the publisher, the editors and the reviewers. Any product that may be evaluated in

this article, or claim that may be made by its manufacturer, is not guaranteed or endorsed by the publisher.

frontiers in Plant Science

ORIGINAL RESEARCH
published: 06 September 2021
doi: 10.3389/fpls.2021.703712

The Algal Polysaccharide Ulvan Induces Resistance in Wheat Against *Zymoseptoria tritici* Without Major Alteration of Leaf Metabolome

Marlon C. de Borba[1,2], Aline C. Velho[1,3], Alessandra Maia-Grondard[4], Raymonde Baltenweck[4], Maryline Magnin-Robert[3], Béatrice Randoux[3], Maxime Holvoet[2], Jean-Louis Hilbert[2], Christophe Flahaut[2], Philippe Reignault[3], Philippe Hugueney[4], Marciel J. Stadnik[1†] and Ali Siah[2*†]*

[1] Laboratory of Plant Pathology, Agricultural Science Center (UFSC-CCA), Federal University of Santa Catarina, Florianópolis, Brazil, [2] Joint Research Unit N° 1158 BioEcoAgro, ULCO, INRAE, University of Lille, Université Liège, UPJV, University of Artois, Lille, France, [3] Unité de Chimie Environnementale et Interactions sur le Vivant (EA 4492), Université du Littoral Côte d'Opale, Calais, France, [4] INRAE, SVQV UMR-A1131, Université de Strasbourg, Colmar, France

OPEN ACCESS

Edited by:
Essaid Ait Barka,
Université de Reims Champagne-Ardenne, France

Reviewed by:
Rahim Mehrabi,
Isfahan University of Technology, Iran
Vineet Kumar,
Forest Research Institute (FRI), India

***Correspondence:**
Ali Siah
ali.siah@junia.com
Marciel J. Stadnik
marciel.stadnik@ufsc.br

† These authors have contributed equally to this work

Specialty section:
This article was submitted to Plant Pathogen Interactions, a section of the journal Frontiers in Plant Science

Received: 30 April 2021
Accepted: 16 July 2021
Published: 06 September 2021

Citation:
de Borba MC, Velho AC, Maia-Grondard A, Baltenweck R, Magnin-Robert M, Randoux B, Holvoet M, Hilbert J-L, Flahaut C, Reignault P, Hugueney P, Stadnik MJ and Siah A (2021) The Algal Polysaccharide Ulvan Induces Resistance in Wheat Against Zymoseptoria tritici Without Major Alteration of Leaf Metabolome. Front. Plant Sci. 12:703712. doi: 10.3389/fpls.2021.703712

This study aimed to examine the ability of ulvan, a water-soluble polysaccharide from the green seaweed *Ulva fasciata*, to provide protection and induce resistance in wheat against the hemibiotrophic fungus *Zymoseptoria tritici*. Matrix-assisted laser desorption/ionization-time-of-flight-mass spectrometry (MALDI-TOF-MS) analysis indicated that ulvan is mainly composed of unsaturated monosaccharides (rhamnose, rhamnose-3-sulfate, and xylose) and numerous uronic acid residues. In the greenhouse, foliar application of ulvan at 10 $mg.ml^{-1}$ 2 days before fungal inoculation reduced disease severity and pycnidium density by 45 and 50%, respectively. Ulvan did not exhibit any direct antifungal activity toward *Z. tritici*, neither *in vitro* nor *in planta*. However, ulvan treatment significantly reduced substomatal colonization and pycnidium formation within the mesophyll of treated leaves. Molecular assays revealed that ulvan spraying elicits, but does not prime, the expression of genes involved in several wheat defense pathways, including pathogenesis-related proteins (β-1,3-endoglucanase and chitinase), reactive oxygen species metabolism (oxalate oxidase), and the octadecanoid pathway (lipoxygenase and allene oxide synthase), while no upregulation was recorded for gene markers of the phenylpropanoid pathway (phenylalanine ammonia-lyase and chalcone synthase). Interestingly, the quantification of 83 metabolites from major chemical families using ultra-high-performance liquid chromatography-mass spectrometry (UHPLC-MS) in both non-infectious and infectious conditions showed no substantial changes in wheat metabolome upon ulvan treatment, suggesting a low metabolic cost associated with ulvan-induced resistance. Our findings provide evidence that ulvan confers protection and triggers defense mechanisms in wheat against *Z. tritici* without major modification of the plant physiology.

Keywords: septoria tritici blotch, green seaweed, induced resistance, MALDI-TOF-MS, gene expression, UHPLC-MS, metabolomics

INTRODUCTION

The Septoria tritici blotch, caused by the hemibiotrophic fungus *Zymoseptoria tritici*, is one of the most devastating diseases of wheat (*Triticum aestivum* L.) worldwide (Fones and Gurr, 2015). The reduction in the photosynthetic leaf area caused by the disease can lead to yield losses of up to 50% or 5–10% when integrated disease management is implemented (Fones and Gurr, 2015). Currently, disease control mainly relies on the use of conventional fungicides (Torriani et al., 2015) and partially resistant cultivars (Ors et al., 2018). However, due to the high genetic diversity and adaptability of *Z. tritici*, the fungus frequently develops resistance to fungicides and often overcomes host resistance, making it one of the most difficult plant pathogens to control (Fones and Gurr, 2015; Torriani et al., 2015). Hence, looking for complementary alternatives, such as the use of plant resistance inducers from natural origin, has been recognized as an eco-friendly strategy to control the STB disease, thus contributing to safer food production.

The life cycle of *Z. tritici* is characterized by two distinct stages, namely, biotrophic (or symptomless latent phase) and necrotrophic phases (Steinberg, 2015). Leaf penetration occurs most frequently by hyphae emerging from germinating and surface-attached conidia that enter through stomata (Steinberg, 2015) or directly *via* the anticlinal and periclinal epidermal cells (Siah et al., 2010a). During this asymptomatic period, the fungus grows extremely slowly between the mesophyll cell layers of the leaf (Keon et al., 2007; Rudd et al., 2015). The transition from the biotrophic to the necrotrophic phase takes place suddenly around 10–15 days after infection and coincides with a sharp increase in fungal growth rate and biomass (Keon et al., 2007; Siah et al., 2010a). This may be supported by the increased apoplastic nutrient availability as a consequence of the loss of host cell-wall integrity (Keon et al., 2007). Finally, the fungus produces asexual spores in the dark-brown pycnidia formed under colonized substomatal cavities (Siah et al., 2010a; Steinberg, 2015).

Ulvan is a water-soluble sulfated heteropolysaccharide extracted from the cell walls of the green macroalgae *Ulva* spp. and is composed mainly of rhamnose, xylose, glucose, uronic acid, and sulfate (Paulert et al., 2009; de Freitas et al., 2015). Ulvan is known to exhibit a broad spectrum of biological activities, including stimulation of plant growth and defense responses (Stadnik and de Freitas, 2014). For instance, when applied onto bean leaves, ulvan is able to reduce the severity of anthracnose (Paulert et al., 2009; de Freitas and Stadnik, 2012), rust (Delgado et al., 2013), and powdery mildew (Jaulneau et al., 2011). In addition, it has shown promising results in the resistance of wheat and barley against the powdery mildew caused by *Blumeria graminis* (Paulert et al., 2010). However, the potential of green algal polysaccharides for controlling STB in wheat has never been examined.

The mode of action of the resistance inducers differs from that of traditional pesticides because they do not directly target the pathogen through antifungal activity, but they inhibit its development indirectly *via* the induction of natural plant defense mechanisms. The status of induced resistance in plants could be related to a direct elicitation of defense responses (i.e., elicitor effect), which occurs in the absence of infection, or to a plant sensitized by a priming agent (i.e., priming effect). This, in turn, results in the expression of earlier and/or stronger basal defense mechanisms upon pathogen attacks (Walters et al., 2005). Although not well understood yet, ulvan seems to induce resistance through the elicitation of defense responses in dicot plants (Cluzet et al., 2004; de Freitas and Stadnik, 2012) and priming in monocot plants (Paulert et al., 2010).

Wheat defense mechanisms against *Z. tritici* are complexes. It has been suggested that the upregulation of pathogenesis-related (PR) proteins (β-1,3-glucanase, *PR-2*; chitinase, *PR-3*) (Adhikari et al., 2007; Shetty et al., 2009) and reactive oxygen species (ROS) metabolism (oxalate oxidase, *OXO*) (Shetty et al., 2007) plays a major role in incompatible interactions, while induction of phenylpropanoids (phenylalanine ammonia-lyase, *PAL*; chalcone synthase, *CHS*) is sometimes observed in partially resistant wheat cultivars (Ors et al., 2018). On the other hand, the expression of genes involved in the octadecanoid pathway (lipoxygenase, *LOX*; allene oxide synthase, *AOS*) seem to be downregulated soon after fungal infection and further upregulated (Rudd et al., 2015; Somai-Jemmali et al., 2017). Although not well explained, the expression of these defense-related genes has been associated with the induction of wheat resistance against *Z. tritici* after the application of resistance inducers (Ors et al., 2019; Somai-Jemmali et al., 2020).

Metabolomics is an emerging and powerful tool aiming at the comprehensive analysis of low-molecular-weight metabolites. Metabolomics has been used for an overview of plant status after several biotic and abiotic stresses, particularly to decipher host resistance or susceptibility following pathogen infection (Rudd et al., 2015; Seybold et al., 2020). Knowing metabolic profiles during plant resistance induction might allow a better characterization of activated defense mechanisms. To date, little is known about the wheat-induced resistance against *Z. tritici* using natural inducers. Thus, the objective of this study was to evaluate the potential of ulvan to protect wheat against *Z. tritici* and determine its effect on plant gene expression and metabolic profile during the biotrophic phase of the fungus life cycle.

MATERIALS AND METHODS

Biological Materials

Wheat plants (*Triticum aestivum* L.) of cv. Alixan, which are susceptible to *Z. tritici* (Ors et al., 2018), were purchased from Limagrain (Saint-Beauzire, France) and used in all experiments. The aggressive monosporic strain of *Z. tritici* T02596 (Mejri et al., 2018) was used in all wheat infection bioassays. The fungus was grown on a potato dextrose agar (PDA) medium at 18°C at a 12-h photoperiod for 7 days. Then, Petri dishes were flooded with 10 ml of distilled water, and the spore suspension was filtered two times to remove mycelial fragments. Spore concentration was determined using a Malassez counting chamber (Paul Marienfeld, Lauda-Königshofen, Germany) and adjusted as needed. Ulvan was obtained as previously described by Paulert et al. (2009) from the green seaweed *Ulva fasciata* and collected on August 2017 at the Barra da Lagoa beach in Florianópolis-SC, Brazil. Briefly,

100 g of dried algae was autoclaved for 2 h at 110°C in 1 L of distilled water. The resulting aqueous solution was filtered and the polysaccharide was precipitated two times with ethanol (3 v) at −20°C: first for 24 h, and afterward for 48 h. The second precipitate of ulvan was collected, dried, and kept at 5°C until use.

Matrix-Assisted Laser Desorption/Ionization-Time-of-Flight-Mass Spectrometry (MALDI-TOF-MS)

Matrix-assisted laser desorption/ionization-time-of-flight-mass spectrometry (MALDI-TOF-MS) analysis was performed using the AutoflexSpeed^{TM} (Bruker, Berlin, Germany) mass spectrometer running the Flexcontrol 3.4 software (Bruker). The mass spectrometer was calibrated according to the recommendations of the manufacturer. Mass spectra were acquired in the negative linear-ion mode using the automatic negative linear method of the manufacturer across a mass-to-charge (m/z) ratio of 100–2,000 atomic mass unit. The mass spectra correspond to mass signals summed from 2,000 laser shots in 100 shot steps performed randomly on different areas of the spot. Ulvan was solubilized at 10 mg.ml^{-1} in ultrapure (MQ) water, while 2,5-dihydroxybenzoic acid (DHB), used as the MALDI matrix, was dissolved at 10 mg.ml^{-1} in acetonitrile/water (3:7; v/v). One microliter of ulvan solution and 1 μl of DHB matrix solution were spotted together on a 384-well polished steel MALDI plate. Samples were allowed to dry and co-crystallize at room temperature before they were loaded into the MALDI-TOF mass spectrometer.

In vitro Antifungal Activity of Ulvan on *Z. tritici*

The direct antifungal effect of ulvan on *Z. tritici* was assessed on both spore germination and mycelial growth. For the spore germination assay, an aliquot of 200 μl of 1 × 10^4 spore ml^{-1} of *Z. tritici* was spread on PDA plates amended or not with ulvan at 10 mg.ml^{-1}. After a 1-day incubation period at 18°C in the dark, the percentage of spore germination was randomly determined from 100 spores using a light microscope at 400× magnification (Siah et al., 2010b). Regarding mycelial growth assay, an aliquot of 5 μl of 1 × 10^5 spore ml^{-1} of the fungus was deposited on the middle of Petri dishes containing PDA amended or not with ulvan at 10 mg.ml^{-1}. After an incubation period of 10 days at 18°C in the dark, the fungal colony diameter was scored from two perpendicular measurements using a caliper (Siah et al., 2010b).

Plant Growth, Treatment, and Inoculation

The wheat seeds of cv. Alixan were pre-germinated in plastic boxes on moist filter paper in the dark under changing temperature conditions, according to Siah et al. (2010a). Twelve wheat germlings were transplanted to 3-L pots (15-cm diameter) containing organic compost as the substrate (Gamm Vert, France). Three pots of 12 plants (i.e., 36 plants) were used as replicates for each condition. Plants were grown under greenhouse conditions (18 ± 3°C, 16 h of light, and a photon flux density of 240 μmol.m^{-2}.s^{-1}) and irrigated according to their water requirements. Three-week-old plants (the third leaf fully expanded stage) were sprayed one time with distilled water (control) or with ulvan solution (10 mg.ml^{-1}), both amended with 0.05% (v/v) polyoxyethylene-sorbitan monolaurate (Tween 20, Sigma-Aldrich, Saint Louis, MO, United States). A solution volume of 30 ml was delivered per pot. Two days after treatment (dat), plants were inoculated by spraying them with a 1 × 10^6 spore ml^{-1} suspension of *Z. tritici* prepared in distilled water with 0.05% Tween 20 and kept under highly humid conditions (∼99% humidity) for 3 days (Siah et al., 2010a). A spore suspension volume of 30 ml was delivered per pot. Mock-inoculated plants were used as control. Disease severity was assessed at 21 days after inoculation (dai) by measuring the percentage of the third leaf area with STB symptoms (chlorosis and necrosis). Pycnidium density was scored on a scale from 0 to 5; with 0 = absence of pycnidia, 1 = 1–19%, 2 = 20–39%, 3 = 40–59%, 4 = 60–79%, and 5 = 80–100% of necrotic leaf area bearing pycnidia, respectively.

In planta Cytological Assays

To assess fungal spore germination and epiphytic hyphal growth (fungal development on the leaf surface), 4-cm third-leaf segments were collected at 1 and 5 dai, respectively, and then immediately immersed in a solution of 0.1% Calcofluor (Fluorescence Brightener 28, Sigma-Aldrich, Saint-Quentin-Fallavier, France) and 0.1 M of Tris-HCl buffer at pH 8.5 for 5 min. Then, leaf segments were washed for 2 min in distilled water, superficially dried at room temperature, placed on a glass slide, covered with a coper slip, and observed microscopically (Eclipse 80i, Nikon, Champigny Sur Marne, France) at 400× magnification under ultraviolet illumination (emission: 365 nm; excitation: 440 nm). The percentage of germinated spores and epiphytic hyphal growth were calculated from 100 spores, which were chosen randomly on the leaf surface. Four categories of germlings were recorded: non-germinated spore (NGS), germinated spore with a short germ tube (GS-SGT), germinated spore with a well-developed germ tube (GS-DGT), and germinated spore with branched hyphae (GS-BH). Pictures were taken with a digital camera (DXM1200C, Nikon) using image capture software (Nis-Elements BR, Nikon).

To measure the colonization of the substomatal cavities, 4-cm third-leaf segments were collected at 21 dai and then bleached in a mixture of absolute ethanol and acetic acid (3:1; v/v) overnight. The cleared leaves were rehydrated in distilled water for 4 h and then fixed in lactoglycerol (lactic acid: glycerol: water; 1:1:1; v/v/v) for 20 min. The fungal structures were stained by immersing the leaf segments in 0.1% Trypan blue (Sigma-Aldrich, Saint Quentin Fallavier, France) dissolved in lactophenol-ethanol (1:2; v/v) at 50°C for 20 min. After washing, the leaf segments were fixed in lactoglycerol, placed on a glass slide, and then observed microscopically at 400× magnification. The colonization of the substomatal cavities was determined from 150 substomatal cavities chosen randomly by assessing the following cytological events: non-colonized stomata (NCS), colonized stomata but not yet filled with a pycnidium (CS), and colonized stomata filled with a pycnidium (P). Pictures were taken using the digital camera, and image capture software is mentioned above.

RNA and Metabolite Extraction

For both plant RNA and metabolite extractions, medial third-leaf segments of approximately 200 mg were sampled at 2 and 7 dat from non-inoculated plants and at 7 dat (corresponding to 5 dai) from inoculated plants and then immediately snap-frozen in liquid nitrogen. Samples collected for RNA extraction were stored at −80°C until analysis, and those harvested for metabolite extraction were lyophilized and weighed.

Total RNA was extracted from 100 mg of frozen leaf samples using the RNeasy Plant Mini Kit (Qiagen, Venlo, Netherlands). Genomic DNA contaminating was removed using DNase RNase-Free Set (Qiagen). The RNA obtained was suspended in 60 μL of RNase-free water and quantified by measuring the absorbance at 260 nm (BioPhotometer, Eppendorf AG, Hamburg, Germany).

For metabolomic analysis, lyophilized leaf samples (i.e., 25–30 mg) were homogenized in a bead mill (TissueLyser II, Qiagen). Polar metabolites were extracted with 25 μl of methanol per mg of dry weight containing 1 $\mu g.ml^{-1}$ of apigenin and 5 $\mu g.ml^{-1}$ of chloramphenicol (Sigma-Aldrich) as internal standards. After vortexing two times for 30 s, the extract was sonicated for 10 min in an ultrasound bath, and then centrifugated at 12,000 × *g* at 21°C for 15 min. Finally, 150 μl of the supernatant was filtered and transferred to a vial and analyzed by ultra-high-performance liquid chromatography-mass spectrometry (UHPLC-MS).

Reverse Transcription-Quantitative PCR (RT-qPCR) Analysis

Reverse transcription of total RNA was carried out using the High Capacity cDNA Reverse Transcription Kit (Applied Biosystems, Waltham, MA, United States) according to the protocol provided by the manufacturer. The PCR reactions were performed with the obtained cDNA to amplify seven target genes: phenylalanine ammonia-lyase (*PAL*), chalcone synthase (*CHS*), lipoxygenase (*LOX*), allene oxide synthase (*AOS*), β-1,3-endoglucanase (*PR-2*), chitinase 2 (*PR-3*), and oxalate oxidase (*OXO*) (Tayeh et al., 2015; Ors et al., 2018) (**Supplementary Table 1**). The β-tubulin 4 (*TUB*) (Tayeh et al., 2013) and class A Apetala 2 (*PetA*) encoding genes were used as housekeeping genes after preliminary assays. Primer efficiencies were calculated by performing real-time PCR on several dilutions of the cDNA samples (>90% of efficiency). Reactions were performed in the real-time PCR detector C1000T (Bio-Rad, Marnes-la-Coquette, France) using the following thermal profile: a denaturation cycle for 3 min at 95°C, followed by an amplification and quantification cycle repeated 39 times (10 s at 95°C for annealing, 30 s at 60°C for extension). Melting curve assays were performed from 65 to 95°C with $0.5°C.s^{-1}$, and melting peaks were visualized to check the specificity of each amplification. The qPCR reaction was performed in duplicates (two technical replicates) for each sample.

UHPLC-MS Analysis

Metabolomic analyses were performed using a Dionex Ultimate 3000 UHPLC system (Thermo Fisher Scientific, Waltham, MA, United States). The chromatographic separations were performed on a Nucleodur C18 HTec column (150 mm × 2 mm, 1.8-μm particle size; Macherey-Nagel, Düren, Germany) maintained at 30°C. The mobile phase consisted of acetonitrile/formic acid (0.1%, v/v, eluant A) and water/formic acid (0.1%, v/v, eluant B) at a flow rate of 0.3 ml min^{-1}. The gradient elution was programmed as follows: 0–1 min, 95% B; 1–2 min, 95–85% B; 2–7 min, 85–0% B; 7–9 min, 100% A. The sample volume injected was 1 μl. The UHPLC system was coupled to an Exactive Orbitrap mass spectrometer (Thermo Fisher Scientific), equipped with an electrospray ionization (ESI) source operating in positive mode. Parameters were set at 300°C for the ion transfer capillary temperature and 2,500 V for the needle voltages. Nebulization with nitrogen sheath gas and auxiliary gas was maintained at 60 and 15 arbitrary units, respectively. The spectra were acquired within the mass-to-charge ratio (*m*/*z*) ranging from 100 to 1,000 atomic mass unit, using a resolution of 50,000 at *m*/*z* 200 atomic mass unit. The system was calibrated internally using dibutyl-phthalate as the lock mass at *m*/*z* 279.1591, giving a mass accuracy lower than 1 ppm. The instruments were controlled using the Xcalibur software (Thermo Fisher Scientific).

Metabolites were sought based on the calculated *m/z* of the corresponding pseudo-molecular ion $[M + H]^+$ from a list of metabolites of interest using a suspect screening approach (Krauss et al., 2010; Flamini et al., 2013). The previous wheat metabolome characterizations were used for a detailed analysis of the metabolites of interest in specific chemical families such as benzoxazinoids (de Bruijn et al., 2016), flavonoids (Wojakowska et al., 2013), and hydroxycinnamic acid amides (Li et al., 2018). Putative metabolite identifications were proposed based on expertized analysis of the corresponding mass spectra and comparison with published literature. Further information was retrieved from the Kyoto Encyclopedia of Genes and Genomes (KEGG[1]) and PubChem[2] databases. Relative quantification of the selected metabolites was performed using the Xcalibur software. For some metabolites, identity was confirmed with the corresponding standard provided by Sigma-Aldrich (France). Liquid chromatography-mass spectrometry (LC-MS) grade methanol and acetonitrile were purchased from Roth Sochiel (France); water was provided by a Millipore water purification system. Apigenin and chloramphenicol were used as internal standards.

Experimental Design and Statistical Analyses

The *in vitro* microscopic assays were conducted in a completely randomized design with five replications, each composed of one Petri dish. All experiments performed *in planta* in the greenhouse, including protection efficacy, cytological, gene expression, and metabolomic analyses, were carried out in a factorial completely randomized design with two factors: treatment (water or ulvan) and inoculation (*Z. tritici* or mock-inoculated plants). Three replications (pots), each composed of three plants, were used for each condition.

After verification of the variance homogeneity of the data sets, data were subjected to ANOVA. Comparisons

[1]http://www.genome.ad.jp/kegg/

[2]http://pubchem.ncbi.nlm.nih.gov

between data obtained for disease severity, pycnidium density, and all assessed *in planta* cytological events, as well as for *in vitro* spore germination and mycelial growth assays, were carried out with Student's *t*-test at a significance level of $P \leq 0.05$. For gene expression analysis, the relative levels of each gene expression normalized to the housekeeping genes *TUB* and *PetA* were represented, at each time point, as Log10 relative expression compared to water-treated control plants (expression value in the control fixed at 1) in both non-infectious and infectious contexts. To assess the effect of the fungus alone on gene expression, water-treated non-inoculated plants were compared with water-treated inoculated ones. Comparisons between data obtained in non-infectious and infectious contexts were performed with the Wilcoxon–Mann–Whitney and Kruskal–Wallis tests at $P \leq 0.05$, respectively. Regarding metabolomic analysis, pairwise comparisons were performed using Tukey's honest significant difference method followed by a false discovery rate (FDR) correction, with FDR < 0.05. Heatmaps were performed using the package *ComplexHeatmap* (Gu et al., 2016) after Log2 transformation data. Principal component analysis (PCA) was constructed in the package *vegan* (Oksanen et al., 2019). The statistical analyses were performed using the software R version 3.5.1 (R Core Team, 2018). All experiments were repeated three times and the values presented in this study are the average of the three experiments.

RESULTS

The Algal Polysaccharide Ulvan Mainly Encompasses Unsaturated Monosaccharides and Numerous Uronic Acid Residues

The molecular heterogeneity of ulvan oligosaccharides ($m/z <$ to 2,000 atomic mass unit) was assessed by a linear negative MALDI-TOF-MS analysis (**Figure 1** and **Supplementary Table 2**). The most intense $[M\text{-}H]^-$ mass signals were assigned to three series (in black, blue, and green) of ulvan monosaccharide composition. The main series (in black) of ulvan oligosaccharides is composed of one unsaturation (Δ, where unsaturation can be located either on Rha3S, Rha, or HexA), one Rha3S, one Xyl, one Rha, and several hexuronic acid residues ranging from one to at least eight. Two oligosaccharide substructures (in green) were composed of two unsaturation $(\Delta)_2$, Rha3S, Xyl, Rha, and $(HexA)_{0-1}$ residues, and two other minor substructures were composed of Rha, Xyl, Rha, and $(HexA)_{0-1}$ residues (in blue) (**Figure 1**).

Ulvan Protects Wheat Against *Z. tritici* and Reduces Both Host Colonization and Fungal Sporulation

The protection efficacy of ulvan in wheat against *Z. tritici* was evaluated in the greenhouse by spraying wheat plants of cv. Alixan with the fungus 2 days before inoculation. The first STB disease symptoms (chlorotic blotches and necrotic spots) appeared at 14 and 16 dai on the water- and ulvan-treated leaves, respectively. At 21 dai, the percentage of necrotic leaf area and index of pycnidium coverage reached 41% and 3.1 in control plants, respectively. Ulvan spraying significantly reduced disease severity by 45% (**Figure 2A**) and pycnidium density by 50% (**Figure 2B**) when compared to the control. Histopathological staining using Trypan blue at 21 dai revealed that the rates of non-colonized substomatal cavities were 55% higher in ulvan-treated leaves in comparison with water-treated ones (**Figures 2C**, **4E,F**). Likewise, plants treated with ulvan showed a significant reduction in 51% in pycnidium formation when compared with the control (**Figures 2C**, **4G,H**).

Ulvan Did Not Display Any Direct Antifungal Activity Toward *Z. tritici* Spores and Mycelium

The direct antifungal effect of ulvan on *Z. tritici* was assessed both *in vitro* and *in planta*. *In vitro* assays highlighted that the percentage of germinated spores did not significantly differ among the PDA plates amended (66%) or not (68%) with ulvan at 10 $mg.ml^{-1}$ (**Figure 3A**). A similar pattern was observed for mycelial growth since no significant effect was observed between fungal colony diameters scored in PDA plates supplemented (8.7 mm) or not (8.1 mm) with ulvan at 10 $mg.ml^{-1}$ (**Figure 3B**).

The effect of ulvan on the *in planta* epiphytic growth of *Z. tritici* was investigated by staining the fungus with Calcofluor. At 1 dai, the percentage of germinated spores over the leaf surface of water-treated plants was 59%. No significant effect of ulvan treatment on the *in planta* spore germination was observed when compared with the control (**Figures 3C**, **4A,B**). At 5 dai, the percentage of non-germinated spores (NGS), germinated spores with a short germ tube (GS-SGT), germinated spores with a well-developed germ tube (GS-DGT), and germinated spores with branched hyphae (GS-BH) were 14.1, 22.5, 27.1, and 37.7% in water-treated plants, respectively. Likewise, ulvan spraying did not significantly impact the fungal epiphytic development *in planta* when compared to the control (**Figures 3D**, **4C,D**).

Ulvan Elicits but Does Not Prime the Expression of Targeted Defense Genes

The relative expression of the seven genes involved in wheat defense reactions—namely, phenylalanine ammonia-lyase (*PAL*), chalcone synthase (*CHS*), lipoxygenase (*LOX*), allene oxide synthase (*AOS*), β-1,3-endoglucanase (*PR-2*), chitinase 2 (*PR-3*), and oxalate oxidase (*OXO*)—were analyzed using RT-qPCR in water- (control) and ulvan-treated plants prior to and after infection with *Z. tritici*. In non-inoculated conditions, at 2 dat, ulvan increased the expression of *PR-2*, *PR-3*, and *OXO* by 8.9-, 2.3-, and 2.9-fold compared with the control, respectively (**Figures 5E–G**). The expression of these three genes remained higher in ulvan-treated non-inoculated plants at 7 dat, i.e., 7.5-, 2.7-, and 4.6-fold for *PR-2*, *PR-3*, and *OXO*, respectively. In

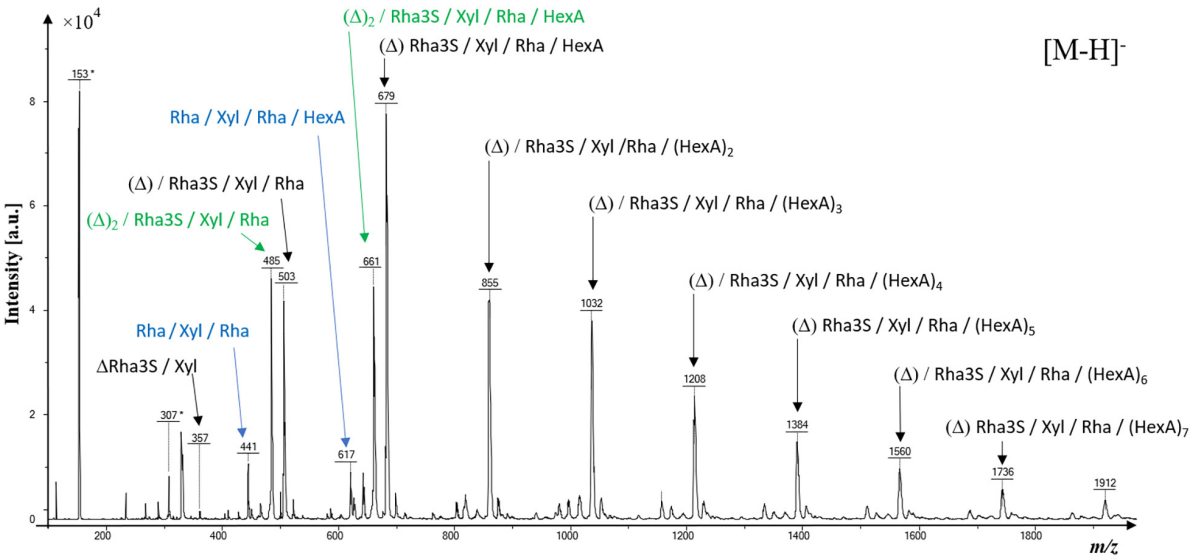

FIGURE 1 | Negative linear matrix-assisted laser desorption/ionization-time-of-flight-mass spectrometry (MALDI-TOF-MS) of ulvan (second precipitate). All mentioned *m/z* ratios correspond to $[M-H]^-$ ions. Note that the *m/z* * correspond to *m/z* of the 2,5-dihydroxybenzoic acid (DHB) matrix negative ions. Rhamnose (Rha); Rhamnose-3-sulfate (Rha3S); Xylose (Xyl); Hexuronic acid (HexA); Unsaturation of monosaccharides are depicted as (Δ).

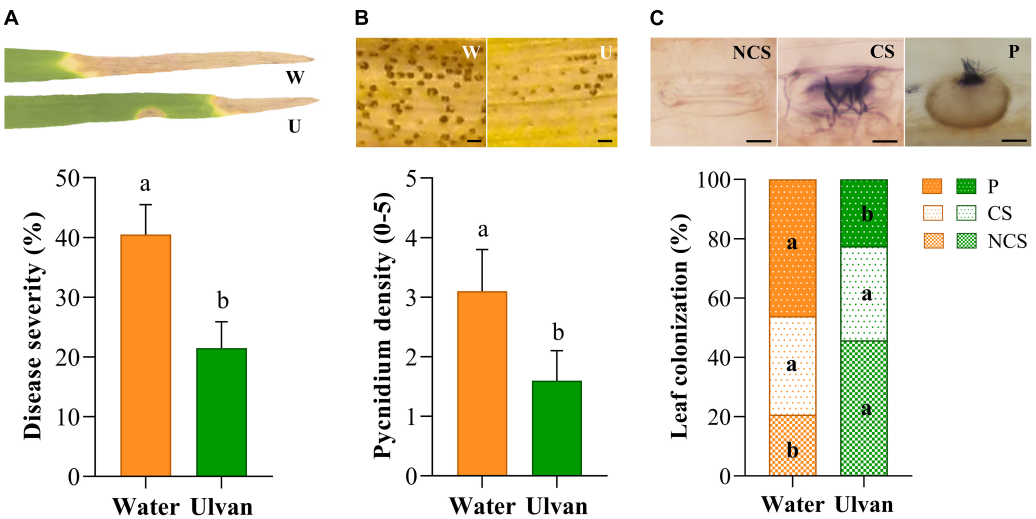

FIGURE 2 | Septoria tritici blotch severity **(A)**, pycnidium density **(B)**, and colonization of substomatal cavities **(C)** on the third leaves of the wheat (cv. Alixan) plants pre-sprayed with water (control) or ulvan (10 $mg.ml^{-1}$) and evaluated at 21 days after inoculation with *Zymoseptoria tritici*. Plants were inoculated 2 days after treatment. Letters indicate significant differences according to Student's *t*-test at $P \leq 0.05$. Bars represent the standard deviations of the mean. W, water; U, Ulvan; NCS, non-colonized stomata; CS, colonized stomata but not yet filled with a pycnidium; P, colonized stomata filled with a pycnidium. Scale bar = 100 μm **(B)** and 10 μm **(C)**.

addition, an upregulation of *LOX* and *AOS* with 7.5-fold was also observed in ulvan-treated non-inoculated plants at 7 dat (**Figures 5C,D**). When compared to non-inoculated plants in absence of ulvan pretreatment, the inoculation with *Z. tritici* induced an upregulation of *AOS*, *PR-2*, *PR-3*, and *OXO* by 3.0-, 12.0-, 2.5-, and 24.4-fold at 5 dai, respectively (**Figures 5D–G**). On the other hand, pretreatment with ulvan repressed the expression of *CHS* by 0.3-fold in infected plants at 5 dai (**Figure 5B**). No significant modulation of *PAL*, *PR-2*, *PR-3*, *AOS*, *LOX*, and *OXO* was observed in ulvan-treated inoculated plants compared to inoculated control ones (**Figures 5A,C–G**).

Ulvan Did Not Alter Wheat Metabolome in Both Non-infectious and Infectious Contexts

To quantify relative amounts of a total of 83 compounds in wheat leaves sprayed or not with ulvan, UHPLC-MS was performed

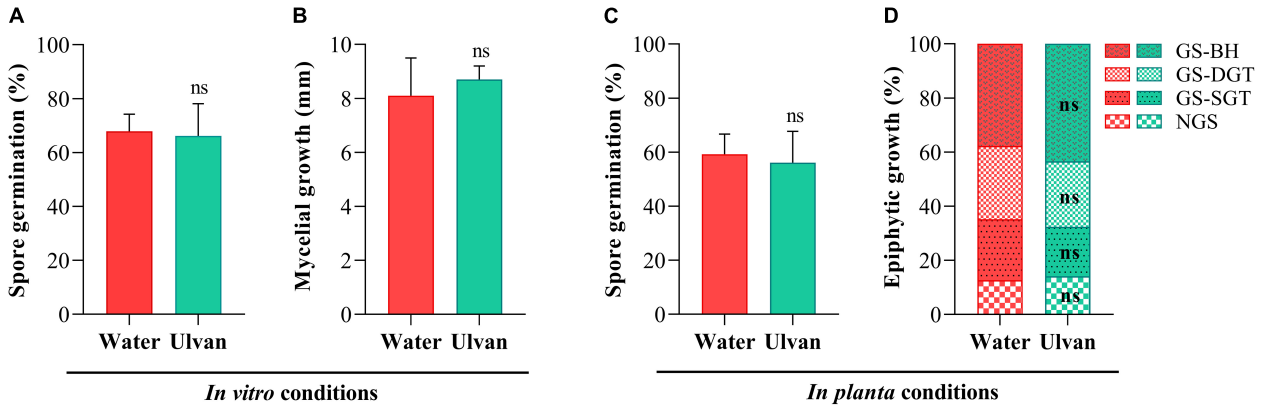

FIGURE 3 | Rates of spore germination **(A)** and mycelial growth **(B)** of *Zymoseptoria tritici* assessed *in vitro* at 1 and 10 days of incubation, respectively, on potato dextrose agar medium amended with water (control) or ulvan (10 mg.ml^{-1}), and spore germination **(C)** and epiphytic hyphal growth **(D)** of *Z. tritici* examined *in planta* at 1 and 5 days after inoculation, respectively, on the third leaves of the wheat plants (cv. Alixan) pre-treated with water (control) or ulvan (10 mg.ml^{-1}) 2 days before fungal inoculation. ns, not significant when compared to the control according to Student's *t*-test at $P \leq 0.05$. NGS, non-germinated spore; GS-SGT, germinated spore with a short germ tube; GS-DGT, germinated spore with a well-developed germ tube; GS-BH, germinated spore with branched hyphae.

(**Supplementary Figure 1** and **Supplementary Table 3**). The selected metabolites were grouped into 10 chemical families, i.e., amines, amino acids, benzoxazinoids, carboxylic acids, coumarins, flavonoids, hormones, hydroxycinnamic acid amides, sugars, and terpenoids. The PCA analysis of metabolite amounts resulted in different groups according to sampling time after ulvan treatment, i.e., 2 and 7 dat and between non-inoculated and inoculated plants at 5 dai, where the first and second component explained 23.8% and 18% of the variation, respectively, totalizing 41.8% of variations (**Figure 6**).

Differential analysis was then performed to identify the potential impact of different treatments on the selected metabolites (**Figure 7**). When comparing treatments in non-inoculated conditions, ulvan did not significantly change the levels of these metabolites, with the exception of spermidine that was significantly downregulated (≤0.55-fold) at 2 dat (**Figures 7A,B** and **Supplementary Table 4**). When compared to non-inoculated plants, the infection of *Z. tritici* upregulated the levels of six metabolites at 5 dai (≥3.3-fold); namely, methylpipecolic acid (amines), valylvaline (amino acids), DIM_2BOA (benzoxazinoids), caffeoylagmatine, caffeoylputrescine, and sinapoylagmatine (hydroxycinnamic acid amides) (**Figures 7C,D** and **Supplementary Table 4**). On the other hand, pretreatment with ulvan did not significantly change the levels of the studied metabolites in inoculated plants at 5 dai when compared with water-treated inoculated controls (**Figure 7E** and **Supplementary Table 4**).

DISCUSSION

Research to develop eco-friendly plant protection compounds without negative impacts on the environment and human health and fitting with the concept of sustainable agriculture is strongly encouraged nowadays. In this study, we report for the first time the potential of ulvan, a sulfated heteropolysaccharide isolated from the green macroalgae *Ulva fasciata*, for conferring significant protection to wheat against *Z. tritici*, a major fungal pathogen in this crop. This finding agrees with previous studies that demonstrated the ability of ulvan to enhance plant resistance against phytopathogens (Stadnik and de Freitas, 2014).

Our results showed that ulvan did not affect neither spore germination nor mycelial or hyphal growth of *Z. tritici* in both *in vitro* and *in planta* assays, thus corroborating previous works where no direct antifungal effect of ulvan toward distinct pathogens including fungi, yeast, and bacteria has been reported (Paulert et al., 2007, 2009; de Freitas and Stadnik, 2012). In contrast, we found that ulvan spraying significantly reduced the colonization of substomatal cavities in wheat leaves; more specifically, the rate of substomatal cavities bearing pycnidia, indicating that the protection conferred by ulvan treatment is associated with the specific defense responses of the plant rather than direct antifungal effects on the pathogen. Consequently, we analyzed the monosaccharide composition of ulvan and performed dedicated gene expression and metabolomic assays to explore the molecular basis of ulvan-induced resistance in the wheat-*Z. tritici* pathosystem.

The MALDI-TOF-MS analysis indicated that ulvan is mainly composed of unsaturated monosaccharides (rhamnose, rhamnose-3-sulfate, and xylose) and numerous uronic acid residues. Rhamnose is a major monosaccharide component of ulvan (Paulert et al., 2009; de Freitas et al., 2015) and is also present in rhamnogalacturonans (Pettolino et al., 2012) and rhamnolipids (Varnier et al., 2009), while uronic acids participate in the composition of polysaccharides in most life forms (Pettolino et al., 2012). Molecules containing rhamnose or uronic acids are known to trigger plant defense responses against pathogens (Varnier et al., 2009; de Freitas et al., 2015). As evidenced by Jaulneau et al. (2010), our work reinforces the proposition that ulvan recognition by the plant may be associated with rhamnose and/or uronic acid residues. However,

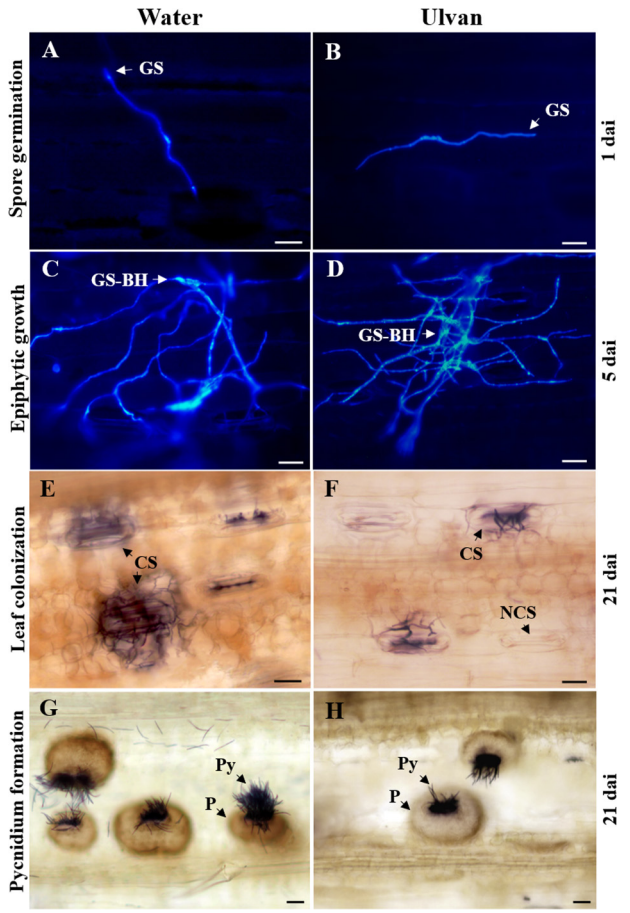

FIGURE 4 | Illustration of spore germination **(A,B)**, epiphytic hyphal growth **(C,D)**, colonization of substomatal cavities **(E,F),** and pycnidium formation **(G,H)** of *Zymoseptoria tritici* on wheat leaves (cv. Alixan) pre-treated with water (control) or ulvan (10 mg.ml^{-1}) and assessed at 1, 5, and 21 days after inoculation, respectively. Plants were inoculated 2 days after treatment. Fungal structures were stained with Calcofluor **(A–D)** and Trypan blue **(E–H)** and visualized under fluorescence microscopy and light microscopy, respectively. GS, germinated spore; GS-BH, germinated spore with branched hyphae; NCS, non-colonized stomata; CS, colonized stomata but not yet filled with a pycnidium; P, colonized stomata filled with a pycnidium; Py, pycnidiospores. Scale bar = 10 μm.

the signaling mechanisms underlying their perception remain to be further determined.

Molecular investigations revealed that ulvan induced several plant defense-related genes in non-inoculated wheat plants, including genes encoding for PR proteins (*PR-2* and *PR-3*), ROS metabolism (*OXO*), and the octadecanoid-based pathway (*LOX* and *AOS*). Interestingly, some of these genes such as *PR-2*, *PR-3*, and *OXO* were upregulated at both 2 and 7 dat, suggesting the eliciting effect of ulvan on wheat plants. The ability of ulvan to elicit the expression of plant defense genes has been previously observed in *Medicago truncatula* (Cluzet et al., 2004). In wheat, the application of extracts from another seaweed, such as the *Ascophyllum nodosum*-based product Dalgin Active®, has been reported to elicit *PR-2* and *LOX* (Somai-Jemmali et al., 2020). As a consequence of this enhanced basal resistance, plants may have more success in defending themselves against further fungal attacks. Indeed, it has been suggested that an upregulation of *PR-2* and *PR-3* genes, encoding for glucanase and chitinase enzymes, respectively, could reduce *Z. tritici* colonization by their known role in digesting β-glucans and chitin of the fungal cell wall, respectively (Shetty et al., 2009; Ors et al., 2019; Somai-Jemmali et al., 2020). In our case, we did not observe a significant upregulation of these targeted genes upon ulvan treatment in infected conditions. Therefore, taken together, our results indicate that the defense mechanisms triggered by ulvan in wheat against *Z. tritici* are more likely associated with an eliciting effect rather than with a priming effect. Accordingly, the eliciting effect of ulvan on glucanase activity was also reported in non-inoculated bean plants, even in those resistant to the hemibiotrophic fungus *Colletotrichum lindemuthianum* (de Freitas and Stadnik, 2012). On the other hand, using a system of suspension-cultured wheat cells, Paulert et al. (2010) concluded that ulvan have the priming effect because they did not elicit the production of hydrogen peroxide alone. Indeed, ulvan-pretreated wheat cells exhibited a stronger chitin-elicited oxidative burst response than the non-pretreated cells. Hence, looking at the earlier times of fungal infection to elucidate if ulvan also has a priming effect on wheat plants will be an exciting challenge for future research.

Wheat infection by *Z. tritici* upregulated the expression of *AOS*, *PR-2*, *PR-3*, and *OXO* genes at 5 dai independently of ulvan pre-treatment. This response may be associated with the basal defense reactions triggered by the plant in an attempt to defend itself against the pathogen, as evidenced by Ors et al. (2018). However, we cannot exclude the possibility that the fungus has invested efforts in activating specific plant defense responses such as *OXO* to support further colonization and disease development as well. This is because *OXO* is responsible for the conversion of oxalic acid and oxygen (O_2) into carbon dioxide (CO_2) and hydrogen peroxide (H_2O_2). Although H_2O_2 can be harmful to *Z. tritici* throughout its life cycle, this fungus can tolerate high levels of H_2O_2 (Shetty et al., 2007) and use it to induce host cell collapse mainly at the transition to the necrotrophic phase and reproduction (Keon et al., 2007). Alternatively, the high expression of *OXO* observed in our study may be the consequence of stress-related responses due to fungal infection rather than an efficient defense mechanism. Indeed, large-scale activation of the ROS metabolism has been observed after infection of *Z. tritici* in susceptible cultivars (Keon et al., 2007; Rudd et al., 2015; Ors et al., 2018).

Pre-treatment of ulvan downregulated the expression of *CHS* at 5 dai, and no modulation of *PAL* was observed at this time point. This result indicates that the biosynthesis of phenylpropanoids is probably not involved in the induction of plant resistance conferred by ulvan in wheat. Accordingly, no significant upregulation of flavonoids or coumarins was observed in our metabolomic analysis. The activation of *PAL* and *CHS* genes has been involved with the basal resistance of wheat (Adhikari et al., 2007; Ors et al., 2018) and after induction by the application of inducers, but mainly in resistant genotypes (Ors et al., 2019). Similarly, no induction of *PAL* was observed after

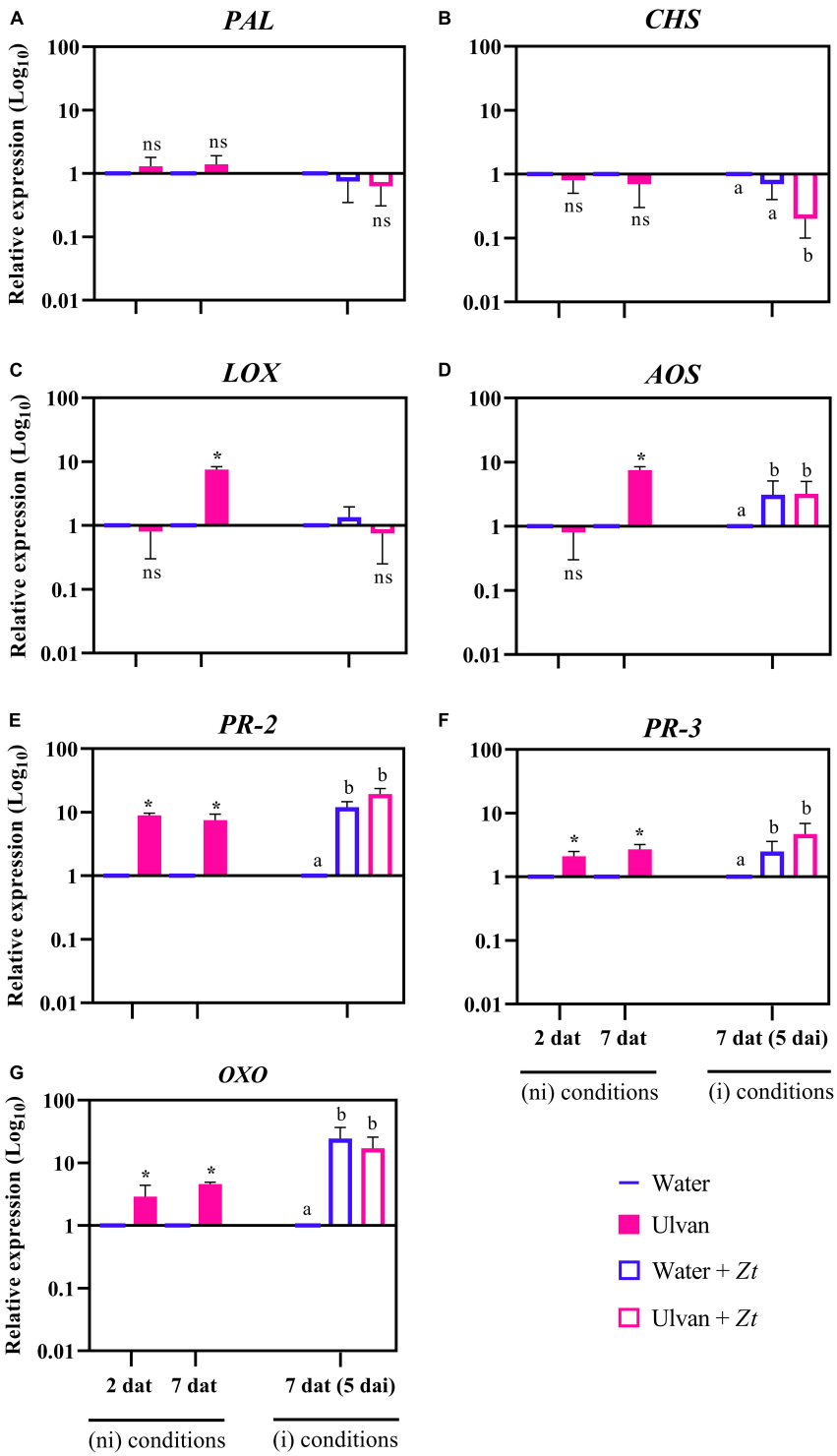

FIGURE 5 | Relative expression of phenylalanine ammonia-lyase (*PAL*; **A**), chalcone synthase (*CHS*; **B**), lipoxygenase (*LOX*; **C**), allene oxide synthase (*AOS*; **D**), β-1,3-endoglucanase (*PR-2*; **E**), chitinase 2 (*PR-3*; **F**), and oxalate oxidase (*OXO*; **G**) in wheat plants (cv. Alixan) at 2 and 7 days after treatment (dat) with ulvan, with 7 dat corresponding to 5 days after inoculation (dai) with *Zymoseptoria tritici* (*Zt*). The relative expression was calculated as Log10 fold change compared to water-sprayed non-inoculated (control) plants at each time point. The expression value of the control was fixed at 1. Asterisks and letters indicate significant differences according to the Wilcoxon–Mann–Whitney and Kruskal–Wallis tests at $P \leq 0.05$, respectively. ns, not significant when compared to the control. Plants were inoculated 2 days after treatment. ni, non-inoculated; i, inoculated.

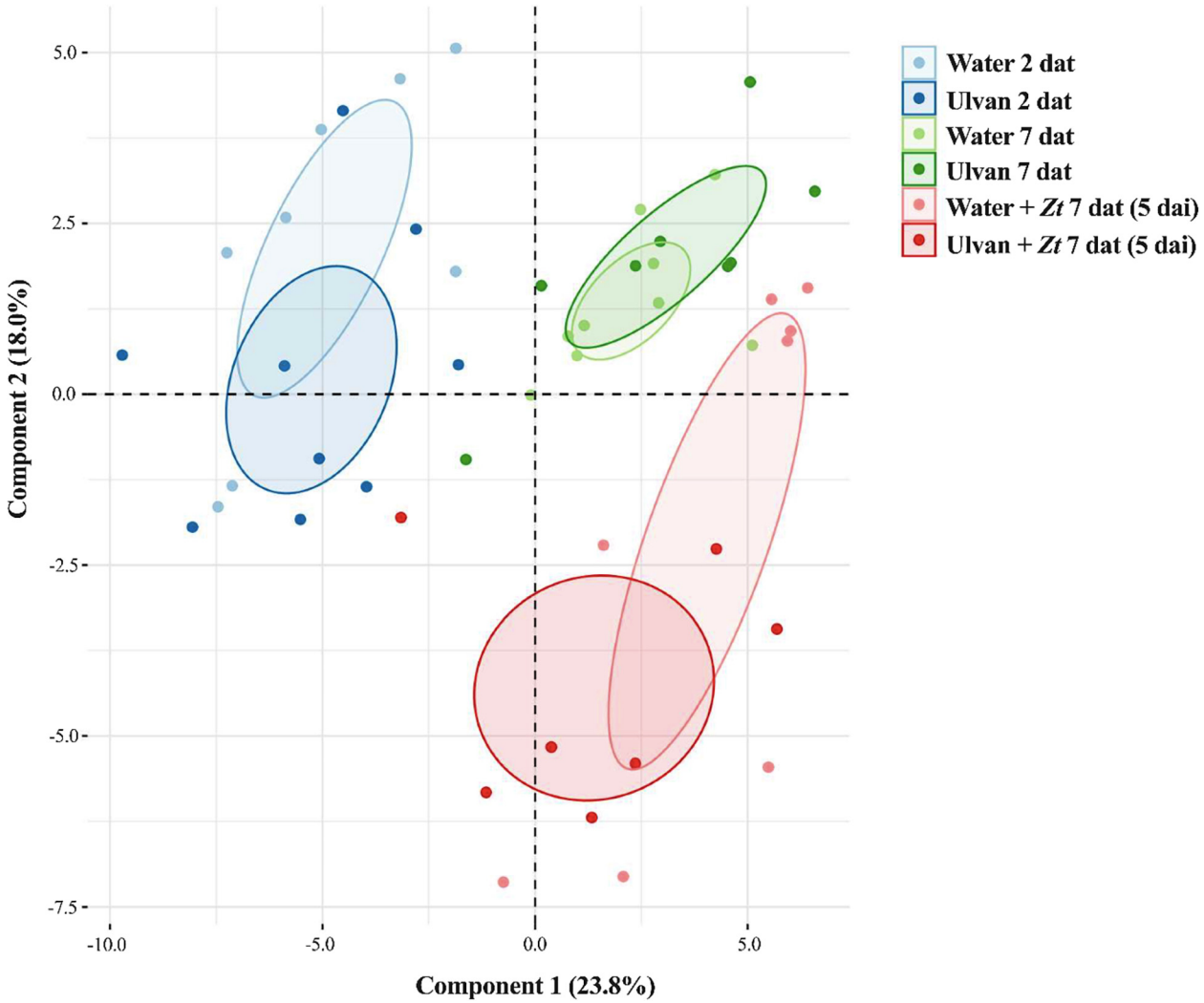

FIGURE 6 | Principal component analysis (PCA) of global wheat leaf metabolite levels at 2 and 7 days after treatment (dat) with ulvan, with 7 dat corresponding to 5 days after inoculation (dai) with *Zymoseptoria tritici* (*Zt*). Plants were inoculated 2 days after treatment.

treatment with the Dalgin Active® inducer in susceptible plants (Somai-Jemmali et al., 2020), suggesting that the activation of the phenylpropanoid pathway in bread wheat may be a cultivar- and/or elicitor-dependent response.

Targeted UHPLC-MS analyses were carried out to quantify the relative amounts of the 83 leaf metabolites belonging to major chemical families. Consistent with previous findings, infection by *Z. tritici* resulted in the accumulation of significant amounts of hydroxycinnamic acid amides (HCAAs) defense compounds (Seybold et al., 2020). Interestingly, the accumulation of a derivative of pipecolic acid, identified as methylpipecolic acid, was highly stimulated upon infection by *Z. tritici*. Lysine metabolism to pipecolic acid derivatives has been shown to be an important activator of defense reactions in several plant species (Hartmann and Zeier, 2018). In contrast, these metabolomic analyses did not reveal substantial changes in the leaf metabolome following ulvan treatment in both non-infected and infected conditions. Indeed, ulvan spraying did not significantly change the levels of the studied metabolites, with the exception of a slight downregulation of spermidine at 2 dat. As the analyzed metabolites were extracted with methanol, we cannot exclude that ulvan treatment may impact methanol-insoluble compounds, such as polymers involved in the reinforcement of cell walls. Altogether, our results suggest that ulvan treatment does not induce major changes in a selection of important leaf metabolites belonging to various chemical families. This observation reinforces the interest in ulvan as a plant health promoter, as the ulvan-conferred protection in wheat does not seem to be associated with important metabolic costs.

The induction of defense responses might be energetically costly for the plant (Walters and Heil, 2007). Such expenses are normally associated with increased demands for nitrogen and carbon skeletons that are provided by the primary metabolic

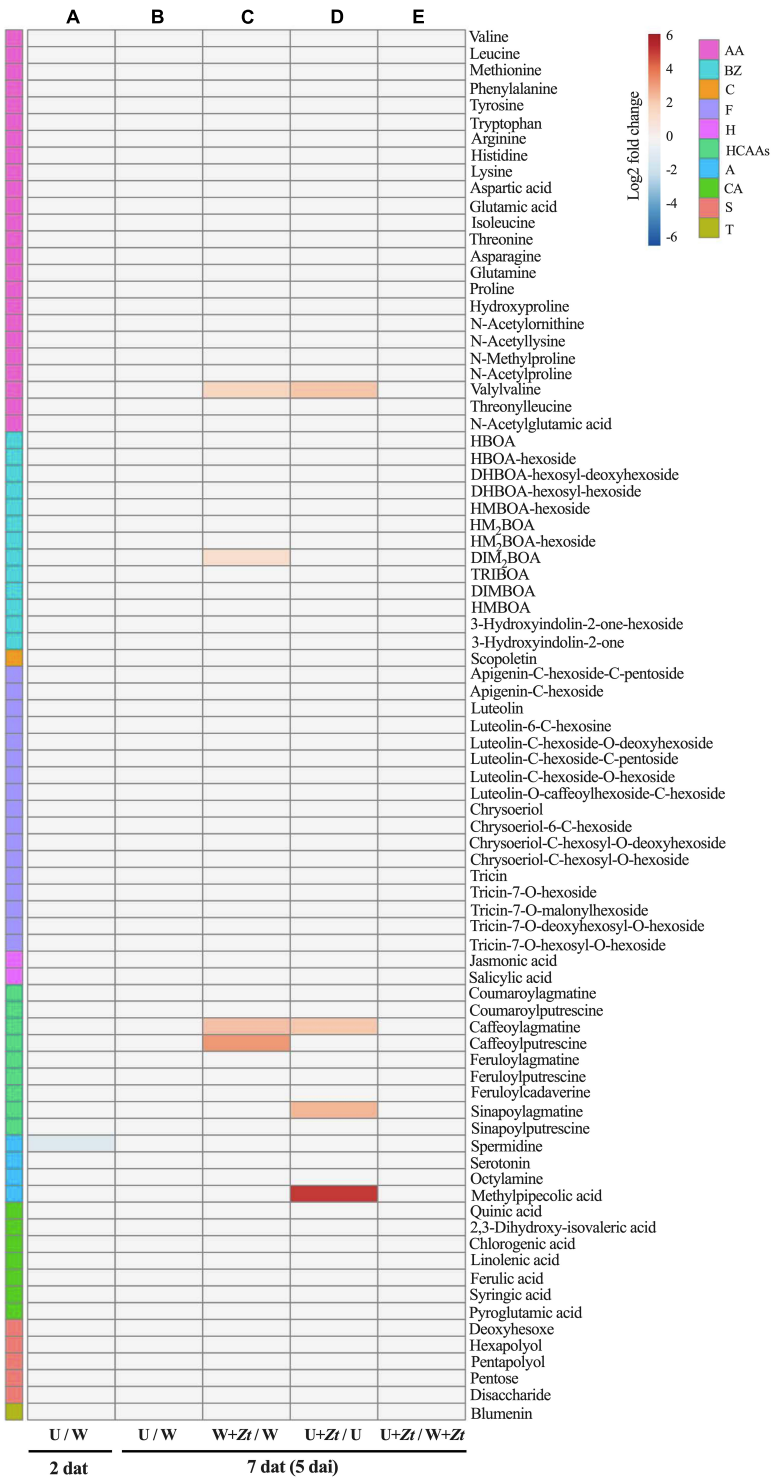

FIGURE 7 | Heatmap of metabolite fold changes in wheat leaves at 2 **(A)** and 7 **(B–E)** days after treatment (dat) with ulvan, with 7 dat corresponding to 5 days after inoculation (dai) with *Zymoseptoria tritici* (*Zt*). Upregulated and downregulated metabolite Log2 fold changes are indicated by red and blue colors, respectively. Metabolites were grouped according to their chemical family as amines (A), amino acids (AA), benzoxazinoids (BZ), carboxylic acids (CA), coumarins (C), flavonoids (F), hormones (H), hydroxycinnamic acid amides (HCAAs), sugars (S), and terpenoids (T). Pairwise comparisons were performed using Tukey's honest significant difference method followed by a false discovery rate (FDR) correction, with FDR < 0.05. For FDR ≥ 0.05, Log2 fold changes were set to 0. W, water; U, ulvan; W + *Zt*, Water + inoculation with *Zt*; U + *Zt*, Ulvan + inoculation with *Zt*.

pathways, such as carbohydrates and amino acids (Bolton, 2009). Our metabolic findings are in agreement with Cluzet et al. (2004), who highlighted that ulvan treatment-induced resistance in *Medicago truncatula* against *Colletotrichum trifolii* infection did not alter plant primary metabolism.

In summary, our study reports for the first time the potential of ulvan to protect wheat against *Z. tritici*. The displayed protection efficacy relies on plant resistance induction since ulvan did not exbibit any direct antifungal effect toward the pathogen in both *in vitro* and *in planta* conditions. Gene expression analysis indicated that ulvan induces resistance in wheat against *Z. tritici via* an eliciting effect rather than a priming effect and that this eliciting effect in wheat relies on the induction of PR protein synthesis, ROS metabolism, and octadecanoids, but do not on the phenylpropanoids. Interestingly, there was no evidence for major alteration in the wheat leaf metabolome upon ulvan treatment during the biotrophic phase of fungal infection, suggesting low plant metabolic and fitness costs associated with ulvan-induced resistance.

DATA AVAILABILITY STATEMENT

The original contributions presented in the study are included in the article/**Supplementary Material**, further inquiries can be directed to the corresponding authors.

AUTHOR CONTRIBUTIONS

MB performed all experiments and wrote the first draft of the manuscript. CF performed the MALDI-TOF-MS analysis. MB, MH, MM-R, BR, and AV performed the gene expression assays and related data analyses. MB, AM-G, RB, and PH performed the metabolomic assays and related data analysis. J-LH contributed to the whole data analyses and the manuscript writing. PR, MS, and AS supervised this study. All authors contributed to the article and approved the submitted version.

FUNDING

This work was supported by the International Cooperation Program CAPES-COFECUB Biostimalg (Grant: 88887.130209/2017-1) and the CPER Alibiotech funded by the European Union, the French State, and the French Region Hauts-de-France.

ACKNOWLEDGMENTS

MB is grateful to the Brazilian agency Coordination for the Improvement of Higher Education Personnel (CAPES) for the doctoral scholarship. MS is a research member of the National Council and Technological Development (CNPq). We are also grateful to the REALCAT platform funded by a French governmental grant administered by the French National Research Agency (ANR) as part of the frame of the "Investments for the Future" program (ANR-11-EQPX-0037).

SUPPLEMENTARY MATERIAL

The Supplementary Material for this article can be found online at: https://www.frontiersin.org/articles/10.3389/fpls.2021.703712/full#supplementary-material

Supplementary Figure 1 | Heatmap of global wheat leaf metabolite levels at 2 and 7 days after treatment (dat) with ulvan, with 7 dat corresponding to 5 days after inoculation (dai) with *Zymoseptoria tritici* (*Zt*). Log10 mean peak area of the indicated metabolites is given by shades of red or blue colors according to the scale bar. Metabolites were grouped according to their chemical family as amines (A), amino acids (AA), benzoxazinoids (BZ), carboxylic acids (CA), coumarins (C), flavonoids (F), hormones (H), hydroxycinnamic acid amides (Hcaas), sugars (S), and terpenoids (T). W, water; U, ulvan; W + *Zt*, Water + inoculation with *Zt*; U + *Zt*, Ulvan + inoculation with *Zt*.

Supplementary Table 1 | Primer sequences, GenBank accession numbers and corresponding references for genes studied in the quantitative reverse-transcription polymerase chain reaction (RT-qPCR) assays.

Supplementary Table 2 | Monosaccharide composition of ulvan and related average theoretical molecular mass.

Supplementary Table 3 | List of the 83 metabolites detected in wheat leaves (cv. Alixan) with ultra-high-performance liquid chromatography-mass spectrometry (UHPLC-MS), using a suspect screening strategy – targeted metabolomic approach.

Supplementary Table 4 | Changes in metabolite levels in wheat leaves at 2 and 7 days after treatment (dat) with ulvan, with 7 dat corresponding to 5 days after inoculation (dai) with *Zymoseptoria tritici*.

REFERENCES

Adhikari, T. B., Balaji, B., Breeden, J., and Goodwin, S. B. (2007). Resistance of wheat to *Mycosphaerella graminicola* involves early and late peaks of gene expression. *Physiol. Mol. Plant Pathol.* 71, 55–68. doi: 10.1016/j.pmpp.2007.10.004

Bolton, M. D. (2009). Primary metabolism and plant defense-fuel for the fire. *Mol. Plant Microbe Interact.* 22, 487–497. doi: 10.1094/MPMI-22-5-0487

Cluzet, S., Torregrosa, C., Jacquet, C., Lafitte, C., Fournier, J., Mercier, L., et al. (2004). Gene expression profiling and protection of *Medicago truncatula* against a fungal infection in response to an elicitor from green algae *Ulva* spp. *Plant Cell Environ.* 27, 917–928. doi: 10.1111/j.1365-3040.2004.01197.x

de Bruijn, W. J., Vincken, J. P., Duran, K., and Gruppen, H. (2016). Mass spectrometric characterization of benzoxazinoid glycosides from *Rhizopus*-elicited wheat (*Triticum aestivum*) seedlings. *J. Agric. Food Chem.* 64, 6267–6276. doi: 10.1021/acs.jafc.6b02889

de Freitas, M. B., Ferreira, L. G., Hawerroth, C., Duarte, M. E. R., Noseda, M. D., and Stadnik, M. J. (2015). Ulvans induce resistance against plant pathogenic fungi independently of their sulfation degree. *Carbohyd. Polym.* 133, 384–390. doi: 10.1016/j.carbpol.2015.07.055

de Freitas, M. B., and Stadnik, M. J. (2012). Race-specific and ulvan-induced defense responses in bean (*Phaseolus vulgaris*) against *Colletotrichum lindemuthianum*. *Physiol. Mol. Plant Pathol.* 78, 8–13. doi: 10.1016/j.pmpp.2011.12.004

Delgado, D. Z., de Freitas, M. B., and Stadnik, M. J. (2013). Effectiveness of saccharin and ulvan as resistance inducers against rust and angular leaf spot

in bean plants (*Phaseolus vulgaris*). *Crop Prot.* 47, 67–73. doi: 10.1016/j.cropro.2013.01.003

Flamini, R., De Rosso, M., De Marchi, F., Dalla Vedova, A., Panighel, A., Gardiman, M., et al. (2013). An innovative approach to grape metabolomics: stilbene profiling by suspect screening analysis. *Metabolomics* 9, 1243–1253. doi: 10.1007/s11306-013-0530-0

Fones, H., and Gurr, S. (2015). The impact of *Septoria tritici* Blotch disease on wheat: an EU perspective. *Fungal Genet. Biol.* 79, 3–7. doi: 10.1016/j.fgb.2015.04.004

Gu, Z., Eils, R., and Schlesner, M. (2016). Complex heatmaps reveal patterns and correlations in multidimensional genomic data. *Bioinformatics* 32, 2847–2849. doi: 10.1093/bioinformatics/btw313

Hartmann, M., and Zeier, J. (2018). L-lysine metabolism to N-hydroxypipecolic acid: an integral immune-activating pathway in plants. *Plant J.* 96, 5–21. doi: 10.1111/tpj.14037

Jaulneau, V., Lafitte, C., Corio-Costet, M. F., Stadnik, M. J., Salamagne, S., Briand, X., et al. (2011). An *Ulva armoricana* extract protects plants against three powdery mildew pathogens. *Eur. J. Plant Pathol.* 131, 393–401. doi: 10.1007/s10658-011-9816-0

Jaulneau, V., Lafitte, C., Jacquet, C., Fournier, S., Salamagne, S., Briand, X., et al. (2010). Ulvan, a sulfated polysaccharide from green algae, activates plant immunity through the jasmonic acid signaling pathway. *J. Biomed Biotechnol.* 2010:525291. doi: 10.1155/2010/525291

Keon, J., Antoniw, J., Carzaniga, R., Deller, S., Ward, J. L., Baker, J. M., et al. (2007). Transcriptional adaptation of *Mycosphaerella graminicola* to programmed cell death (PCD) of its susceptible wheat host. *Mol. Plant Microbe Interact.* 20, 178–193. doi: 10.1094/MPMI-20-2-0178

Krauss, M., Singer, H., and Hollender, J. (2010). LC-high resolution MS in environmental analysis: from target screening to the identification of unknowns. *Anal. Bioanal. Chem.* 397, 943–951. doi: 10.1007/s00216-010-3608-9

Li, Z., Zhao, C., Zhao, X., Xia, Y., Sun, X., Xie, W., et al. (2018). Deep annotation of hydroxycinnamic acid amides in plants based on ultra-high-performance liquid chromatography-high-resolution mass spectrometry and its in silico database. *Anal. Chem.* 90, 14321–14330. doi: 10.1021/acs.analchem.8b03654

Mejri, S., Siah, A., Coutte, F., Magnin-Robert, M., Randoux, B., Tisserant, B., et al. (2018). Biocontrol of the wheat pathogen *Zymoseptoria tritici* using cyclic lipopeptides from *Bacillus subtilis*. *Environ. Sci. Pollut. Res.* 25, 29822–29833. doi: 10.1007/s11356-017-9241-9

Oksanen, F. J., Blanchet, G., Friendly, M., Kindt, R., Legendre, P., McGlinn, D., et al. (2019). *vegan: Community Ecology Package*. Available online at: https://CRAN.R-project.org/package=vegan (accessed December 20, 2020).

Ors, M., Randoux, B., Siah, A., Couleaud, G., Maumené, C., Sahmer, K., et al. (2019). A plant nutrient-and microbial protein-based resistance inducer elicits wheat cultivar-dependent resistance against *Zymoseptoria tritici*. *Phytopathology* 109, 2033–2045. doi: 10.1094/PHYTO-03-19-0075-R

Ors, M. E., Randoux, B., Selim, S., Siah, A., Couleaud, G., Maumené, C., et al. (2018). Cultivar-dependent partial resistance and associated defence mechanisms in wheat against *Zymoseptoria tritici*. *Plant Pathol.* 67, 561–572. doi: 10.1111/ppa.12760

Paulert, R., Ebbinghaus, D., Urlass, C., and Moerschbacher, B. M. (2010). Priming of the oxidative burst in rice and wheat cell cultures by ulvan, a polysaccharide from green macroalgae, and enhanced resistance against powdery mildew in wheat and barley plants. *Plant Pathol.* 59, 634–642. doi: 10.1111/j.1365-3059.2010.02300.x

Paulert, R., Smania, A., Stadnik, M. J., and Pizzolatti, M. G. (2007). Antifungal and antibacterial properties of the ulvan and crude extracts from the green seaweed *Ulva fasciata* Delile. *Algol. Stud.* 123, 123–129. doi: 10.1127/1864-1318/2007/0123-0123

Paulert, R., Talamini, V., Cassolato, J. E. F., Duarte, M. E. R., Noseda, M. D., Smania, A., et al. (2009). Effects of sulfated polysaccharide and alcoholic extracts from green seaweed *Ulva fasciata* on anthracnose severity and growth of common bean (*Phaseolus vulgaris* L.). *J. Plant Dis. Prot.* 116, 263–270. doi: 10.1007/BF03356321

Pettolino, F. A., Walsh, C., Fincher, G. B., and Bacic, A. (2012). Determining the polysaccharide composition of plant cell walls. *Nat. Protoc.* 7, 1590–1607. doi: 10.1038/nprot.2012.081

R Core Team (2018). *R Version 3.5.0. R: A Language and Environment for Statistical Computing*. Vienna: R Foundation for Statistical Computing.

Rudd, J. J., Kanyuka, K., Hassani-Pak, K., Derbyshire, M., Andongabo, A., Devonshire, J., et al. (2015). Transcriptome and metabolite profiling of the infection cycle of *Zymoseptoria tritici* on wheat reveals a biphasic interaction with plant immunity involving differential pathogen chromosomal contributions and a variation on the hemibiotrophic lifestyle definition. *Plant Physiol.* 167, 1158–1185. doi: 10.1104/pp.114.255927

Seybold, H., Demetrowitsch, T. J., Hassani, M. A., Szymczak, S., Reim, E., Haueisen, J., et al. (2020). A fungal pathogen induces systemic susceptibility and systemic shifts in wheat metabolome and microbiome composition. *Nat. Commun.* 11:1910. doi: 10.1038/s41467-020-15633-x

Shetty, N. P., Jensen, J. D., Knudsen, A., Finnie, C., Geshi, N., Blennow, A., et al. (2009). Effects of β-1,3-glucan from *Septoria tritici* on structural defence responses in wheat. *J. Exp. Bot.* 60, 4287–4300. doi: 10.1093/jxb/erp269

Shetty, N. P., Mehrabi, R., Lütken, H., Haldrup, A., Kema, G. H., Collinge, D. B., et al. (2007). Role of hydrogen peroxide during the interaction between the hemibiotrophic fungal pathogen *Septoria tritici* and wheat. *New Phytol.* 174, 637–647. doi: 10.1111/j.1469-8137.2007.02026.x

Siah, A., Deweer, C., Duyme, F., Sanssené, J., Durand, R., Halama, P., et al. (2010a). Correlation of in planta endo-beta-1,4-xylanase activity with the necrotrophic phase of the hemibiotrophic fungus *Mycosphaerella graminicola*. *Plant Pathol.* 59, 661–670. doi: 10.1111/j.1365-3059.2010.02303.x

Siah, A., Deweer, C., Morand, E., Reignault, P., and Halama, P. (2010b). Azoxystrobin resistance of French *Mycosphaerella graminicola* strains assessed by four *in vitro* bioassays and by screening of G143A substitution. *Crop Prot.* 29, 737–743. doi: 10.1016/j.cropro.2010.02.012

Somai-Jemmali, L., Randoux, B., Siah, A., Magnin-Robert, M., Halama, P., Reignault, P., et al. (2017). Similar infection process and induced defense patterns during compatible interactions between *Zymoseptoria tritici* and both bread and durum wheat species. *Eur. J. Plant Pathol.* 147, 787–801. doi: 10.1007/s10658-016-1043-2

Somai-Jemmali, L., Siah, A., Randoux, B., Magnin-Robert, M., Halama, P., Hamada, W., et al. (2020). Brown alga *Ascophyllum nodosum* extract-based product, Dalgin Active®, triggers defense mechanisms and confers protection in both bread and durum wheat against *Zymoseptoria tritici*. *J. Appl. Phycol.* 32, 3387–3399. doi: 10.1007/s10811-020-02200-6

Stadnik, M. J., and de Freitas, M. B. (2014). Algal polysaccharides as source of plant resistance inducers. *Trop. Plant Pathol.* 39, 111–118. doi: 10.1590/S1982-56762014000200001

Steinberg, G. (2015). Cell biology of *Zymoseptoria tritici*: pathogen cell organization and wheat infection. *Fungal Genet. Biol.* 79, 17–23. doi: 10.1016/j.fgb.2015.04.002

Tayeh, C., Randoux, B., Bourdon, N., and Reignault, P. (2013). Lipid metabolism is differentially modulated by salicylic acid and heptanoyl salicylic acid during the induction of resistance in wheat against powdery mildew. *J Plant Physiol.* 170, 1620–1629. doi: 10.1016/j.jplph.2013.06.015

Tayeh, C., Randoux, B., Tisserant, B., Khong, G., Jacques, P., and Reignault, P. (2015). Are ineffective defence reactions potential target for induced resistance during the compatible wheat-powdery mildew interaction? *Plant Physiol. Biochem.* 96, 9–19. doi: 10.1016/j.plaphy.2015.07.015

Torriani, S. F. F., Melichar, J. P. E., Mills, C., Pain, N., Sierotzki, H., and Courbot, M. (2015). *Zymoseptoria tritici*: a major threat to wheat production, integrated approaches to control. *Fungal Genet. Biol.* 79, 8–12. doi: 10.1016/j.fgb.2015.04.010

Varnier, A. L., Sanchez, L., Vatsa, P., Boudesocque, L., Garcia-Brugger, A., Rabenoelina, F., et al. (2009). Bacterial rhamnolipids are novel MAMPs conferring resistance to *Botrytis cinerea* in grapevine. *Plant Cell Environ.* 32, 178–193. doi: 10.1111/j.1365-3040.2008.01911.x

Walters, D., and Heil, M. (2007). Costs and trade-offs associated with induced resistance. *Physiol. Mol. Plant Pathol.* 71, 3–17. doi: 10.1016/j.pmpp.2007.09.008

Walters, D., Walsh, D., Newton, A., and Lyon, G. (2005). Induced resistance for plant disease control: maximizing the efficacy of resistance elicitors. *Phytopathology* 95, 1368–1373. doi: 10.1094/PHYTO-95-1368

Wojakowska, A., Perkowski, J., Góral, T., and Stobiecki, M. (2013). Structural characterization of flavonoid glycosides from leaves of wheat (*Triticum aestivum* L.) using LC/MS/MS profiling of the target compounds. *J. Mass Spectrom.* 48, 329–339. doi: 10.1002/jms.3160

Conflict of Interest: The authors declare that the research was conducted in the absence of any commercial or financial relationships that could be construed as a potential conflict of interest.

Publisher's Note: All claims expressed in this article are solely those of the authors and do not necessarily represent those of their affiliated organizations, or those of the publisher, the editors and the reviewers. Any product that may be evaluated in this article, or claim that may be made by its manufacturer, is not guaranteed or endorsed by the publisher.

frontiers in Plant Science

ORIGINAL RESEARCH
published: 07 October 2021
doi: 10.3389/fpls.2021.741342

A *Valsa mali* Effector Protein 1 Targets Apple (*Malus domestica*) Pathogenesis-Related 10 Protein to Promote Virulence

*Weidong Wang[1,2], Jiajun Nie[1,2], Luqiong Lv[1,2], Wan Gong[1,2], Shuaile Wang[1,2], Mingming Yang[1,2], Liangsheng Xu[1,2], Mingjun Li[1,3], Hongxia Du[1,2] and Lili Huang[1,2]**

[1] State Key Laboratory of Crop Stress Biology for Arid Areas, Yangling, China, [2] College of Plant Protection, Northwest A&F University, Yangling, China, [3] College of Horticulture, Northwest A&F University, Yangling, China

To successfully colonize the plants, the pathogenic microbes secrete a mass of effector proteins which manipulate host immunity. Apple valsa canker is a destructive disease caused by the weakly parasitic fungus *Valsa mali*. A previous study indicated that the *V. mali* effector protein 1 (*VmEP1*) is an essential virulence factor. However, the pathogenic mechanism of *VmEP1* in *V*. *mali* remains poorly understood. In this study, we found that the apple (*Malus domestica*) pathogenesis-related 10 proteins (*MdPR10*) are the virulence target of *VmEP1* using a yeast two-hybrid screening. By bimolecular fluorescence (BiFC) and coimmunoprecipitation (Co-IP), we confirmed that the *VmEP1* interacts with *MdPR10 in vivo*. Silencing of *MdPR10* notably enhanced the *V*. *mali* infection, and overexpression of *MdPR10* markedly reduced its infection, which corroborates its positive role in plant immunity against *V*. *mali*. Furthermore, we showed that the co-expression of *VmEP1* with *MdPR10* compromised the *MdPR10*-mediated resistance to *V*. *mali*. Taken together, our results revealed a mechanism by which a *V*. *mali* effector protein suppresses the host immune responses by interfering with the *MdPR10*-mediated resistance to *V*. *mali* during the infection.

Keywords: defense response, *Valsa mali*, PR10, plant immunity, callose deposition

OPEN ACCESS

Edited by:
Rachid Lahlali, Ecole Nationale d'Agriculture de Meknès, Morocco

Reviewed by:
Hyong Woo Choi, Andong National University, South Korea
Miaoying Tian, University of Hawaii at Manoa, United States

****Correspondence:***
Lili Huang
huanglili@nwsuaf.edu.cn

Specialty section:
This article was submitted to Plant Pathogen Interactions, a section of the journal Frontiers in Plant Science

Received: *14 July 2021*
Accepted: *13 September 2021*
Published: *07 October 2021*

Citation:
Wang W, Nie J, Lv L, Gong W, Wang S, Yang M, Xu L, Li M, Du H and Huang L (2021) A Valsa mali Effector Protein 1 Targets Apple (Malus domestica) Pathogenesis-Related 10 Protein to Promote Virulence. Front. Plant Sci. 12:741342. doi: 10.3389/fpls.2021.741342

INTRODUCTION

The plants rely mainly on an innate complicated defense system to systematically counteract pathogen invasion. For successful infection and colonization in the hosts, the virulent pathogens deploy abundant effector proteins (EPs) which play a diverse number of roles in pathogenicity of the plant cells to modulate the plant immunity (Uhse and Djamei, 2018). The ascomycete *Valsa mali* has been reported to produce 193 secretory proteins with unknown functions, 101 of which are *V*. *mali*-specific (Li et al., 2015). These EPs are divided into two classes based on their function, inducing cell death elicitors, such as VmE02 (Nie et al., 2019) and VmHEP1 (Zhang et al., 2019), and the cell death suppressors, such as VmEP1 (Li et al., 2015) and VmPxE1 (Zhang M. et al., 2018). Among them, a deletion mutant of VmEP1 (VM1G_02400), which is a virulence factor of *V*. *mali*, showed a significantly reduction of virulence on the apple twigs and leaves (Li et al., 2015). However, how VmEP1 manipulates the host immunity is still not clear.

Several EPs have been reported to suppress the host immunity by targeting the positive regulators of immunity (Jwa and Hwang, 2017; Qi et al., 2019; Tang et al., 2020; Yang et al., 2020, 2021; Ai et al., 2021). For example, *Pseudomonas syringae* effector HopAI1 suppresses the PAMP-induced plants immunity (Zhang et al., 2007) by targeting the mitogen-activated protein kinase (MAPK), which plays roles in both the basal defense and interactions involving the R-gene-mediated resistance (Pedley and Martin, 2005). Conserved fungal effector NIS1, from *Magnaporthe oryzae*, suppresses the plants immunity by targeting PRR-associated kinases BAK1 and BIK1, which are positive regulators in the immune signaling pathway (Irieda et al., 2019; van der Burgh et al., 2019). In addition, many positive regulators targeted by the EPs have been reported. However, it remains unclear whether *V. mali* effector VmEP1 also targets the positive factors of immunity to suppress host immunity.

Pathogenesis-related (PR) proteins, which are key to the defense of plants, are able to enhance the disease resistance against both the biotrophic and necrotrophic phytopathogens (Honee, 1999; Jiang et al., 2015; Dai et al., 2016; Wu et al., 2016). Based on the protein sequence similarities, enzymatic activities, or other biological features, PR proteins are grouped into 17 families (Sels et al., 2008; Kim et al., 2014). Some, such as PR2, PR3, PR4, PR5, PR10, and PR12, possess significant antimicrobial activity (Loon and Strien, 1999; Chadha and Das, 2006; Sels et al., 2008; Taheri and Tarighi, 2010), and some can activate the systemic acquired resistance (SAR) pathway in the plants to defend against the phytopathogens (Ahuja et al., 2012; Navarova et al., 2012; Ali et al., 2017). Therefore, quite a few PR proteins are considered to be positive regulators of plant immunity. For this, the PR proteins can frequently be targeted by pathogen effectors. For example, the barley PR17 proteins are targeted by effector CSEP0055 from powdery mildew (Zhang et al., 2012), and wheat PR1 proteins are targeted by SnTox3 from *Parastagonospora nodorum* (Breen et al., 2016). Nonetheless, whether other PR proteins are targeted by pathogen effectors is largely unknown.

The pathogenesis-related 10 (PR10) proteins play diverse roles in the plant developmental processes, secondary metabolism, and antimicrobial activity (Choi et al., 2012). The *PR10* genes can be activated by the biotic stresses, such as microbial attacks, fungal elicitors, or wounding stresses, as well as abiotic stresses, such as salt and drought (Choi et al., 2012). In particularly, it has been shown that *PR10* from apple (*Malus domestica*) was activated when exposed to the pathogens, such as viruses and fungi (Pühringer et al., 2000; Poupard et al., 2003; Chevalier et al., 2008; Liu et al., 2021), acibenzolar-S-methyl (ASM) (Ziadil et al., 2001), ethephon, and wounding (Poupard et al., 2003), indicating that in apple, PR10 plays an important role in response to the biotic and abiotic stresses.

In this study, we showed that apple PR10 (MdPR10) was targeted by VmEP1, a virulence-essential EP from *V. mali* (Li et al., 2015). The transient expression of *MdPR10* in apple induced callose deposition and enhanced resistance to *V. mali*, whereas gene silencing of *MdPR10* in apple leaves enhanced sensitivity to *V. mali*, indicating that MdPR10 positively contributes to apple immunity and disease resistance, but it is unclear whether it plays a regulatory role, or directly contribute to it. We further found that the transient expression of VmEP1 compromised MdPR10-induced callose deposition and attenuated MdPR10-mediated resistance to *V. mali*. Our results highlight a mechanism in which a *V. mali* effector promoted pathogen infection by targeting a PR10 protein which positively contributes to the apple immunity.

MATERIALS AND METHODS

Microbe and Plant Growth Conditions

The wild-type strain of *V. mali* 03-8 and *Sclerotinia sclerotiorum* were obtained from the Laboratory of Integrated Management of Plant Disease in the College of Plant Protection, Northwest A&F University, Shaanxi, Yangling, China (Wu et al., 2018). *Valsa mali*, *S. sclerotiorum*, and *Phytophthora capsici* were cultured on potato dextrose agar (PDA) at 25°C. *Agrobacterium tumefaciens* strains were routinely cultured on a yeast-extract and peptone (YEP) medium at 28°C and *Escherichia coli* strains DH5α were cultured on a Luria-Bertani medium (LB) at 37°C.

The tissue-cultured plantlets of apple (*M. domestica* "Gala 3") were grown on a Murashige and Skoog (MS) agar medium containing 0.3 mg/L 6-benzyl aminopurine (6-BA) and 0.2 mg/L indoleacetic acid (IAA) (Sun et al., 2018). They were cultured under conditions of 25°C, 60 μmol/m^2/s, and a 14 h photoperiod. *Nicotiana benthamiana* were grown in a greenhouse under a 16 h 25°C:8 h 22°C, high light intensity:darkness regime.

Infection Assays on Leaves

Valsa mali and S. *sclerotiorum* were cultured on PDA for 2 days. The agar disks containing mycelium of *V. mali* or S. *sclerotiorum* were taken from the edge of a growing colony. The stab inoculation method was used on the infiltrated leaves of apple and *N. benthamiana* (Wu et al., 2018). The inoculated samples were incubated at 25°C for 36 h. The size of lesions on apple and *N. benthamiana* were measured by Image J software and the crossing method, respectively. The apple leaves were then collected to measure the biomass of *V. mali*. All the treatments were performed on at least 30 apple leaves or 10 *N. benthamiana* leaves, and all the experiments were repeated three times.

Valsa mali biomass was measured using a quantitative polymerase chain reaction (qPCR) with *V. mali*-specific glyceraldehyde-3-phosphate dehydrogenase (G6PDH) primers (Yin et al., 2013) related to the apple elongation factor 1 alpha gene (EF-1a) (Yin et al., 2016) at 36 h post infiltration (hpi). Genomic DNA was isolated using a Super Plant Genomic DNA Kit (Polysaccharides and Polyphenolics-rich) (Tiangen, Beijing, China) from 0.5 g apple leaves that included all the infected tissue and healthy tissue without petioles. Quantification of *V. mali* biomass assay was performed three times, and each experiment with three replicates.

Plasmid Construction

All the constructs were cloned by homologous recombination with 15–20 bp of vector sequences at the 5′ terminus of each primer using a ClonExpress II One Step Cloning Kit (Vazyme Biotech, Nanjing, China). The VmEP1 (lacking the

signal peptide-encoding region) was cloned from the cDNA of *V. mali* using gene-specific primers and was inserted into PICH86988, resulting in PICH86988-HA-VmEP1 used to perform a co-immunoprecipitation (Co-IP) assay. *MdPR10* and *NbPR10*, without terminator codons, were ligated into pCAMBIA1302 between the Nco1 and Spe1 sites, resulting in pCAMBIA1302-*MdPR10-GFP* and pCAMBIA1302-*NbPR10-GFP* for a Co-IP assay and a transient expression assay. The *VmEP1* and *MdPR10* amplified fragments were cloned into nYFP or cYFP, resulting in nYFP-MdPR10 and cYFP-VmEP1 used for carrying out a bimolecular fluorescence complementation (BiFC) assay. Individual colonies of each construct were tested by PCR and verified by sequencing. For yeast two-hybrid (Y2H) assays, VmEP1 fragment without signal peptide-encoding region was cloned into the pKGBKT7 vector using the *EcoR1* and *BamH1* sites to form the bait plasmid BD-VmEP1. MdPR10 was cloned into the pGADT7 vector using the *EcoR1* and *BamH1* sites to form the AD-MdPR10 plasmid. Loss-of-function MdPR10 plasmid was produced by cloning the reverse partially specific sequences of gene *MdPR10* into pFGC5941, carrying the *Nco*I and *Bam*HI digestion sites and resulting in pFGC5941-MdPR10 to produce siRNA (hpRNAi-MdPR10) (Zhang Q. et al., 2018). The constructs used for virus-induced gene silencing (VIGS) in *N. benthamiana* were generated in the tobacco rattle virus 2 (TRV2) vector (Liu et al., 2002) using the *N. benthamiana* cDNA library for gene fragment amplification. All the constructs were validated by sequencing in Sangon (Sangon Biotech, Shanghai, China). All the primers used above are listed in **Supplementary Table 1**.

Transient Expression in *Nicotiana benthamiana* and *Malus domestica*

The constructs were transformed into *Agrobacterium* strain GV3101 (pSoup-P19) by electric shock transformation. GV3101 (pSoup-P19) containing plasmids were grown in YEP medium supplemented with appropriated antibiotics at 28°C for 16–18 h until optical density $(OD)_{600}$ = 0.8. The bacterial cells were harvested and resuspended in the infiltration buffer (10 mM MES, 10 mM $MgCl_2$, and 200 μM acetosyringone), adjusted to the required OD_{600}, and incubated for 3 h before use. The plasmids were infiltrated into 4-week-old *N. benthamiana* leaves by injection; each plasmid was infiltrated into more than five *N. benthamiana* plants (∼20 leaves). For co-expression of multiple constructs, the Agrobacterium suspensions carrying the different constructs were thoroughly mixed before infiltration.

The transient expression on the apple leaves was performed as previously reported (Zhang Q. et al., 2018), with slight improvements. Agrobacterium suspensions used for transient expression in apple were used to prepare 50 ml, and the processing method was as described above. The pCAMBIA1302 constructs and pFGC5941 constructs were infiltrated into the leaves of 5-week-old tissue-cultured plantlets under a vacuum of 100 kPa for 10 min, and the infiltrated plantlets were returned to the MS medium and cultured in a growth cabinet. The infiltrated plantlets of overexpression and gene silencing were used for the experiments after 2 and 7 days of culture, respectively. Each plasmid was infiltrated into more than the eight apple plantlets (∼40 leaves).

Yeast Two-Hybrid Assay

A Y2H system was performed to screen for VmEP1-interacting proteins (Ito et al., 2001). The cDNA library was constructed into the prey vector pGADT7 using mRNA isolated from the junction of diseased (infected by *V. mali* wild type strain 03-8) and healthy twigs. The recombinant BD-VmEP1 and pGADT7-cDNA libraries were co-transformed into yeast strain AH109 using the lithium acetate method according to the Yeast Protocols Handbook (Clontech, United States). To verify the interaction between VmEP1 and MdPR10, BD-VmEP1 and AD-MdPR10 were co-transformed into the yeast strain AH109. The yeast transformants were cultured on synthetic dropout medium lacking leucine, tryptothan, and medium lacking leucine, tryptophan, and histidine (SD/-Leu-Trp-His), and the positive colonies were transferred to synthetic dropout medium lacking leucine, tryptophan, and histidine and containing X-α-Gal (SD/-Leu-Trp-His + X-α-Gal) for confirmation of the interaction. The yeast transformation and interaction tests were performed following the instructions in the Yeast Protocols Handbook (Clontech, United States).

Tobacco Rattle Virus-Based Virus-Induced Gene Silencing in *Nicotiana benthamiana*

Virus-induced gene silencing (VIGS) in plant was performed as previously described (Lu et al., 2003). A 300-bp sequence of *NbPR10*, predicted by sol genomics network (SGN) VIGS tool[1], was amplified and cloned into pBinary TRV2 vectors between the *BamH1* and *EcoR1* sites in the antisense orientation. A TRV2 construct expressing green fluorescent protein (GFP) served as a control. The primers used for PCR amplification are listed in **Supplementary Table 1**. The two largest leaves of four-leaf-stage *N. benthamiana* plants were pressure-infiltrated with GV3101 *A. tumefaciens* strains containing a mixture of TRV1 (OD_{600} = 0.4) and the VIGS construct or GFP control of each target protein at OD_{600} = 0.5. The plants were used for assays or check gene-silencing levels by real-time quantitative PCR (qRT-PCR) 3 weeks later. *A. tumefaciens* transient expressions in combination with *P. capsici* infection were carried out as described previously described.

RNA Extraction and Reverse Transcription-Quantitative Polymerase Chain Reaction

The samples were collected and ground in liquid nitrogen. For each sample, the total RNA was extracted using an EasyPure® Plant RNA Kit (cat. ER301, Transgen, Beijing, China) following the instructions of manufacturer, and genomic DNA was freed by treatment with DNAse 1. A NanoDrop spectrophotometer (ND-1000, Wilmington, DE, United States) was used to quantify RNA. cDNA was synthesized using MultiScribe™ Reverse

[1]https://vigs.solgenomics.net/

Transcriptase (Thermo Fisher Scientific, MA, United States). The qRT-PCR was performed using a Roche LightCycler® 96 SW1.1 Real-Time PCR System (Roche, IN, United States) with 2 × RealStar Green Power Mixture (GeneStar, Beijing, China). The EF-1a from *Malus* was used as an endogenous reference gene (Yin et al., 2016). The relative transcript level of each gene was calculated by the $2^{-\Delta\Delta CT}$ method (Livak and Schmittgen, 2001). All the treatments were performed in the three replicates, and all the experiments were repeated three times. The data from the three replicates were used to calculate the means and SDs. A statistical analysis was performed using Student's *t*-test implemented by SPSS software (IBM Corp., Armonk, NY, United States) ($P < 0.05$). The PCR was performed under the following conditions: 95°C (10 min), 40 cycles at 95°C (15 s), 60°C (30 s), and 72°C (30 s), followed by a melting curve step, 95°C (15 s), 60°C (60 s), and 95°C (15 s). The gene-specific primers used for the qRT-PCR are listed in **Supplementary Table 1**.

The heterologous expression of *VmEP1* was verified by semi-quantitative PCR (the primers are shown in the **Supplementary Table 1**). cDNA products measuring 2 μl served as templates and were amplified with 2xTaq Plus MasterMix (Dye) (CWBIO, China), and in the presence of the specific primers for *VmEP1*. The gene-specific primers used for RT-PCR are listed in **Supplementary Table 1**. The reactions were carried out using a Life Technologies ProFlex PCR System (United States). The PCR was performed under the following conditions: 95°C (3 min); 30 cycles at 95°C (30 s), 58°C (30 s), and 72°C (30 s); 72°C (2 min); 4°C holding. The PCR products were loaded onto 1% agarose gels with Gel Green (COFIT® Bioscience, China). Images of the agarose gels were acquired with a G:BOX F3 Gel Documentation System (Syngene, MD, United States).

Immunoprecipitation

The protein fusions were overexpressed in *N. benthamiana* using *Agrobacterium*-mediated transient expression. The leaf samples were collected at 48 hpi. The proteins were extracted using native lysis buffer (50 mM Tris–HCl pH 7.5, 150 mM NaCl, 1 mM EDTA, 0.5% NP-40, 1 × protease inhibitor mixture) with protease inhibitor mixture and 1 mM PMSF. To immunoprecipitated GFP-tagged MdPR10 or NbPR10, the protein extracts were incubated with GFP-Trap®_A magnetic beads (Chromotec) for 2 h on a rotator at 4°C. The resulting samples were analyzed by immunoblotting. The samples were loaded onto a 10% sodium dodecyl sulfate–polyacrylamide gel electrophoresis (SDS-PAGE) gel run with 1 × SDS running buffer for 30 min at 10 mA and 2 h at 15 mA. The gels were blotted onto a nitrocellulose membrane for 2 h at 65 V, then stained with Ponceau solution to show loading and transfer. The membranes were blocked in 5% milk in 1 × TBST [TBS (50 mM Tris–HCl, 150 mM NaCl, and pH 7.4) with Tween-20 0.1% (vol/vol)] for 1 h before the addition of primary antibodies overnight: either a monoclonal GFP antibody raised in mouse at 1:1,000 dilution (cat. AF0159; Beyotime) or a monoclonal hemagglutinin (HA) antibody raised in mouse at 1:1,000 (cat. no. 26183; Abcam). The membrane was washed with 1 × TBST (0.1% Tween 20) three times for 10 min each before the addition of the secondary antibody at 1:8,000 dilution with goat anti-mouse lgG-HRP antibody (cat. A0216; Beyotime) for 1 h. ECL Western Blotting Substrate (cat. PE0030; Beijing Solarbio Science and Technology, Beijing, China) was used according to the instructions of manufacturer.

Callose Staining

Callose deposition of *N. benthamiana* and apple leaves were stained with aniline blue as described (Adam and Somerville, 1996) and observed using a fluorescence microscope. Callose accumulation was quantified using Image J software and data were analyzed by Student's *t*-test or Tukey's multiple comparisons test.

Confocal Fluorescence Microscopy

The patches of *N. benthamiana* leaves were imaged 48 h after agro-infiltration using an Olympus FV3000 laser scanning microscope (Olympus Corporation, Tokyo, Japan). The GFP and yellow fluorescent protein (YFP) were imaged at excitation/emission wavelengths of 488 and 561 nm, respectively.

RESULTS

Transient Expression of a *Valsa mali* Effector Protein 1 in Plant Enhances Susceptibility to Pathogens

The VmEP1 was previously demonstrated to contribute to *V. mali* full virulence (Li et al., 2015). As an approach to illustrate this, VmEP1 lacking the signal peptide was transiently expressed in the apple leaves followed by inoculation with *V. mali*. As a result, the average number of lesions in the leaves expressing *VmEP1* increased by ∼49% when compared with those expressing GFP control (**Figures 1A,B**). The relative biomass of *V. mali* in the apple leaves expressing *VmEP1* was about 1.3 times that of the control (**Figure 1C**). The expression of *VmEP1* was determined by semiquantitative RT-PCR (**Figure 1D**). These results indicated that the transient expression of *VmEP1* in the apple leaves enhanced the host susceptibility to *V. mali*.

We also tested whether VmEP1 could facilitate the infection of other phytopathogens. For this, the VmEP1 was transiently expressed in the model plant *N. benthamiana* prior to inoculation with *P. capsici* and *S. sclerotiorum*. As shown (**Supplementary Figures 1A–D**), the average lesion diameters caused by *P. capsica* and *S. sclerotiorum* in the leaves expressing VmEP1 were ∼19 and ∼14% higher than those expressing the GFP control, respectively. These results indicated that VmEP1 could enhance the plant susceptibility to both oomycetes (*P. capsici*) and fungi (*V. mali* and *S. sclerotiorum*).

A *Valsa mali* Effector Protein 1 Interacts With Apple (*Malus domestica*) Pathogenesis-Related Protein 10

To clarify the underlying virulence mechanism of VmEP1, we aimed to find those host components that it targets.

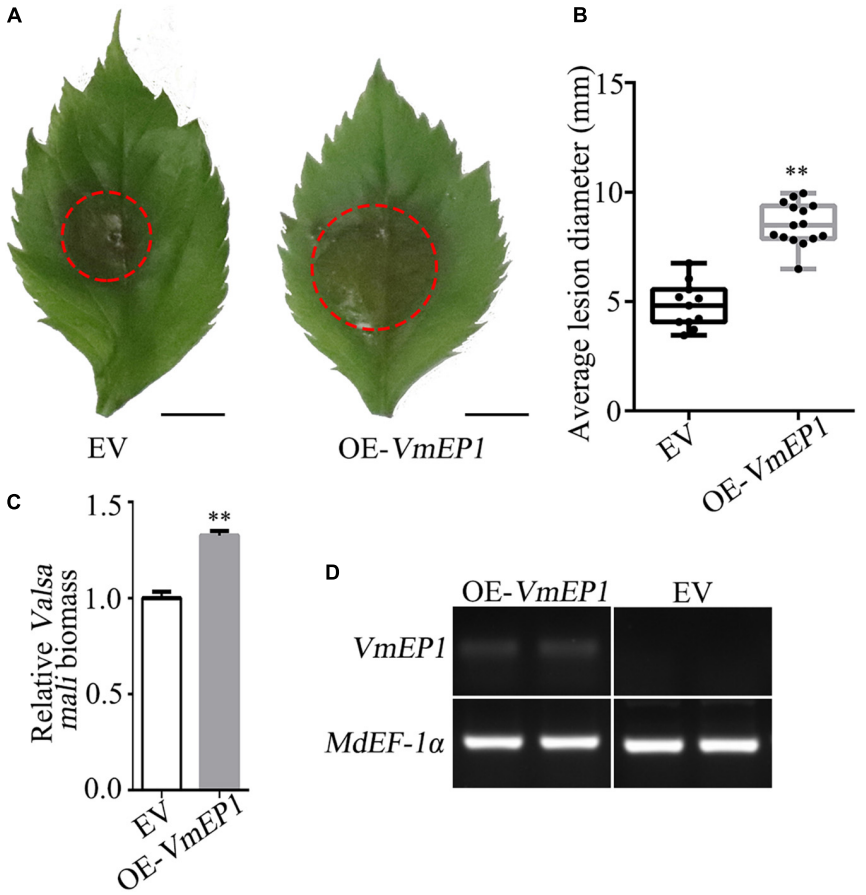

FIGURE 1 | The transient expression of *Valsa mali* effector protein 1 (*VmEP1*) in apple facilitates *V. mali* infection. **(A)** Representative disease symptoms of the apple leave overexpressing *VmEP1* at 36 hpi of *V. mali*. Bars = 5 mm. **(B)** The average lesion diameter of apple leaves in which *VmEP1* is overexpression was evaluated at 36 hpi of *V. mali*. **(C)** *V. mali* biomass was measured with qPCR at 36 hpi of *V. mali*. The relative *V. mali* biomasses were normalized to the mean of the wild-type. **(D)** A semiquantitative RT-PCR analysis to assess the expression of *VmEP1*. **(A–D)** EV, pCAMBIA1302 empty vector; OE-*VmEP1*, apple leaves overexpressing *VmEP1*. Mean ± SD; $n > 10$; $^{**}P < 0.01$; Student's *t*-test.

For this, we adopted the Y2H assay approach to screen the candidate targets using VmEP1 as bait. MdPR10 was one of the candidate proteins screened by Y2H assay (**Figure 2A**). To validate the VmEP1-MdPR10 interaction, a reciprocal BiFC assay was first performed. It showed that VmEP1 interacted with MdPR10 *in vivo* (**Figure 2**). To further confirm their interaction, we performed a Co-IP assay in *N. benthamiana*. As shown in **Figure 2C**, a specific signal for VmEP1-HA was clearly observed in the MdPR10-GFP immunoprecipitated (**Figure 2C**), indicating that VmEP1 interacted with MdPR10 in the plants.

Since VmEP1 also facilitates pathogen infection in *N. benthamiana*, we analyzed the homologous sequence of MdPR10 in *N. benthamiana* (**Supplementary Figure 2A**) and tested whether it interacted with VmEP1 similarly. As expected, the BiFC and Co-IP assays showed that the yellow fluorescence and a specific signal for VmEP1 were observed (**Supplementary Figures 2B,C**), indicating that the VmEP1 also interacted with *N. benthamiana* PR10 (NbPR10). In addition, we tested the interaction between an empty vector cYFP and nYFP. The yellow fluorescence was not detected (**Supplementary Figure 3**), indicating the results observed were all positive results.

Apple (*Malus domestica*) Pathogenesis-Related Protein 10 Positively Contributes to Plant Immunity

To investigate the role of MdPR10 during phytopathogen infection, we infiltrated *A. tumefaciens* cells carrying an MdPR10 fusion construct in the apple leaves, followed by inoculation with *V. mali*. The average lesion diameter of apple leaves expressing MdPR10 was ∼43% smaller than that of the control (**Figures 3A,B**). Moreover, the relative biomass of *V. mali* in the apple leaves expressing MdPR10 was ∼0.6 times that of the control (**Figure 3C**). The qRT-PCR results showed that the gene expression level of MdPR10 increased significantly (**Figure 3D**) and immunoblot analysis of MdPR10-GFP indicated MdPR10 was successfully expressed (**Figure 3E**). We also inoculated the apple leaves with *Colletotrichum gloeosporioides*. The results showed that the lesion diameter on the apple leaves expressing

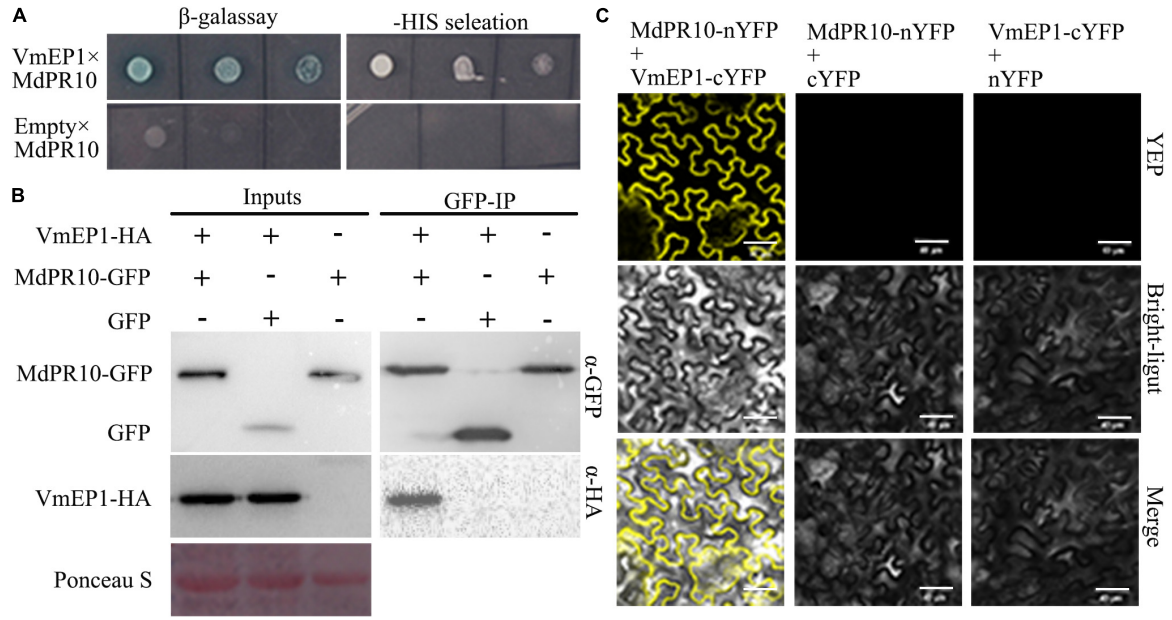

FIGURE 2 | Interaction between *VmEP1* and *Malus domestica* pathogenesis-related 10 protein (*MdPR10*) *in vitro* and *vivo*. **(A)** The positive yeast clones were cultured on SD-4 + X-α-Gal with ladder concentration of yeast suspension (10^{-1}, 10^{-2}, and 10^{-3}) for further confirmation. **(B)** Bimolecular fluorescence complementation showed that *VmEP1* interacted with *MdPR10* in the leaf cells of *N. benthamiana*. VmEP1-cYFP and MdPR10-nYFP were co-expressed in *N. benthamiana* by agroinfiltration. The yellow fluorescence was observed 48–72 h post infiltration (Bars = 20 μm). **(C)** *In vivo* Co-IP assay of HA: *VmEP1* (without the signal peptide sequence) and green fluorescent protein (GFP)-*MdPR10*. Both the genes were expressed in *N. benthamiana* leaves using agro-infection. The input experiment was performed by western blot with the HA antibody and GFP antibody to confirm the expression of the two proteins. The mixed proteins were blended with GFP-trap agarose beads. The final eluent was analyzed by immunoblot using the above-mentioned antibodies to detect *VmEP1* and *MdPR10*. This assay was repeated three times.

MdPR10 decreased (**Supplementary Figure 4**). To expound on these results, we further silenced MdPR10 in the apple leaves by *Agrobacterium*-mediated transient expression and inoculated the leaves with *V. mali*. The average lesion diameter of the apple leaves silencing MdPR10 was ∼25% higher than that of the control (**Figures 3F,G**). The relative biomass of *V. mali* in the apple leaves silencing MdPR10 was ∼1.27 times that of the control (**Figure 3H**). The qRT-PCR analysis showed that the transcript levels of MdPR10 were reduced by ∼50% (**Figure 3L**). **Figure 3M** illustrates a schematic diagram of the construction of the MdPR10 silencing vector. These results collectively suggested that MdPR10 positively contributed to the apple immunity and disease resistance.

To further confirm the above results, we transiently expressed *MdPR10* in *N. benthamiana* and inoculated with *P. capsici*. The average lesion diameter of *N. benthamiana* leaves expressing *MdPR10* was ∼32% smaller than that of the control (**Supplementary Figures 5A,B**). Furthermore, we silenced *NbPR10* in *N. benthamiana* by VIGS and inoculated *P. capsici*. It showed that the average lesion diameter of *N. benthamiana* leaves silencing *NbPR10* was ∼29% larger than that of the control (**Supplementary Figures 5C,D**). The silencing efficiency of *NbPR10* was tested by qRT-PCR, and the result showed that the *NbPR10* expression level was reduced by ∼80% (**Supplementary Figure 4E**). These results indicated that NbPR10 positively contributed to the plant immunity and disease resistance as well.

To address if the PR10 is a virulence target of VmEP1, *VmEP1* deletion mutants (Li et al., 2015) were inoculated on the apple leaves silencing *MdPR10*. The average lesion diameter of the *VmEP1* deletion mutants was ∼14% higher than that of the control (**Figures 3I,J**). The relative biomass of *V. mali* in the apple leaves silencing MdPR10 was significantly greater than that of the control (**Figure 3L**). These results suggested that PR10 was a functional target for VmEP1. The relative lesion diameter growth rate of *V. mali* (∼25%) was higher than that of the *VmEP1* deletion mutants (∼15%), indicating PR10 was essential for VmEP1 virulence function. These results indicated that the PR10 was a functional target for VmEP1.

A *Valsa mali* Effector Protein 1 Suppresses Apple (*Malus domestica*) Pathogenesis-Related 10 Proteins- and Pathogen-Associated Molecular Pattern-Triggered Callose Deposition

We detected the callose deposition by staining with aniline blue after transient expression of *MdPR10*. The results showed that the accumulation of callose was much greater in the apple leaves expressing *MdPR10* than that of the empty vector (**Figure 4**). However, the callose deposition in the apple leaves co-expressing *MdPR10* and *VmEP1* was clearly attenuated, compared with the experimental group expressing *MdPR10* alone (**Figure 4**). To validate these results, we detected the transcript level of *MdCalS5*,

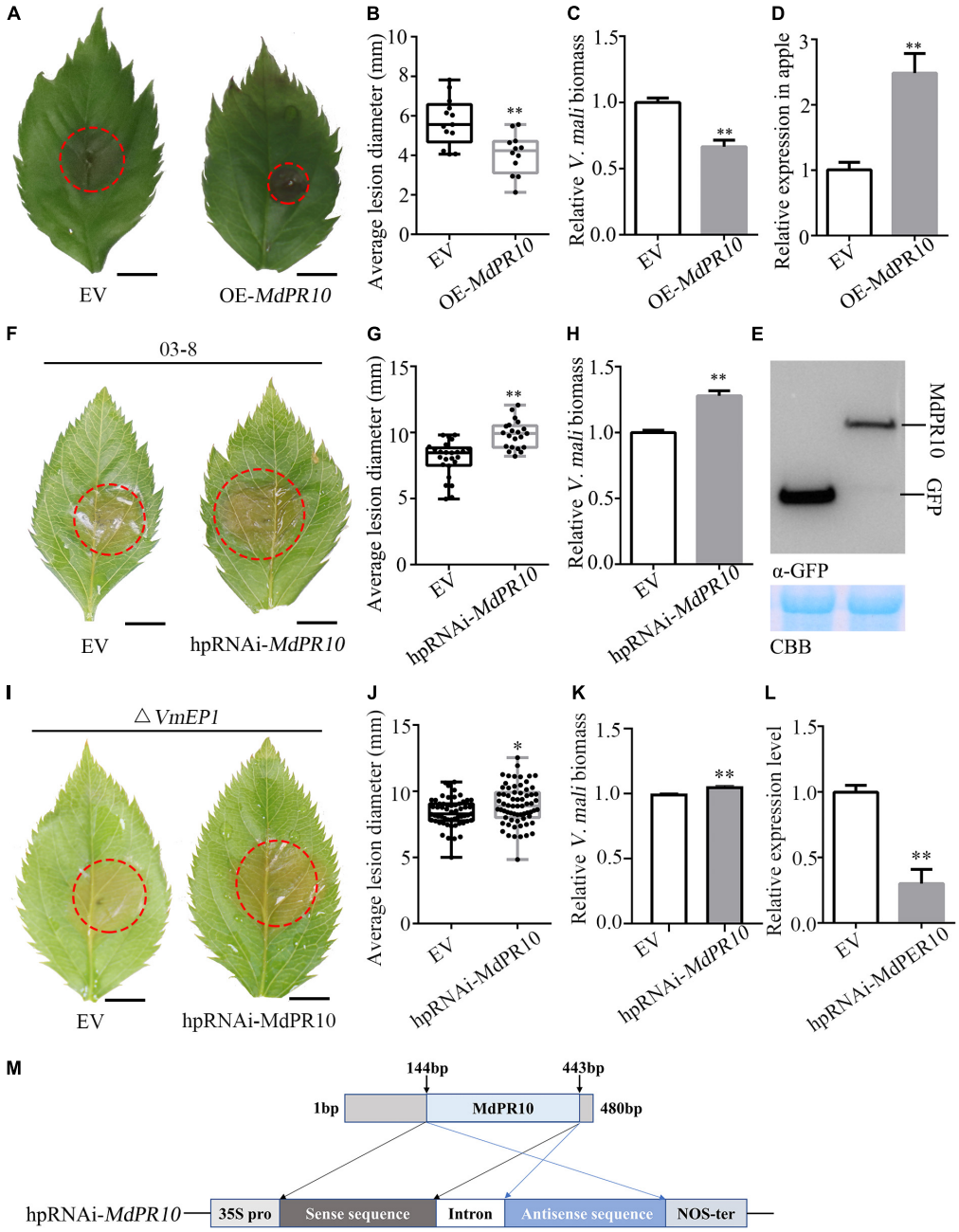

FIGURE 3 | Apple (*Malus domestica*) pathogenesis-related protein 10 positively contributes apple resistance to *V. mali*. **(A)** Representative disease symptoms of the apple leaves transiently expressing *MdPR10* at 36 h after inoculation of *V. mali*. Bars = 5 mm. **(B)** The average lesion diameter in the apple leaves in which MdPR10 is transiently expressed was evaluated at 36 hpi of *V. mali*. **(C)** The mRNA level of *MdPR10* in the apple leaves, as revealed by reverse transcription-quantitative polymerase chain reaction (RT-qPCR) 2 days after infiltration of OE-*MdPR10*. **(D)** *V. mali* biomass was measured with qPCR at 36 hpi. **(A–D)** EV, pCAMBIA1302 empty vector; OE-*MdPR10*, the apple leaves overexpressing *MdPR10*. **(E)** Immunoblot analysis of proteins in apple transiently expressing GFP control and MdPR10 fused with GFP tag. **(F)** Representative disease symptoms of the apple leaves in which *MdPR10* is silenced at 36 hpi of *V. mali*. Bars = 5 mm. **(G)** The average lesion diameter in the apple leaves in which MdPR10 is silenced was evaluated at 36 hpi of *V. mali*. **(H)** *V. mali* biomass was measured with qPCR at 36 hpi of *V. mali*. Relative *V. mali* biomasses were normalized to the mean of the wild-type. **(I)** Representative disease symptoms of the apple leaves silencing *MdPR10* after inoculation of *VmEP1* deletion mutants of *V. mali*. Bars = 5 mm. **(J)** The average lesion diameter in the apple leaves in which MdPR10 is silenced was evaluated at 36 h after the inoculation of *VmEP1* deletion mutants of *V. mali*. **(K)** The *V. mali* biomass was measured with qPCR at 36 hpi of the *VmEP1* deletion mutants of *V. mali*. The relative *V. mali* biomasses were normalized to the mean of the wild-type. **(L)** Silence efficiency detection of MdPR10 in apple leaves by RT-qPCR 5 days after the infiltration of hpRNAi-*MdPR10*. **(M)** Schematic of the constructs used to silence MdPR10. hpRNAi-*MdPR10* were cloned into the pFGC5941 binary vector. In panels **(E–L)** EV, pFGC5941 empty vector; hpRNAi-*MdPR10*, apple leaves in which *MdPR10* is silenced. In panels **(B,F,J)** mean ± SD; $n > 10$; $^{*}P < 0.05$, $^{**}P < 0.01$; Student's *t*-test. In panels **(C,D,G,H)** mean ± SD; $n = 3$; $^{**}P < 0.01$; Student's *t*-test. The genome DNA of the apple leaves was extracted and the relative *V. mali* biomass was estimated by DNA-based quantitative PCR (qPCR). These experiments were repeated three times with similar results.

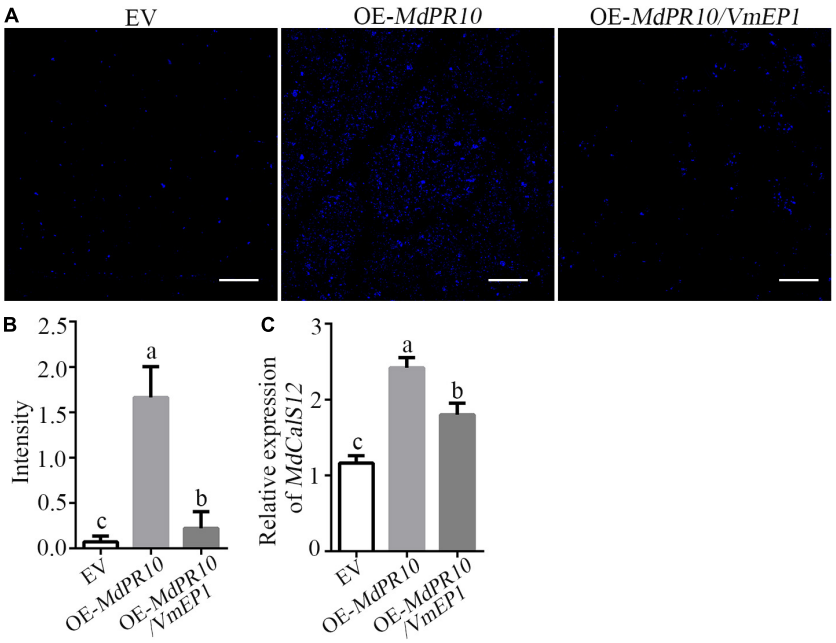

FIGURE 4 | A *Valsa mali* effector protein 1 suppresses *MdPR10*-mediated callose deposition. **(A)** Aniline blue staining with leaves at 48 h after expression of *MdPR10* or co-expression of *MdPR10* and *VmEP1* in the apple leaves. Bars = 100 μm. The expression of EV as control. Bars = 50 μm. **(B)** Quantification of the callose deposition in apple leaf tissues, as determined by ImageJ software. Mean ± SD; n > 10; a, b, and c indicate *t-test* $P < 0.05$; Duncan's multiple range test. **(C)** The mRNA level of *MdCalS5* in the apple plantlets, as revealed by qRT-PCR 2 days after infiltration of OE-*MdPR10*. The transcript levels were analyzed by qRT-PCR and normalized to that in the EV using the EF-1α gene as an internal reference. Mean ± SD; $n = 3$; a, b, and c indicate *t-test* $P < 0.05$; Duncan's multiple range test. These experiments were repeated three times with similar results. Panels **(A–C)** EV, pCAMBIA1302 empty vector.

a key enzyme for callose synthesis (Xie et al., 2012), by qRT-PCR. It showed that the expression level of *MdCalS5* in the apple leaves expressing *MdPR10* was about two times higher than the control expressing the empty vector alone. Additionally, the co-expression of MdPR10 and VmEP1 attenuated the transcript level of *MdCalS5* by ∼34% compared with the apple leaves expressing *MdPR10* (**Figure 4C**). These results indicated MdPR10 triggered callose deposition, and VmEP1 inhibited the response mediated by MdPR10.

To verify whether the expression of VmEP1 affected the pathogen-associated molecular pattern (PAMP)-triggered callose accumulation, we examined the callose deposition in *N. benthamiana* leaves after treatment with INF1 elicitin (Kamoun et al., 1997), a PAMP of *Phytophthora infestans* (Kamoun et al., 1998). The result showed that VmEP1 significantly suppressed the callose deposition induced by INF1 (**Supplementary Figure 6**). Together, these results indicated that VmEP1 could effectively inhibit the accumulation of callose in the plants.

A *Valsa mali* Effector Protein 1 Compromises Apple (*Malus domestica*) Pathogenesis-Related 10 Proteins-Mediated Resistance

Since VmEP1 attenuated the accumulation of callose induced by MdPR10, we speculated that VmEP1 might affect the resistance of MdPR10 to phytopathogens. To test this hypothesis, MdPR10 and VmEP1 were transiently co-expressed in apple. A *V. mali* inoculation assay showed that the average lesion diameter of the apple leaves co-expressing VmEP1 and MdPR10 was similar with that of the control, and was about 43% higher than the average lesion diameter of the apple leaves expressing MdPR10 (**Figures 5A,B**). These results indicated that the function of MdPR10 to suppress the infection of *V. mali* was weakened by VmEP1. The changed trend of relative *V. mali* biomass was consistent with the average lesion diameter (**Figure 5C**). Immunoblot analysis showed that MdPR10 successfully expressed (**Figure 5D**). These results showed that VmEP1 promoted infection of phytopathogens by inhibiting the callose deposition induced by MdPR10.

DISCUSSION

To resist the biotic and abiotic stress, the plants initiate a series of immune responses, such as reactive oxygen species (ROS) bursts, biosynthesis of phytohormones, the expression of a large number of defense-related genes, and callose deposition. The callose deposition at the cell wall is an early defense response (Jones and Dangl, 2006; Schwessinger and Ronald, 2012), which is associated with cell death (Han and Hwang, 2017). In *Arabidopsis*, the measuring callose deposition has become a popular model system to quantify the plant immunity activity (Luna et al., 2011), since pathogen invasion could be slowed by the cell walls thickened by the deposition of callose (Nishimura et al., 2003).

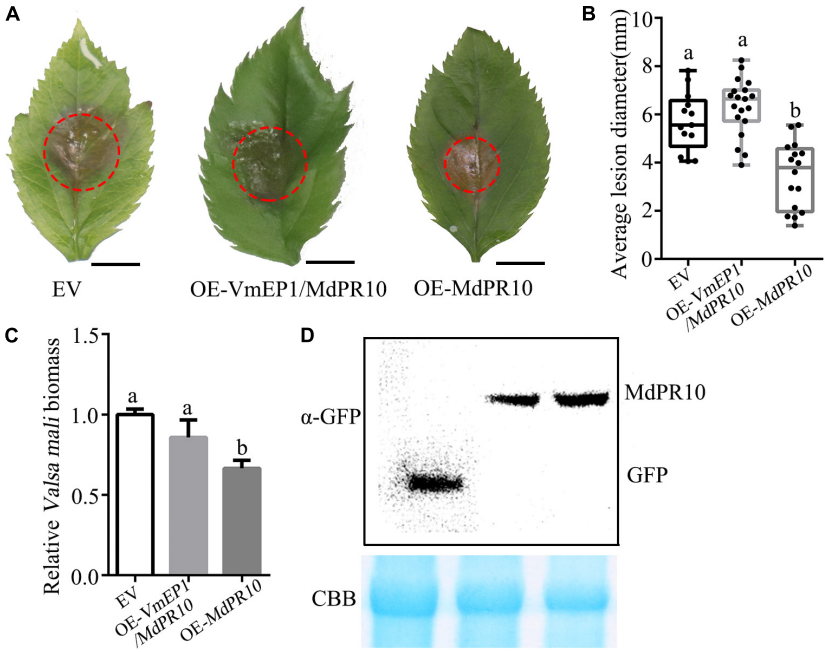

FIGURE 5 | A *Valsa mali* effector protein 1 attenuates the MdPR10-mediated resistance to *V. mali*. **(A)** Representative disease symptoms of the apple leaves overexpressing the genes at 36 hpi of *V. mali*. Bars = 5 mm. **(B)** The average lesion diameter in the apple leaves in which genes overexpression was evaluated at 36 hpi of *V. mali*. Means ± SDs; $n > 15$; a and b indicate *t-test* $P < 0.05$; Duncan's multiple range test. **(C)** *V. mali* biomass was measured with qPCR at 36 hpi of *V. mali*. The relative *V. mali* biomasses were normalized to the mean of the control. Means ± SDs; $n = 3$; a and b indicate *t-test* $P < 0.05$; Duncan's multiple range test. The genome DNA of apple leaves was extracted and the relative *V. mali* biomass was estimated by DNA-based quantitative PCR (qPCR). These experiments were repeated three times with similar results. **(D)** Immunoblot analysis of the expressed proteins were performed with anti-GFP antibody. CBB staining (bottom) was used as a loading control.

From the previous studies, we knew that the overexpression of *CaPR10* and *PpPR10* can induce the callose deposition (Choi et al., 2012; Castro et al., 2016), PR10 of *Malus sieversii* is upregulated after infection with a 15-fold higher increase than the control (Liu et al., 2021), and the transient expression of PR10 enhances the resistance to phytopathogens, such as PR-10 from *Panax ginseng* C. A. Meyer (Pulla et al., 2010), *Zea mays* (Xie et al., 2010), and strawberry (*Fragaria x ananassa*) (Besbes et al., 2019). This means the PR10 proteins, one of the pathogenesis-related groups, may contribute to plant resistance by inducing the callose deposition. In this study, we found that the overexpression of *MdPR10* induced callose deposition in the apple leaves (**Figure 4**) and enhanced the resistance of apple leaves to *V. mali* (**Figures 3A–C**). Our experimental results confirmed the previous studies, but the mechanism of immune activation of PR10 is still unclear.

Conversely, to successfully invade and colonize their host plants, the phytopathogenic bacteria, fungi, and oomycetes can secret diverse groups of EPs to inhibit the callose deposition, such as PsCRN63 from *Phytophthora sojae* (Li et al., 2016), PSTha5a23 from *Puccinia striiformis* f. sp. tritici (Cheng et al., 2017), and Cce1 from *Ustilago maydis* (Seitner et al., 2018). In our study, we found that the EP VmEP1 could not only inhibit the accumulation of callose (**Figure 4** and **Supplementary Figure 6**), but also promote the infection of *V. mali* (**Figure 1** and **Supplementary Figure 1**) by interaction with MdPR10 (**Figure 2**). The phytophthora effectors can affect the various aspects of the host plant immune systems to manipulate the host immunity, such as plant cell proteases, phytohormones, RNAs, the MAPK pathway, catalase, the ubiquitin proteasome pathway, the endoplasmic reticulum, nucleotide binding leucine-rich repeat (NB-LRR) proteins, and the cell membrane (Wang and Jiao, 2019). It has also been reported that PR10 interacting with effector CSEP0064/BEC1054, secreted by the fungal pathogen *Blumeria graminis*, may modulate the antimicrobial activity of these defense-related polypeptides (Dodds et al., 2019). Hence, we speculate that VmEP1 disturbs the host plant immune systems by interacting and interfering with MdPR10. However, it is still unknown how the effectors manipulate the function of PR10 proteins to interfere in the host plant immune response. Interestingly, the overexpression of *PR10* can activate a plant defense response, which is increased by its interaction with leucine-rich repeat (LRR1) proteins (Choi et al., 2012). Therefore, we put forward a hypothesis that VmEP1 and LRR1 may competitively interact with PR10, resulting in the weakening or disappearance of the interaction between LRR1 and PR10. Of course, this hypothesis needs to be verified by further research.

In summary, this study helps illustrate the mechanism of how VmEP1 aids infection of *V. mali*. MdPR10 was identified as a target of VmEP1 and a mediator of the defense response of the plants to inhibit the infection of phytopathogens. For

successful colonization, *V. mali* secretes effector VmEP1 to disturb MdPR10 resistance to *V. mali*. The discovery of MdPR10-enhanced resistance to *V. mali* will provide a new guidance for breeders to engineer the disease-resistant plants. Further studies are needed to explain how VmEP1 interferes in the function of MdPR10.

DATA AVAILABILITY STATEMENT

The original contributions presented in the study are included in the article/**Supplementary Material**, further inquiries can be directed to the corresponding author.

AUTHOR CONTRIBUTIONS

WW and LH designed the research. WW mainly contributed to the all experiments. WG, LL, SW, and HD assisted with specific experiments. JN, MY, LX, and ML assisted with preparation of the manuscript. LH revised the manuscript. All authors contributed to the article and approved the submitted version.

FUNDING

This work was supported by the National Natural Science Foundation of China (No. 31471732) and the Science and Technology Major Project of Shanxi Province (No. 2020zdzx03-03-01).

ACKNOWLEDGMENTS

The authors thank Qing Ma for providing the TRV plasmids, Xili Liu for providing the isolate of *P. capsici* (LT1534), and Jun Guo for preparing the manuscript.

SUPPLEMENTARY MATERIAL

The Supplementary Material for this article can be found online at: https://www.frontiersin.org/articles/10.3389/fpls.2021.741342/full#supplementary-material

REFERENCES

Adam, L., and Somerville, S. C. (1996). Genetic characterization of five powdery mildew disease resistance loci in Arabidopsis thaliana. *Plant J.* 9, 341–356. doi: 10.1046/j.1365-313x.1996.09030341.x

Ahuja, I., Kissen, R., and Bones, A. M. (2012). Phytoalexins in defense against pathogens. *Trends Plant Sci.* 17, 73–90. doi: 10.1016/j.tplants.2011.11.002

Ai, G., Xia, Q., Song, T., Li, T., Zhu, H., Peng, H., et al. (2021). A Phytophthora sojae CRN effector mediates phosphorylation and degradation of plant aquaporin proteins to suppress host immune signaling. *PLoS Pathog.* 17:e1009388. doi: 10.1371/journal.ppat.1009388

Ali, S., Mir, Z. A., Tyagi, A., Bhat, J. A., Chandrashekar, N., Papolu, P. K., et al. (2017). Identification and comparative analysis of *Brassica juncea* pathogenesis-related genes in response to hormonal, biotic and abiotic stresses. *Acta Physiol. Plant.* 39:268. doi: 10.1007/s11738-017-2565-8

Besbes, F., Habegger, R., and Schwab, W. (2019). Induction of PR-10 genes and metabolites in strawberry plants in response to *Verticillium dahliae* infection. *BMC Plant Biol.* 19:128. doi: 10.1186/s12870-019-1718-x

Breen, S., Williams, S. J., Winterberg, B., Kobe, B., and Solomon, P. S. (2016). Wheat PR-1 proteins are targeted by necrotrophic pathogen effector proteins. *Plant J.* 88, 13–25. doi: 10.1111/tpj.13228

Castro, A., Vidal, S., and Ponce de Leon, I. (2016). Moss Pathogenesis-Related-10 Protein Enhances Resistance to *Pythium irregulare* in *Physcomitrella patens* and *Arabidopsis thaliana*. *Front. Plant Sci.* 7:580. doi: 10.3389/fpls.2016.00580

Chadha, P., and Das, R. H. (2006). A pathogenesis related protein, AhPR10 from peanut: an insight of its mode of antifungal activity. *Planta* 225, 213–222. doi: 10.1007/s00425-006-0344-7

Cheng, Y., Wu, K., Yao, J., Li, S., Wang, X., Huang, L., et al. (2017). PSTha5a23, a candidate effector from the obligate biotrophic pathogen Puccinia striiformis f. sp. tritici, is involved in plant defense suppression and rust pathogenicity. *Environ. Microbiol.* 19, 1717–1729. doi: 10.1111/1462-2920.13610

Chevalier, M., Parisi, L., Gueye, B., Campion, C., Simoneau, P., and Poupard, P. (2008). Specific activation of PR-10 pathogenesis-related genes in apple by an incompatible race of *Venturia inaequalis*. *Biol. Plant.* 52, 718–722. doi: 10.1007/s10535-008-0138-9

Choi, D. S., Hwang, I. S., and Hwang, B. K. (2012). Requirement of the cytosolic interaction between PATHOGENESIS-RELATED PROTEIN10 and LEUCINE-RICH REPEAT PROTEIN1 for cell death and defense signaling in pepper. *Plant Cell* 24, 1675–1690. doi: 10.1105/tpc.112.095869

Dai, L., Wang, D., Xie, X., Zhang, C., Wang, X., Xu, Y., et al. (2016). The Novel Gene VpPR4-1 from *Vitis pseudoreticulata* Increases Powdery Mildew Resistance in Transgenic *Vitis vinifera* L. *Front. Plant Sci.* 7:695. doi: 10.3389/fpls.2016.00695

Dodds, P. N., Pennington, H. G., Jones, R., Kwon, S., Bonciani, G., Thieron, H., et al. (2019). The fungal ribonuclease-like effector protein CSEP0064/BEC1054 represses plant immunity and interferes with degradation of host ribosomal RNA. *PLoS Pathog.* 15:e1007620. doi: 10.1371/journal.ppat.1007620

Han, S. W., and Hwang, B. K. (2017). Molecular functions of *Xanthomonas* type III effector AvrBsT and its plant interactors in cell death and defense signaling. *Planta* 245, 237–253. doi: 10.1007/s00425-016-2628-x

Honee, G. (1999). Engineered resistance against fungal plant pathogens. *Eur. J. Plant Pathol.* 105, 319–326. doi: 10.1023/A:1008715520415

Irieda, H., Inoue, Y., Mori, M., Yamada, K., Oshikawa, Y., Saitoh, H., et al. (2019). Conserved fungal effector suppresses PAMP-triggered immunity by targeting plant immune kinases. *Proc. Natl. Acad. Sci. U. S. A.* 116, 496–505. doi: 10.1073/pnas.1807297116

Ito, T., Chiba, T., Ozawa, R., Yoshida, M., Hattori, M., and Sakaki, Y. (2001). A comprehensive two-hybrid analysis to explore the yeast protein interactome. *Proc. Natl. Acad. Sci. U. S. A.* 98, 4569–4574. doi: 10.1073/pnas.061034498

Jiang, L., Wu, J., Fan, S., Li, W., Dong, L., Cheng, Q., et al. (2015). Isolation and Characterization of a Novel Pathogenesis-Related Protein Gene (*GmPRP*) with Induced Expression in Soybean (*Glycine max*) during Infection with *Phytophthora sojae*. *PLoS One* 10:e0129932. doi: 10.1371/journal.pone.0129932

Jones, J. D., and Dangl, J. L. (2006). The plant immune system. *Nature* 444, 323–329. doi: 10.1038/nature05286

Jwa, N. S., and Hwang, B. K. (2017). Convergent Evolution of Pathogen Effectors toward Reactive Oxygen Species Signaling Networks in Plants. *Front. Plant Sci.* 8:1687. doi: 10.3389/fpls.2017.01687

Kamoun, S., vanWest, P., deJong, A. J., deGroot, K. E., Vleeshouwers, V. G. A. A., and Govers, F. (1997). A gene encoding a protein elicitor of Phytophthora infestans is down-regulated during infection of potato. *Molecular Plant-Microbe Interactions* 10, 13–20.

Kamoun, S., Van West, P., Vleeshouwers, V. G., De Groot, K. E., and Govers, F. (1998). Resistance of *Nicotiana benthamiana* to *Phytophthora infestans* is

mediated by the recognition of the elicitor protein INF1. *Plant Cell* 10, 1413–1425. doi: 10.1105/tpc.10.9.1413

Kim, Y. J., Jang, M. G., Lee, H. J., Jang, G. H., Sukweenadhi, J., Kwon, W. S., et al. (2014). Functional characterization of the pathogenesis-related protein family 10 gene, *PgPR10-4*, from *Panax ginseng* in response to environmental stresses. *Plant Cell Tissue Organ Cult.* 118, 531–543. doi: 10.1007/s11240-014-0505-5

Li, Q., Zhang, M., Shen, D., Liu, T., Chen, Y., Zhou, J. M., et al. (2016). A *Phytophthora sojae* effector PsCRN63 forms homo-/hetero-dimers to suppress plant immunity via an inverted association manner. *Sci. Rep.* 6:26951. doi: 10.1038/srep26951

Li, Z., Yin, Z., Fan, Y., Xu, M., Kang, Z., and Huang, L. (2015). Candidate effector proteins of the necrotrophic apple canker pathogen *Valsa mali* can suppress BAX-induced PCD. *Front. Plant Sci.* 6:579. doi: 10.3389/fpls.2015.00579

Liu, X., Li, X., Wen, X., Zhang, Y., Ding, Y., Zhang, Y., et al. (2021). PacBio full-length transcriptome of wild apple (*Malus sieversii*) provides insights into canker disease dynamic response. *BMC Genomics* 22:52. doi: 10.1186/s12864-021-07366-y

Liu, Y., Schiff, M., Marathe, R., and Dinesh-Kumar, S. P. (2002). Tobacco Rar1, EDS1 and NPR1/NIM1 like genes are required for N-mediated resistance to tobacco mosaic virus. *Plant J.* 30, 415–429.

Livak, K. J., and Schmittgen, T. D. (2001). Analysis of relative gene expression data using real-time quantitative PCR and the 2(-Delta Delta C(T)) Method. *Methods* 25, 402–408. doi: 10.1006/meth.2001.1262

Loon, L. C. V., and Strien, E. A. V. (1999). The families of pathogenesis-related proteins, their activities, and comparative analysis of PR-1 type proteins. *Physiol. Mol. Plant Pathol.* 55, 85–97. doi: 10.1006/pmpp.1999.0213

Lu, R., Martin-Hernandez, A. M., Peart, J. R., Malcuit, I., and Baulcombe, D. C. (2003). Virus-induced gene silencing in plants. *Methods* 30, 296–303. doi: 10.1016/S1046-2023(03)00037-9

Luna, E., Pastor, V., Robert, J., Flors, V., Mauch-Mani, B., and Ton, J. (2011). Callose deposition: a multifaceted plant defense response. *Mol. Plant Microbe Interact* 24, 183–193. doi: 10.1094/MPMI-07-10-0149

Navarova, H., Bernsdorff, F., Doring, A. C., and Zeier, J. (2012). Pipecolic acid, an endogenous mediator of defense amplification and priming, is a critical regulator of inducible plant immunity. *Plant Cell* 24, 5123–5141. doi: 10.1105/tpc.112.103564

Nie, J., Yin, Z., Li, Z., Wu, Y., and Huang, L. (2019). A small cysteine-rich protein from two kingdoms of microbes is recognized as a novel pathogen-associated molecular pattern. *New Phytol.* 222, 995–1011. doi: 10.1111/nph.15631

Nishimura, M. T., Stein, M., Hou, B. H., Vogel, J. P., Edwards, H., and Somerville, S. C. (2003). Loss of a Callose Synthase Results in Salicylic Acid–Dependent Disease Resistance. *Science* 3011, 969–972. doi: 10.1126/science.1086716

Pedley, K. F., and Martin, G. B. (2005). Role of mitogen-activated protein kinases in plant immunity. *Curr. Opin. Plant Biol.* 8, 541–547. doi: 10.1016/j.pbi.2005.07.006

Poupard, P., Parisi, L., Campion, C., Ziadi, S., and Simoneau, P. (2003). A wound- and ethephon-inducible PR-10 gene subclass from apple is differentially expressed during infection with a compatible and an incompatible race of *Venturia inaequalis*. *Physiol. Mol. Plant Pathol.* 62, 3–12. doi: 10.1016/S0885-5765(03)00008-0

Pühringer, H., Moll, D., Hoffmann-Sommergruber, K., Watillon, B., Katinger, H., Machado, M. L. D., et al. (2000). The promoter of an apple *Ypr10* gene, encoding the major allergen Mal d 1, is stress- and pathogen-inducible. *Plant Sci.* 152, 35–50. doi: 10.1016/S0168-9452(99)00222-8

Pulla, R. K., Lee, O. R., In, J. G., Kim, Y. J., Senthil, K., and Yang, D. C. (2010). Expression and functional characterization of pathogenesis-related protein family 10 gene, *PgPR10-2*, from *Panax ginseng* C.A. Meyer. *Physiol. Mol. Plant Pathol.* 74, 323–329. doi: 10.1016/j.pmpp.2010.05.001

Qi, T., Guo, J., Liu, P., He, F., Wan, C., Islam, M. A., et al. (2019). Stripe Rust Effector PstGSRE1 Disrupts Nuclear Localization of ROS-Promoting Transcription Factor TaLOL2 to Defeat ROS-Induced Defense in Wheat. *Mol. Plant* 12, 1624–1638. doi: 10.1016/j.molp.2019.09.010

Schwessinger, B., and Ronald, P. C. (2012). Plant innate immunity: perception of conserved microbial signatures. *Annu. Rev. Plant Biol.* 63, 451–482. doi: 10.1146/annurev-arplant-042811-105518

Seitner, D., Uhse, S., Gallei, M., and Djamei, A. (2018). The core effector Cce1 is required for early infection of maize by *Ustilago maydis*. *Mol. Plant Pathol.* 19, 2277–2287. doi: 10.1111/mpp.12698

Sels, J., Mathys, J., De Coninck, B. M., Cammue, B. P., and De Bolle, M. F. (2008). Plant pathogenesis-related (PR) proteins: a focus on PR peptides. *Plant Physiol. Biochem.* 46, 941–950. doi: 10.1016/j.plaphy.2008.06.011

Sun, X., Wang, P., Jia, X., Huo, L., Che, R., and Ma, F. (2018). Improvement of drought tolerance by overexpressing MdATG18a is mediated by modified antioxidant system and activated autophagy in transgenic apple. *Plant Biotechnol. J.* 16, 545–557. doi: 10.1111/pbi.12794

Taheri, P., and Tarighi, S. (2010). Cytomolecular aspects of rice sheath blight caused by *Rhizoctonia solani*. *Eur. J. Plant Pathol.* 129, 511–528. doi: 10.1007/s10658-010-9725-7

Tang, L., Yang, G., Ma, M., Liu, X., Li, B., Xie, J., et al. (2020). An effector of a necrotrophic fungal pathogen targets the calcium-sensing receptor in chloroplasts to inhibit host resistance. *Mol. Plant Pathol.* 21, 686–701. doi: 10.1111/mpp.12922

Uhse, S., and Djamei, A. (2018). Effectors of plant-colonizing fungi and beyond. *PLoS Pathog.* 14:e1006992. doi: 10.1371/journal.ppat.1006992

van der Burgh, A. M., Postma, J., Robatzek, S., and Joosten, M. (2019). Kinase activity of SOBIR1 and BAK1 is required for immune signalling. *Mol. Plant Pathol.* 20, 410–422. doi: 10.1111/mpp.12767

Wang, W., and Jiao, F. (2019). Effectors of *Phytophthora pathogens* are powerful weapons for manipulating host immunity. *Planta* 250, 413–425. doi: 10.1007/s00425-019-03219-x

Wu, J., Kim, S. G., Kang, K. Y., Kim, J. G., Park, S. R., Gupta, R., et al. (2016). Overexpression of a Pathogenesis-Related Protein 10 Enhances Biotic and Abiotic Stress Tolerance in Rice. *Plant Pathol. J.* 32, 552–562. doi: 10.5423/PPJ.OA.06.2016.0141

Wu, Y., Xu, L., Yin, Z., Dai, Q., Gao, X., Feng, H., et al. (2018). Two members of the velvet family, VmVeA and VmVelB, affect conidiation, virulence and pectinase expression in *Valsa mali*. *Mol. Plant Pathol.* 19, 1639–1651. doi: 10.1111/mpp.12645

Xie, B., Deng, Y., Kanaoka, M. M., Okada, K., and Hong, Z. (2012). Expression of Arabidopsis callose synthase 5 results in callose accumulation and cell wall permeability alteration. *Plant Sci.* 183, 1–8. doi: 10.1016/j.plantsci.2011.10.015

Xie, Y. R., Chen, Z. Y., Brown, R. L., and Bhatnagar, D. (2010). Expression and functional characterization of two pathogenesis-related protein 10 genes from *Zea mays*. *J. Plant Physiol.* 167, 121–130. doi: 10.1016/j.jplph.2009.07.004

Yang, B., Yang, S., Guo, B., Wang, Y., Zheng, W., Tian, M., et al. (2021). The Phytophthora effector Avh241 interacts with host NDR1-like proteins to manipulate plant immunity. *J. Integr. Plant Biol.* 63, 1382–1396. doi: 10.1111/jipb.13082

Yang, Q., Huai, B., Lu, Y., Cai, K., Guo, J., Zhu, X., et al. (2020). A stripe rust effector Pst18363 targets and stabilises TaNUDX23 that promotes stripe rust disease. *New Phytol.* 225, 880–895. doi: 10.1111/nph.16199

Yin, Z., Ke, X., Huang, D., Gao, X., Voegele, R. T., Kang, Z., et al. (2013). Validation of reference genes for gene expression analysis in Valsa mali var. mali using real-time quantitative PCR. *World J. Microbiol. Biotechnol.* 29, 1563–1571. doi: 10.1007/s11274-013-1320-6

Yin, Z., Ke, X., Kang, Z., and Huang, L. (2016). Apple resistance responses against Valsa mali revealed by transcriptomics analyses. *Physiol. Mol. Plant Pathol.* 93, 85–92. doi: 10.1016/j.pmpp.2016.01.004

Zhang, J., Shao, F., Li, Y., Cui, H., Chen, L., Li, H., et al. (2007). A *Pseudomonas* syringae effector inactivates MAPKs to suppress PAMP-induced immunity in plants. *Cell Host Microbe* 1, 175–185. doi: 10.1016/j.chom.2007.03.006

Zhang, M., Feng, H., Zhao, Y., Song, L., Gao, C., Xu, X., et al. (2018). *Valsa mali* Pathogenic Effector VmPxE1 Contributes to Full Virulence and Interacts With the Host Peroxidase MdAPX1 as a Potential Target. *Front. Microbiol.* 9:821. doi: 10.3389/fmicb.2018.00821

Zhang, Q., Ma, C., Zhang, Y., Gu, Z., Li, W., Duan, X., et al. (2018). A Single-Nucleotide Polymorphism in the Promoter of a Hairpin RNA Contributes to *Alternaria alternata* Leaf Spot Resistance in Apple (*Malus x domestica*). *Plant Cell* 30, 1924–1942. doi: 10.1105/tpc.18.00042

Zhang, M., Xie, S., Zhao, Y., Meng, X., Song, L., Feng, H., et al. (2019). Hce2 domain-containing effectors contribute to the full virulence of *Valsa mali* in a redundant manner. *Mol. Plant Pathol.* 20, 843–856. doi: 10.1111/mpp.12796

Zhang, W. J., Pedersen, C., Kwaaitaal, M., Gregersen, P. L., Morch, S. M., Hanisch, S., et al. (2012). Interaction of barley powdery mildew effector candidate CSEP0055 with the defence protein PR17c. *Mol. Plant Pathol.* 13, 1110–1119. doi: 10.1111/j.1364-3703.2012.00820.x

Ziadil, S., Poupard, P., Brisset, M. N., Paulin, J. P., and Simoneau, P. (2001). Characterization in apple leaves of two subclasses of *PR-10* transcripts inducible by acibenzolar-S-methyl, a functional analogue of salicylic acid. *Physiol. Mol. Plant Pathol.* 59, 33–43. doi: 10.1006/pmpp.2001.0343

Conflict of Interest: The authors declare that the research was conducted in the absence of any commercial or financial relationships that could be construed as a potential conflict of interest.

Publisher's Note: All claims expressed in this article are solely those of the authors and do not necessarily represent those of their affiliated organizations, or those of the publisher, the editors and the reviewers. Any product that may be evaluated in this article, or claim that may be made by its manufacturer, is not guaranteed or endorsed by the publisher.

frontiers in Plant Science

ORIGINAL RESEARCH
published: 19 November 2021
doi: 10.3389/fpls.2021.685533

JAZ8 Interacts With VirE3 Attenuating Agrobacterium Mediated Root Tumorigenesis

Shijuan Li[1], Bingliang Xu[1], Xiaolei Niu[2]*, Xiang Lu[3], Jianping Cheng[3], Meiliang Zhou[4]* and Paul J. J. Hooykaas[5]*

[1] College of Plant Protection, Gansu Agricultural University, Lanzhou, China, [2] Hainan Key Laboratory for Sustainable Utilization of Tropical Bioresource, College of Tropical Crops, Hainan University, Haikou, China, [3] College of Agriculture, Guizhou University, Guiyang, China, [4] Institute of Crop Sciences, Chinese Academy of Agricultural Sciences, Beijing, China, [5] Department of Molecular and Developmental Genetics, Institute of Biology, Leiden University, Leiden, Netherlands

Agrobacterium tumefaciens can cause crown gall tumors by transferring both an oncogenic piece of DNA (T-DNA) and several effector proteins into a wide range of host plants. For the translocated effector VirE3 multiple functions have been reported. It acts as a transcription factor in the nucleus binding to the *Arabidopsis thaliana* pBrp TFIIB-like protein to activate the expression of *VBF*, an F-box protein involved in degradation of the VirE2 and VIP1 proteins, facilitating *Agrobacterium*-mediated transformation. Also VirE3 has been found at the plasma membrane, where it could interact with VirE2. Here, we identified AtJAZ8 in a yeast two-hybrid screening with VirE3 as a bait and confirmed the interaction by pull-down and bimolecular fluorescence complementation assays. We also found that the deletion of *virE3* reduced *Agrobacterium* virulence in a root tumor assay. Overexpression of *virE3* in Arabidopsis enhanced tumorigenesis, whereas overexpression of *AtJAZ8* in Arabidopsis significantly decreased the numbers of tumors formed. Further experiments demonstrated that AtJAZ8 inhibited the activity of VirE3 as a plant transcriptional regulator, and overexpression of *AtJAZ8* in Arabidopsis activated *AtPR1* gene expression while it repressed the expression of *AtPDF1.2*. Conversely, overexpression of *virE3* in Arabidopsis suppressed the expression of *AtPR1* whereas activated the expression of *AtPDF1.2*. Our results proposed a novel mechanism of counter defense signaling pathways used by *Agrobacterium*, suggesting that VirE3 and JAZ8 may antagonistically modulate the salicylic acid/jasmonic acid (SA/JA)-mediated plant defense signaling response during *Agrobacterium* infection.

Keywords: ***Agrobacterium tumefaciens*, *Arabidopsis thaliana*, VirE3, JAZ8, jasmonates**

OPEN ACCESS

Edited by:
Brigitte Mauch-Mani, Université de Neuchâtel, Switzerland

Reviewed by:
Andrew N. Binns, University of Pennsylvania, United States
Essaid Ait Barka, Université de Reims Champagne-Ardenne, France

***Correspondence:**
Bingliang Xu
xubl@gsau.edu.cn
Xiaolei Niu
ninterxll@hainanu.edu.cn
Meiliang Zhou
zhoumeiliang@caas.cn

Specialty section:
This article was submitted to Plant Pathogen Interactions, a section of the journal Frontiers in Plant Science

Received: *25 March 2021*
Accepted: *11 October 2021*
Published: *19 November 2021*

Citation:
Li S, Xu B, Niu X, Lu X, Cheng J, Zhou M and Hooykaas PJJ (2021) JAZ8 Interacts With VirE3 Attenuating Agrobacterium Mediated Root Tumorigenesis. Front. Plant Sci. 12:685533. doi: 10.3389/fpls.2021.685533

INTRODUCTION

The plant pathogen *Agrobacterium tumefaciens*, a soil-borne gram negative bacterium, provokes crown gall disease in dicotyledonous plant species, which is characterized by neoplastic growth at infection sites (McCullen and Binns, 2006; Guo et al., 2019). During infection, *Agrobacterium* transfers a single-stranded DNA segment from its tumor-inducing (Ti) plasmid, the T-DNA, into the plant cell, where it integrates into the chromosomes (Beijersbergen and Hooykaas, 1993; Gelvin, 2000, 2003, 2021; Citovsky et al., 2007; Guo et al., 2019). Expression of the oncogenic genes located

on T-DNA in transformed plant cells promotes uncontrolled cell proliferation and results in the formation of crown gall tumors (Nester et al., 1984). Under laboratory conditions, *Agrobacterium* is also able to transform non-plant organisms, such as the yeast *Saccharomyces cerevisiae* and fungi (Bundock and Hooykaas, 1996; Piers et al., 1996; de Groot et al., 1998). By taking advantage of this unique ability of interkingdom gene transfer, *Agrobacterium* has been widely used in creating transgenic plants and fungi for research and biotechnology through a method known as the *Agrobacterium*-mediated transformation (AMT).

Besides the T-region, the virulence (vir) region in the Ti plasmid embraces a series of genes that are essential for AMT, which facilitate T-DNA processing, delivery, and integration into host cell nucleus. Within *Agrobacterium*, the virulence protein VirD2, in conjunction with VirD1, recognizes and generates nicks in the border sequence surrounding the T-DNA region, releasing the T-strand from the Ti plasmid (Yanofsky et al., 1986; Herrera-Estrella et al., 1988). VirD2 remains covalently attached to the 5′ end of the T-strand in *Agrobacterium,* and then the VirD2–T-strand complex is delivered into host cells through a type IV secretion system (T4SS) composed of 11 VirB proteins and VirD4 (Young and Nester, 1988; Christie et al., 2005; Li and Christie, 2018). In host cells, the nuclear localization signal (NLS) of the VirD2 protein pilots the T-strand to the nucleus (Howard et al., 1992; Shurvinton et al., 1992; Tinland et al., 1992; Rossi et al., 1993). In addition, some of the virulence proteins, nowadays referred to as effector proteins, including VirE2, VirE3, VirD5, and VirF are directly translocated into host cells *via* the T4SS independent of the T-strand (Vergunst, 2000; Schrammeijer, 2003). VirE2 is a single-strand DNA binding protein which is supposed to coat the T-strand in the host cytoplasm to form a T-complex, protecting the T-strand from degradation by host nucleases (Citovsky et al., 1989; Gelvin, 1998; Abu-Arish et al., 2004). VirE2 can interact with VIP1, a host bZIP transcription factor, which relocalizes from the cytoplasm to the nucleus to activate defense-related genes upon *Agrobacterium* infection (Tzfira, 2001; Djamei et al., 2007). It has been reported that VIP1 assists in the nuclear entry of the T-complex and facilitates transformation (Tzfira, 2001; Li et al., 2005; Djamei et al., 2007). However, the importance of VIP in AMT is controversial, as no difference in transformation susceptibility between wild-type and *vip1-1* mutant was observed, and a recent report pointed out that VIP1 and its homologs are not required for AMT (Shi et al., 2014; Lapham et al., 2018). The VirF protein is a host–range factor (Melchers et al., 1990; Jarchow et al., 1991) and contains an F-box motif by which it interacts with plant Arabidopsis Skp1–like (ASK1) to form an Skp1–Cullin–F-box (SCF) E3 ubiquitin ligase in the host cell (Jarchow et al., 1991; Schrammeijer et al., 2001). The SCF^{virF} is thought to use the host ubiquitin-26S proteasome system to promote proteolysis of VirE2, VIP1, and some other host proteins in nucleus (Tzfira et al., 2004; Zaltsman et al., 2012; García-Cano et al., 2018). Degradation of VirE2 and VIP1 uncoats the T-complex and thus, may enable integration of T-DNA into the host genome (Tzfira et al., 2004). In addition, proteasomal degradation of Arabidopsis transcription factor VIP1 and VFP4 may dampen the defense response of the host cells (Djamei et al., 2007; García-Cano et al., 2018). Some plant species like Arabidopsis, encode an endogenous F-box protein "VBF," which can functionally replace VirF, and therefore, do not require VirF for transformation (Zaltsman et al., 2010).

VirE3 is another translocated effector that has been shown to interact with VirE2 and bind to plant importin-a, possibly acting as an "adapter" molecule between VirE2 and importin-a to assist the nuclear import of the T-complex, thereby mimicking the function of VIP1 (Lacroix et al., 2004). More recently, an interaction between VirE3 and VirE2 was found to take place at the plasma membrane, suggesting that VirE3 may be involved in the early stage of T-complex formation (Li et al., 2018). Besides, VirE3 can act as a transcriptional activator in the nucleus to modulate the plant gene expression profile through interaction with pBrp, a plant specific general transcription factor belonging to the TFIIB family (García-Rodríguez et al., 2006). One of the genes strongly induced by VirE3 was pointed out to be the gene encoding VBF, thus explaining why simultaneous deletion of *virF* and *virE3* results in a much stronger deficiency of tumorigenicity than observed in the single mutant (Niu et al., 2015). Another gene highly induced by VirE3 was *NIMIN1*, which operates as a negative regulator by binding to NPR1 and reduces salicylic acid (SA)-mediated *PR1* gene expression and attenuates the defense response (Weigel et al., 2005; Niu et al., 2015). Here, we found that *Agrobacterium* VirE3 can interact with Arabidopsis JAZ8 and that overexpression of *virE3* promotes tumor formation, whereas *JAZ8* overexpression makes roots recalcitrant to tumorigenesis by *Agrobacterium*. JAZ proteins are best known as repressors of the jasmonate response, which recruit general corepressors to prevent the transcriptional activity of MYC transcription factors (Pauwels and Goossens, 2011; Howe et al., 2018). We found that the activity of VirE3 as a plant transcription regulator was repressed by JAZ8. The jasmonic acid (JA)-regulated *PDF1.2* gene expression was elevated in the *virE3*-overexpressor plant line, but the SA-mediated *PR1* gene expression was reduced in the *virE3*-overexpressor plant line. Our results suggest the VirE3 and JAZ8 may antagonistically modulate each other's activity, and that *Agrobacterium* uses VirE3 to shift the plant defense response during AMT from SA signaling to JA signaling, which is less deleterious for biotrophic pathogens.

MATERIALS AND METHODS

Plasmid Constructs

Supplementary Tables 1–3 list the primer sequences, plasmids, and strains used in this study, respectively. The *JAZ8* coding sequence was amplified by PCR using cDNA of Col-0 *Arabidopsis thaliana* with the primer set JAZ8-1302-F and JAZ8-1302-R. The PCR fragment was inserted into pCAMBIA1302 by homologous recombination, yielding *JAZ8* overexpression construct JAZ8-1302. The *JAZ8* sequence was amplified by PCR on plasmid JAZ8-1302 using primers listed in **Supplementary Table 1** for JAZ8-pAS2.1, JAZ8-ZIM-pAS2.1, JAZ8NT-pAS2.1,

JAZ8CT-pAS2.1, JAZ8-pMAL-c5X, JAZ8-cYFP, and pRT101-JAZ8 constructs. The PCR fragments were digested and inserted into pAS2.1, pMAL-c5X, pRTL2-HAYC, and pRT101, yielding corresponding constructs.

The *virE3* coding sequence was amplified by PCR on plasmid pRT101-VirE3 (Niu et al., 2015) using primers listed in **Supplementary Table 1** for virE3-pACT, virE3-pGEX6P-1, and virE3-nYFP constructs. The resulting PCR fragment was digested and inserted into the pACT2, pGEX-6P-1, and pRTL2-EEYN vector, yielding corresponding constructs. All constructs were verified by sequencing.

Plant Materials, Growth Conditions, and Plant Transformation

The genetic background of ecotype Col-0 was used as wild type *Arabidopsis thaliana*. JAZ8-1302 (pCAMBIA1302) construct and 1,302 empty vector were used for Arabidopsis transformation. All plasmids used in this work are listed in **Supplementary Table 2**. The construct JAZ8-1302 and the empty vector 1,302 (used as control) were introduced into GV3101 by electroporation. Arabidopsis were transformed using the floral dip method (Clough and Bent, 1998) and grown at 21°C in a growth chamber (16-h light/8-h dark, 2,500 lux). Seeds from the dipped plants were harvested and planted on MS medium containing 30 mg L^{-1} hygromycin. The transgenic plants were verified by PCR of *Hph* gene. The positive seedlings were transferred to soil and grown until new seeds could be harvested. The TAM-*virE3* transgenic plant lines used in this study were from Niu et al. (2015).

Yeast Two-Hybrid Assays

The truncated VirE3 (pASE3ΔC) without autoactivation activity was used as a bait in yeast two-hybrid screening (García-Rodríguez et al., 2006). The Arabidopsis cDNA library representing 5.7×10^5 primary transformants was generated by Zhou (Zhou et al., 2017). The bait plasmid pASE3ΔC and Arabidopsis cDNA library was cotransformed into yeast strain PJ69-4A using the PEG-lithium acetate method (Gietz et al., 1992; James et al., 1996). Full-length JAZ8 (AT1G30135), JAZ8NT (aa 1–101), JAZ8CT (aa 101–127), and JAZ8-ZIM (aa 13–101) were cloned in pAS2.1 (acc. No. U30497). The corresponding vectors were cotransformed with empty pACT2 (acc. No. U29899) and pACT2-VirE3, respectively, to yeast strain PJ69-4A. Empty pAS2.1 and pACT2 were used as negative control. Yeast two-hybrid assays were conducted by the cotransformation of bait and prey plasmids into yeast strain PJ69-4A as described by Zhou (Zhou et al., 2017). Transformants were allowed to grow for 4 days at 28°C on synthetic defined (SD)-glucose plates lacking leucine, tryptophan, and histidine (-LWH). Then cells were incubated overnight in liquid SD–LWH medium and 4 μl of 100-fold dilutions were spotted on SD-LWH plate to grow for 4 days at 28°C. The experiments were repeated three times.

In vitro Pull-Down Assay

The *JAZ8* coding sequence was cloned into pMAL-c5X through *Nde*I and *Bam*HI sites for fusion with MBP tag. Full-length CDS of *virE3* was cloned into pGEX6P-1 through *Bam*HI and *Sal*I sites for fusion with GST tag. Constructs JAZ8-pMAL-c5X and virE3-PGEX6P were transformed into *E. coli* strain BL21 (DE3) pLysS, separately and screened by 20 μg/ml chloramphenicol and 100 μg/ml carbenicillin. Protein expression of MBP-JAZ8 and GST-VirE3 were induced by 1 mM IPTG. The MBP-fusion proteins and GST-fusion proteins were extracted and immobilized onto MBP and GST agarose beads. For pull-down assays, proteins attached to the beads were subsequently examined by SDS-PAGE and detected with anti-MBP and anti-GST antibody, respectively. Detection was performed by incubating the blots in 8 ml western lighting reagent and then exposure to X-ray films.

Bimolecular Fluorescence Complementation Assays

virE3 was fused with the N-terminal part of the improved yellow fluorescent protein (YFP) in pRTL2-EEYN to produce VirE3-nYFP. *JAZ8* was fused with the C-terminal part of YFP in pRTL2-HAYC to produce JAZ8-cYFP (Bracha-Drori et al., 2004). VirE3-nYFP was transiently cotransformed with JAZ8-cYFP into the Arabidopsis leaf protoplast. Images of transfected protoplasts were acquired with a Leica DM IRBE confocal laser scanning microscope equipped an excitation at 514 nm and a band mission was detected at 530–600 nm. Microscopic images were analyzed using Image J software.

Agrobacterium-Mediated Arabidopsis Root Tumor Assay

The *Agrobacterium* tumorigenic strain LBA 1010 (WT) and LBA 2564 (-*virE3*) were used for tumorigenesis assays on Arabidopsis Col-0 wild-type, *JAZ8*-OE, and *virE3*-OE plant lines. Arabidopsis root tumor assay was carried out as described previously with minor modifications (Valvekens et al., 1988; Czako et al., 1993). In brief, Arabidopsis seeds of Col-0, *JAZ8*-OE, and *virE3*-OE plant lines, respectively, were sterilized and incubated in liquid B5 medium at 4°C for 2 days. Then, the seeds in liquid B5 medium were incubated on a shaker (120 rpm) in growth room (21°C, 16 h light/8hrs dark, 2,000 lux) for 10 days. The root segments pooled from 10-day-old plant of Col-0, *JAZ8*-OE, and *virE3*-OE plants, respectively, were incubated with *Agrobacterium* LBA1010 and LBA2564 (OD_{620} = 0.2) for 2 min. The infected roots were cut into 4 mm (named explants) and dried on sterile filter paper, transferred to B5 agar plants containing 100 μM acetosyringone for cocultivation for 2 days in the growth room (25°C, 2,000 lux). After cocultivation, root explants were washed with liquid B5 and then transferred to B5 plates supplemented with 100 μg/ml timentin for 3 weeks until calli/tumors were formed. The percentage of roots that form tumors was calculated by counting tumors on 100 to 120 explants. Three independent replicates of 100 to 120 explants were used for each line.

Arabidopsis Leaf Protoplast Transient Expression Assay

Plasmid *VBF*-promoter-GUS was obtained by inserting the promoter sequence of *VBF* (857bp) into plasmid GUSXX

(Niu et al., 2015). Full length of *virE3* and *JAZ8* were inserted into plasmid pRT101. Plasmids carrying *VBF*-promoter-GUS and plasmids expressing VirE3 and/or JAZ8 were cotransformed into Arabidopsis Col-0 leaf protoplasts by polyethylene-glycol-mediated transformation as previously described (Schirawski et al., 2000). Cotransformation of pRT101 with GUSXX plasmids was used as control (Töpfer et al., 1987). Protoplasts were incubated at 25°C for 16 h and harvested by centrifugation. The GUS activity assays were performed as described (Niu et al., 2015). Relative expression levels of *virE3, AtJAZ8, AtPR1,* and *AtPDF1.2* were measured.

Illumina mRNA-Seq Library Preparation and Sequencing

Arabidopsis seeds harvested from three independent *JAZ8*-OE and 1,302 plant lines were grown vertically on MS plates. RNA isolated from 10-day-old seedlings were used for Illumina sequencing. Illumina mRNA-seq libraries were generated and sequenced by Majorbio Cloud Platform[1]. The resulting libraries were checked and quantified. The libraries were multiplexed, clustered, and sequenced on an Illumina HiSeq 2000. Sequence reads of low quality and reads containing adaptor sequences were removed. To validate the RNA-seq results, total RNA was extracted from three independent *JAZ8*-OE and 1,302 plant lines using the same protocol for RNA-seq. cDNA was generated from total RNA. qRT-PCR was performed by Universal SYBR Green Master mix according to the manufacturer's instructions. The relative amount of gene expression level was calculated using $2^{-\Delta\Delta Ct}$ method. *EF1a* (At5G09810) was used as the reference gene.

Quantification of *AtPR1* and *AtPDF1.2* in *Agrobacterium* Infected Seedlings

Arabidopsis seeds of Col-0, *JAZ8*-OE, and *VirE3*-OE were sterilized and incubated in liquid B5 medium at 4°C for 2 days. Then, the seeds in liquid B5 medium were incubated on a shaker (120 rpm) in growth room (21°C, 16-h light/8-h dark, 2,000 lux) for 10 days. *Agrobacterium* strains LBA1100 and LBA2564 were preadjusted to OD600 = 0.2. Seedlings of the Col-0, *JAZ8*-OE, and *virE3*-OE were infected by *Agrobacterium* strains LBA1100 and LBA2564 for 2 min. The infected seedlings were taken out and immediately frozen in liquid nitrogen at different time points. RNA was extracted for qRT-PCR analysis. Quantitative RT-PCR analysis was carried out using Bio-Rad iCycler iQ5. The first strand of cDNA was synthesized by HiScript® III RT SuperMix for qPCR (+ gDNA wiper) kit. Specific primers were designed for *AtPR1*, *AtPDF1.2,* and *EF1a* reference gene by primer 5. The primers are listed in **Supplementary Table 1**. The qRT-PCR reactions were as follows: 95°C 30 s; 95°C 10 s, 60°C 30 s, followed by 40 cycles. Relative expression levels of *AtPR1* and *AtPDF1.2* were calculated by $2^{-\Delta\Delta CT}$ methods. All dates are collected from three biological replicates.

[1]http://login.majorbio.com/login

Statistical Analysis

The data were analyzed by Excel and SPSS software, and Duncan's new complex range method was used to compare the differences among the treatments. P value < 0.05 was considered to be significant.

RESULTS

VirE3 Interacts With JAZ8

Early publications reported that VirE3 was bound with pBrp to facilitate AMT through modulating gene expression profiles in the host cell (García-Rodríguez et al., 2006). To gain further insight into the function of VirE3 within the host cells during *Agrobacterium* infection, we used the yeast two-hybrid system (Y2H) to screen for interactors of VirE3. Due to the transcriptional activation activity of the full-length VirE3 in yeast strain PJ69-4A, the truncated VirE3 (pASE3ΔC) without autoactivation activity (García-Rodríguez et al., 2006) was used as a bait and an Arabidopsis cDNA library (Zhou et al., 2017) was used as a prey. Five colonies were found to grow on minimal medium without histidine. Recovered prey plasmids were retransformed with pASE3ΔC into yeast strain PJ69-4A, and only two of these plasmids could grow on selective medium. From these candidate VirE3 interactors, only one cDNA sequence was in frame with the GAL4 activation domain and encoded the JAZ8 protein (AT1G30135). Our Y2H screening thus identified the Jasmonate ZIM-domain protein JAZ8 as a positive interactor of VirE3. To investigate which domain of JAZ8 was responsible for interaction with VirE3, we divided JAZ8 into N-terminal (JAZ8NT), ZIM domain containing (JAZ8-ZIM), and C-terminal fragments (JAZ8CT). JAZ8NT contained an EAR and a ZIM domain, whereas the JAZ8-ZIM and JAZ8CT only contained the ZIM domain and Jas domain, respectively (**Figure 1A**). We then cloned the full-length VirE3 into the activation domain (AD) and the different truncated versions of JAZ8 into the binding domain (BD) to verify the interaction in the Y2H system. We found that JAZ8, JAZ8NT, and JAZ8-ZIM interacted with VirE3 but not JAZ8CT. These results indicate that the ZIM domain of JAZ8 is responsible for the interaction between VirE3 and JAZ8 (**Figure 1B**). We further applied pull-down assays to verify the interaction between VirE3 and JAZ8 *in vitro*. GST-tagged VirE3 and maltose binding protein (MBP)-fused JAZ8 (MBP-JAZ8) were heterologously expressed in *E. coli* BL21 (DE3) cells and MBP-pull-down assays were performed using two fusion proteins. MBP-JAZ8 resin was incubated with GST-VirE3 and then separated on SDS-PAGE for immunoblotting with anti-GST antibody. As shown in **Figure 1C**, the negative control (MBP resin) was unable to pull-down GST-VirE3, whereas the GST-VirE3 was efficiently precipitated by MBP-JAZ8, indicating that VirE3 can physically interact with JAZ8 *in vitro*. We next used bimolecular fluorescence complementation (BiFC) assays to verify the interaction of VirE3 and JAZ8 proteins *in planta*. VirE3 was fused with the N-terminal part of the improved YFP in pRTL2-EEYN to produce VirE3-nYFP, and JAZ8 was fused with the C-terminal part of YFP in pRTL2-EEYN to produce JAZ8-cYFP. VirE3-nYFP was transiently coexpressed with JAZ8-cYFP

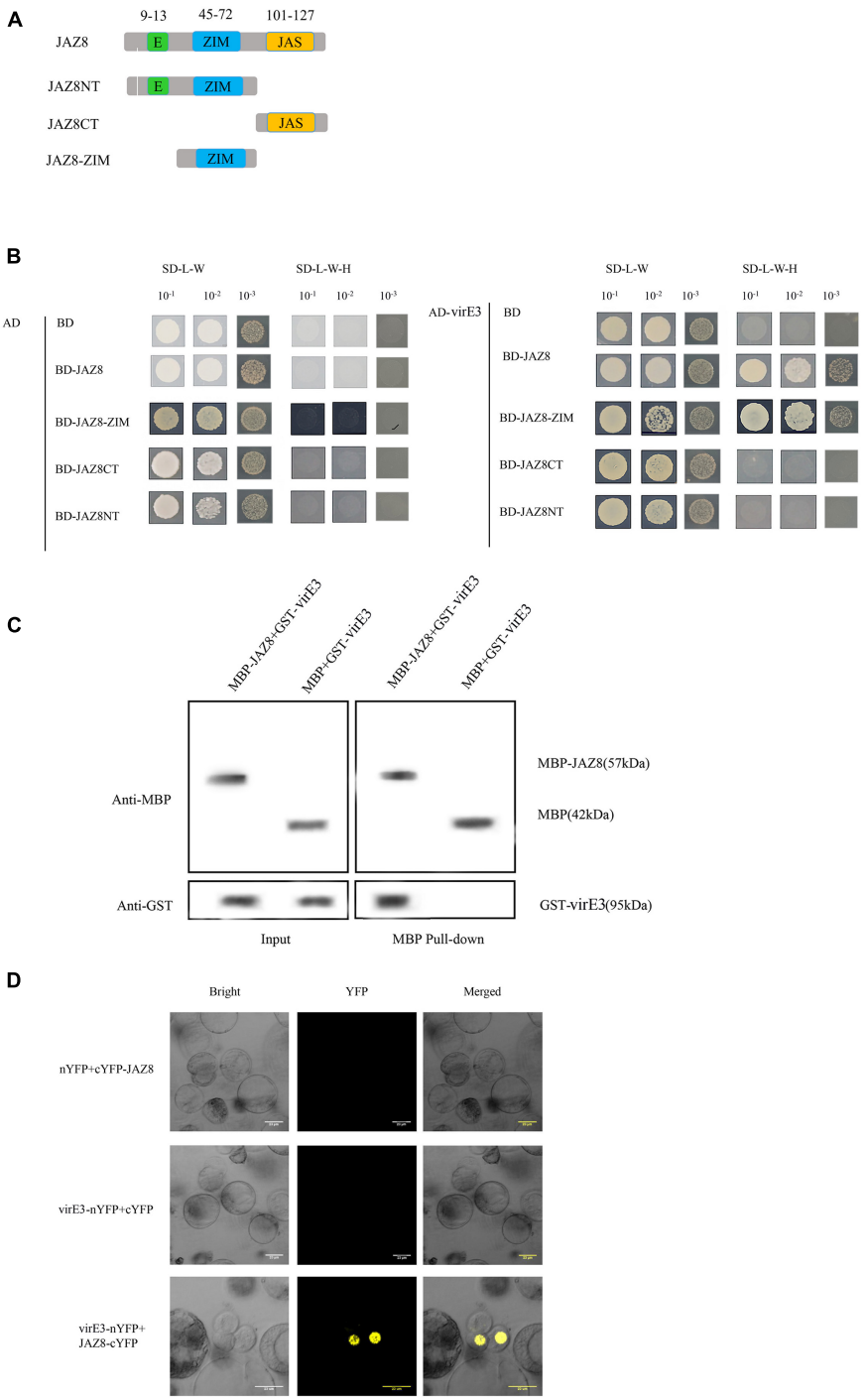

FIGURE 1 | VirE3 interacts with AtJAZ8 *in vivo* and *in vitro.* **(A)** Schematic representation of JAZ8 constructs used for yeast two-hybrid assay. Numbers represent amino acid positions in full-length JAZ8. **(B)** Yeast two-hybrid assay. Full length of JAZ8 and the truncated fragments of JAZ8NT (aa 1–101), JAZ8CT (aa 101–127), JAZ8-ZIM (aa 13–101) were cloned into pAS2.1 (BD). The *virE3* was cloned into pACT2 (AD). The indicated prey and bait constructs were cotransformed into yeast strain PJ69-4A. The transformants were first screened on synthetic defined (SD) medium minus tryptophan and leucine (SD/-Trp-Leu) and the positive yeast cells were subcultured on SD medium minus tryptophan, leucine and histidine at 30°C for 4 days. pAS2.1 and pACT2 were used as the negative control. **(C)** Maltose-binding protein (MBP) pulldown assay. The MBP pull-down proteins were detected by Western blotting (WB) using anti-GST or anti-MBP antibody. MBP alone was used as the negative control. Input, protein samples without pull-down were analyzed by Western blotting. **(D)** Bimolecular fluorescence complementation (BIFC) assay. The constructs 35S::VirE3-nYFP and 35S::AtJAZ8-cYFP were transiently co-transformed into Arabidopsis protoplast and the transformed cells were observed under a confocal microscope. 35S::nYFP and 35S:: cYFP were used as negative control.

in Arabidopsis protoplasts. We found that co-expression of VirE3-nYFP with JAZ8-cYFP resulted in strong YFP fluorescence in the nucleus of Arabidopsis mesophyll protoplasts (**Figure 1D**), whereas no YFP fluorescence was detected in negative controls (VirE3-nYFP coexpressed with cYFP or nYFP coexpressed with cYFP-JAZ8). Taken together, the Y2H assays, pull-down assays, and BiFC assays consistently demonstrate that VirE3 interacts with JAZ8 protein *in vitro* and *in vivo*.

Effects of VirE3 and JAZ8 on *Agrobacterium*-Mediated Arabidopsis Root Tumorigenesis

It has been reported that VirE3 plays a role in tumorigenesis; however, mutation of *virE3* led to hardly any attenuation in tumor formation on the stems of six plant species including *Nicotiana glauca, Nicotiana tabacum, Helianthus annuus, Lycopersicon esculentum, Kalanchoe tubiflora,* and *Kalanchoe daigramontiana* (García-Rodríguez et al., 2006). To better understand the role of VirE3 in tumorigenesis, the *Agrobacterium* wild-type strain (LBA1010) and a *virE3* deletion strain (LBA2564) were compared in more quantitative root transformation assays on Arabidopsis Col-0. As shown in **Figure 2A**, the *virE3* mutant developed a lower number of tumors compared with LBA1010 (average 32 versus 39% of inoculated roots showing tumors). Analysis by the Student's *t*-test confirmed that tumorigenesis of LBA1010 and LBA2564 on Arabidopsis Col-0 was significantly different. To determine whether overexpression of *virE3* in Arabidopsis could increase susceptibility to *Agrobacterium* infection, we used a transgenic line of Arabidopsis that expresses the *virE3* coding sequence under the control of the tamoxifen-inducible promoter (Niu et al., 2015). After induction by tamoxifen (**Figure 2C**) the roots of *virE3*-OE line1 were transformed by LBA1010 and LBA2564 and the fractions of roots that formed tumors were calculated. As shown in **Figure 2B**, the *virE3*-OE line1 was much more susceptible to *Agrobacterium* LBA1010 and LBA2564 infection with tumors forming in 52 and 41% of the inoculated roots for wild type and *virE3* mutant, respectively. Apparently, increasing the amount of VirE3 can enhance tumor formation even by the wild type *Agrobacterium* strain. The difference in tumorigenesis between LBA1010 and LBA2564 on *virE3*-OE line1 was statistically significant, suggesting that translocated VirE3 from LBA1010 also still contributes to tumor formation.

As we found that VirE3 can interact with JAZ8, we further investigated the role of JAZ8 in tumor formation by *Agrobacterium*. To this end, transgenic plant lines that constitutively expressed the *JAZ8* coding sequence under the CaMV 35S promoter were generated. Two independent T1 transgenic lines, designated *JAZ8*-OE1 and *JAZ8*-OE2, both showed about ninefold higher levels of *JAZ8* transcript accumulation in their roots compared with Col-0 wild type by qRT-PCR analysis. The roots of *JAZ8*-OE line1 were transformed by LBA1010 and LBA2564 and the fraction of roots on which tumors were formed was calculated. Interestingly, we found that on *JAZ8*-OE line1 much less tumors were formed by our wild type strain LBA1010 than on Arabidopsis Col-0 (27 versus 39% of inoculated roots showing tumors, statistically significant). When the *virE3* mutant LBA2564 was used for inoculation of the *JAZ8*-OE roots, the fraction of roots forming tumors was even lower with tumorigenesis seen on only about 22% of the roots (**Figure 2B**). Our results indicate that JAZ8 counters

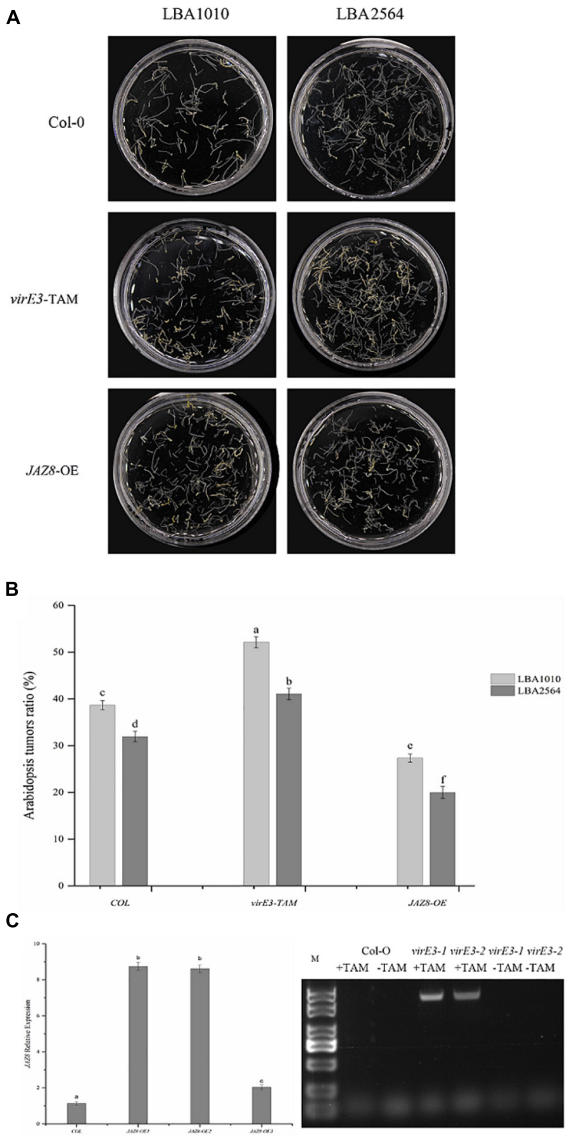

FIGURE 2 | Efficiency of *Agrobacterium*-mediated root transformation in *virE3* and *JAZ8* overexpressor lines (*virE3*-TAM and *JAZ8*-OE lines) as compared with wild-type plants (Col-0) by *Agrobacterium* strain LBA1010 and *virE3* deletion mutant LBA2564. **(A)** Tumors developed on root explants. Root segments of Columbia, *virE3*-TAM1 and *JAZ8*-OE1 lines were infected with tumorigenic *Agrobacterium* strain LBA1010 and its *virE3* deletion mutant LBA2564. The root segments were photographed and scored 30 days after infection. **(B)** Quantification of the tumorigenicity showed in panel **(A)**. Error bars in B indicate SEM. Differences in tumorigenicity indicated by different letters are statistically significant (*P* values < 0.05) and by the same letter are not statistically significant. **(C)** Gene expression analysis of *JAZ8* and *virE3* in transgenic over-expressor plant lines.

Agrobacterium virulence, whereas VirE3 enhances *Agrobacterium* tumorigenicity on Arabidopsis roots.

JAZ8 Reduces Activity of VirE3 as a Transcriptional Activator

VirE3 can act as a plant transcription factor which activates genes such as Arabidopsis *VBF,* which are needed for tumorigenesis (Niu et al., 2015). JAZ8 belongs to the plant-specific TIFY family of transcriptional regulators that repress JA-regulated defense responses by binding to MYC transcription factors (Shyu et al., 2012). To find out whether JAZ8 could reduce the transcriptional activity of VirE3, the effect of JAZ8 on the VirE3-dependent activation of *VBF* (At1G56250) promoter was investigated in a protoplast transactivation assay. The 857 bp of *VBF* promoter was fused to the GUS reporter, and the full length of *virE3* or *JAZ8* coding sequences wase cloned into the pRT101 plasmid, in which *virE3* or *JAZ8* was expressed from the CaMV 35S promoter. Arabidopsis protoplasts were cotransformed with the *VBF*-promoter-GUS reporter plasmid and at the same time with the effector plasmid pRT101-VirE3 and/or pRT101-JAZ8. First we measured whether the *JAZ8* and *virE3* construct were expressed in Arabidopsis protoplasts by RT-PCR. As shown in **Figure 3B**, the mRNA expression level of *JAZ8* was around 30-fold higher in protoplasts transformed with plasmid pRT101-JAZ8 and also in protoplasts transformed by pRT101-JAZ8 together with pRT101-VirE3 compared with that in Col-0 protoplasts. The mRNA expression of *virE3* was also confirmed by RT-PCR analysis in protoplasts transformed with plasmid pRT101-VirE3 and plasmids pRT101-VirE3 together with pRT101-JAZ8 (**Figure 3C**). These results indicate that the mRNAs of both genes are indeed expressed in the transformed protoplasts and that the expression of the *JAZ8* gene does not negatively affect the expression of *virE3* and vice versa. Subsequently, we tested the effect of JAZ8 and VirE3 on the activity of the *VBF* promoter. As shown in **Figure 3A**, expression of JAZ8 alone barely affected the activity of the *VBF* promoter, whereas VirE3, as expected, activated the *VBF* promoter by approximately threefold. In contrast, co-expression of VirE3 and JAZ8 together led to a twofold reduced activity of the *VBF* promoter as compared with that in the presence of VirE3 alone. As JAZ8 is known to affect the JA response and promote the SA defense response, we also tested whether VirE3 could affect these defense responses. To this end, we measured the mRNA levels of *PR1* (SA response) and *PDF1.2* (JA response) in the same transformed protoplasts. Interestingly, we found that the expression level of *PR1* was reduced in protoplasts transformed with pRT101-VirE3 and elevated in protoplasts transformed with pRT101-JAZ8. Reversely, the expression level of *PDF1.2* was elevated in protoplasts transformed with pRT101-VirE3 and decreased in protoplasts transformed with pRT101-JAZ8 (**Figure 3B**). In summary, our results indicate that JAZ8 can repress the transcriptional activity of VirE3 on activating the expression of *VBF*. Also overexpression of VirE3 reduced *PR1* gene expression and elevated *PDF1.2* expression, whereas overexpression of *JAZ8* elevated *PR1* gene expression and reduced *PR1* expression.

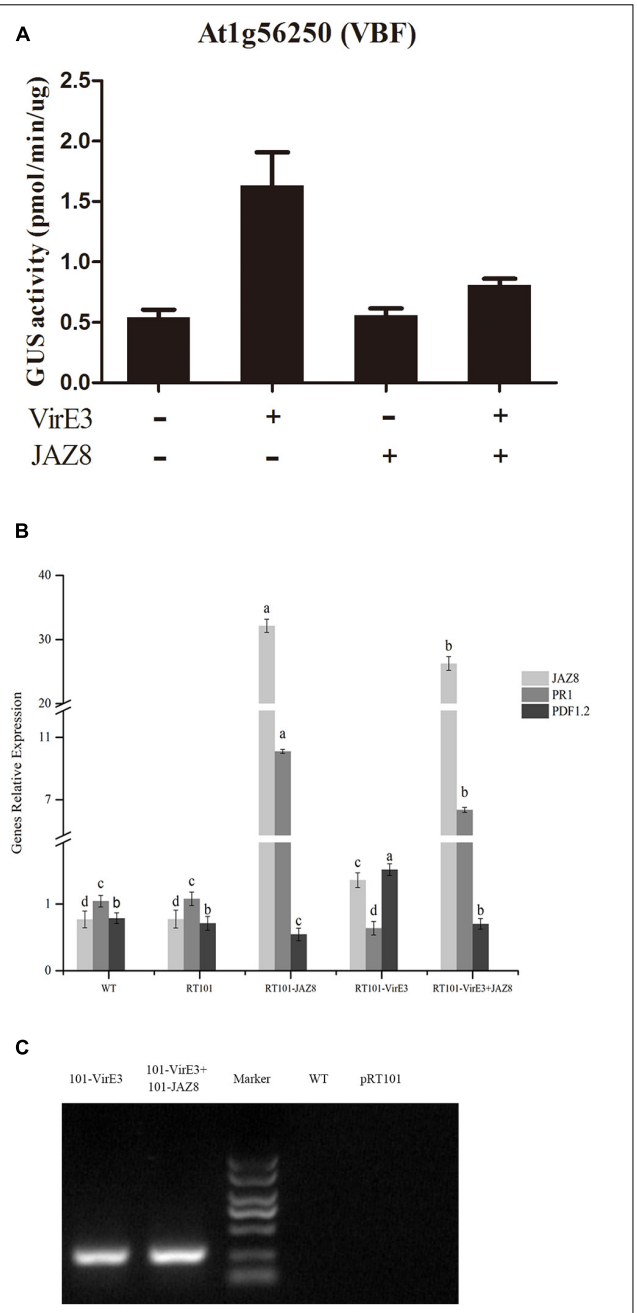

FIGURE 3 | Protoplast expression analysis of the promoters of At1G56250 (*VBF*) and the gene expression analysis of *PR1*, *PDF1.2*, *JAZ8,* and *virE3*. **(A)** JAZ8 inhibits VirE3-dependent activation of the At1G56250 (*VBF*) (857 bp) promoters in Arabidopsis protoplasts. **(B)** qPCR analysis of the expression level of *PR1*, *PDF1.2*, *JAZ8* in protoplasts transfected with corresponding plasmids. **(C)** RT-PCR analysis of the expression of *virE3* in protoplast transformed with corresponding plasmids.

Effect of *JAZ8* Overexpression on the Arabidopsis Transcriptome

As a transcriptional repressor of the jasmonate downstream signaling pathway, JAZ8 most likely affects plant susceptibility

to *Agrobacterium* by regulating the expression of plant defense responsive genes that interfere with the *Agrobacterium* infection. To investigate the role of JAZ8 on the transcription of defense responsive genes, we carried out transcriptome profiling by comparing *AtJAZ8* overexpressor lines with control lines using RNA-seq analysis. Total RNA samples extracted from seedlings were analyzed for gene expression using RNA-seq. Using DESeq to calculate differentially expressed genes (DEGs), we identified a total of 696 genes that were either up- or down-regulated (FDR < 0.001 and log2FC > 2) in JAZ8-OE plant lines compared with the control lines (**Supplementary Table 1**). Raw data have been deposited in the NCBI SRA database (BioProject accession number: PRJNA719307). To validate the RNA-seq results, six DEGs from *AtJAZ8* overexpressor plants were randomly selected for analysis by quantitative RT-PCR. As shown in **Figure 4A**, the results obtained from qRT-PCR analysis are in general agreement with the RNA-seq results. We then used GO annotation (TAIR10) to assign genes to functional categories and performed function enrichment analysis on the DEGs. The 428 genes upregulated in the *JAZ8*-OE line were enriched for genes implicated in regulation of SA metabolic process, regulation of defense response to bacterium, regulation of plant-type hypersensitive response, and also defense response (**Figure 4B**). By contrast, the 268 genes downregulated in the *JAZ8*-OE line were enriched for genes related to defense response, immune system process, response to JA, etc. (**Figure 4C**). Our results suggest that JAZ8 generally affects genes involved in plant defense responses. Interestingly, we found that the expression level of pathogenesis-related gene 1 (*AtPR1*) in *JAZ8*-OE was around five times (5.48) higher than in control lines, indicating JAZ8 may activate the SA-mediated signaling pathway against *Agrobacterium* infection.

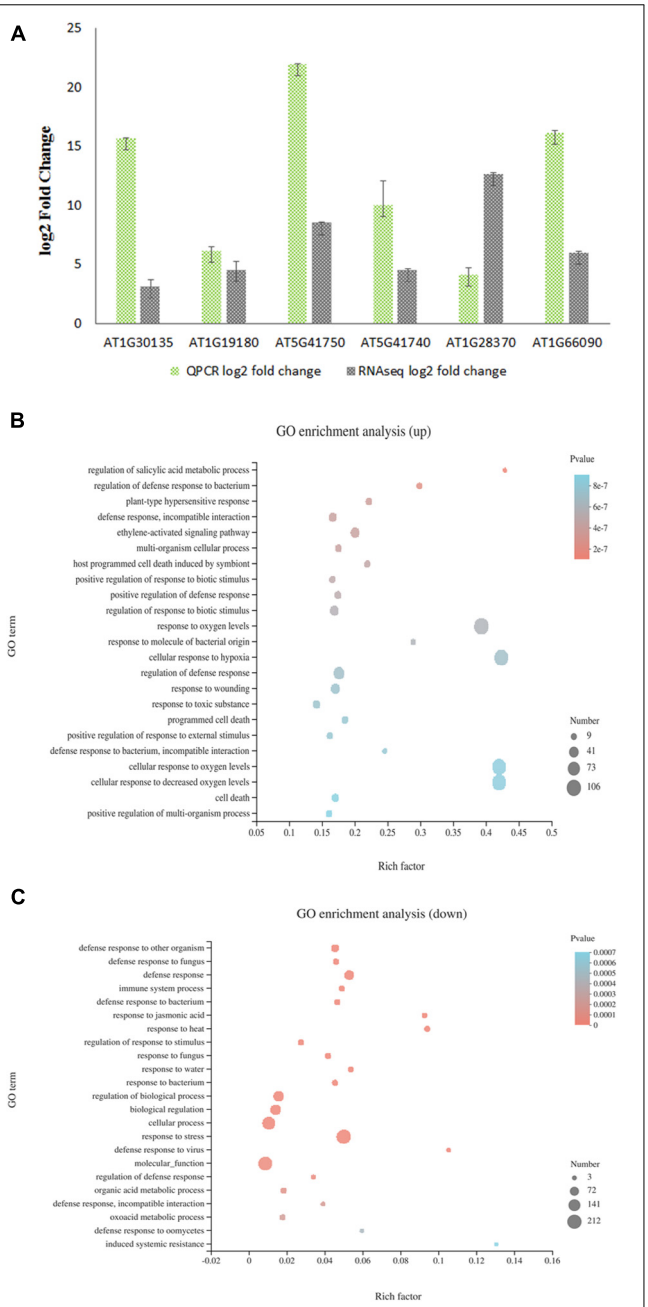

FIGURE 4 | Transcript profiling of *AtJAZ8* overexpressor plants. **(A)** Validation of the RNA-Seq data by quantitative RT-PCR. Six differential expression genes in *AtJAZ8* overexpressor plants compared with control plant lines in the RNA-seq experiment were selected for validation by qRT-PCR. **(B)** GO term enrichment for 428 upregulated genes using Database for Annotation and Visualization. **(C)** GO term enrichment for 268 downregulated genes using Database for Annotation and Visualization.

JAZ8 Antagonizes VirE3 on Expression of *AtPR1*

We have shown that the percentage of root tumors was highly decreased in *JAZ8*-OE lines and increased in *virE3*-OE lines. To investigate the plant defense genes responsible for *Agrobacterium* mediated root tumorigenesis, the expression level of Arabidopsis *pathogenesis-related GENE 1* (*AtPR1*) and Arabidopsis *PLANT DEFENSIN 1.2*(*AtPDF1.2*) were measured by qRT-PCR in wild type Col-0, *JAZ8*-OE, and *virE3*-OE plant lines infected by *Agrobacterium* strains LBA1100 (wild-type) and LBA2564 (*virE3* deletion mutant) at different time points. To compare the gene expression level at different time points infected by two *Agrobacterium* strains LBA1100 and LBA2564, we normalized the expression level of *AtPR1* and *AtPDF1.2* to the Col-0 at 0 h before infection by qRT-PCR analysis. As shown in **Figure 5A**, 24 h after *Agrobacterium* infection, the expression level of *AtPR1* was significantly reduced in *virE3*-OE plant line compared with that in Col-0 and *JAZ8*-OE plant line, whereas the expression level of *AtPR1* gene was the highest in the *JAZ8*-OE plant line. Our results showed that VirE3 inhibits the expression of *AtPR1* gene and JAZ8 promotes *AtPR1* gene expression probably by repressing the JA-responsive defense pathway. The expression pattern of *AtPR1* in plant lines was negatively well correlated with the root tumorigenicity by *Agrobacterium*. On the contrary, after *Agrobacterium* infection, the expression level of *AtPDF1.2* was highest in *virE3*-OE plant line and lowest in *JAZ8*-OE plant line, indicating VirE3 might

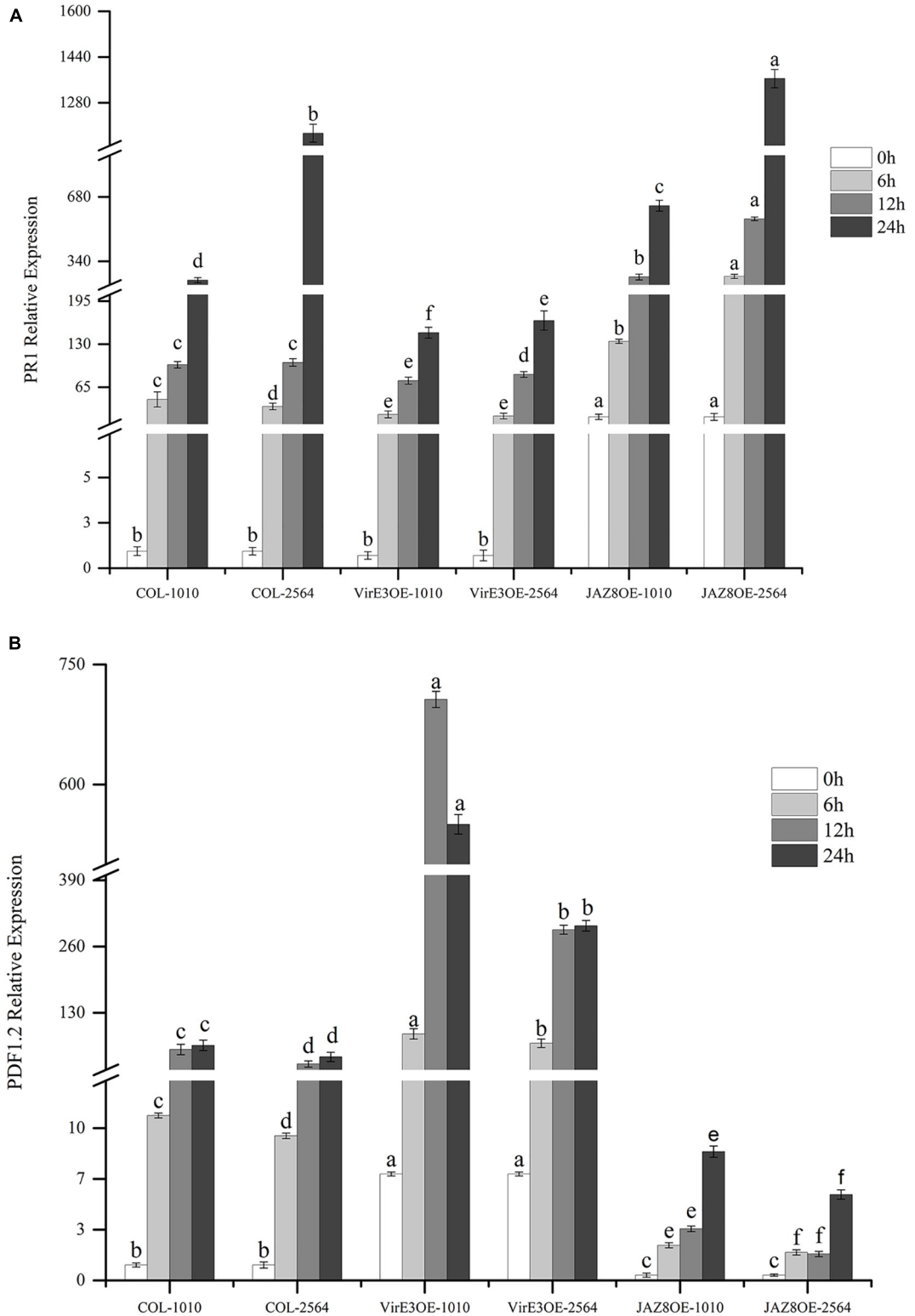

FIGURE 5 | Quantification of *AtPR1* and *AtPDF1.2* gene expression level in Col-0, *virE3*-OE and *JAZ8*-OE1 lines after infection with *Agrobacterium* LBA1010 and LBA2564 at different time points. **(A)** qRT-PCR analysis of *AtPR1* gene expression pattern. **(B)** qRT-PCR analysis of *AtPDF1.2* gene expression pattern. *EF1a* was used as internal control for data normalization. The expression level of *PR1* and *PDF1.2* in the wild-type Col-0 at 0 h was set to 1.0, and error bars represent SEM of three independent biological replicates. The expression values of *PR1* and *PDF1.2* in *virE3*-OE and *JAZ8*-OE lines were compared to the control Col-0 at each corresponding condition. Differences indicated by different letters are statistically significant (P values < 0.05) and by the same letter are not statistically significant.

activate the JA-induced signaling pathway by repressing *AtPR1* gene expression (**Figure 5B**). Our results showed that JAZ8 may antagonize VirE3 on activating the expression of *AtPR1* gene, which in turn attenuates *Agrobacterium* tumorigenesis on Arabidopsis root.

DISCUSSION

Agrobacterium delivers several virulence proteins, including VirD2, VirE2, VirE3, VirF, and VirD5 to plant cell for successful T-DNA integration and tumorigenesis (Lacroix and Citovsky, 2019). One of the translocated effector proteins, VirE3, is highly conserved among different *Agrobacterium* and rhizobia species, suggesting that VirE3 may play an important role during AMT. However, it was reported that VirE3 was not essential for AMT by octopine strains and a *virE3* mutation did not significantly affect tumor formation on the stems of several plant species, and its contribution to tumorigenesis could only be seen in *virE3 virF* double mutants (García-Rodríguez et al., 2006). A recent report showed that VirE3 is required for full virulence of the agropine/succinamopine strain EHA105, which does not have a close homolog of octopine Ti *virF*. Deletion of *virE3* resulted in a decreased transformation efficiency in the transient transformation assays of *Nicotiana benthamiana* leaves (Li et al., 2018, 2020). In contrast, another report showed constitutive overexpression of *virE2* or *virE3* under CaMV 35S promoter in Arabidopsis-induced plant defense responses and conferred resistance to *Agrobacterium* infection (Duan et al., 2018). Our results showed that VirE3 is required for tumorigenesis of oncogenic wild type *Agrobacterium* LBA1010. Deletion of *virE3* attenuated *Agrobacterium* virulence in root tumor assay, whereas transient overexpression of *virE3* enhanced *Agrobacterium* tumorigenesis (**Figure 2A**). The different results reported may be due to the different methods used for the transformation or to the different plant species or *Agrobacterium* strains used.

Upon attack by pathogens, plants possess highly sophisticated mechanisms to induce the expression of defense genes to restrict pathogen invasion. The phytohormones SA and JA, as key signaling molecules, play important roles in regulating the activation of the induced defense responses. Silencing of SA biosynthetic and signaling genes in *N. benthamiana* increases susceptibility to crown gall disease (Yuan et al., 2007; Anand et al., 2008). One of the crucial effects of SA in plant defense is to activate the expression of pathogenesis related genes such as *PR1*, resulting in both local and systemic acquired resistance to the pathogens. However, *Agrobacterium* has evolved strategies to dampen this host defense response. It has been reported that infection by *Agrobacterium* decreases the level of free SA in roots, leading to reduced *PR1* gene expression and a diminished systemic-acquired resistance (SAR) (Gaspar et al., 2004). Otherwise it has been reported that *Agrobacterium* infection triggers the activation of mitogen-activated protein kinase (MAPK) MPK3, which phosphorylates the transcription factor VIP1, leading to its relocalization from the cytoplasm to the nucleus, and also in the of induction of stress-related genes. This can indirectly lead to increased *PR1* gene expression (Djamei et al., 2007). However, the translocated effector VirE3 was shown to induce the expression of *NIMIN1* (Niu et al., 2015). The NIMIN1 protein binds to NPR1/NIM1 and prevents the induction of *PR1* and SAR (Niu et al., 2015). It has been shown that exogenous application of SA also affects *Agrobacterium* itself and inhibits induction of its virulence genes, and thus decreases its infectivity (Yuan et al., 2007). A recent publication revealed that SA is used by *Agrobacterium* to turn down the expression of its virulence genes late in infection. To this end *Agrobacterium* expresses the hydrolase SghA to liberate plant SA from the storage form, SA-glucoside (Wang et al., 2019).

Our new results showed that *VirE3* enhances *Agrobacterium* tumorigenesis by reducing *PR1* defense gene expression at the early stage (**Figure 5A**). Using yeast two-hybrid screening, we found that VirE3 can interact with Jasmonate ZIM domain (JAZ) repressor JAZ8 *via* its ZIM domain. JAZ proteins are suppressors of JA-induced transcriptional response, reducing the transcription of JA-responsive genes such as *PDF1.2*. Our results are in line with this and show that JAZ8 suppresses the JA-dependent defense response as seen by the downregulation of *PDF1.2*, and promotes the SA-dependent response as seen by enhanced *PR1* gene expression with increased levels of JAZ8 expression (**Figure 5B**). JAZ8-OE in turn attenuates Agrobacterium tumorigenesis as shown in **Figure 2B**. We found that the effector proteinVirE3 binds to and thereby counteracts the activity of JAZ8 and thus promotes tumorigenesis by *Agrobacterium*. In the presence of VirE3, the expression of JA-defense genes is increased and the expression level of SA-defense genes decreased.

In conclusion, our data shown herein revealed that the effector protein VirE3 is required for the full virulence of *Agrobacterium* by counteracting the transcriptional repressor activity of JAZ8, thus promoting the JA defense response and diminishing the SA defense response. Such a strategy is not uncommon for plant pathogenic bacteria. Plant pathogenic *Pseudomonas syringae* bacteria secrete coronatine, a jasmonate mimic, to enhance the JA defense response. Other strains may deliver Hop effector proteins *via* a Type3 secretion system such as HopZ1 that bind to and modify JAZ proteins leading to their destruction (Jiang et al., 2013). Whether *Agrobacterium* VirE3 binding to JAZ8 similarly leads to its degradation requires further study.

DATA AVAILABILITY STATEMENT

The original contributions presented in the study are publicly available. This data can be found here: NCBI repository, accession number: PRJNA719307 (https://www.ncbi.nlm.nih.gov/bioproject/PRJNA719307).

AUTHOR CONTRIBUTIONS

BX, MZ, XN, and PH conceived and designed the experiment. SL performed the experiments. XN and SL wrote the manuscript.

MZ, XL, and JC provided critical analysis of the design and data. All authors read and approved the final manuscript.

FUNDING

This work was financially supported by the Natural Science Foundation of Hainan Province (No. 2019RC013) and Hainan Provincial Department of Education (Hnjg2019ZD-2). The funding agencies had no role in the design, analysis, and interpretation of the data, or writing of the manuscript.

SUPPLEMENTARY MATERIAL

The Supplementary Material for this article can be found online at: https://www.frontiersin.org/articles/10.3389/fpls.2021.685533/full#supplementary-material

REFERENCES

Abu-Arish, A., Frenkiel-Krispin, D., Fricke, T., Tzfira, T., Citovsky, V., Wolf, S. G., et al. (2004). Three-dimensional reconstruction of Agrobacterium VirE2 protein with single-stranded DNA. *J. Biol. Chem.* 279, 25359–25363. doi: 10.1074/jbc.m401804200

Anand, A., Uppalapati, S. R., Ryu, C.-M., Allen, S. N., Kang, L., Tang, Y., et al. (2008). Salicylic acid and systemic acquired resistance play a role in attenuating crown gall disease caused by *Agrobacterium tumefaciens*. *Plant Physiol.* 146, 703–715. doi: 10.1104/pp.107.111302

Beijersbergen, A., and Hooykaas, P. J. J. (1993). The virulence system of *Agrobacterium Tumefaciens*. *Methods Mol. Biol.* 14, 37–49.

Bracha-Drori, K., Shichrur, K., Katz, A., Oliva, M., Angelovici, R., Yalovsky, S., et al. (2004). Detection of protein-protein interactions in plants using bimolecular fluorescence complementation. *Plant J.* 40, 419–427.

Bundock, P., and Hooykaas, P. J. J. (1996). Integration of *Agrobacterium tumefaciens* T-DNA in the *Saccharomyces cerevisiae* genome by illegitimate recombination. *Proc. Natl. Acad. Sci. U.S.A.* 93, 15272–15275. doi: 10.1073/pnas.93.26.15272

Christie, P. J., Atmakuri, K., Krishnamoorthy, V., Jakubowski, S., and Cascales, E. (2005). Biogenesis, architecture, and function of bacterial type Iv secretion systems. *Annu. Rev. Microbiol.* 59, 451–485.

Citovsky, V., Kozlovsky, S. V., Lacroix, B., Zaltsman, A., Dafny-Yelin, M., Vyas, S., et al. (2007). Biological systems of the host cell involved in Agrobacterium infection. *Cell Microbiol.* 9, 9–20. doi: 10.1111/j.1462-5822.2006.00830.x

Citovsky, V., Wong, M. L., and Zambryski, P. (1989). Cooperative interaction of Agrobacterium VirE2 protein with single-stranded DNA: implications for the T-DNA transfer process. *Proc. Natl. Acad. Sci. U.S.A.* 86, 1193–1197. doi: 10.1073/pnas.86.4.1193

Clough, S. J., and Bent, A. F. (1998). Floral dip: a simplified method for Agrobacterium-mediated transformation of *Arabidopsis thaliana*. *Plant J.* 16, 735–743. doi: 10.1046/j.1365-313x.1998.00343.x

Czako, M., Wilson, J., Yu, X., and Marton, L. (1993). Sustained root culture for generation and vegetative propagation of transgenic *Arabidopsis thaliana*. *Plant Cell Rep.* 12, 603–606. doi: 10.1007/BF00232807

de Groot, M. J. A., Bundock, P., Hooykaas, P. J. J., and Beijersbergen, A. G. M. (1998). *Agrobacterium tumefaciens*-mediated transformation of filamentous fungi. *Nat. Biotechnol.* 16, 839–842. doi: 10.1038/nbt0998-839

Djamei, A., Pitzschke, A., Nakagami, H., Rajh, I., and Hirt, H. (2007). Trojan horse strategy in Agrobacterium transformation: abusing MAPK defense signaling. *Science* 318, 453–456. doi: 10.1126/science.1148110

Duan, K., Willig, C. J., De Tar, J. R., Spollen, W. G., and Zhang, Z. J. (2018). Transcriptomic analysis of arabidopsis seedlings in response to an agrobacterium-mediated transformation process. *Mol. Plant Microbe Interact.* 31, 445–459. doi: 10.1094/MPMI-10-17-0249-R

García-Cano, E., Hak, H., Magori, S., Lazarowitz, S. G., and Citovsky, V. (2018). The Agrobacterium F-Box protein effector VirF destabilizes the Arabidopsis GLABROUS1 enhancer/binding protein-like transcription factor VFP4, a transcriptional activator of defense response genes. *Mol. Plant Microbe Interact.* 31, 576–586. doi: 10.1094/MPMI-07-17-0188-FI

García-Rodríguez, F. M., Schrammeijer, B., and Hooykaas, P. J. J. (2006). The Agrobacterium VirE3 effector protein: a potential plant transcriptional activator. *Nucleic Acids Res.* 34, 6496–6504. doi: 10.1093/nar/gkl877

Gaspar, Y. M., Nam, J., Schultz, C. J., Lee, L.-Y., Gilson, P. R., Gelvin, S. B., et al. (2004). Characterization of the Arabidopsis lysine-rich Arabinogalactan-Protein AtAGP17 Mutant (rat1) that results in a decreased efficiency of agrobacterium transformation. *Plant Physiol.* 135, 2162–2171. doi: 10.1104/pp.104.045542

Gelvin, S. B. (1998). Agrobacterium VirE2 proteins can form a complex with T strands in the plant Cytoplasm. *J. Bacteriol.* 180, 4300–4302. doi: 10.1128/JB.180.16.4300-4302.1998

Gelvin, S. B. (2000). Agrobacteriumandplantgenesinvolved Int-DNA transfer andintegration. *Annu. Rev. Plant Physiol. Plant Mol. Biol.* 51, 223–256.

Gelvin, S. B. (2003). Agrobacterium-mediated plant transformation: the biology behind the "Gene-Jockeying". tool. *Microbiol. Mol. Biol. Rev.* 67, 16–37. doi: 10.1128/MMBR.67.1.16-37.2003

Gelvin, S. B. (2021). Plant DNA repair and Agrobacterium T-DNA integration. *Int. J. Mol. Sci.* 22:8458. doi: 10.3390/ijms22168458

Gietz, D., St Jean, A., Woods, R. A., and Schiestl, R. H. (1992). Improved method for high efficiency transformation of intact yeast cells. *Nucleic Acids Res.* 20:1425.

Guo, M., Ye, J., Gao, D., Xu, N., and Yang, J. (2019). Agrobacterium-mediated horizontal gene transfer: mechanism, biotechnological application, potential risk and forestalling strategy. *Biotechnol. Adv.* 37, 259–270. doi: 10.1016/j.biotechadv.2018.12.008

Herrera-Estrella, A., Chen, Z. M., Van Montagu, M., and Wang, K. (1988). VirD proteins of *Agrobacterium tumefaciens* are required for the formation of a covalent DNA-protein complex at the 5' terminus of T-strand molecules. *EMBO J.* 7, 4055–4062. doi: 10.1002/j.1460-2075.1988.tb03299.x

Howard, E. A., Zupan, J. R., Citovsky, V., and Zambryski, P. C. (1992). The VirD2 protein of a. tumefaciens contains a C-terminal bipartite nuclear localization signal: implications for nuclear uptake of DNA in plant cells. *Cell* 68, 109–118. doi: 10.1016/0092-8674(92)90210-4

Howe, G. A., Major, I. T., and Koo, A. J. (2018). Modularity in jasmonate signaling for multistress resilience. *Annu. Rev. Plant Biol.* 69, 387–415. doi: 10.1146/annurev-arplant-042817-040047

James, P., Halladay, J., and Craig, E. A. (1996). Genomic libraries and a host strain designed for highly efficient two-hybrid selection in yeast. *Genetics* 144, 1425–1436. doi: 10.1093/genetics/144.4.1425

Jarchow, E., Grimsley, N. H., and Hohn, B. (1991). virF, the host-range-determining virulence gene of *Agrobacterium tumefaciens*, affects T-DNA transfer to Zea mays. *Proc. Natl. Acad. Sci. U.S.A.* 88, 10426–10430. doi: 10.1073/pnas.88.23.10426

Jiang, S., Yao, J., Ma, K. W., Zhou, H., Song, J., He, S. Y., et al. (2013). Bacterial effector activates jasmonate signaling by directly targeting JAZ transcriptional repressors. *PLoS Pathog.* 9:e1003715. doi: 10.1371/journal.ppat.1003715

Lacroix, B. T., Vaidya, M., Tzfira, T., and Citovsky, V. (2004). The VirE3 protein of Agrobacterium mimics a host cell function required for plant genetic transformation. *EMBO J.* 24, 428–437. doi: 10.1038/sj.emboj.7600524

Lacroix, B., and Citovsky, V. (2019). Pathways of DNA transfer to plants from *Agrobacterium tumefaciens* and related bacterial species. *Annu. Rev. Phytopathol.* 57, 231–251. doi: 10.1146/annurev-phyto-082718-100101

Lapham, R., Lee, L.-Y., Tsugama, D., Lee, S., Mengiste, T., and Gelvin, S. B. (2018). VIP1 and its homologs are not required for agrobacterium-mediated transformation, but play a role in botrytis and salt stress responses. *Front. Plant Sci.* 9:749.

Li, J., Krichevsky, A., Vaidya, M., Tzfira, T., and Citovsky, V. (2005). Uncoupling of the functions of the Arabidopsis VIP1 protein in transient and stable plant

genetic transformation by Agrobacterium. *Proc. Natl. Acad. Sci. U.S.A.* 102, 5733–5738. doi: 10.1073/pnas.0404118102

Li, X., Tu, H., and Pan, S. Q. (2018). Agrobacterium delivers anchorage protein VirE3 for companion VirE2 to aggregate at host entry sites for T-DNA protection. *Cell Rep.* 25, 302–311.e306. doi: 10.1016/j.celrep.2018.09.023

Li, X., Zhu, T., Tu, H., and Pan, S. Q. (2020). Agrobacterium VirE3 uses its two tandem domains at the C-terminus to retain its companion VirE2 on the Cytoplasmic side of the host plasma membrane. *Front. Plant Sci.* 11:464. doi: 10.3389/fpls.2020.00464

Li, Y. G., and Christie, P. J. (2018). The Agrobacterium VirB/VirD4 T4SS: mechanism and architecture defined through in vivo mutagenesis and chimeric systems. *Curr. Top. Microbiol. Immunol.* 418, 233–260. doi: 10.1007/82_2018_94

McCullen, C. A., and Binns, A. N. (2006). *Agrobacterium tumefaciens* and plant cell interactions and activities required for interkingdom macromolecular transfer. *Annu. Rev. Cell Dev. Biol.* 22, 101–127. doi: 10.1146/annurev.cellbio.22.011105.102022

Melchers, L. S., Maroney, M. J., den Dulk-Ras, A., Thompson, D. V., van Vuuren, H. A., Schilperoort, R. A., et al. (1990). Octopine and nopaline strains of *Agrobacterium tumefaciens* differ in virulence; molecular characterization of the virF locus. *Plant Mol. Biol.* 14, 249–259. doi: 10.1007/BF00018565

Nester, E. W., Gordon, M. P., Amasino, R. M., and Yanofsky, M. F. (1984). Crown gall: a molecular and physiological analysis. *Annu. Rev. Plant Physiol.* 35, 387–413.

Niu, X., Zhou, M., Henkel, C. V., van Heusden, G. P. H., and Hooykaas, P. J. J. (2015). The *Agrobacterium tumefaciens* virulence protein VirE3 is a transcriptional activator of the F-box geneVBF. *Plant J.* 84, 914–924. doi: 10.1111/tpj.13048

Pauwels, L., and Goossens, A. (2011). The JAZ proteins: a crucial interface in the jasmonate signaling cascade. *Plant Cell* 23, 3089–3100. doi: 10.1105/tpc.111.089300

Piers, K. L., Heath, J. D., Liang, X., Stephens, K. M., and Nester, E. W. (1996). *Agrobacterium tumefaciens*-mediated transformation of yeast. *Proc. Natl. Acad. Sci. U.S.A.* 93, 1613–1618.

Rossi, L., Hohn, B., and Tinland, B. (1993). The VirD2 protein of *Agrobacterlum tumefaciens* carries nuclear localization signals important for transfer of T-DNA to plants. *Mol. Gen. Genet. MGG* 239, 345–353. doi: 10.1007/BF00276932

Schirawski, J., Planchais, S., and Haenni, A.-L. (2000). An improved protocol for the preparation of protoplasts from an established *Arabidopsis thaliana* cell suspension culture and infection with RNA of turnip yellow mosaic tymovirus: a simple and reliable method. *J. Virol. Methods* 86, 85–94. doi: 10.1016/s0166-0934(99)00173-1

Schrammeijer, B. (2003). Analysis of Vir protein translocation from *Agrobacterium tumefaciens* using *Saccharomyces cerevisiae* as a model: evidence for transport of a novel effector protein VirE3. *Nucleic Acids Res.* 31, 860–868. doi: 10.1093/nar/gkg179

Schrammeijer, B., Risseeuw, E., Pansegrau, W., Regensburg-Tuïnk, T. J. G., Crosby, W. L., and Hooykaas, P. J. J. (2001). Interaction of the virulence protein VirF of *Agrobacterium tumefaciens* with plant homologs of the yeast Skp1 protein. *Curr. Biol.* 11, 258–262. doi: 10.1016/s0960-9822(01)00069-0

Shi, Y., Lee, L.-Y., and Gelvin, S. B. (2014). Is VIP1 important for Agrobacterium-mediated transformation? *Plant J.* 79, 848–860. doi: 10.1111/tpj.12596

Shurvinton, C. E., Hodges, L., and Ream, W. (1992). A nuclear localization signal and the C-terminal omega sequence in the *Agrobacterium tumefaciens* VirD2 endonuclease are important for tumor formation. *Proc. Natl. Acad. Sci. U.S.A.* 89, 11837–11841. doi: 10.1073/pnas.89.24.11837

Shyu, C., Figueroa, P., DePew, C. L., Cooke, T. F., Sheard, L. B., Moreno, J. E., et al. (2012). JAZ8 lacks a canonical degron and has an EAR motif that mediates transcriptional repression of jasmonate responses in Arabidopsis. *Plant Cell* 24, 536–550. doi: 10.1105/tpc.111.093005

Tinland, B., Koukolikova-Nicola, Z., Hall, M. N., and Hohn, B. (1992). The T-DNA-linked VirD2 protein contains two distinct functional nuclear localization signals. *Proc. Natl. Acad. Sci. U.S.A.* 89, 7442–7446. doi: 10.1073/pnas.89.16.7442

Töpfer, R., Matzeit, V., Gronenborn, B., Schell, J., and Steinbiss, H.-H. (1987). A set of plant expression vectors for transcriptional and translational fusions. *Nucleic Acids Res.* 15, 5890–5890. doi: 10.1093/nar/15.14.5890

Tzfira, T. (2001). VIP1, an Arabidopsis protein that interacts with Agrobacterium VirE2, is involved in VirE2 nuclear import and Agrobacterium infectivity. *EMBO J.* 20, 3596–3607.

Tzfira, T., Vaidya, M., and Citovsky, V. (2004). Involvement of targeted proteolysis in plant genetic transformation by Agrobacterium. *Nature* 431, 87–92. doi: 10.1038/nature02857

Valvekens, D., Van Montagu, M., and Van Lijsebettens, M. (1988). *Agrobacterium tumefaciens*-mediated transformation of Arabidopsis thaliana root explants by using kanamycin selection. *Proc. Natl. Acad. Sci. U.S.A.* 85, 5536–5540. doi: 10.1073/pnas.85.15.5536

Vergunst, A. C. (2000). VirB/D4-dependent protein translocation from agrobacterium into plant cells. *Science* 290, 979–982. doi: 10.1126/science.290.5493.979

Wang, C., Ye, F., Chang, C., Liu, X., Wang, J., Wang, J., et al. (2019). Agrobacteria reprogram virulence gene expression by controlled release of host-conjugated signals. *Proc. Natl. Acad. Sci. U.S.A.* 116, 22331–22340. doi: 10.1073/pnas.1903695116

Weigel, R. R., Pfitzner, U. M., and Gatz, C. (2005). Interaction of NIMIN1 with NPR1 modulates PR gene expression in arabidopsis. *Plant Cell* 17, 1279–1291. doi: 10.1105/tpc.104.027441

Yanofsky, M. F., Porter, S. G., Young, C., Albright, L. M., Gordon, M. P., and Nester, E. W. (1986). The virD operon of *Agrobacterium tumefaciens* encodes a site-specific endonuclease. *Cell* 47, 471–477. doi: 10.1016/0092-8674(86)90604-5

Young, C., and Nester, E. W. (1988). Association of the virD2 protein with the 5' end of T strands in *Agrobacterium tumefaciens*. *J. Bacteriol.* 170, 3367–3374. doi: 10.1128/jb.170.8.3367-3374.1988

Yuan, Z. C., Edlind, M. P., Liu, P., Saenkham, P., Banta, L. M., Wise, A. A., et al. (2007). The plant signal salicylic acid shuts down expression of the vir regulon and activates quormone-quenching genes in Agrobacterium. *Proc. Natl. Acad. Sci. U.S.A.* 104, 11790–11795. doi: 10.1073/pnas.0704866104

Zaltsman, A., Krichevsky, A., Loyter, A., and Citovsky, V. (2010). Agrobacterium induces expression of a host F-Box protein required for tumorigenicity. *Cell Host Microbe* 7, 197–209. doi: 10.1016/j.chom.2010.02.009

Zaltsman, A., Lacroix, B., Gafni, Y., and Citovsky, V. (2012). Disassembly of synthetic Agrobacterium T-DNA-protein complexes via the host SCFVBF ubiquitin-ligase complex pathway. *Proc. Natl. Acad. Sci. U.S.A.* 110, 169–174. doi: 10.1073/pnas.1210921110

Zhou, M., Zhang, K., Sun, Z., Yan, M., Chen, C., and Zhang, X. (2017). LNK1 and LNK2 corepressors interact with the MYB3 transcription factor in phenylpropanoid biosynthesis. *Plant Physiol.* 174, 1348–1358. doi: 10.1104/pp.17.00160

Conflict of Interest: The authors declare that the research was conducted in the absence of any commercial or financial relationships that could be construed as a potential conflict of interest.

Publisher's Note: All claims expressed in this article are solely those of the authors and do not necessarily represent those of their affiliated organizations, or those of the publisher, the editors and the reviewers. Any product that may be evaluated in this article, or claim that may be made by its manufacturer, is not guaranteed or endorsed by the publisher.

frontiers in Plant Science

ORIGINAL RESEARCH
published: 30 November 2021
doi: 10.3389/fpls.2021.754391

Transcriptomic Response of Huanglongbing-Infected *Citrus sinensis* Following Field Application of a Microbial Fermentation Product

Richard D. Lally[1], Kathleen Donaleshen[2], Ulalo Chirwa[2], Katie Eastridge[2], Wesley Saintilnord[3], Edward Dickinson[2], Richard Murphy[1], Steven Borst[2], Karina Horgan[1] and Karl Dawson[2]*

[1]Alltech Ireland, Dunboyne, Ireland, [2]Alltech, Nicholasville, KY, United States, [3]Department of Molecular and Cellular Biochemistry, University of Kentucky, Lexington, KY, United States

OPEN ACCESS

Edited by:
Essaid Ait Barka, Université de Reims Champagne-Ardenne, France

Reviewed by:
Rachid Lahlali, Ecole Nationale d'Agriculture de Meknès, Morocco
Antonio Cellini, University of Bologna, Italy

***Correspondence:**
Richard D. Lally
lallyr43@yahoo.com

Specialty section:
This article was submitted to Plant Pathogen Interactions, a section of the journal Frontiers in Plant Science

Received: *06 August 2021*
Accepted: *05 November 2021*
Published: *30 November 2021*

Citation:
Lally RD, Donaleshen K, Chirwa U, Eastridge K, Saintilnord W, Dickinson E, Murphy R, Borst S, Horgan K and Dawson K (2021) Transcriptomic Response of Huanglongbing-Infected Citrus sinensis Following Field Application of a Microbial Fermentation Product. Front. Plant Sci. 12:754391. doi: 10.3389/fpls.2021.754391

Huanglongbing (HLB) is considered the most destructive disease in *Citrus* production and threatens the future of the industry. Microbial-derived defense elicitors have gained recognition for their role in plant defense priming. This work assessed a 5% (V/V) microbial fermentation application (MFA) and its role in the elicitation of defense responses in HLB-infected *Citrus sinensis* trees following a foliar application with a pump sprayer. Using a PCR detection method, HLB infection levels were monitored in healthy and infected trees for 20 months. Nutrient analysis assessed N, P, K, Ca, Mg, Mn, Zn, Fe, B, and Cu concentrations in the trees. MFA significantly increased Cu concentrations in treated trees and resulted in the stabilization of disease index (DI) in infected trees. Initial real-time qPCR analysis of defense-associated genes showed a significant increase in pathogenesis-related protein 2 (PR2) and phenylalanine ammonia lyase (PAL) gene expression in healthy and HLB-infected trees in response to MFA. Gene expression of PR2 and PAL peaked 6 h post-microbial fermentation application during an 8-h sampling period. A transcriptomic assessment using GeneChip microarray of the hour 6 samples revealed differential expression of 565 genes when MFA was applied to healthy trees and 909 genes when applied infected citrus trees when compared to their respective controls. There were 403 uniquely differentially expressed genes in response to MFA following an intersectional analysis of both healthy and infected citrus trees. The transcriptomic analysis revealed that several genes associated with plant development, growth, and defense were upregulated in response to MFA, including multiple PR genes, lignin formation genes, ROS-related genes, hormone synthases, and hormone regulators. This study provides further evidence that MFA may play an important role as a plant elicitor in an integrated pest management strategy in citrus and other agronomically important crops.

Keywords: *Citrus*, citrus greening, HLB, huanglongbing, microbial elicitors, fermentation

INTRODUCTION

Huanglongbing (HLB) is a phloem-limited bacterial disease that infects citrus trees of all kinds, caused by *Candidatus liberibacter* (Jagoueix et al., 1996; Hansen et al., 2008; Duan et al., 2009). It is delivered to the phloem tissue by the Asian citrus psyllid vector and slowly kills trees over a period of several years (Bové, 2006). HLB has devastated the citrus industry in the United States, resulting in severe economic deterioration in affected regions (Dala-Paula et al., 2019; Singerman and Rogers, 2020). Efforts to control and manage HLB have been unsuccessful leading to yearly declines in citrus production. In areas where the disease is not broadly prevalent, management strategies include scouting and destroying infected trees. Aggressive management strategies are recommended for highly infected areas including the use of insecticides, antimicrobials, thermotherapy, antibiotics, and novel therapeutic agents (Davis et al., 2000; Bové, 2006; Das et al., 2014; Gardner et al., 2020). However, effective treatment and a commercially viable cure for the disease have not been found. Defense elicitors in crops have been under investigation as possible solutions to alleviate symptoms of various agronomic diseases. Elicitors upregulate the expression of defense proteins that in turn activate both systemic and local defense responses in treated plants (Montesano et al., 2003). In situations where this activity is observed, the reduction of diseases results in healthier plants and higher yielding crops. In multiple studies, HLB has been observed to interrupt the normal biochemical pathways in citrus. In *Citrus limon*, HLB infection facilitated the downregulation of catalases, chitinases, lectin-related proteins, and miraculin-like proteins (Nwugo et al., 2013). These metabolic changes ultimately lead to increased bacterial spread and susceptibility to other problematic pathogens. Among its repertoire of virulence tools, HLB encodes a salicylic acid hydroxylase, which degrades the plant hormone salicylic acid (Li et al., 2017). HLB also contains peroxiredoxins that increase oxidative stress tolerance, leading to increased HLB fitness *in planta* (Jain et al., 2015, 2018). The routine activation of a plants defense in response to an elicitor could perhaps reduce the success of HLB in citrus.

Microbial fermentation application (MFA), a previously described elicitor program, is formulated with a bacterial fermentation media, yeast cell wall extract, and a Cu component. It has been shown to reduce powdery mildew infection in wheat (Twamley et al., 2019). The authors also concluded that MFA upregulated pathogenesis-related protein 1 (PR 1), pathogenesis-related protein 4 (PR 4), pathogenesis-related protein 5 (PR 5), and pathogenesis-related protein 9 (PR 9) gene expression (Twamley et al., 2019). Upregulation of PR1 is an indicator of increased systemic acquired resistance (SAR) in plants (Ryals et al., 1996) and influences salicylic acid accumulation at the site of infection by various pathogens. The expression of PR1 increases plant tolerance to fungal, oomycete, and bacterial pathogenic challenges (Alexander et al., 1993; Jirage et al., 1999; Zhang et al., 1999). PR5 are a group of thaumatin-like proteins that are also associated with SAR and general defense responses. These are induced in response to various fungal and bacterial challenges (Li et al., 2015b; Chen et al., 2017). Peroxidases, such as PR9, are also widely involved in plant defense (Kawano, 2003) and have been observed in response to bacterial and fungal pathogen infections or exposure.

In this study, MFA was investigated for its potential role in activating citrus defenses against HLB. The previous research in wheat and soybean demonstrates that microbial fermentation products increase the expression of defense networks and aid in the improvement of crop quality parameters or can reduce the burden of disease (Twamley et al., 2019; Schulman et al., 2021; Twamley et al., 2021). If the upregulation of a systemic defense network can be achieved in a similar way in citrus, HLB might be suppressed using the MFA program. Additionally, MFA may affect the plant tissue Cu concentration, as a further mechanism for the restriction of HLB population. To this end, citrus gene expression, nutrient composition, and assessment of routine use of MFA on HLB infection levels quantified by PCR in a field study over the course of 20 months were examined. This experiment monitored four treatment groups consisting of an uninfected control, infected trees, uninfected trees with MFA treatment, and infected trees with MFA treatment. Citrus petiole samples were observed routinely throughout the trial to determine the level of HLB infection and how it progressed in response to each treatment. Leaf tissue nutrient analysis was conducted to determine whether nutrient concentrations were influenced in each treatment group. Gene expression of PR2 and phenylalanine ammonia lyase (PAL) was assessed to determine the impact of MFA on defense gene expression between 0 and 8 h post-MFA treatment. Samples from the hour 6 time point were used for a transcriptomic assessment using microarray.

MATERIALS AND METHODS

Microbial Fermentation Application

Microbial fermentation application as previously described by Twamley et al. (2019) was a applied as a 5% (V/V) suspension in water for this experiment. MFA contains co-products from bacterial and yeast fermentation processes. Applications were made once monthly to the foliar portion of each tree using a handheld pressurized pump sprayer, for the duration of the experiment. The MFA used in this study was supplied by Alltech Crop Science, KY, United States.

Field Trial Design

The field trial was conducted for 20 months in a privately owned citrus grove in central Florida (Haines City, FL, United States; latitude 28.14297 and longitude −81.69818). A total of 64 *Citrus sinensis* trees were planted in four rows over a 2-acre trial site. To minimize the risk of HLB infection, all the trees were contained in individual plastic protective covers. The trees were split into four groups for the study and were randomly assigned across the four rows. Several trees were removed from the trial due to hurricane damage and unsuccessful infection grafting. The remaining trees were divided across

four experimental groups, which included: HLB negative trees (referred to herein as control) $n = 11$, HLB positive trees (referred to herein as infected) $n = 17$, HLB positive trees with monthly treatments of MFA (referred to herein as MFA + infection) $n = 20$, and HLB negative trees with monthly treatments of MFA (referred to herein as MFA) $n = 12$. HLB positive groups were infected by grafting HLB positive bud wood onto healthy citrus trees. Grafting was achieved by sourcing infected bud wood from highly symptomatic mature *C. sinensis* trees, which were obtained from a mature symptomatic tree from the same grove. Bud wood of a length of 6–8 cm was shaped with a longitudinal cut which was compatible with a cut in the receiving trees. Grafts were firmly secured with 2-cm-wide plastic wrap. HLB infection levels were monitored at 0, 3, 4, 6, 8, and 20 months by PCR to determine infection progression and to ensure negative groups remained uninfected. After the grafts were established monthly, applications of a 5% (V/V) MFA treatment were applied to healthy and infected citrus trees. Simultaneously water was applied to a control and the infected control groups. All treatments were applied as a foliar spray and were delivered by pump pressurized equipment, and each treatment was applied until the leaf surfaces were saturated. Each tree received approximately 200 ml of each treatment.

Tissue Sampling and RNA Extraction

After the 15th MFA treatment, samples were taken for qPCR analysis and gene transcriptomic analysis. This gave the trial and disease enough time to establish and receive routine doses of MFA before transcriptomic and nutrient analysis. Seven trees were randomly selected per treatment, and leaf tissue samples were harvested at 0, 2, 4, 6, and 8 h post-treatment application. In total, 6 leaves were randomly sampled from each of the selected trees for each time point. Leaves were sealed in plastic zip bags and frozen immediately on dry ice. Tissue samples were transported on dry ice and immediately stored at −80°C at their destination. Leaf tissue was ground to a fine powder under liquid nitrogen, and the frozen powdered tissue was then processed using an RNeasy Plant mini kit (Qiagen, Hilden, Germany) according to the manufacturer's instructions. An on-column DNA digestion was conducted using the RNase-Free DNase kit (Qiagen, Hilden, Germany) to remove any DNA from the extracted RNA. Purified samples were eluted into a 1.5-ml tube and stored at −80°C until use. Sample quality was evaluated by both NanoDrop (Thermo Fisher Scientific, Waltham, MA, United States) and 2100 Bioanalyzer analysis (Agilent Technologies, Santa Clara, CA, United States) according to the manufacturer's instructions (Thermo Fisher Scientific, Waltham, MA, United States). Samples with a 230/260 and 260/280 ratio value lower than 2 were rejected and reprocessed. Samples with a RNA Integrity Number (RIN) values >7 were considered acceptable for downstream analysis.

RT-qPCR Gene Expression Analysis

A total RNA concentration of 2 µg was converted to cDNA using the High-Capacity cDNA Reverse Transcription Kit (Thermo Fisher Scientific, Waltham, MA, United States) according to the manufacturer's instructions. Following the reverse transcription step, the cDNA was diluted 1:20 in nuclease-free water. Target genes encoding for PAL (GenBank accession No. XM_006481430.3) F: 5′-TTGAACTGGGGAGTGA TGGC-3′; R: 5′-CCACTTTGACTTGGGCGTTG-3′ (this study designed with Primer 3) and PR2 (GenBank accession No. XM_015534320.2) FW-F: 5′-ACTTCGCTCAGTACCTTG TTC-3′; R: 5′-GGCAGTGGAAACCTTGATTTG-3′ (Dutt et al., 2015) were considered with 18S (GenBank accession No. XR_003063242.1) F: 5′-GCTTAGGCCAAGGAAGTTTG-3′ R: 5′-TCTATCCCCATCACGATGAA-3′ (Albrecht and Bowman, 2012) as a house keeping gene for examining the relative gene expression of citrus-specific defense indicators.

Reactions were conducted at a volume of 20 µl with 10 µl Fast SYBR Green Master Mix (Thermo Fisher Scientific, Waltham, MA, United States), 0.1 µl F and 0.1 µl R primers at a concentration of 10 µM each, 8.8 µl of nuclease-free water, and 1 µl of cDNA template. The quantitative program started with a melt step at 95°C for 20 s and then cycled 40 times with an annealing temperature of 60°C for 30 s and a melting temperature at 95°C for 3 s. Each plate was run with technical duplicates for each sample and a negative control for each target gene. Data were statistically analyzed as $2^{-(\Delta ct)}$ data and converted to fold change values for presentation (Schmittgen and Livak, 2008). Fold change values were calculated with the equation $2^{-(\Delta\Delta ct)}$ using the ratio of target gene to control gene. All qPCR analysis was performed on the Applied Biosystems 7500 Fast Real-Time PCR instrument.

Citrus Transcriptomic Analysis

Leaf samples collected at 6 h for the initial qPCR analysis were processed for transcriptomic analysis ($n = 5$), using microarray technology. The Affymetrix GeneChip hybridization protocol was used to generate transcriptomic data and was conducted according to the manufacturers protocol for the 3′ IVT PLUS Reagent Kit (Thermo Fisher Scientific, Waltham, MA, United States). Briefly, RNA was isolated as described above and was processed for use with the Affymetrix Citrus genome GeneChip array. Total RNA was prepared to a total reaction concentration of 15 µg and used to generate first-strand and second-strand cDNA. Following this, cRNAs were labeled in the presence of biotinylated ribonucleotide analogues (3′ IVT Biotin Label); after purification and fragmentation, a total concentration of 15 µg of cRNAs was used in a hybridization mixture containing added hybridization controls. A total of 200 µl of the mixture was hybridized on arrays for 16 h at 45°C. Post-hybridization, GeneChips were washed and double-stained using the Affymetrix GeneChip fluidics station 450. Chips were then scanned using the Affymetrix GeneChip scanner 2500. Data were exported as CEL files to the Transcriptome Analysis Console (TAC; Thermo Fisher Scientific, Waltham, MA, United States), and data were filtered to include only genes that were expressed to +2 or −2 fold change with a significance threshold of $p \leq 0.05$ following analysis using the RMA model (Millenaar et al., 2006). All data used for analysis are available in **Supplementary File 1**.

Leaf Nutrient Analysis

Citrus leaves, 25–30 per tree, were randomly picked and placed in nitrogen-free tissue sampling bags at the time of the gene transcription analysis. Bags were transported and submitted to Central Florida Soil Laboratory (Bartow, FL, United States). Citrus leaves were washed in 3% hydrochloric acid to remove surface residues and contaminants prior to processing. Samples were prepared using a dry ash method. ICP-OES analysis was used to quantify K, Ca, Mg, Cu, Mn, Zn, Fe, and B (Hansen et al., 2013). N and P concentrations were assessed using a LECO instrument (St. Joseph, MI, United States).

HLB Progression

Bacterial concentration tests were conducted by submitting leaf tissue samples to Southern Gardens Diagnostic Laboratory (Clewiston, FL, United States). Every tree in the experiment was tested for HLB throughout the study. Once tress were HLB positive as confirmed by a PCR Ct value <33, leaf samples were taken at 0, 3, 4, 6, 8, and 20 months into the trial. Month 0 coincided with the first MFA treatment. Six leaves from each tree were sampled and pooled in plastic zip sealed bags and immediately frozen on dry ice. From each sample bag, 100 mg of petiole was randomly obtained from across the leaves and placed in extraction buffer. Samples were processed using an automated plant DNA isolation method using Qiagen plant DNA extraction reagents (Qiagen, Hilden, Germany). Assay conditions and primers were prepared according to (Li et al., 2006). Ct values were reported as Ct per 10 ng μl^{-1} of petiole DNA. The disease index (DI %) was calculated as previously described by. In short, HLB disease severity was assigned a grade from 0 to 4, where 0 = Ct value ≥36.0 (undetectable), 1 = 32.0 ≤ C_t value <36 (low HLB infection), 2 = 28 ≤ C_t value <32 (moderate HLB infection), 3 = 24 ≤ C_t value <28 (high HLB infection), and 4 = C_t value <24 (very high HLB infection). Those values were converted to DI % using the formula described by Yang et al. (2016). Changes in the distribution of disease severity of the infection were measured by examining the changes in the DI in individual trees during the period between 8 and 20 months of the trial.

Statistical Analysis

Statistical testing for HLB concentrations, nutrient, mineral analysis, and qPCR was all computed using R (R-Core-Team, 2020), with all data initially tested with a one-way ANOVA. Where significant differences were detected between groups ($p < 0.05$), the data were then subjected to a Tukey's HSD test, and data achieving a $p < 0.05$ were accepted as significantly different. The distribution of the change of disease severity was compared with a Pearson's Chi-squared test in JMP version 16.0.0 (SAS, Cary, NC, United States). Gene expression data were subjected to independent statistical validation using the TAC console as described in citrus transcriptome analysis section above. Any gene expression results with a value of $p < 0.05$ were considered significantly different where fold changes were greater than +2 or less than −2.

RESULTS

HLB Progression

Huanglongbing prevalence was monitored throughout the experimental period. Uninfected control and MFA trees had no detectable infections for the duration of the trial (**Figure 1**). The infected and MFA + infected groups showed a steady rise in HLB prevalence over the 6 months after graft inoculation (**Figure 1A**). A numeric difference was observed between both the infected and MFA + infected with the MFA-treated trees scoring a lower average DI rating of 13.3% at 20 months although this was not significant ($p = 0.25$; **Figure 1B**).

The ability of the MFA treatment to modulate the progression of the disease and propagation of the infective agent was evaluated during the last 12 months of the trial by following the severity of the infections (DI values) in individual trees. Significant changes were recorded in the progression of DI in disease challenged (infected) trees treated with MFA and untreated trees (**Table 1**). A smaller proportion of trees showed increases in the DI ($p = 0.044$), and greater proportion showed decreased DI ($p = 0.008$) in the MFA-treated group during this period.

Nutrient Analysis of Leaf Tissue Following MFA Treatment of Control and Infected *Citrus sinensis*

Leaf tissue mineral analysis results indicated that Cu concentrations were significantly higher in trees that received the MFA (**Table 2**). When compared to the control, both MFA ($p = 0.0063$) and MFA + infection ($p = 0.0003$) resulted in significantly higher leaf tissue Cu concentrations, and both were also greater when compared to the infected samples (MFA $p = 0.0003$ and MFA + infected $p = 0.046$). There was a lower Ca concentration in MFA + infected treatment when compared to the control trees ($p = 0.0036$). The results also indicated that Mg concentration was lower in the infected group when compared to the control ($p = 0.009$) and MFA group ($p = 0.004$). The concentrations of the remaining nutrients tested (N, P, K, Mn, Zn, Fe, and B) were unaltered as result of MFA or the HLB disease.

Gene Expression Analysis of *Citrus sinensis* in Response to MFA in Control and Infected Trees

RT-qPCR analysis of two citrus defense-associated genes was performed in a time point-based assessment (**Figure 2**). PR2 gene expression increased in MFA and MFA + infected trees 2 h after MFA treatment and remained significantly upregulated relatively to the untreated controls at all remaining time points (**Figure 2A**). The maximum expression level increase for PR2 was observed 6 h after the MFA treatment was made, with increases of 5.4-fold ($p = 0.001$) and 5.9-fold ($p = 0.001$) in MFA and MFA + infected groups, respectively, when compared to the control.

Phenylalanine ammonia lyase expression levels were also significantly increased in MFA and MFA + infected trees (**Figure 2B**) 6 h post-application. MFA and MFA + infection

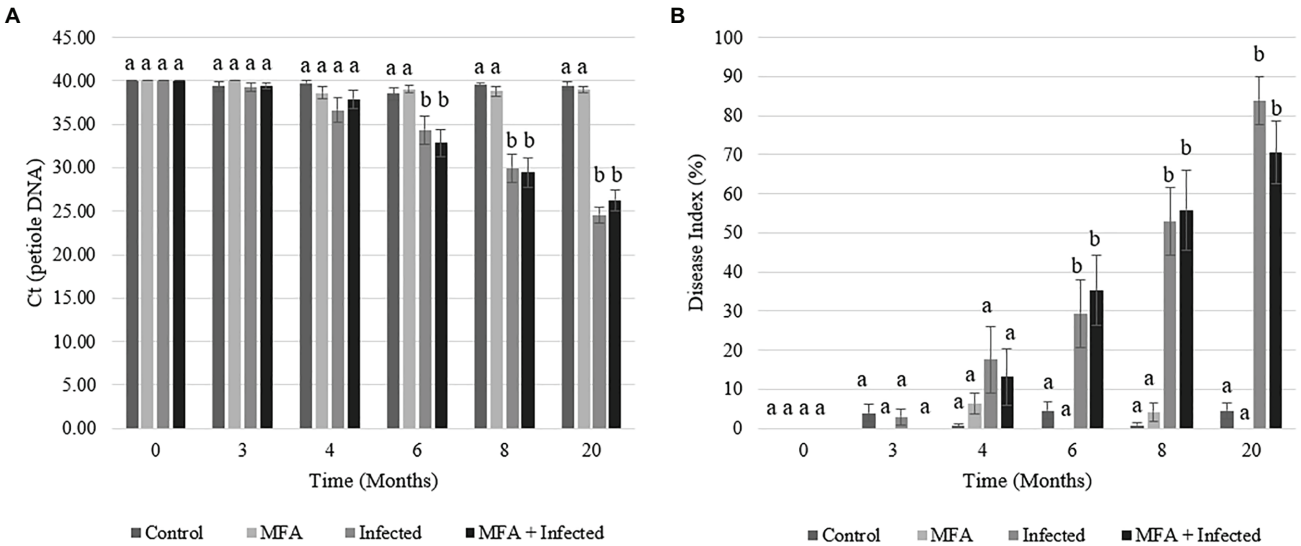

FIGURE 1 | Huanglongbing (HLB) prevalence and disease progression in *Citrus sinensis* over the duration of the field investigation. **(A)** HLB infection as C_t of petiole DNA measurements was made in infected and uninfected citrus tissue for the duration of the trial. **(B)** Disease index over time. Data represent average disease index rating over time in each experimental group. Letters that are the same within each time point indicate no differences between groups. Error bars represent ± SEM.

TABLE 1 | Disease progression in trees during the period between 8 and 20 months of the trial as measured by changes in the severity of infection (DI) in individual trees.

Condition	Treatment	Number of trees showing increased severity of infection (change in DI > 0)		Number of trees showing decreased severity of infection (change in DI < 0)	
		Fraction	Percent	Fraction	Percent
Unchallenged trees	Control	1/11	9%	0/11	0%
	MFA	0/12	0%	2/12	17%
Infected trees	Infected	12/17[a]	71%	0/17[a]	0%
	MFA + Infected	7/20[b]	35%	5/20[b]	25%
All trees	No MFA Treatment	13/28[a]	46%	0/28[a]	0%
	MFA Treated	7/32[b]	21%	7/32[b]	21%

Differences in superscripts (a, b) indicate the distribution of the change in disease severity (DI) differs between the MFA treated and untreated groups of trees ($p < 0.05$).

increased to 6.9-fold ($p = 0.01$) and 11.0-fold ($p = 0.03$), respectively, when compared to untreated controls. PAL expression remained high in the MFA + infected trees 8 h after application with a fold change of 5.4 ($p = 0.02$).

Transcriptomic Assessment of Control and Infected Trees in Response to MFA

As the highest expression levels for both defense genes following treatment with MFA were observed at 6 h (**Figure 2**), RNA samples from the control, infected, MFA and MFA + infected trees/groups were assessed *via* GeneChip microarray ($n = 5$). The results revealed 171 differentially expressed genes between the control and infected group. In both MFA-treated groups, a greater incidence of significantly differentially expressed genes was noted. Five hundred and sixty-five genes were differentially expressed between the control and MFA. Nine hundred and nine genes were differentially expressed between infected and MFA + infected groups (**Figure 3A**).

These results revealed a pattern of uniquely expressed genes in response to the MFA treatment in both infected and healthy citrus trees. Each group had uniquely expressed genes associated with their experimental conditions. The groups were assessed using the following comparisons: control vs. infected, control vs. MFA, and infected vs. MFA + infected. The control vs. infected group had 142 uniquely expressed genes between the groups representing 11.8% of the gene expression differences. Control vs. MFA had 139 genes that were unique to that group. The infected vs. MFA + infected contained 490 unique genes. There were 403 genes that were differentially expressed and were shared between the two groups MFA vs. MFA + infection and control vs. MFA, indicating a cluster of unique genes regulated by MFA (**Figure 3B**).

Principal component analysis (PCA) presented in **Figure 3** reveals clustering of distinct groupings of the MFA-treated trees, with MFA-treated clustering together and the untreated groups being completely distinct.

TABLE 2 | Leaf tissue nutrient analysis from *Citrus sinensis* after long-term MFA treatment.

	%					Ppm				
Treatment	**N**	**P**	**K**	**Ca**	**Mg**	**Mn**	**Zn**	**Fe**	**B**	**Cu**
Control	3.22 ± 0.11^{a}	0.18 ± 0.01^{a}	1.98 ± 0.08^{a}	3.76 ± 0.27^{a}	0.28 ± 0.01^{a}	39.80 ± 6.36^{a}	41.80 ± 5.12^{a}	88.40 ± 6.23^{a}	168.00 ± 16.44^{a}	9.8 ± 0.7^{a}
Infected	2.98 ± 0.14^{a}	0.16 ± 0.01^{a}	1.84 ± 0.05^{a}	3.22 ± 0.17^{ab}	0.22 ± 0.01^{b}	38.40 ± 5.10^{a}	35.40 ± 0.07^{a}	73.80 ± 7.17^{a}	185.40 ± 16.26^{a}	9.4 ± 0.3^{a}
MFA	3.18 ± 0.09^{a}	0.20 ± 0.01^{a}	1.82 ± 0.07^{a}	2.92 ± 0.15^{ab}	0.29 ± 0.01^{a}	48.00 ± 14.27^{a}	44.80 ± 2.42^{a}	86.00 ± 9.35^{a}	162.80 ± 36.69^{a}	32.4 ± 5.4^{b}
MFA + Infected	3.04 ± 0.07^{a}	0.19 ± 0.01^{a}	2.00 ± 0.11^{a}	2.44 ± 0.25^{b}	0.25 ± 0.01^{ab}	37.20 ± 9.90^{a}	40.20 ± 4.82^{a}	71.00 ± 5.37^{a}	184.00 ± 15.37^{a}	26.8 ± 6.69^{b}

Data presented represent means of each treatment group for each mineral or nutrient tested. Letters that are the same within each column indicate no differences between groups (n = 5). Error is represented as ± SEM.

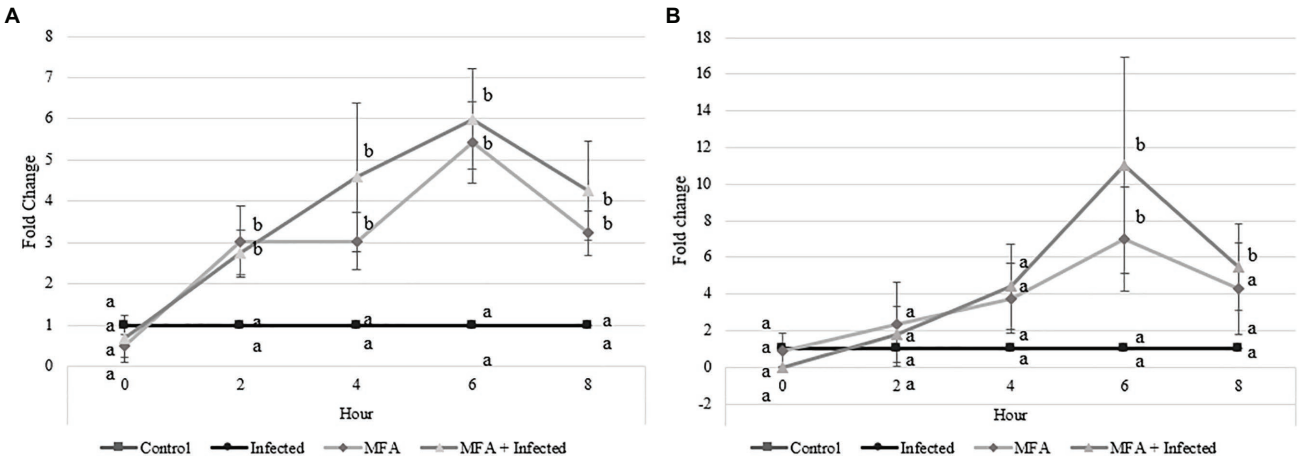

FIGURE 2 | Impact of microbial fermentation application (MFA) on gene expression levels of defense genes in healthy and infected *Citrus sinensis* trees. Data represent gene expression of **(A)** beta-1,3-endoglucanase (PR2) and **(B)** phenylalanine ammonia lyase (PAL) over 5 time points 0, 2, 4, 6, and 8 h after MFA treatment ($n = 7$). Both treatments were normalized to their respective controls. MFA trees were normalized to control trees, and MFA + infected trees were normalized to the infected group. Letters that are the same within each time point indicate no differences between groups ($p > 0.05$). Error bars indicate ± SEM.

Analysis of Control vs. Infected

The set of genes reported when the control was compared to the infected citrus samples revealed 171 differentially expressed genes, 150 of which were upregulated and 21 were downregulated in infected trees when compared to the control. The range of upregulation was recorded from 2 to 11.43 fold and −2 to −5.03 fold change for the downregulated genes. The top 10 upregulated and downregulated genes are presented in **Table 3**, and the full comparative set is available in **Supplementary File 1**. Among the known genes, there was a number that may reveal the impact of HLB on various citrus metabolic processes. Genes associated with early nodulin-like protein 3-like gene, Kinesin-4-like, gibberellin regulated protein, probable polygalacturonase-like, trans-resveratrol di-O-methyltransferase-like, and probable leucine-rich repeat receptor-like protein kinase At1g68400-like were all upregulated. Indicators of defense and stress responses such as peroxidase 30-like, protein Aspartic protease in guard cell 1-like, hypersensitive-induced response protein 2-like, phenylalanine ammonia-lyase-like, and miraculin-like and thaumatin-like protein-like were also upregulated. Genes that may be involved in carbohydrate accumulation such as sucrose synthase 6-like, expansin-A4-like, extensin-2-like, and cellulose synthase-like protein G2-like were also upregulated. Among the downregulated genes were hormone-related genes like auxin-responsive protein IAA29-like, brassinosteroid-regulated protein BRU1-like, and ethylene-responsive transcription factor ERF023-like. Fe(II) transport protein 3, chloroplastic-like, adenylate isopentenyltransferase 3, chloroplastic-like, xyloglucan endotransglucosylase/hydrolase protein 22-like, probable xyloglucan endotransglucosylase/hydrolase protein 23-like, ATC protein, and serine/threonine-protein phosphatase 6 regulatory ankyrin repeat subunit C-like were also impacted. Several genes are currently unknown or were hypothetical proteins including the highest upregulated and downregulated genes (**Table 3**).

Analysis of Control vs. MFA

A comparison of gene expression in control citrus trees with MFA-treated citrus trees revealed 565 differentially expressed genes. 516 of these genes were upregulated, and 49 were downregulated. 2–56.5 fold changes were observed in the group of upregulated genes, and −2 to −3.8 fold change was noted in the downregulated group (**Table 4** and the full comparative

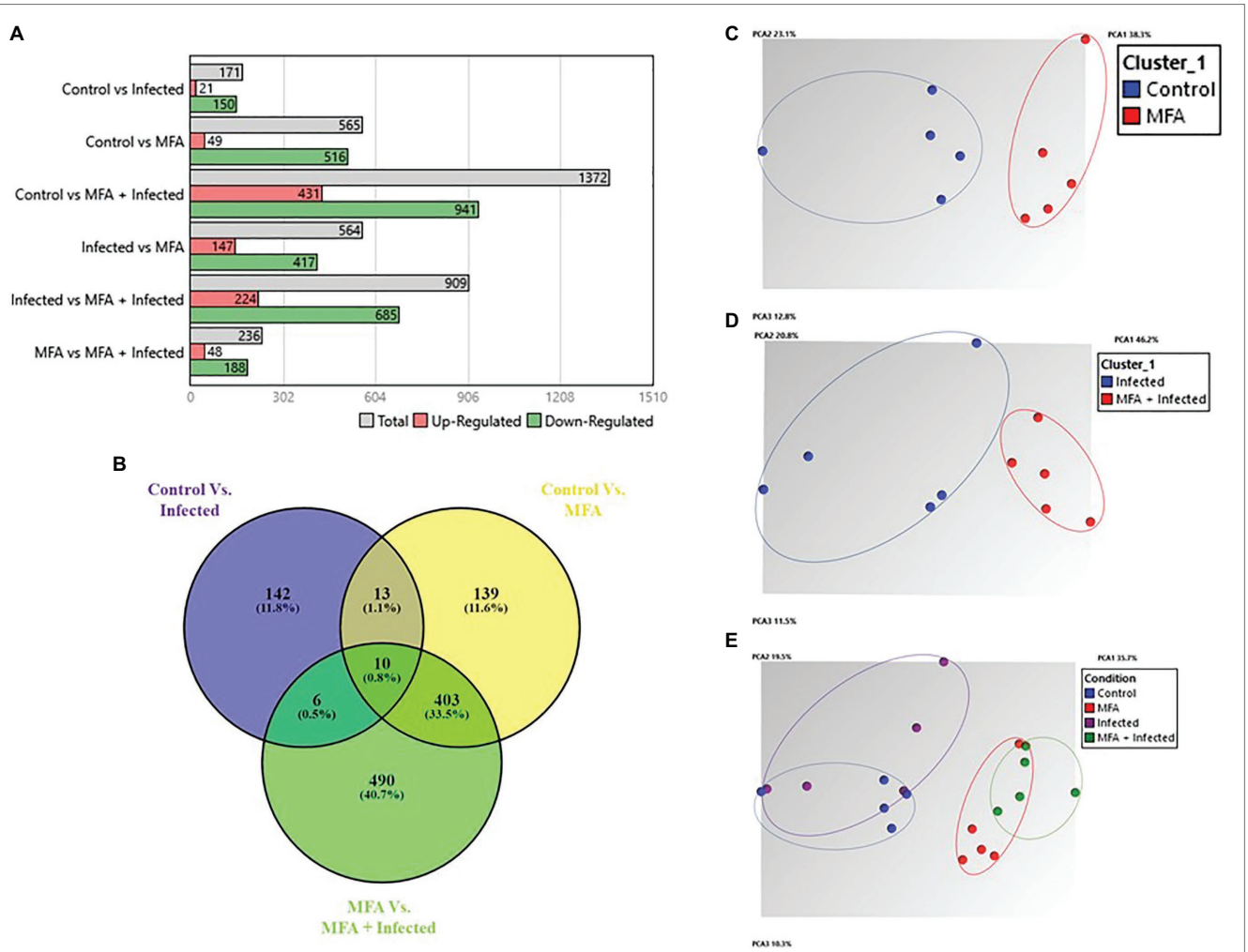

FIGURE 3 | Summary of gene expression data from *Citrus sinensis*. **(A)** Number of significantly differentially expressed genes between different combinations of experimental groups. **(B)** Venn diagram displaying number of intersecting genes between healthy and HLB-infected *Citrus sinensis* following treatment with MFA. Venn diagram was generated by comparing gene expression sets. Venn diagram displays the common tally of genes that are impacted by the experimental conditions. Numbers represent significantly differentially expressed genes ($p < 0.05$), and percentages represent the percentage of the total tally. (Oliveros, 2007–2015). Venny 2.1.0. https://bioinfogp.cnb.csic.es/tools/venny/. **(C–E)** Principal component analysis (PCA) plots indicating relationships between differentially expressed genes in MFA-treated samples and control treatments. Oval shapes indicate treatment grouping (control, infected, MFA, MFA + infected). **A**, **C**, **D**, and **E** graphs were generated by the TAC console.

set is available in **Supplementary File 1**). This comparison revealed that genes related to defense regulation 1-aminocy clopropane-1-carboxylate synthase 1-like, Laccase-7-like, O-methyltransferase homologue, blue copper protein-like, BAHD acyltransferase At5g47980-like, cytochrome P450 83B1-like, phenylalanine ammonia-lyase-like, chitinase CHI1, ethylene-responsive transcription factor 1B-like, glucan endo-1,3-beta-glucosidase, basic isoform-like, and peroxidase C3-like were influenced. Downregulated genes included auxin-induced protein 22D-like, protein ECERIFERUM 1-like, regulator of chromosome condensation-like protein, purple acid phosphatase 8-like, expansin-A5-like, auxin-induced protein 22D-like, translocator protein homolog, and uncharacterized proteins and hypothetical proteins (**Table 4**).

Analysis of Infected vs. MFA + Infected

When gene expression in the infected trees was compared to the MFA + infected citrus trees, 909 differentially expressed genes were observed. 685 of these genes were upregulated, and 224 were downregulated in MFA + infected samples. 2–43.2 fold changes were observed in the group of upregulated genes, and 2 to −11.1 fold change was observed in the downregulated group. A sample of these genes is presented in **Table 5**, and the full comparative set is available in **Supplementary File 1**. The analysis revealed an upregulation in laccase-7-like, 1-aminocyclopropane-1-carboxylate synthase 1-like, BAHD acyltransferase At5g47980-like, blue copper protein-like, and genes associated with defense responses. This includes endochitinase 1-like, glucan endo-1,3-beta-glucosidase, basic isoform-like, ethylene-induced esterase,

TABLE 3 | A sample of the differentially expressed genes in the control vs. infected groups.

Gene ID	Description	Fold change	*p*
Upregulated			
Cit.10009.1.S1_s_at	Unknown	11.43	0.0281
Cit.15054.1.S1_at	Hypothetical protein	11.07	0.0067
Cit.7276.1.S1_at	Uncharacterized LOC102630205	10.49	0.0042
Cit.23470.1.S1_s_at	Uncharacterized LOC102625551	9.73	0.0064
Cit.7727.1.S1_at	Early nodulin-like protein 3-like	9.56	0.0020
Cit.20586.1.S1_at	Unknown	8	0.0383
Cit.30043.1.S1_at	Unnamed protein product homologue (*Arabidopsis thaliana*)	7.68	0.0104
Cit.7736.1.S1_at	Unnamed protein homologue (*Arabidopsis thaliana*)	7.68	0.0104
Cit.29883.1.S1_a_at	Kinesin-4-like	6.59	0.0097
Cit.681.1.S1_x_at	Unknown	6.09	0.0203
Downregulated			
Cit.13366.1.S1_at	Chalcone synthase homologue (*Cardamine amara*)	−5.03	0.0297
Cit.5973.1.S1_s_at	Serine/threonine-protein phosphatase 6 regulatory ankyrin repeat subunit C-like	−4.67	0.0182
Cit.17562.1.S1_at	Serine/threonine-protein phosphatase 6 regulatory ankyrin repeat subunit C-like	−3.93	0.0205
Cit.31451.1.S1_s_at	ATC protein	−3.34	0.0021
Cit.17724.1.S1_s_at	Xyloglucan endotransglucosylase/hydrolase protein 22-like	−2.76	0.0009
Cit.13424.1.S1_at	Putative cytochrome P450 protein homologue (*Arabidopsis thaliana*)	−2.68	0.0026
Cit.9523.1.S1_s_at	Translocator protein homolog	−2.67	0.0354
Cit.18045.1.S1_s_at	Ethylene-responsive transcription factor ERF023-like	−2.65	0.0011
Cit.30513.1.S1_x_at	Syringolide-induced protein 19-1-5 homologue (*Glycine max*)	−2.62	6.27E-06
Cit.9421.1.S1_s_at	Probable xyloglucan endotransglucosylase/hydrolase protein 23-like	−2.6	5.70E-05

phenylalanine ammonia-lyase-like, and peroxidase 15-like proteins. There were also a number of unknown and uncharacterized genes upregulated. Among the most downregulated genes were chalcone synthase-related genes and homologues, a Protein ECERIFERUM 1-like, glycine-rich cell wall structural protein 1-like and GDSL esterase/lipase EXL1-like, and putative copia-like retrotransposon protein homologue (**Table 5**).

Common Upregulated Genes Shared by MFA-Treated Trees

There were 403 genes directly influenced by MFA, following the Venn analysis of intersecting genes between control vs. MFA and infected vs. MFA + infected (**Figure 3**). The genes uniquely responsive to the MFA treatment are highlighted here. Among the top upregulated genes in the two sample sets include Laccase-7-like which plays a role in lignin polymerization and anthocyanin degradation. The gene BAHD acyltransferase At5g47980-like was also upregulated in the two groups. BAHD acyltransferases are involved in the production of defense and anti-herbivory compounds. The blue copper protein-like gene, which is involved in redox reactions, was also highly upregulated in the two groups possibly reflective of the higher Cu concentrations in the MFA-treated trees.

Increased expression was recorded in several plant hormone response genes which may indicate the type of defense response induced by MFA. This included genes associated with ethylene concentration including ACC oxidase, 1-aminocyclopropane-1-carboxylate synthase 1-like, ethylene-responsive transcription factor 1A-like, and protein reversion-to-ethylene sensitivity1-like. Abscisic acid-associated genes were among the groups of upregulated genes and included CYSTM1 family protein A-like, exocyst complex component EXO70B1-like, zeaxanthin epoxidase, chloroplastic-like, and threonine dehydratase biosynthetic chloroplastic-like protein. There were also several indole-3-acetic acid (IAA)-related genes downregulated in the leaf tissue in response to MFA which may have indicated a reduction in IAA production in the trees. These included a IAA-amino acid hydrolase ILR1-like 6-like, probable indole-3-acetic acid-amido synthetase GH3.1-like, and a auxin-induced protein 22D-like.

Among the genes that were influenced, increased expression was observed in multiple PR genes such as PR2, PR4, and PR5; genes involved in the phenylpropanoid biosynthesis. These included shikimate O-hydroxycinnamoyltransferase-like, 4-coumarate–CoA ligase-like 10-like, and feruloyl CoA ortho-hydroxylase 1-like genes. Upregulated lignin-specific genes included caffeoyl-CoA O-methyltransferase-like, cinnamoyl-CoA reductase 1-like, and caffeic acid 3-O-methyltransferase-like genes.

A number of genes associated with oxidative responses were also increased in response to MFA. This includes ROS regulators such as peroxidases. Genes associated with respiratory burst oxidase homolog protein D-like, cinnamate 4-hydroxylase CYP73, and peroxisomal membrane protein PMP22-like were also

TABLE 4 | A sample of the differentially expressed genes in the control vs. MFA-treated groups.

Gene ID	Description	Fold change	*p*
Upregulated			
Cit.17838.1.S1_at	Uncharacterized LOC102619854	56.59	1.52E-05
Cit.3761.1.S1_x_at	Uncharacterized LOC102619665	39.39	5.42E-07
Cit.1441.1.S1_at	Acetyltransferase-like protein homologue (*Arabidopsis thaliana*)	33.12	3.13E-10
Cit.18037.1.S1_at	1-aminocyclopropane-1-carboxylate synthase 1-like	29.49	4E-11
Cit.2409.1.S1_s_at	laccase-7-like	22.38	1.4E-12
Cit.17291.1.S1_at	O-methyltransferase homologue (*Populus balsamifera subsp. trichocarpa x Populus deltoides*)	22.32	6.30E-09
Cit.17178.1.S1_x_at	Unknown	21.27	1.53E-07
Cit.3377.1.S1_at	Blue copper protein-like	20.96	6.6E-10
Cit.29411.1.S1_s_at	BAHD acyltransferase At5g47980-like	20.23	1.56E-10
Cit.7362.1.S1_at	Cytochrome P450 83B1-like	19.53	7.3E-10
Downregulated			
Cit.16432.1.S1_at	Hypothetical protein	−3.83	0.0002
Cit.9523.1.S1_s_at	Translocator protein homolog	−3.48	0.0339
Cit.3534.1.S1_s_at	Uncharacterized LOC102616771	−3.18	0.0153
Cit.21126.1.S1_s_at	Auxin-induced protein 22D-like	−3	5E-05
Cit.2093.1.S1_s_at	Expansin-A5-like	−2.66	0.0483
Cit.8231.1.S1_s_at	Purple acid phosphatase 8-like	−2.62	0.0022
Cit.29521.1.S1_x_at	Regulator of chromosome condensation-like protein homolog (*Arabidopsis thaliana*)	−2.6	0.0009
Cit.29521.1.S1_at	Regulator of chromosome condensation-like protein homolog (*Arabidopsis thaliana*)	−2.55	0.0014
Cit.38030.1.S1_at	Protein ECERIFERUM 1-like	−2.51	0.0006
Cit.17407.1.S1_at	Auxin-induced protein 22D-like	−2.46	6E-05

upregulated. Several transcriptional activators increased in response to MFA. These included WRKY transcriptional factors, myb-related proteins, NAC domain-containing proteins, scarecrow-like protein 14-like, and transcription factor RAX2-like. Genes associated with cell growth, cell remodeling, and cell structure were also upregulated. These included extensin, LOB domain-containing protein 11-like, receptor-like serine/threonine-protein kinase SD1-8-like, QWRF motif-containing protein 8-like and metalloendoproteinase 1-like, probable galacturonosyltransferase-like 10-like, early nodulin-93-like, and alkaline/neutral invertase CINV2-like.

Genes associated with alkaloid biosynthesis were also upregulated in response to MFA. These included cannabidiolic acid synthase-like 2-like, anthranilate synthase component I-1, chloroplastic-like, tropinone reductase-like 1-like anthranilate N-methyltransferase-like, taxadien-5-alpha-ol O-acetyltransferase-like, and codeine O-demethylase-like. Transport genes were among a series of upregulated genes in the citrus trees in response to MFA. These are involved with ABC transporters and iron transport. Other genes (**Supplementary File 1**) are possibly involved in brassinosteroid biosynthesis, anthocyanin synthesis, lipase activity, senescence, elicitor and wound responses, ubiquidation, SAR, homeostasis, amino acid synthesis, endopeptidase inhibition, and energy metabolism.

DISCUSSION

This study examined the impact of a microbial preparation, MFA, against HLB in young citrus trees. The study assessed four experimental groups: control, infected, MFA treated, and MFA treated + infected. The results presented here indicate that MFA increased the transcriptional activity of citrus defense mechanisms, elevated Cu concentrations in citrus leaf tissue, and stabilized HLB infection in treated plants (**Figure 1, Table 1**).

Following monthly treatments of MFA over the experimental period (**Figure 1**), there was a consistent increase in disease severity over time in infected trees which is consistent with previous observations (Li et al., 2018). A DI reduction of 13.3% in MFA-treated trees was observed at 20 months, but this infection rate did not significantly deviate from the untreated infected group (**Figure 1B**). Monitoring of the distribution of change in DI revealed that MFA, when all trees and infected trees were considered, resulted in significant stabilization of disease progression in the MFA-treated groups (**Table 1**). PR2 was significantly increased 2 h after MFA treatment (**Figure 2A**), and PAL was also significantly increased 6 h after treatment in response to MFA (**Figure 2B**). In addition to this, a transcriptomic assessment revealed an array of defense mechanisms that were upregulated in response to MFA. The previous work examined the impact of plant defense elicitors on HLB in a field evaluation. Li et al. (2015a) and Li et al. (2018) found a consistent reduction in disease severity when β-aminobutyric acid (BABA), benzothiadiazole (BTH), ascorbic acid (AA), and salicylic acid (SA) were applied to citrus. Induction of PR2 was observed after BABA and BTH applications, suggesting its implication in the defense against HLB.

The significant increases in Cu concentrations of citrus leaves following treatment with MFA (**Table 2**) observed in this study can be attributed to the Cu in the application which significantly increased the mineral in healthy and infected trees to 32.4 and 26.8 ppm, respectively. Copper nutrition is critical in citrus development. Its deficiency is commonly associated with rapid growth in non-bearing trees following periods of high nitrogen fertilizer usage, and this leads to distorted leaf and twig growth and visual leaf chlorosis (Yruela,

TABLE 5 | A sample of the differentially expressed genes in the infected vs. MFA + infected groups.

Gene ID	Description	Fold change	*p*
Upregulated			
Cit.2409.1.S1_s_at	Laccase-7-like	43.29	4.46E-14
Cit.1441.1.S1_at	Unknown	43.23	1.43E-10
Cit.26572.1.S1_at	Uncharacterized LOC102607820	37.15	2.50E-08
Cit.3761.1.S1_x_at	Uncharacterized LOC102619665	32.54	3.29E-07
Cit.18037.1.S1_at	1-aminocyclopropane-1-carboxylate synthase 1-like	31.54	2.58E-11
Cit.29411.1.S1_s_at	BAHD acyltransferase At5g47980-like	27.46	4.49E-11
Cit.26572.1.S1_s_at	Uncharacterized LOC102607820	24.17	9.71E-09
Cit.17178.1.S1_x_at	Unknown	22.58	1.72E-07
Cit.3377.1.S1_at	Blue copper protein-like	21.58	3.80E-10
Cit.17838.1.S1_at	Uncharacterized LOC102619854	21.44	9.41E-05
Downregulated			
Cit.35493.1.S1_s_at	Uncharacterized LOC102612783	−11.1	0.0364
Cit.21179.1.S1_at	Chalcone synthase 2 homologue (*Citrus sinensis*)	−7.53	0.0003
Cit.8600.1.S1_x_at	Chalcone synthase 2 homologue (*Citrus sinensis*)	−5.22	0.0007
Cit.19520.1.S1_s_at	Chalcone synthase 2-like	−4.7	0.001
Cit.38030.1.S1_at	Protein ECERIFERUM 1-like	−4.5	3.57E-05
Cit.30458.1.S1_s_at	Chalcone synthase 2-like	−3.97	0.0016
Cit.19520.1.S1_x_at	Chalcone synthase 2-like	−3.89	0.0014
Cit.34812.1.S1_s_at	Glycine-rich cell wall structural protein 1-like	−3.8	0.0052
Cit.39287.1.S1_s_at	GDSL esterase/lipase EXL1-like	−3.7	0.0037
Cit.27421.1.S1_at	Putative copia-like retrotransposon protein homologue (*Oryza sativa*)	−3.52	0.0009

2009; Hippler et al., 2017). Cu is poorly mobile in the phloem. Its application is recommended during periods of new vegetative growth (Marschner, 2012; Hippler et al., 2017) and should be regularly applied as foliar and ground fertilizer (Hippler et al., 2018). Cu is an important cofactor for many enzymes such as superoxide dismutase, amino oxidase, laccase, blue copper protein, and plastocyanin, but it also plays an important role for the transcription of protein trafficking machinery and oxidative phosphorylation (Yruela, 2005, 2009). Applications that increase Cu uptake in citrus could therefore be deemed valuable for agronomic purposes. Cu as a phytosanitary application has been used in the control of pathogens for many years (Russell, 2005; Hippler et al., 2017) and is considered a potent antimicrobial element (Vincent et al., 2018). The Cu portion of MFA may have contributed to the stabilization of HLB DI. In an investigation into the impact of micronutrients on HLB in *C. sinensis*, Da Silva et al. (2020) examined the use of copper hydroxide fertilizer on HLB in citrus. These authors reported that although leaf Cu concentrations reached 20 ppm, there was no significant impact on HLB concentrations. The authors also reported that individual Cu fertilizer treatments helped mitigate the impact of HLB on starch metabolism a fundamental issue in trees infected with the disease. For this reason, MFA could potentially play a role in alleviating HLB symptoms by delivering higher Cu concentrations in infected citrus trees. However, the added elicitation of defense responses by MFA may have contributed to stabilization of disease progression. A previous investigation which compared $CuSO_4$, MFA without $CuSO_4$ and MFA reported that MFA had a significant impact on the induction of defense-related genes and on the control of powdery mildew in wheat (Twamley et al., 2019). The evidence presented suggests that MFA as a combined formulation (fermentation media and $CuSO_4$) gave the greatest control of disease and was the most effective at priming defense-related responses. This observation was further supported when MFA demonstrated greater antifungal activity against *Zymoseptoria tritici* compared to individual treatments of $CuSO_4$ and MFA without $CuSO_4$ at reduced concentrations *in vitro* (Twamley et al., 2021). Twamley et al. (2021) also indicated that MFA-treated plants resulted in grain yield and quality improvements in healthy MFA-treated plants. The authors suggest that this could be a function of peptide or amino acid complexes that might have greater bioactive properties and that could help limit the oxidative damage caused by Cu in plants. This suggests that the microbial preparation with $CuSO_4$ (MFA) possibly responds better than $CuSO_4$ or the fermentation media in isolation. The formulation may have a unique synergistic mechanism as a combined product. This may suggest that in the current study, the total preparation is conferring the benefits observed in the data for citrus and not just the $CuSO_4$ or fermentation media in isolation. However, a more comprehensive study should be conducted to confirm this. Excessive Cu use will continue to be regulated against due to its negative environmental impact. Issues such as accumulation and the selection of Cu resistant pathogens in the natural environment are of primary concern (Lamichhane et al., 2018). Environmentally safe microbial preparations that can prime plant natural defenses may play a role in reducing the use of Cu as a phytosanitary application.

Transcriptomic analysis gives an insight into what cellular processes are dormant or active in response to either a disease, challenge, or a nutritional treatment. In the control vs. infected trees, there were several differentially expressed genes associated with HLB infection. In previous studies conducted in greenhouses, HLB infection significantly impacted between 604and 633 genes (245–589 upregulated and 22–350 downregulated; Kim et al., 2009; Mafra et al., 2013; Fu et al., 2016; Hu et al., 2017). In the present study, HLB infection impacted a total of 171 genes (150 upregulated and 21 downregulated), in a field infection model. The most common issues associated with HLB are alterations in transcriptional processes related to defense, oxidative stress, carbohydrate metabolism, cell structure and organization, transcription factors, hormone signaling, and phloem blockage (Kim et al., 2009; Albrecht and Bowman,

2012; Mafra et al., 2013; Martinelli et al., 2013; Fu et al., 2016; Hu et al., 2017). Each of these processes are believed to contribute to the rapid development of disease symptoms, ultimately leading to declining tree health and death. Similar patterns for many of the previously reported correlations (**Table 3** and **Supplementary File 1**) were observed in this study. Peroxidase, thaumatin-like protein, beta-galactosidase 1-like, hypersensitive-induced response protein 2-like, and elicitor-induced gene product homologue were upregulated in response to HLB infection. These are indicators of defense and oxidative stress-related responses in citrus and have previously been associated with HLB infection (Kim et al., 2009; Fu et al., 2016). Pathways associated with secondary metabolite biosynthesis were also upregulated, including multiple PAL genes, flavanone synthase genes, isoflavone 4′-O-methyltransferase-like gene, (E)-beta-farnesene synthase, and a trans-resveratrol di-O-methyltransferase-like gene. Phenylpropanoids are both associated with defense and the syntheses of flavonoids and terpenes which both play a role in the attraction of pollinating insects, defense against herbivories, and in the establishment of disease resistance. Previous studies have indicated that HLB impacts phenylpropanoid and terpene synthesis (Albrecht and Bowman, 2012; Fu et al., 2016; Hu et al., 2017).

Genes involved with carbohydrate metabolism and cell wall modification were also significantly impacted. Early nodulin, extensins, probable polygalacturonase, sucrose synthase, xyloglucan endotransglucosylase/hydrolase, cellulose synthase, and pectinesterase inhibitor were included in the group of upregulated genes responding to HLB infection in this study. The previous work has identified transcriptomic signatures that demonstrate the impact of HLB on carbohydrate metabolism (Fu et al., 2016, Hu et al., 2017) where expansins, xyloglucan endotransglucosylase/hydrolase proteins, cellulose synthesis, and pectinase-related genes were previously reported as differentially impacted in response to HLB. Genes involved in hormone signaling were also significantly impacted between control and HLB-infected trees; specifically, three gibberellin-regulated genes and a HVA22-like gene were upregulated in the HLB-infected tissue. Auxin-responsive protein, brassinosteroid-regulated gene, ethylene-induced esterase homologue, and an ethylene-responsive transcription factor were all downregulated. Phytohormones are believed to be impacted due to the cellular processes that are distorted as a result of changes in cell growth and defense responses. Zheng and Zhao (2013) saw similar changes in phytohormone production including auxin-, ethylene-, and gibberellin-related genes which may play a role in the mediation of citrus responses to HLB.

Many of the genes impacted following MFA treatment are associated with a strong localized and systemic defense responses. These included direct defense genes and numerous genes involved in the regulation of biotic defense responses. The defense stimulatory response may have supported the 13.3% reduction in DI (**Figure 1**). Disease progression was also significantly stabilized (**Table 1**) in MFA-treated trees. The transcriptome analysis revealed an increase in many direct defense-related enzymes but also a series of pathways involved in secondary metabolite biosynthesis and the production of antimicrobial compounds (**Tables 4** and **5**, and **Supplementary File 1**). Microbial elicitors have been successful in the past in the induction of resistance to bacterial, fungal, and oomycete pathogens (Thakur and Sohal, 2013). MFA contains both bacterial and yeast fermentation media, and both components may play a role in initiating gene transcription responses and have benefited plants in the past (Wiesel et al., 2014). The application of a yeast suspension to Arabidopsis saw the development of resistance to both *Pseudomonas syringae* and *Botrytis cinerea* infections (Raacke et al., 2006). The study also uncovered the ability of the yeast application to stimulate the expression of several plant defense systems including SAR, detoxification, and the jasmonate/ethylene pathways (Raacke et al., 2006). Yeast cell wall extracts are also well-documented inducers of plant defense, observed to regulate plant stomatal closure and mediate ROS responses following their use in various plant models (Khokon et al., 2010; Wiesel et al., 2014). A study that investigated ROS generation in rice in response to a N-acetylchitooligosaccharide demonstrated its role in plant defense elicitation (Kuchitsu et al., 1995). In Arabidopsis, chitin elicitors also increased ROS generation while contributing to both fungal and bacterial suppression (Egusa et al., 2015). The benefits of bacterial derived elicitors for plants have also been reported. They trigger induced systemic resistance (ISR) in plants and have other secondary benefits to plant health (Choi and Klessig, 2016; Ek-Ramos et al., 2019). ISR is understood to be important in cell wall thickening or destruction of infected cells, which helps cut off nutrients and access to invading pathogens. This has been effective against a range of plant pathogens in greenhouse and field settings (Lugtenberg et al., 2002; Aloo et al., 2019).

Phenylpropanoids produce an array of secondary metabolites derived from intermediates of the shikimate pathway (Fraser and Chapple, 2011). They contribute to a plant's response to biotic and abiotic stimuli. PAL catalyzes the non-oxidative deamination of phenylalanine to trans-cinnamate and directs carbon flow from the shikimate pathway to general phenylpropanoid biosynthesis (Vogt, 2010). Phenylpropanoids are also understood to be involved in a plants overall defense strategy. They form preformed defenses, inducible defense responses, physical barriers and act as signaling molecules (Dixon et al., 2002). They are also well documented in plants in response to pathogens and in the development of resistance to disease. This data provides evidence that MFA may result in the beneficial upregulation of the phenylpropanoid pathways, and several phenylalanine ammonia-lyase-like genes were upregulated and complimented with shikimate O-hydroxycinnamoyltransferase-like, 4-coumarate--CoA ligase-like, and feruloyl CoA ortho-hydroxylase. There were significant increases in the lignin synthetic genes including caffeoyl-CoA O-methyltransferase-like, cinnamoyl-CoA reductase 1-like, and caffeic acid 3-O-methyltransferase-like which could be indicative of enhanced lignin formation. Laccase-7-like and blue copper protein was among the top 10 highest upregulated genes in healthy and infected trees where MFA was applied (**Tables 4** and **5**). Laccases are multi-copper enzymes that catalyze substrate oxidation and that reduce molecular oxygen to water. Laccases are also involved in Cu-facilitated lignification of cell walls

contributing to defense, structure, and rigidity (Janusz et al., 2020). Xu et al. (2019) indicated that citrus laccases respond to environmental stress and are involved in lignin synthesis, and Cu ions are bound in several sites in laccases by Type 1 blue copper proteins (Printz et al., 2016), making blue copper proteins essential in the formation and function of laccases. Based on the transcriptomic evidence provided in this study, MFA potentially may play a crucial role in the activation of the phenylpropanoid pathway and facilitates lignin formation in citrus cell walls.

In this study, several PR genes were upregulated by MFA, including chitinase, endochitinase, endo-1,3-beta-glucosidase, osmotin, peroxidases, and thaumatin-like proteins (PR2, PR3, PR5, PR8, and PR9). Plants produce several direct defense mechanisms when initially challenged by pathogens. The importance of PR gene expression in citrus biotic responses has previously been reported (Campos et al., 2007) and highlights their role in pathogen defense responses. PR gene expression was expected to be upregulated as the data generated in the initial RT-qPCR experiment revealed significant upregulation of PR2 prior to microarray transcriptomic analysis (**Figure 2**).

Plant hormones are known to be important in plant growth, development, and cell signaling. They are also understood to be crucial in plant defense responses (Bari and Jones, 2009). In this study, there were several differentially expressed genes involved with plant hormone synthesis and regulation in response to MFA. This included genes associated with IAA, ethylene, and abscisic acid. There were also a small number of genes associated with brassinosteroids, salicylic acid, and jasmonic acid. Ethylene is produced from methionine by ACC synthase (ACS) and ACC oxidase (ACO) from its precursor 1-aminocyclopropane-1-carboxylic acid (ACC). The results presented herein revealed that S-adenosylmethionine synthase-like genes ACC synthase and a homologue were upregulated in response to MFA. Two ACC oxidases and ACC oxidase homologues were upregulated in response to MFA. Ethylene-responsive transcription factor-like genes 1A (2), 1B (2), 5, and 113 were also upregulated in MFA-treated plants. These ethylene-responsive transcription factors bind to the GCC-box pathogenesis-related promoter responding to pathogens and increasing the expression of PR genes (Zhou et al., 1997; Fujimoto et al., 2000; Sakuma et al., 2002).

CONCLUSION

This work provides evidence that MFA when applied to infected and healthy citrus trees increases Cu concentration, stabilizes HLB disease progression, and increases the expression of defense-related genes 2 h after its application in a field setting. Transcriptomic assessment revealed that MFA increased the expression of 565 genes in healthy citrus trees and 909 genes in HLB-infected trees. This included traits associated with plant growth, development, and defense. There are very few successful applications that can be integrated into citrus production systems to help manage HLB. Provided herein are promising data suggesting a microbial preparation may help slow the progression of HLB in a field scenario. Further work is required to determine the mode of action of the application. Due to the limits in phytosanitary use of Cu, future work will address whether the efficacy of $CuSO_4$ contained in MFA is enhanced by its microbe-derived fraction, thus allowing for a reduced Cu input in the environment. Work will also aim to determine the impact of MFA on mature HLB-infected citrus trees in multiyear studies. MFA may also play a role in the management of other problematic pathogens; future research will aim to determine whether MFA has a broader application in agronomy.

DATA AVAILABILITY STATEMENT

The original contributions presented in the study are publicly available. This data can be found here: ArrayExpress accession E-MTAB-10919.

AUTHOR CONTRIBUTIONS

RL, KDo, SB, and KDa designed set up and managed the experiment and its logistics. RL, KDo, UC, WS, and ED applied treatments, sampled the trial, and prepared the samples for mineral and qPCR analysis. RL, KDo, and KE prepared and ran the transcriptomic samples. RL, RM, SB, KH, and KDa managed and supported the overall study. RL, KH, and KDa prepared and wrote the manuscript. All authors contributed to the interpretation of the data prior to preparing the manuscript. All authors contributed to the article and approved the submitted version.

FUNDING

This work was funded in full by Alltech and Alltech Crop Science. Alltech provided the research facilities and financial support for this work.

ACKNOWLEDGMENTS

The authors would also like to acknowledge Dr. Pearse Lyons for his personal and financial contribution to this project. His passion for research and a wiliness to address the global citrus greening problem led to the initiation of this work. This paper is dedicated to the memory of him.

SUPPLEMENTARY MATERIAL

The Supplementary Material for this article can be found online at: https://www.frontiersin.org/articles/10.3389/fpls.2021.754391/full#supplementary-material

REFERENCES

Albrecht, U., and Bowman, K. D. (2012). Transcriptional response of susceptible and tolerant citrus to infection with *Candidatus Liberibacter* asiaticus. *Plant Sci.* 185–186, 118–130. doi: 10.1016/j.plantsci.2011.09.008

Alexander, D., Goodman, R. M., Gut-Rella, M., Glascock, C., Weymann, K., Friedrich, L., et al. (1993). Increased tolerance to two oomycete pathogens in transgenic tobacco expressing pathogenesis-related protein 1a. *Proc. Natl. Acad. Sci. U. S. A.* 90, 7327–7331. doi: 10.1073/pnas.90.15.7327

Aloo, B. N., Makumba, B. A., and Mbega, E. R. (2019). The potential of *Bacilli rhizobacteria* for sustainable crop production and environmental sustainability. *Microbiol. Res.* 219, 26–39. doi: 10.1016/j.micres.2018.10.011

Bari, R., and Jones, J. D. (2009). Role of plant hormones in plant defence responses. *Plant Mol. Biol.* 69, 473–488. doi: 10.1007/s11103-008-9435-0

Bové, J. M. (2006). Huanglongbing: a destructive, newly-emerging, century-old disease of citrus. *J. Plant Pathol.* 88, 7–37. doi: 10.4454/jpp.v88i1.828

Campos, M. A., Rosa, D. D., Teixeira, J. É. C., Targon, M. L. P. N., Souza, A. A., Paiva, L. V., et al. (2007). PR gene families of citrus: their organ specific-biotic and abiotic inducible expression profiles based on ESTs approach. *Genet. Mol. Biol.* 30, 917–930. doi: 10.1590/S1415-47572007000500020

Chen, T., Duan, L., Zhou, B., Yu, H., Zhu, H., Cao, Y., et al. (2017). Interplay of pathogen-induced defense responses and symbiotic establishment in *Medicago truncatula*. *Front. Microbiol.* 8:973. doi: 10.3389/fmicb.2017.00973

Choi, H. W., and Klessig, D. F. (2016). DAMPs, MAMPs, and NAMPs in plant innate immunity. *BMC Plant Biol.* 16:232. doi: 10.1186/s12870-016-0921-2

Da Silva, J. R., De Alvarenga, F. V., Boaretto, R. M., Lopes, J. R. S., Quaggio, J. A., Coletta Filho, H. D., et al. (2020). Following the effects of micronutrient supply in HLB-infected trees: plant responses and '*Candidatus Liberibacter* asiaticus' acquisition by the Asian citrus psyllid. *Trop. Plant Pathol.* 45, 597–610. doi: 10.1007/s40858-020-00370-9

Dala-Paula, B. M., Plotto, A., Bai, J., Manthey, J. A., Baldwin, E. A., Ferrarezi, R. S., et al. (2019). Effect of Huanglongbing or greening disease on Orange juice quality, a review. *Front. Plant Sci.* 9:1976. doi: 10.3389/fpls.2018.01976

Das, A. K., Nerkar, S., Bawage, S., and Kumar, A. (2014). Current distribution of Huanglongbing (citrus greening disease) in India as diagnosed by real-time PCR. *J. Phytopathol.* 162, 402–406. doi: 10.1111/jph.12195

Davis, R. I., Jacobson, S. C., Rahamma, S., and Gunua, T. G. (2000). Surveillance for citrus huanglongbing (greening) disease in New Guinea and North Queensland. *Australas. Plant Pathol.* 29:226. doi: 10.1071/AP00043

Dixon, R. A., Achnine, L., Kota, P., Liu, C.-J., Reddy, M. S. S., and Wang, L. (2002). The phenylpropanoid pathway and plant defence—a genomics perspective. *Mol. Plant Pathol.* 3, 371–390. doi: 10.1046/j.1364-3703.2002.00131.x

Duan, Y., Zhou, L., Hall, D. G., Li, W., Doddapaneni, H., Lin, H., et al. (2009). Complete genome sequence of citrus huanglongbing bacterium, '*Candidatus Liberibacter* asiaticus' obtained through metagenomics. *Mol. Plant-Microbe Interact.* 22, 1011–1020. doi: 10.1094/MPMI-22-8-1011

Dutt, M., Barthe, G., Irey, M., and Grosser, J. (2015). Transgenic citrus expressing an Arabidopsis NPR1 gene exhibit enhanced resistance against huanglongbing (HLB; citrus greening). *PLoS One* 10:e0137134. doi: 10.1371/journal.pone.0137134

Egusa, M., Matsui, H., Urakami, T., Okuda, S., Ifuku, S., Nakagami, H., et al. (2015). Chitin nanofiber elucidates the elicitor activity of polymeric chitin in plants. *Front. Plant Sci.* 6:1098. doi: 10.3389/fpls.2015.01098

Ek-Ramos, M. J., Gomez-Flores, R., Orozco-Flores, A. A., Rodríguez-Padilla, C., González-Ochoa, G., and Tamez-Guerra, P. (2019). Bioactive products From plant-Endophytic gram-positive bacteria. *Front. Microbiol.* 10:463. doi: 10.3389/fmicb.2019.00463

Fraser, C. M., and Chapple, C. (2011). The phenylpropanoid pathway in *Arabidopsis*. *Arabidopsis Book* 9:e0152. doi: 10.1199/tab.0152

Fu, S., Shao, J., Zhou, C., and Hartung, J. S. (2016). Transcriptome analysis of sweet orange trees infected with '*Candidatus Liberibacter* asiaticus' and two strains of *citrus tristeza* virus. *BMC Genomics* 17:349. doi: 10.1186/s12864-016-2663-9

Fujimoto, S. Y., Ohta, M., Usui, A., Shinshi, H., and Ohme-Takagi, M. (2000). Arabidopsis ethylene-responsive element binding factors act as transcriptional activators or repressors of GCC box-mediated gene expression. *Plant Cell* 12, 393–404. doi: 10.1105/tpc.12.3.393

Gardner, C. L., Da Silva, D. R., Pagliai, F. A., Pan, L., Padgett-Pagliai, K. A., Blaustein, R. A., et al. (2020). Assessment of unconventional antimicrobial compounds for the control of '*Candidatus Liberibacter* asiaticus', the causative agent of citrus greening disease. *Sci. Rep.* 10:5395. doi: 10.1038/s41598-020-62246-x

Hansen, T. H., De Bang, T. C., Laursen, K. H., Pedas, P., Husted, S., and Schjoerring, J. K. (2013). "Multielement plant tissue analysis using ICP spectrometry," in *Plant Mineral Nutrients: Methods and Protocols*. ed. F. J. M. Maathuis (Totowa, NJ: Humana Press).

Hansen, A. K., Trumble, J. T., Stouthamer, R., and Paine, T. D. (2008). A new Huanglongbing species, "*Candidatus Liberibacter* psyllaurous," found to infect tomato and potato, is vectored by the psyllid *Bactericera cockerelli* (Sulc). *Appl. Environ. Microbiol.* 74, 5862–5865. doi: 10.1128/AEM.01268-08

Hippler, F. W. R., Boaretto, R. M., Quaggio, J. A., and Mattos Júnior, D. (2017). Copper in citrus production: required but avoided. *Citrus Res. Technol.* 38, 99–106. doi: 10.4322/crt.ICC067

Hippler, F. W. R., Boaretto, R. M., Teixeira, L. A. J., Quaggio, J. A., and Mattos-Jr, D. D. (2018). Copper supply and fruit yield of young citrus trees: fertiliser sources and application methods. *Bragantia* 77, 365–371. doi: 10.1590/1678-4499.2017125

Hu, Y., Zhong, X., Liu, X., Lou, B., Zhou, C., and Wang, X. (2017). Comparative transcriptome analysis unveils the tolerance mechanisms of *Citrus hystrix* in response to '*Candidatus Liberibacter* asiaticus' infection. *PLoS One* 12:e0189229. doi: 10.1371/journal.pone.0189229

Jagoueix, S., Bové, J. M., and Garnier, M. (1996). PCR detection of the two 'Candidatus' Liberobacter species associated with greening disease of citrus. *Mol. Cell. Probes* 10, 43–50. doi: 10.1006/mcpr.1996.0006

Jain, M., Fleites, L. A., and Gabriel, D. W. (2015). Prophage-encoded peroxidase in '*Candidatus Liberibacter* asiaticus' is a secreted effector that suppresses plant defenses. *Mol. Plant-Microbe Interact.* 28, 1330–1337. doi: 10.1094/MPMI-07-15-0145-R

Jain, M., Munoz-Bodnar, A., Zhang, S., and Gabriel, D. W. (2018). A secreted '*Candidatus Liberibacter* asiaticus' peroxiredoxin simultaneously suppresses both localized and systemic innate immune responses in planta. *Mol. Plant-Microbe Interact.* 31, 1312–1322. doi: 10.1094/MPMI-03-18-0068-R

Janusz, G., Pawlik, A., Świderska-Burek, U., Polak, J., Sulej, J., Jarosz-Wilkołazka, A., et al. (2020). Laccase properties, physiological functions, and evolution. *Int. J. Mol. Sci.* 21:966. doi: 10.3390/ijms21030966

Jirage, D., Tootle, T. L., Reuber, T. L., Frost, L. N., Feys, B. J., Parker, J. E., et al. (1999). *Arabidopsis thaliana* PAD4 encodes a lipase-like gene that is important for salicylic acid signaling. *Proc. Natl. Acad. Sci. U. S. A.* 96, 13583–13588. doi: 10.1073/pnas.96.23.13583

Kawano, T. (2003). Roles of the reactive oxygen species-generating peroxidase reactions in plant defense and growth induction. *Plant Cell Rep.* 21, 829–837. doi: 10.1007/s00299-003-0591-z

Khokon, M. A., Hossain, M. A., Munemasa, S., Uraji, M., Nakamura, Y., Mori, I. C., et al. (2010). Yeast elicitor-induced stomatal closure and peroxidase-mediated ROS production in Arabidopsis. *Plant Cell Physiol.* 51, 1915–1921. doi: 10.1093/pcp/pcq145

Kim, J. S., Sagaram, U. S., Burns, J. K., Li, J. L., and Wang, N. (2009). Response of sweet orange (*Citrus sinensis*) to '*Candidatus Liberibacter* asiaticus' infection: microscopy and microarray analyses. *Phytopathology* 99, 50–57. doi: 10.1094/PHYTO-99-1-0050

Kuchitsu, K., Kosaka, H., Shiga, T., and Shibuya, N. (1995). EPR evidence for generation of hydroxyl radical triggered by N-acetylchitooligosaccharide elicitor and a protein phosphatase inhibitor in suspension-cultured rice cells. *Protoplasma* 188, 138–142. doi: 10.1007/BF01276805

Lamichhane, J. R., Osdaghi, E., Behlau, F., Köhl, J., Jones, J. B., and Aubertot, J.-N. (2018). Thirteen decades of antimicrobial copper compounds applied in agriculture. A review. *Agron. Sustain. Dev.* 38:28. doi: 10.1007/s13593-018-0503-9

Li, X.-Y., Gao, L., Zhang, W.-H., Liu, J.-K., Zhang, Y.-J., Wang, H.-Y., et al. (2015b). Characteristic expression of wheat PR5 gene in response to infection by the leaf rust pathogen, *Puccinia triticina*. *J. Plant Interact.* 10, 132–141. doi: 10.1080/17429145.2015.1036140

Li, W., Hartung, J. S., and Levy, L. (2006). Quantitative real-time PCR for detection and identification of *Candidatus Liberibacter* species associated with citrus huanglongbing. *J. Microbiol. Methods* 66, 104–115. doi: 10.1016/j.mimet.2005.10.018

Li, J., Li, L., Pang, Z., Kolbasov, V. G., Ehsani, R., Carter, E. W., et al. (2018). Developing citrus Huanglongbing (HLB) management strategies based on the severity of symptoms in HLB-endemic citrus-producing regions. *Phytopathology* 109, 582–592. doi: 10.1094/PHYTO-08-18-0287-R

Li, J., Pang, Z., Trivedi, P., Zhou, X., Ying, X., Jia, H., et al. (2017). '*Candidatus Liberibacter* asiaticus' encodes a functional salicylic acid (SA) hydroxylase that degrades SA to suppress plant defenses. *Mol. Plant-Microbe Interact.* 30, 620–630. doi: 10.1094/MPMI-12-16-0257-R

Li, J., Trivedi, P., and Wang, N. (2015a). Field evaluation of plant defense inducers for the control of citrus Huanglongbing. *Phytopathology* 106, 37–46. doi: 10.1094/PHYTO-08-15-0196-R

Lugtenberg, B. J. J., Chin-A-Woeng, T. F. C., and Bloemberg, G. V. (2002). Microbe–plant interactions: principles and mechanisms. *Antonie Van Leeuwenhoek* 81, 373–383. doi: 10.1023/A:1020596903142

Mafra, V., Martins, P. K., Francisco, C. S., Ribeiro-Alves, M., Freitas-Astúa, J., and Machado, M. A. (2013). *Candidatus Liberibacter* americanus induces significant reprogramming of the transcriptome of the susceptible citrus genotype. *BMC Genomics* 14:247. doi: 10.1186/1471-2164-14-247

Marschner, H. (2012). "Marschner's mineral nutrition of higher plants" in *Marschner's Mineral Nutrition of Higher Plants*. *3rd edn*. P. Marschner. (San Diego: Academic Press).

Martinelli, F., Reagan, R. L., Uratsu, S. L., Phu, M. L., Albrecht, U., Zhao, W., et al. (2013). Gene regulatory networks elucidating huanglongbing disease mechanisms. *PLoS One* 8:e74256. doi: 10.1371/journal.pone.0074256

Millenaar, F. F., Okyere, J., May, S. T., Van Zanten, M., Voesenek, L. A. C. J., and Peeters, A. J. M. (2006). How to decide? Different methods of calculating gene expression from short oligonucleotide array data will give different results. *BMC Bioinformatics* 7:137. doi: 10.1186/1471-2105-7-137

Montesano, M., Brader, G., and Palva, E. T. (2003). Pathogen derived elicitors: searching for receptors in plants. *Mol. Plant Pathol.* 4, 73–79. doi: 10.1046/j.1364-3703.2003.00150.x

Nwugo, C. C., Duan, Y., and Lin, H. (2013). Study on citrus response to Huanglongbing highlights a down-regulation of defense-related proteins in lemon plants Upon 'Ca Liberibacter asiaticus' infection. *PLoS One* 8:e67442. doi: 10.1371/journal.pone.0067442

Oliveros, J. C. (2007–2015). Venny. An interactive tool for comparing lists with Venn's diagrams [online]. Available at: https://bioinfogp.cnb.csic.es/tools/venny/index.html (Accessed April 12, 2021).

Printz, B., Lutts, S., Hausman, J.-F., and Sergeant, K. (2016). Copper trafficking in plants and its implication on cell wall dynamics. *Front. Plant Sci.* 7:601. doi: 10.3389/fpls.2016.00601

Raacke, I. C., Von Rad, U., Mueller, M. J., and Berger, S. (2006). Yeast increases resistance in Arabidopsis against *Pseudomonas syringae* and *Botrytis cinerea* by salicylic acid-dependent as well as -independent mechanisms. *Mol. Plant-Microbe Interact.* 19, 1138–1146. doi: 10.1094/MPMI-19-1138

R-Core-Team (2020). R: A language and environment for statistical computing. R Foundation for Statistical Computing.

Russell, P. E. (2005). A century of fungicide evolution. *J. Agric. Sci.* 143, 11–25. doi: 10.1017/S0021859605004971

Ryals, J. A., Neuenschwander, U. H., Willits, M. G., Molina, A., Steiner, H. Y., and Hunt, M. D. (1996). Systemic acquired resistance. *Plant Cell* 8, 1809–1819.

Sakuma, Y., Liu, Q., Dubouzet, J. G., Abe, H., Shinozaki, K., and Yamaguchi-Shinozaki, K. (2002). DNA-binding specificity of the ERF/AP2 domain of *Arabidopsis* DREBs, transcription factors involved in dehydration- and cold-inducible gene expression. *Biochem. Biophys. Res. Commun.* 290, 998–1009. doi: 10.1006/bbrc.2001.6299

Schmittgen, T. D., and Livak, K. J. (2008). Analyzing real-time PCR data by the comparative CT method. *Nat. Protoc.* 3, 1101–1108. doi: 10.1038/nprot.2008.73

Schulman, P., Ribeiro, T. H. C., Fokar, M., Chalfun-Junior, A., Lally, R. D., Paré, P. W., et al. (2021). A microbial fermentation product induces defense-related transcriptional changes and the accumulation of phenolic compounds in Glycine max. *Phytopathology*. doi: 10.1094/PHYTO-06-21-0227-R

Singerman, A., and Rogers, M. E. (2020). The economic challenges of dealing with citrus greening: the case of Florida. *J. Integr. Pest Manag.* 11. doi: 10.1093/jipm/pmz037

Thakur, M., and Sohal, B. S. (2013). Role of elicitors in inducing resistance in plants against pathogen infection: A review. *ISRN Biochem.* 2013:762412. doi: 10.1155/2013/762412

Twamley, T., Gaffney, M., and Feechan, A. (2019). A microbial fermentation mixture primes for resistance against powdery mildew in wheat. *Front. Plant Sci.* 10:1241. doi: 10.3389/fpls.2019.01241

Twamley, T., Gaffney, M., and Feechan, A. (2021). A microbial fermentation mixture reduces Fusarium head blight and promotes grain weight but does not impact *Septoria tritici* blotch. *Eur. J. Plant Pathol.* doi: 10.1007/s10658-021-02396-4

Vincent, M., Duval, R. E., Hartemann, P., and Engels-Deutsch, M. (2018). Contact killing and antimicrobial properties of copper. *J. Appl. Microbiol.* 124, 1032–1046. doi: 10.1111/jam.13681

Vogt, T. (2010). Phenylpropanoid biosynthesis. *Mol. Plant* 3, 2–20. doi: 10.1093/mp/ssp106

Wiesel, L., Newton, A. C., Elliott, I., Booty, D., Gilroy, E. M., Birch, P. R. J., et al. (2014). Molecular effects of resistance elicitors from biological origin and their potential for crop protection. *Front. Plant Sci.* 5:655. doi: 10.3389/fpls.2014.00655

Xu, X., Zhou, Y., Wang, B., Ding, L., Wang, Y., Luo, L., et al. (2019). Genome-wide identification and characterization of laccase gene family in *Citrus sinensis*. *Gene* 689, 114–123. doi: 10.1016/j.gene.2018.12.015

Yang, C., Powell, C. A., Duan, Y., Shatters, R., Fang, J., and Zhang, M. (2016). Deciphering the bacterial microbiome in Huanglongbing-affected citrus treated with thermotherapy and sulfonamide antibiotics. *PLoS One* 11:e0155472. doi: 10.1371/journal.pone.0155472

Yruela, I. (2005). Copper in plants. *Braz. J. Plant Physiol.* 17, 145–156. doi: 10.1590/S1677-04202005000100012

Yruela, I. (2009). Copper in plants: acquisition, transport and interactions. *Funct. Plant Biol.* 36, 409–430. doi: 10.1071/FP08288

Zhang, Y., Fan, W., Kinkema, M., Li, X., and Dong, X. (1999). Interaction of NPR1 with basic leucine zipper protein transcription factors that bind sequences required for salicylic acid induction of the PR-1 gene. *Proc. Natl. Acad. Sci. U. S. A.* 96, 6523–6528. doi: 10.1073/pnas.96.11.6523

Zheng, Z.-L., and Zhao, Y. (2013). Transcriptome comparison and gene coexpression network analysis provide a systems view of citrus response to '*Candidatus Liberibacter* asiaticus' infection. *BMC Genomics* 14:27. doi: 10.1186/1471-2164-14-27

Zhou, J., Tang, X., and Martin, G. B. (1997). The Pto kinase conferring resistance to tomato bacterial speck disease interacts with proteins that bind a cis-element of pathogenesis-related genes. *EMBO J.* 16, 3207–3218. doi: 10.1093/emboj/16.11.3207

Conflict of Interest: All the authors were paid employees of Alltech during their contributions to this project. Alltech innovate and manufacture crop input products for the agronomic industry.

Publisher's Note: All claims expressed in this article are solely those of the authors and do not necessarily represent those of their affiliated organizations, or those of the publisher, the editors and the reviewers. Any product that may be evaluated in this article, or claim that may be made by its manufacturer, is not guaranteed or endorsed by the publisher.

frontiers | Frontiers in Plant Science

ORIGINAL RESEARCH
published: 20 May 2022
doi: 10.3389/fpls.2022.893858

Arabinogalactan Protein-Like Proteins From *Ulva lactuca* Activate Immune Responses and Plant Resistance in an Oilseed Crop

Tereza Přerovská[1], Barbora Jindřichová[2], Svatopluk Henke[3], Jean-Claude Yvin[4], Vincent Ferrieres[1], Lenka Burketová[2], Petra Lipovová[3†] and Eric Nguema-Ona[4†]*

[1]Ecole Nationale Supérieure de Chimie de Rennes, CNRS, ISCR-UMR 6226, Univ Rennes, Rennes, France, [2]Laboratory of Pathological Plant Physiology, Institute of Experimental Botany of the Czech Academy of Sciences, Prague, Czechia, [3]Department of Biochemistry and Microbiology, University of Chemistry and Technology Prague, Prague, Czechia, [4]Agro Innovation International TIMAC AGRO, Laboratoire de Nutrition Végétale, Pôle Stress Biotique, Saint Malo, France

OPEN ACCESS

Edited by:
Brigitte Mauch-Mani,
Université de Neuchâtel, Switzerland

Reviewed by:
Edita Tylová,
Charles University, Czechia
Birgit Classen,
University of Kiel, Germany
Ning Zhang,
Boyce Thompson Institute (BTI), United States

***Correspondence:**
Eric Nguema-Ona
Eric.NguemaOna@roullier.com

[†]These authors have contributed equally to this work and share last authorship

Specialty section:
This article was submitted to Plant Pathogen Interactions, a section of the journal Frontiers in Plant Science

Received: 10 March 2022
Accepted: 22 April 2022
Published: 20 May 2022

Citation:
Přerovská T, Jindřichová B, Henke S, Yvin J-C, Ferrieres V, Burketová L, Lipovová P and Nguema-Ona E (2022) Arabinogalactan Protein-Like Proteins From Ulva lactuca Activate Immune Responses and Plant Resistance in an Oilseed Crop. Front. Plant Sci. 13:893858. doi: 10.3389/fpls.2022.893858

Natural compounds isolated from macroalgae are promising, ecofriendly, and multifunctional bioinoculants, which have been tested and used in agriculture. Ulvans, for instance, one of the major polysaccharides present in *Ulva* spp. cell walls, have been tested for their plant growth-promoting properties as well as their ability to activate plant immune defense, on a large variety of crops. Recently, we have characterized for the first time an arabinogalactan protein-like (AGP-like) from *Ulva lactuca*, which exhibits several features associated to land plant AGPs. In land plant, AGPs were shown to play a role in several plant biological functions, including cell morphogenesis, reproduction, and plant-microbe interactions. Thus, isolated AGP-like proteins may be good candidates for either the plant growth-promoting properties or the activation of plant immune defense. Here, we have isolated an AGP-like enriched fraction from *Ulva lactuca* and we have evaluated its ability to (i) protect oilseed rape (*Brassica napus*) cotyledons against *Leptosphaeria maculans*, and (ii) its ability to activate immune responses. Preventive application of the *Ulva* AGP-like enriched fraction on oilseed rape, followed by cotyledon inoculation with the fungal hemibiotroph *L. maculans*, resulted in a major reduction of infection propagation. The noticed reduction correlated with an accumulation of H_2O_2 in treated cotyledons and with the activation of SA and ET signaling pathways in oilseed rape cotyledons. In parallel, an ulvan was also isolated from *Ulva lactuca*. Preventive application of ulvan also enhanced plant resistance against *L. maculans*. Surprisingly, reduction of infection severity was only observed at high concentration of ulvan. Here, no such significant changes in gene expression and H_2O_2 production were observed. Together, this study indicates that *U. lactuca* AGP-like glycoproteins exhibit promising elicitor activity and that plant eliciting properties of *Ulva* extract, might result not only from an ulvan-originated eliciting activities, but also AGP-like originated.

Keywords: Arabinogalactan proteins, plant defense, elicitor, hemibiotrophic fungus, plant immunity, *Ulva lactuca*

INTRODUCTION

The whole agricultural sector is facing the forthcoming challenges to keep up productivity with a growing global population (Ray et al., 2013). Nowadays, high and continuous agricultural productivity is dependent on the use of chemical fertilizers and pesticides. Nevertheless, the excessive use of these compounds has adverse effects on human health and the environment (Carvalho, 2006). The recent progress in the use of either natural plant growth-promoting substances or microorganisms (also termed plant biostimulants) has allowed a reduction and optimized use of fertilizers. This combination of mineral nutrients and biostimulants allows a better nutrient use efficiency, a better crop tolerance against abiotic stresses, and indirectly, a better quality and an improved yield of the crops (Rouphael and Colla, 2020; du Jardin et al., 2020). Likewise, microorganisms/organisms or natural substances were also tested and used in agriculture as agents able to interfere by different means with the occurrence of plant diseases caused by pathogens. Natural substances encompass various types of biomolecules, which can be extracted from a vast number of plant species. Among these natural substances, plant elicitors are described as substances able to activate plant immune system, and further, to protect crop against various kind of pathogens and parasites both in conventional and organic agriculture (Wiesel et al., 2014; Jamiolkowska, 2020).

Plants have indeed developed an efficient immune system described in the zig-zag model from Jones and Dangl (2006), which can be triggered *via* (i) the perception of plant elicitors or pathogen/microbial/damage-associated molecular patterns (P/M/DAMPs) also known as pathogen-associated molecular pattern PAMP-triggered immunity (PTI) or (ii) specific pathogens' effectors (effector-triggered immunity, ETI; Jones and Dangl, 2006). In field conditions, the mobilization of PTI by plant defence elicitors could lead to a pesticide reduction. In PTI, the recognition of plant elicitors by cell surface pattern-recognition receptors (PRRs) induces a series of early events, such as reactive oxygen species (ROS), nitric oxide production, and intracellular calcium influx. Then, intermediate events consist of activation of mitogen-activated protein kinases (MAPK) and phytohormone signaling (salicylic acid—SA, jasmonic acid—JA, and/or ethylene—ET; Bigeard et al., 2015). These signaling cascades trigger the induction of defense genes leading to the production of various defense-related compounds such as pathogensis-related (PR) proteins (Van Loon et al., 2006) or specialized antimicrobial compounds (Boller and Felix, 2009).

Many plant elicitors, also called PAMPs, which have been so far isolated and tested in both laboratory and field experiments, originated from microbes (MAMPs; e.g., flagellin; Zipfel et al., 2004), or plant themselves (DAMPs; oligogalacturonides; Hahn et al., 1981; Benedetti et al., 2015). A third category, called exogenous elicitors, which includes seaweed-based natural substances, was also reported to activate PTI. Interestingly, many macroalgae-based extracts were also reported to exhibit plant growth-promoting properties. Carrageenans are galactan-based polysaccharides commonly found in red macroalgae and were reported to exhibit plant-eliciting properties (Mercier et al., 2001). Laminarins, β-glucan-containing polysaccharides of brown macroalgae were also reported to exhibit plant-eliciting properties (Klarzynski et al., 2000; Aziz et al., 2003). Finally, ulvan polysaccharide, constitutive component of the cell walls of the green macroalgae *Ulva* genus was also reported to activate PTI (Cluzet et al., 2004; Jaulneau et al., 2010; Martin et al., 2020; Borba et al., 2021).

Ulva spp. belong to the class of Ulvophyceae, a group of green marine benthic algae, which dominates shallow marine environments and displays outstanding diversity regarding cytological and morphological characteristics (Wichard et al., 2015). *Ulva* spp. were shown to contain macro- and micronutrients, phytohormones, osmoprotectants, and other compounds with possible biological activities (Chbani et al., 2015; Shoubaky and Salem, 2016; Nabti et al., 2017). The presence of these compounds may accounts for well documented, *Ulva* extract-dependent, plant-growth promoting properties (Gireesh et al., 2011; Divya et al., 2015; Castellanos-Barriga et al., 2017; Paulert et al., 2021; Shefer et al., 2022). In addition to ulvans, *Ulva* spp. was also reported to contain fibrillar cellulose, mannan, or xylan polysaccharides in their cell walls (Domozych et al., 2012).

One class of proteins, the arabinogalactan proteins (AGPs), found in algal, moss, fern, and flowering plant cells walls and are strongly implicated in developmental processes (Lee et al., 2005; Nguema-Ona et al., 2012; Bartels and Classen, 2017; Renzaglia et al., 2017; Happ and Classen, 2019; Palacio-López et al., 2019) as well as in interaction with microorganisms (Nguema-Ona et al., 2013; Mareri et al., 2019). AGPs are proteoglycans consisting of two distinct moieties, the carbohydrate and the protein domain. The carbohydrate component typically accounts for 90%–98% of an AGP by weight and is rich in arabinose and galactose residues. The protein moiety, accounting for less than 10% of an AGP by weight is hydroxyproline-rich (Showalter, 2001; Seifert and Roberts, 2007). However, there is a wide range of variability in the structure and composition of both the carbohydrate and the polypetide parts. Based on the amino acid sequence and composition, AGPs were initially categorized into classical AGPs [consisting of a P/Hyp-rich domain heavily *O*-glycosylated, a hydrophobic C-terminal (C-ter) domain required for anchorage to the plasma membrane, and a signal peptide sequence] and non-classical AGPs (sometimes *N*-glycosylated and lacking the C-ter domain; Nguema-Ona et al., 2012). Non-classical AGPs also tend to be less heavily glycosylated (Showalter, 2001; Ma et al., 2018).

Although AGPs and AGP-like structures were reported to occur across the green and brown algae lineages, contrasting with the wealth of information available on land plant AGPs, much less is known about AGP occurrence, structure, and function in algae (Sørensen et al., 2011; Hervé et al., 2015; Palacio-López et al., 2019). Using immunocytochemistry and Yariv reagent, the presence of AGPs was described in several green microalgae of the freshwater-originated Charophyta division, specifically in Desmidiaceae, Coleochaetacea, Mesotaeniacea, Zygnemataceae, Chlorokybaceae, and Peniaceae families (Domozych et al., 2007, 2009; Eder et al., 2008; Sørensen et al., 2011; Palacio-López et al., 2019; Pfeifer et al., 2021).

Furthermore, AGPs were detected as well in the Charale order, representing the multicellular algae with stem-like and leaf-like structures (Domozych et al., 2010). Within the Chlorophyta division, AGPs were also reported in Oedogoniaceae and Codiaceae families (Estevez et al., 2008, 2009; Fernández et al., 2010, 2015). Very recently, AGP-like glycoproteins were isolated for the first time from *Ulva lactuca* (Přerovská et al., 2021). In this study, *Ulva* AGP-like glycoproteins exhibited a contrasting reactivity with primary anti-AGP antibodies as well as with Yariv reagent when compared to AGP glycoproteins isolated from *Solanum lycopersicum*. While the amino acid analysis of the AGP-like glycoproteins purified by the β-D-glucosyl Yariv reagent showed a similarity between *Ulva* AGP-like glycoproteins and land plant AGPs, saccharide analysis revealed unique glycosylation of the *Ulva lactuca* AGP-like glycoproteins. Surprisingly, arabinose and galactose were not the most prevalent monosaccharides and the most outstanding was the presence of 3-*O*-methyl-hexose, which has never been described in the AGPs (Přerovská et al., 2021). Nevertheless, methylation of AGP glycans was previously reported (Bartels et al., 2017; Bartels and Classen, 2017; Happ and Classen, 2019; Temple et al., 2019; Pfeifer et al., 2020). Moreover, methylated glycoproteins and polysaccharides are widely distributed within algal cell walls (Ogawa et al., 2001; Bollig et al., 2007; Capek et al., 2008; Levy-Ontman et al., 2011; Staudacher, 2012; Mathieu-Rivet et al., 2014; Mócsai et al., 2019; Pfeifer and Classen 2020).

In the present study, an AGP-like enriched fraction from *Ulva lactuca* has been purified and chemically characterized. In order to find out if the *Ulva* AGP-like enriched fraction would exhibit plant eliciting properties, the fraction was tested for its ability to elicit the activation of PTI on oilseed rape (*Brassica napus*). Oilseed rape is widely grown in Europe, Canada, China, and Australia, and ranks second as oilseed production right after soybean (Neik et al., 2020; Raboanatahiry et al., 2021). Oilseed rape is confronted by a plethora of pathogenic agents, including *Plasmodiophora brassicae*, *Leptosphaeria maculans*, *Sclerotinia sclerotiorumm*, *Hyaloperonospora parasitica*, and others (Becker et al., 2017; Neik et al., 2017, 2020). *Leptosphaeria maculans* is a hemibiotrophic fungal pathogen causing blackleg disease, also called phoma stem canker (Lipková et al., 2021). The disease causes annually 10%–20% of yield losses (Van de Wouw and Howlett, 2020). The AGP-like enriched fraction was further tested for its ability to reduce the occurrence and the spread of blackleg disease on oilseed rape cotyledons. All along this work, the level of activation of PTI as well as the efficacy of the AGP-like enriched fraction was evaluated. In parallel, an ulvan was also isolated and its ability to both activate immune responses and to protect oilseed rape, was evaluated and compared to the AGP-like enriched fraction. Our results showed that the AGP-like enriched fraction was able to significantly activate PTI, and further, to protect the oilseed rape cotyledons from the occurrence and the spread of *L. maculans*. Interestingly, plants treated with the AGP-like enriched fraction showed a concentration-dependent reduction in the severity of *L. maculans* infection, while ulvan was effective only at the highest tested concentration. Likewise, the level of activation of PTI was more pronounced following the application of the AGP-like enriched fraction compared to the ulvan.

MATERIALS AND METHODS

Biological Materials

U. lactuca materials collected in Brittany (France) were purchased from the European Marine Biological Resource Center (EMBRC, Station Biologique de Roscoff; https://embrc-france.obs-banyuls.fr) in 2017. *U. lactuca* was identified based on the sequence and phylogenetic analysis of rubisco large subunit (*rbcL*), internal transcribe spacer (ITS), and *tuf*A (plastid elongation factor) genes according to Vieira et al. (2016) and Lin et al. (2012). The material used for further extractions and analyses was freeze-dried and ground to a fine powder in CryoMill.

B. napus cultivar Columbus plants were grown hydroponically in perlite nourished with Steiner's nutrient solution (Steiner, 1984) under controlled conditions (14/10 h, 22/20°C, day/night). For inoculation tests, gene expression tests and hydrogen peroxide detection cotyledon leaves were used.

The fungus *L. maculans* (anamorph *Phoma lingam*) isolate JN2 (Balesdent et al., 2001) was cultivated on V8 solidified medium (20% V8 vegetable juice, Campbell, 3 g·L^{-1} $CaCO_3$, and 15 g·L^{-1} agar, autoclaved). Sporulation cultures and conidia suspension were prepared according to Šašek et al. (2012a). After harvesting, the spores were diluted to 10^8 spore·ml^{-1} and stored at −20°C for a maximum of 6 months.

Ulvan Extraction

Based on Yaich et al. (2013), 12.5 g of ground lyophilized *U. lactuca* was resuspended in 200 ml 50 mM HCl pH 2 and was incubated at 90°C for 3 h. After the extraction, the suspension was centrifuged for 10 min at 7,000 *g* at room temperature. The pH of the supernatant was adjusted to 3.5 by 1 M NaOH and precipitated overnight by three volumes of ethanol at 4°C. The pellet was obtained by centrifugation for 10 min at 7,000 *g* at 10°C, and the precipitate was washed three times by 50, 75, and 100% ethanol, centrifuged, dried, and lyophilized.

Preparation of AGP-Like Enriched Fraction

1 g of ground freeze-dried *U. lactuca* was extracted with 4 ml of extraction buffer: 50 mM 4-morpholineethanesulfonic acid (MES) buffer pH 6, 0.2 M $CaCl_2$, and 1 mM phenylmethylsulfonyl fluoride (PMSF). The extractions mixture was incubated 24 h at 4°C using a rotary mixer. Extraction mixture was centrifuged at 22,000 *g* for 20 min at 4°C.

For purification, the column XK 16/40 (GE Healthcare, United States) was fully packed by Q Sepharose® Fast Flow resin (GE Healthcare, United States). Subsequently, 50 ml of crude extract was 10 times diluted by 25 mM MES buffer pH 6 and left overnight at 4°C to precipitate. The AGP-like glycoproteins remained in the supernatant after the extract precipitation. The extract was then centrifuged, filtered by 0.45 µm, and loaded to the column by sample pump. The sample loading was followed by 200 ml 25 mM

MES buffer pH 6 column wash, followed by 100 ml buffer with 0.2 M NaCl, and then step change to buffer with 0.5 M NaCl and after that linear gradient to 1.2 M NaCl on 150 ml. The next step was linear gradient 1.2–2 M NaCl in buffer on 50 ml. The column was reequilibrated by 200 ml wash with 2 M NaCl and 200 ml 25 mM MES buffer pH 6. The flow rate was 2.5 ml•min^{-1}. Localization of AGP-like glycoprotein in collected fractions was done by western blot assay and control for the presence of ulvan was done by TBO assay. Positive fractions were pulled together, desalted by dialysis using 100 kDa MWCO dialysis tubing (Repligen, United States) for 3 days against distilled water and lyophilized.

Sodium Dodecylsulfate-Polyacrylamide Gel Electrophoresis and Western Blot

Samples were mixed with Laemmli sample buffer with a reducing agent, boiled for 10 min and 4–25 µl were loaded on 4%–15% Mini-PROTEAN® TGX Stain-Free™ precast polyacrylamide gels (Bio-Rad, United States). Gels were run at a constant current 200 V for approximately 35 min, and then they were stained by Pierce Silver Stain Kit (Thermo Fisher Scientific, United States). Separated proteins were transferred to the nitrocellulose membrane *via* the Trans-Blot Turbo system (Bio-Rad, United States), using the 10-min program for high molecular weight proteins, and were checked for the efficiency of transfer. The membrane was blocked with 5% low-fat milk in Tris-buffered saline (TBS) with 0.05% Tween 20 (v/v; TBST) overnight at 4°C on a rocking platform. JIM16 primary antibody (PlantProbes, United Kingdom) was used in 1:500 dilution in 5% low-fat milk in TBST for 1.5 h at room temperature on a rocking platform 100 rpm. After washing with TBST three times for 20 min at room temperature on a rocking platform, blots were incubated with an anti-rat IgG secondary antibody (Sigma Aldrich, United States) coupled to horseradish peroxidase in dilution 1:10,000 in 5% low-fat milk in TBST for 1.5 h at room temperature on the rocking platform 100 rpm. After washing as described before, the membranes were developed in SuperSignal West Femto Maximum Sensitivity Substrate (Thermo Fisher Scientific, United States) for 5 min at room temperature and the chemiluminescence was detected by ChemiDoc Imaging System (Bio-Rad, United States).

FT-IR Analysis

FT-IR spectra (4,000–400 cm^{-1}) were measured on Nicolet 6700 FT-IR spectrometer (Thermo Fisher Scientific, United States) using KBr tablets (transmission), 64 scans were accumulated with a spectral resolution of 2.0 cm^{-1}. The spectra were smoothed, baseline-corrected and the normalization has been done in Omnic 8.0 (Thermo Fisher Scientific, United States). Finally, the spectra were exported in ASCII format to Origin Pro software (Microcal Origin, United States) for the preparation of graphs.

Determination of Sulfated Polysaccharides by Toluidine Blue O

Based on Hahn et al. (2016), toluidine blue O (TBO) was dissolved in 20 mM maleic acid buffer pH 1 to a final concentration of 0.06 mmol·L^{-1}. For measurement of calibration curves, ulvan (prepared according to the section "Ulvan Extraction") and dextran sulfate in concentrations 0, 0.1, 0.25, 0.5, 0.75, and 1 mg·ml^{-1} were used. About 100 µl of calibration or sample solutions were mixed with 900 µl of TBO reagent, and the absorbance was measured at 632 nm. For the blank measurement was used distilled water.

Determination of Protein Content by Bicinchoninic Acid Assay

Protein content was measured by Bicinchoninic Acid (BCA) Protein Macro Assay Kit (Serva, DE) according to the product manual. Briefly, for measurement of calibration line, the bovine serum albumin in concentrations 0, 0.025, 0.05, 0.1, 0.25, 0.5, 0.75, and 1 mg·ml^{-1} was used. About 50 µl of standards or samples were mixed with 1 ml of BCA reagent. In blank measurement was used just distilled water. The solutions were incubated at 37°C for 30 min and absorbance was read at 562 nm.

Determination of Total Saccharide Content by Anthrone Assay

Based on Yemm and Willis (1954), anthrone reagent was prepared by dissolving 0.2 g of anthrone in a mixture of 5 ml of ethanol and 95 ml of 75% sulfuric acid on ice. For measurement of calibration line, glucose in concentrations 0, 0.01, 0.1, 1, 10, and 100 µg•ml^{-1} was used. The 100 µl of samples (0.1 mg•ml^{-1}) or calibration solutions were mixed with 500 µl of anthrone reagent on ice. Afterward, the mixture was incubated for 10 min at 100°C, chilled on ice, and the saccharide content was determined spectrophotometrically at 625 nm.

Determination of Uronic Acid Content

Based on Blumenkrantz and Asboe-Hansen (1973), galacturonic acid was used for measurement of the calibration line in concentrations 0, 40, 80, 120, 160, 200, and 240 µg•ml^{-1}. Samples (1 mg•ml^{-1}) and calibration solutions were diluted by distilled water 1:4 to final volume 500 µl and 3 ml of 12.5 mM sodium tetraborate decahydrate (0.478 g dissolved in 100 ml of 96% sulfuric acid) was added and the mixture was vortexed. The tubes were kept at 100°C for 5 min, chilled on ice and 50 µl of 0.15% (w/v) 3-hydroxybiphenyl in 0.5% NaOH was added. In the case of individual sample blank measurements, the use of 3-hydroxybiphenyl was omitted and only 0.5% NaOH was added. The solutions were vortexed and kept at room temperature for 30 min. The absorbance was measured at 520 nm. From the samples control solution of β-glucan (1 mg•mL^{-1}), as correction of neutral saccharide interference, was also subtracted.

Saccharide Composition Analysis by High-Performance Anion-Exchange Chromatography

1 mg of samples were dissolved in 1 ml of 1 M H_2SO_4 and were hydrolyzed for 8 h at 90°C. To neutralize the samples, 300 mg of $BaCO_3$ were added and incubated overnight on vortex. Samples were centrifuged at 10,000 g for 15 min, the

supernatants were filtrated, and pH was checked (Přerovská et al., 2021). If needed, samples were further diluted to get within the calibration range of the following analysis.

The samples were analyzed using high-performance anion-exchange chromatography (HPAEC) with pulsed amperometric detection (PAD) system Dionex DX-600 (Dionex, United States) with anion-exchange column CarboPac PA1, 2 mm × 250 mm (Thermo Fisher Scientific, United States) for the possible presence of about 20 saccharides and sugar alcohols (modified method according to Hardy et al., 1988; Přerovská et al., 2021 and Nagel et al., 2014). The Dionex ECD-50 detector (Dow, United States) was switched to the PAD mode. The injection volume was 10 µl. The mobile phase flow rate was 0.25 ml•min^{-1}, and the column temperature was maintained at 25°C. The program starts at 0 min with a column in 100 mM NaOH, the NaOAc concentration is gradually increased to 240 mM during 50 min while maintaining the NaOH concentration at 100 mmol•L^{-1}. Then, within 0.5 min, there is a change to 100 mM NaOH/600 mM NaOAc and in such a way regeneration takes place until 55 min. Afterward, within 0.5 min, there is a smooth change to 200 mM NaOH regenerating the column until 58 min, and finally within 0.5 min there is another change to 100 mM NaOH causing reequilibration of the column until 65 min.

In vitro Antifungal Assay

Antifungal activity of AGP-like enriched fraction and ulvan was measured according to the method previously described by Jindřichová et al. (2014). Briefly, GFP-tagged *L. maculans* (Šašek et al., 2012b) was suspended into 5×10^4 spore•ml^{-1} in a Gamborg B5 medium (Duchefa, Netherlands) supplemented with 0.3% sucrose and 10 mM MES pH 6.8. About 50 µl of conidia suspension was pipetted into black 96-well plate and then added 50 µl of test solutions (final concentration 0.01, 0.05, and 0.1 mg•ml^{-1}). AGP-like enriched fraction and ulvan were dissolved in 10 mM MES pH 6.8. As a growth control, 10 mM MES pH 6.8 was used. As positive control, 32 mM tebuconazole was used in form of commercial fungicide Horizon 250 EW (Bayer CropScience AG, Germany). The covered and micropore tape sealed plate was cultivated at 26°C and in the dark. Relative fluorescence was measured using Infinite F200 plate reader (TECAN, Switzerland) with filters for excitation 485/20 nm and for emission 535/25 nm every 24 h for 5 days. Fluorescent values were averaged for each treatment and difference between 96 and 0 h of control treatment was set as 100% of growth of *L. maculans*.

Plant Treatment

Cotyledons of 12-day-old plants were used for AGP-like enriched fraction and ulvan solutions treatment. Lyophilized extracts of AGP-like enriched fraction and ulvan were dissolved in distilled water. For dissolving, solutions were slightly heated in water bath. As negative control treatment with distilled water was used and as positive control 32 µM benzothiadiazole (BTH), a synthetic analogue of salicylic acid, in the form of the commercial preparation Bion 50WG (Syngenta, Zambia) was used in induced resistance test. For all experiments, 12 plants were used for each treatment. Cotyledons were treated by infiltration using a syringe without needle until full leaf saturation. The final concentrations of AGP-like enriched fraction and ulvan were 0.01, 0.02, 0.05, and 0.1 mg•ml^{-1}.

Induced Resistance Test

The 14-day-old plants were inoculated by conidia suspension of *L. maculans* in concentration 10^5 spore•ml^{-1}. Inoculation was performed by infiltration using needleless syringe until complete leaf saturation. Infected leaves were evaluated by image analysis using the APS Asses 2.0 software (APS Press, United States). The lesion area relative to the cotyledon area was averaged for each treatment and compared to the control (water) treatment, representing 100%.

Determination of Hydrogen Peroxide

Based on Thordal-Christensen et al. (1997), the presence of hydrogen peroxide was determined by the polymerization of 3,3′-diaminobenzidine (DAB). DAB solution (1 mg•ml^{-1} in 10 mM Tris/HCl pH 7.8) was infiltrated into the cotyledons by vacuum infiltration. Infiltrated leaves were incubated for 4 h in dark at room temperature. Afterward, the chlorophyll was removed by several washes with 96% ethanol. Before scanning, the leaves were rehydrated by consecutive 75, 50, 25, and 0% ethanol washes. For longer storage were leaves kept in 50% glycerol. DAB forms a reddish–brown polymerization product in the presence of H_2O_2 and peroxidase (PX).

Gene Transcription Analysis

RNA was isolated 24 h after plant treatment with studied compounds using commercial kit Spectrum™ Plant Total RNA Kit (Sigma Aldrich, United States). About 100 mg of plant material (10–12 disks with radius 6 mm) was used for isolation; four samples were collected from 12 plants. RNA was isolated according to the manufacturer manual and the concentration of isolated RNA was determined spectrophotometrically by NanoDrop 1000 (Thermo Scientific, United States). Isolated RNA (2.5 µg) was treated with DNA-free™ DNA Removal Kit (Ambion, United States) to remove possible contamination by genomic DNA. Isolated RNA was transcribed to cDNA *via* reverse transcription using M-MLV RNase H-point mutant (Promega, United States) and anchored oligo dT21 primer (Metabion, Germany). The qPCR reaction contained the equivalent of 6.25 ng of RNA in LightCycler® 480 SYBR Green I Master (Roche, Switzerland), in case of *ACS2* and *NCED3*, RNA equivalent was 25 ng. The final volume of reaction was 10 µl and was performed in a 96-well plate using LightCycler® 480 (Roche, Switzerland). The PCR conditions were 95°C for 10 min followed by 45 cycles of 95°C for 10 s, 55°C for 20 s, and 72°C for 20 s, followed by a melting curve analysis. Threshold cycles and melting curves were calculated using LightCycler®480 software. Level of relative transcription was calculated with an efficiency correction and normalized to the reference gene *Actin*. A list of primers is shown in **Supplementary Table S1**.

Statistical Analysis

The experiments were carried out in three independent biological replicates (i.e., three separate experiments not conducted in parallel at the same time). Data were analyzed using pair *t*-test or one-way ANOVA with *post hoc* Tukey test ($p < 0.05$). All statistical analysis were performed using GraphPad Prism 8 software.

RESULTS

Preparation of AGP-Like Enriched Fraction and Its Characterization

Based on physicochemical properties of both, AGPs and ulvan, ion-exchange (IEX) chromatography was chosen for their separation. In order to get rid of ulvan, purification procedure was optimized. The effectivity of separation was established based on the separation of AGP-like glycoproteins localized by western blot, and ulvan, whose localization was determined by TBO assay. The best results were achieved using Q Sepharose® Fast Flow resin and 25 mM MES buffer pH 6 and for the elution gradient of 2 M NaCl was chosen. The combination of step and linear elution gradient proved to be the most effective. Once the suitable protocol was found out, the purification was scaled up and the example chromatogram of chosen ion-exchange purification is presented in **Supplementary Figure 1A**.

The majority of proteins were localized within the peak containing AGP-like glycoproteins, represented by western blot positive fractions (**Supplementary Figure S1B**, lanes 6–8). On the other hand, the ulvan peak represented by TBO positive fractions contained almost no proteins (**Supplementary Figure S1B**, lane 9). The results of the western blot showed the presence of two high molecular weight AGP-like glycoproteins in JIM16 positive fractions. These fractions were collected and dialyzed against water for 3 days using a membrane with 100 kDa MWCO to desalt the sample and at the same time to remove low molecular weight compounds including the unwanted proteins. The dialyzed JIM16 positive fractions (AGP-like enriched fraction) were lyophilized afterwards and used for biological assays on plants.

Ulvan from *U. lactuca* was chosen as a control during the biological assays on plants, because of its well-documented elicitor activity. Ulvan from *U. lactuca* was prepared according to Yaich et al. (2013) and the yield was approximately 18% (w/w). To check the result of ulvan extraction, the sample was analyzed by FT-IR analysis (**Supplementary Figure 2**).

The measured FT-IR spectrum corresponded well to the already measured spectra of ulvan in the literature and contained all the bands typical for ulvan structure (Robic et al., 2009): the OH groups gave a signal at 3,420 cm^{-1}, the uronic acids afforded expected signals at 1,634 and 1,428 cm^{-1}, the sulfate groups absorbed at 1,258 and 1,225 cm^{-1}, the glycosidic linkages absorbance band was at 1,138–1,127 cm^{-1}, and the sugar-rings signals were assigned in the range of 110 and 990 cm^{-1} (**Supplementary Figure 2B**). However, some differences were noticed since the maximum absorption band at 1,135 cm^{-1} (1,055 cm^{-1} in Robic et al., 2009), and a shoulder between 1,220 and 1,130 cm^{-1} (not so significant in Robic et al., 2009) were observed. Although the ulvan extraction was successful, spotted differences might be pointing out to the slightly different structure of ulvan or presence of contamination within the sample. The presence of the bands at 656 and 645 cm^{-1} in the FT-IR spectrum suggested contamination by inorganic sulfates or phosphates.

Ulvan and AGP-like enriched fraction used for biological tests on plants were characterized mainly in terms of their glycosylation, which is assumed to be responsible for the AGPs functionality in plant development and defense responses (Lopez-Hernandez et al., 2020; Villa-Rivera et al., 2021).

Firstly, all the samples were analyzed in terms of the total protein content and composition of AGP-like glycoproteins (**Figure 1A**). Even though almost no proteins and mainly smear typical for polysaccharides could be seen in the case of the extracted ulvan (**Figure 1A**; lane 1), the presence of proteins confirms the contamination of extracted ulvan. The AGP-like enriched fraction contained a high amount of proteins with a molecular weight below 75 kDa (**Figure 1A**; lane 2). Surprisingly, even though the majority of the unwanted proteins had molecular weight below 75 kDa, they were not removed by 3-day 100 kDa MWCO dialysis at all. Nevertheless, the JIM16 antibody had a strong response with the sample after

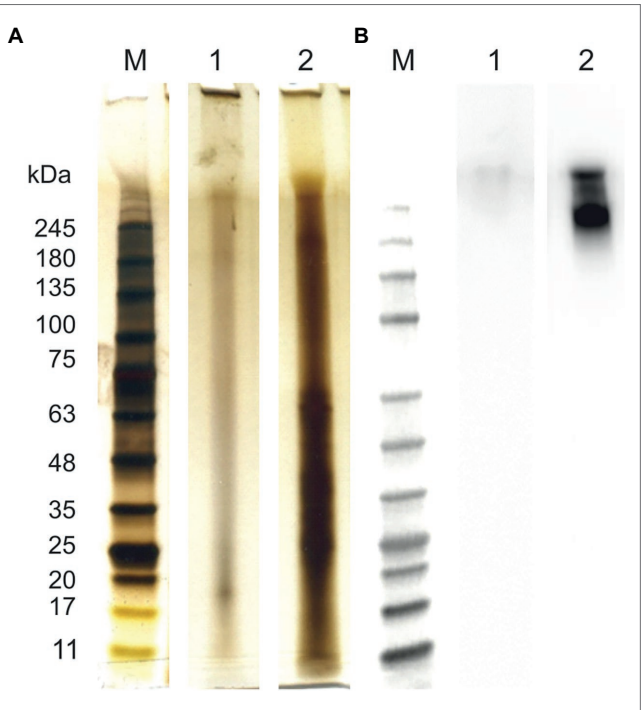

FIGURE 1 | Protein characterization of arabinogalactan protein (AGP)-like enriched fraction (AGPs) and ulvan. Samples were analyzed using SDS-PAGE and silver staininig **(A)** and immunolabeling with anti-AGP JIM16 primary antibody, 10 s exposition time **(B)**. (1) Ulvan; (2) AGPs. For the SDS-PAGE separation were used 4%–15% gradient precast polyacrylamide gels. Prestained Protein Ladder—Broad molecular weight (10–245 kDa, ab116028) was used.

IEX purification (**Figure 1B**; lane 2). Besides, an almost invisible response could be seen also in extracted ulvan (**Figure 1B**; lane 1). These findings further correspond to their spectrophotometric analysis of protein, total saccharide, and uronic acid content (**Table 1**).

The neutral saccharide composition differed greatly between the samples (**Table 1B**). Although the ulvan composition corresponded to the information present in the literature, surprising was the presence of unidentified monosaccharides (Yaich et al., 2013). One of these unidentified monosaccharides (retention time 3.15 min) was previously identified as 3-*O*-methyl-hexose, possibly 3-*O*-methyl-galactose, which has never been described in ulvan structure and might originate from the contaminating proteins (Přerovská et al., 2021). This saccharide was the most prevalent saccharide within AGP-like enriched fraction, followed by rhamnose, saccharide with retention time 4.63 min, saccharide with retention time min 3.92 min, and arabinose. The content of the remaining saccharides did not exceed 10%. Interestingly, the saccharide with retention time 3.92 min could be found only in this sample.

Moreover, the composition of negatively charged monosaccharides was completely different too (**Table 1C**). Ulvan negatively charged monosaccharide composition is almost identical to the *Ulva* extract with the majority of negatively charged monosaccharide with retention time 36.47 min. The data for *Ulva* extract were previously published in Přerovská et al. (2021). After IEX purification of *Ulva* extract the amount of this unidentified negatively charged monosaccharide, glucuronic, and iduronic acid decreased, whereas a significant amount of negatively charged monosaccharide with retention time 25.15 min and galacturonic acid appeared in the sample.

For the simplification, the term AGP-like enriched fraction will be in following text shortened to AGPs. It is a mixture of AGP-like glycoproteins and other proteins. However, low molecular weight compounds such as phytohormones and the vast majority of ulvans were removed from the sample during preparation. It is important to keep in mind that the structure and composition of *U. lactuca* AGP-like glycoproteins differ significantly from the AGPs of classical terrestrial plants (Seifert and Roberts, 2007; Přerovská et al., 2021).

TABLE 1 | The characterisation of samples.

	A—Total content		
	AGPs	**Ulvan**	
Protein	0.346 ± 0.027	0.041 ± 0.004	
Total saccharides	0.191 ± 0.027	0.276 ± 0.037	
Uronic acids	0.082 ± 0.002	0.200 ± 0.010	
B—Neutral monosaccharide composition			
Retention time (min)	**AGPs**	**Ulvan**	
2.93	1.4 ± 0.3	Traces	Fucose
3.15	27.7 ± 2.3	6.8 ± 0.5	3-*O*-methyl-hexose[a]
3.42	15.7 ± 0.5	71.5 ± 2.8	Rhamnose
3.92	12.5 ± 0.3	n.d.	-[b]
4.13	10.0 ± 0.8	Traces	Arabinose
4.63	15.5 ± 0.1	0.8 ± 0.1	-[b]
4.83	4.5 ± 0.1	2.3 ± 0.2	Mannose
5.05	7.3 ± 0.1	9.8 ± 0.2	Galactose
5.07	1.8 ± 0.1	traces	Glucose
5.27	3.8 ± 0.1	8.0 ± 0.5	Xylose
C—Negatively charged monosaccharide composition			
Retention time (min)	**AGPs**	**Ulvan**	
25.15	13.9 ± 0.9	n.d.	-[c]
25.83	23.4 ± 0.3	n.d.	Galacturonic acid
27.65	30.7 ± 0.8	33.4 ± 1.3	Glucuronic acid
33.90	3.7 ± 0.1	6.4 ± 0.2	Iduronic acid
36.47	28.4 ± 0.2	60.2 ± 1.9	-[c]

(A) *Basic characterization of the samples by spectrophotometric methods. Protein, total saccharide, and uronic acid mass fraction of Ulva lactuca ulvan, and AGP-like enriched fraction. Protein content was measured by the Bicinchoninic Acid (BCA) method, total saccharide content by anthrone method, and uronic acid content by the 3-hydroxybiphenyl method. Values in the table represent the mean ± SE (n = 9, collected from three independent experiments).* **(B)** *Neutral monosaccharide composition (mass % of total neutral saccharides) of Ulva lactuca ulvan, and AGP-like enriched fraction. Values in the table represent the mean ± SE (n = 9, collected from three independent experiments).* **(C)** *Negatively charged monosaccharide composition (mass % of total negatively charged monosaccharides) of Ulva lactuca ulvan, and AGP-like enriched fraction. Values in the table represent the mean ± SE (n = 4, collected from two independent experiments).*

[a]*Approximate content, the concentration calculated with a coefficient of 3-O-methyl-glucose.*

[b]*Approximate content, the concentration calculated with average coefficient of all standards.*

[c]*Approximate content, the concentration calculated with an average coefficient of all uronic acid standards.*

Traces: content < 0.5%; n.d., not detected.

AGP-Like Enriched Fraction Protects *Brassica napus* Against *Leptosphaeria maculans*

The protection efficacy of five different concentrations of algal elicitors (AGPs or ulvan) in *B. napus* against *L. maculans* was assessed by infiltration of *B. napus* cotyledons 2 days prior to inoculation with the pathogen. Once the lesions have developed (11 days after inoculation), the cotyledons were scanned to evaluate the lesion area (**Figure 2A**).

The grey-brown areas represent the *L. maculans* lesions. From the images themselves it was obvious, that AGPs caused a significant reduction in disease progression in concentration-dependent manner with concentration 1 mg·ml^{-1} being as effective as 32 μM benzothiadiazole (BTH), which was used as a positive control. BTH is a synthetic analog of salicylic acid able to induce SA-mediated stress response, which plays a major role in the defense against hemibiotrophic pathogens. Moreover, the lesion area was evaluated by image analysis, when the lesion area relative to the cotyledon area was averaged for each treatment and compared to the control treatment, expressed as 100%. Each treatment was represented by 12 plants and the whole experiment was repeated three times (**Figure 2B**).

The concentration-dependent effect of AGPs on the reduction of *L. maculans* infection is even more profound from the graph (**Figure 2B**). As positive control was used treatment with BTH, which diminished infection propagation by 99%–92% compared to control plants. Even the second-lowest tested concentration

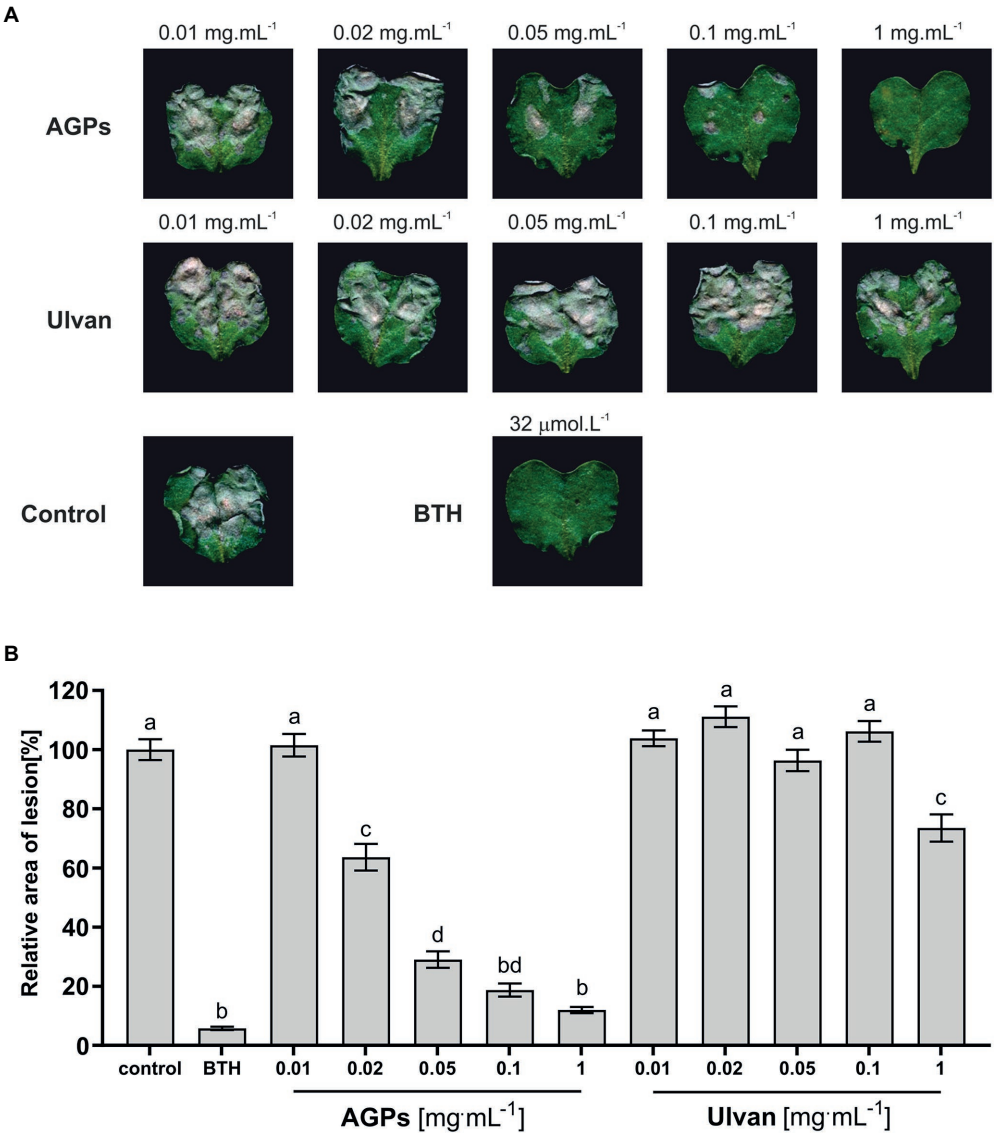

FIGURE 2 | Effect of algal elicitors on the progression of *L. maculans* infection in *B. napus* cotyledons. Cotyledons were treated with AGP-like enriched fraction (AGPs), ulvan extracted according to Yaich et al. (2013) (Ulvan), distilled water (negative control), and 32 μM BTH (benzothiadiazole, positive control) 2 days before inoculation with *L. maculans*. Symptoms of *L. maculans* infection on cotyledons of *B. napus* 11 days after inoculation **(A)**. Disease symptoms were evaluated as a percentage of the lesion area to the leaf area 11 days after inoculation **(B)**. The algal elicitors were tested in concentrations 0.01, 0.02, 0.05, 0.1, and 1 mg·ml^{-1}. The graph presented data from three biological replicates. Statistically significant differences determined by the one-way ANOVA and Tukey *post-hoc* test ($p < 0.05$). Each column is presented as the mean ± SE ($n = 72$). Different letters indicate significant difference.

(0.02 mg·ml^{-1}) led to a decrease in the relative area of lesions by 45%–30%. The pretreatment with the highest tested concentration (1 mg·ml^{-1}) resulted in a major reduction of infection propagation by 94%–83%, which was almost as efficient as the use of commercial elicitor BTH. Unexpectedly, the ulvan pretreatment had much lower elicitor activity, when only the highest tested concentration caused a statistically significant drop in lesion relative area by 47%–15%. Besides, greater variability between individual biological repetitions could be observed in the case of ulvan results, especially at higher concentrations.

AGP-Like Enriched Fraction Did Not Display Any Direct Antifungal Activity Against *Leptosphaeria maculans*

To exclude a direct antifungal effect of the tested compounds, the direct antifungal effect of AGPs and ulvan on *L. maculans* was examined *in vitro*. The assay showed that the relative fluorescence of growing mycelium of *L. maculans* did not significantly differ among the control and AGPs. Interestingly, ulvan in all tested concentrations improved *L. maculans* growth (**Figure 3**).

AGP-Like Enriched Fraction Induced Production of H_2O_2 in *Brassica napus* Cotyledons

Hydrogen peroxide represents important ROS, which has been shown to participate in cell signaling regulation, differentiation, programmed cell death, cell wall formation, and stress responses to both abiotic and biotic factors (Huang et al., 2019).

The formation of ROS is the first defense response of plants to biotic and abiotic stress and was suggested to play a pivotal role in the establishment of SAR with H_2O_2 as intra- and intercellular messenger (Barna et al., 2012). Thus, the effect of AGPs from *U. lactuca* and extracted ulvan on the formation of H_2O_2 was examined (**Figure 4A**).

The infiltration of AGPs sample into the cotyledons of *B. napus* leads to the accumulation of H_2O_2 in a concentration-dependent manner. Only weak accumulation of H_2O_2 was detected after treatment with ulvan regardless of the concentration used. In the case of water infiltration, H_2O_2 accumulation was not observed. To determine the origin of produced hydrogen peroxide, relative gene expression of two NADPH oxidases, also called respiratory burst oxidase homologues (RBOHs) was assessed (**Figure 4B**). Although RBOH family has more members, RBOH D and RBOH F are believed to be the key players in the ROS production during the stress responses (Chapman et al., 2019).

Treatment of *B. napus* cotyledons with AGPs and ulvan 24 h prior measurement resulted in increased expression of *RBOH F* by 2.9- and 1.9-fold compared to control, respectively. In the case of *RBOH D*, the expression level remained unchanged.

AGP-Like Enriched Fraction Induced Expression of Plant Defense Genes

To further understand the mechanisms behind improved *B. napus* resistance to *L. maculans* infection, the effect of AGPs on the activation of signaling pathways was tested and compared to control and ulvan treatment. Marker genes linked to the individual signaling pathways were chosen and their changes in expression 24 h after elicitor infiltration were observed. Corresponding to the previous results of inoculation assay, the treatment with AGPs caused statistically significant changes of gene expression in the *B. napus* cotyledons (**Figure 5**).

The relative expression of the nine genes involved in *B. napus* defense reactions—namely, *pathogenesis-related gene 1* (*PR1*), *isochorismate synthase 1* (*ICS1*), *phenylalanine ammonia-lyase* (*PAL*), *ACC synthase* (*ACS2*), *β-chitinase* (*βCHI*), *vegetative storage protein* (*VSP*), *allene oxide synthase* (*AOS*), transcription factor *responsive to desiccation 26* (*RD26*), and *9-cis-epoxycarotenoid dioxygenase 3* (*NCED3*)—were analyzed using RT-qPCR in water- (Control), AGPs-, and ulvan-treated plants. The treatment with AGPs led to the activation of the salicylic acid signaling pathway based on increased expression of SA responsive gene *PR1* (94.4-fold) as well as SA biosynthetic gene *ICS1* (8.9-fold). Though, the biggest change in gene expression could be observed in the case of *ACS2* (316.6-fold), pointing to strong activation of ethylene signaling pathway. Although the elevated level of *βCHI* expression (95.9-fold) indicates the involvement of the JA/ET signaling pathway, marker genes for jasmonic acid pathway *AOS* and *VSP* were downregulated by 0.4- and 0.2-fold, respectively. On contrary, ulvan in addition to the upregulation of *βCHI* (3.8-fold) also increased expression of *VSP* (2.6-fold), suggesting activation of JA/ET signaling pathway. Moreover, marker genes of abscisic acid pathway, *RD26* and *NCED3*, were downregulated by both AGPs (0.6- and 0.6-fold) and ulvan (0.6- and 0.7-fold). The changes in expression of the other marker genes were not statistically significant. The results suggest an unusual synergistic role of SA and ET signaling pathways during the AGPs induced resistance.

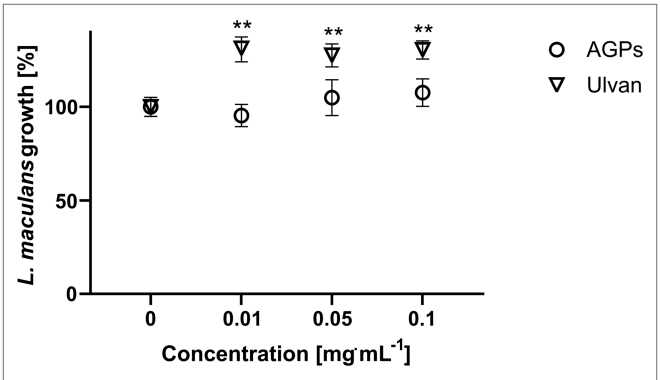

FIGURE 3 | Antifungal effect of AGP-like enriched fraction (AGPs) and ulvan on *L. maculans* growth. Spores of *L. maculans* tagged with GFP were cultivated with different concentrations of AGPs and ulvan extracted according to Yaich et al. (2013) (Ulvan) for 96 h in a microtitre plate. The growth of mycelium was quantified as an increase in GFP fluorescence. The data are presented as the mean ± SE values ($n = 6$). Statistically significant differences determined by the *t*-test are marked either with an $^*p < 0.05$ or $^{**}p < 0.01$, all samples were compared to the control (10 mM MES pH 6.8).

DISCUSSION

Seaweed extracts are already used in agriculture for their growth-promoting activity and ability to enhance plant stress tolerance for decades (Battacharyya et al., 2015). Although *Ascophyllum nodosum* products are the most commercially used (Sharma et al., 2014), *Ulva* sp. extracts have also high potential and have been the topic of various research papers (Dominguez and Loret, 2019). The most crucial challenge in seaweed biostimulant development is to choose the right extraction protocol, which will harvest all desired molecules with biostimulant activity. The protocol immensely affects the composition of final product and various protocols were established over the years. Although novel extraction technologies such as supercritical fluid extraction or microwave-assisted extraction are available, at the industrial level, the most common method is heating of algal biomass with potassium or sodium hydroxide solutions under pressure. Such harsh conditions can lead to the loss of some bioactive compounds plus result in uncontrolled fragmentation of polysaccharide chains, which consequently affect the biostimulant activity of the formulation

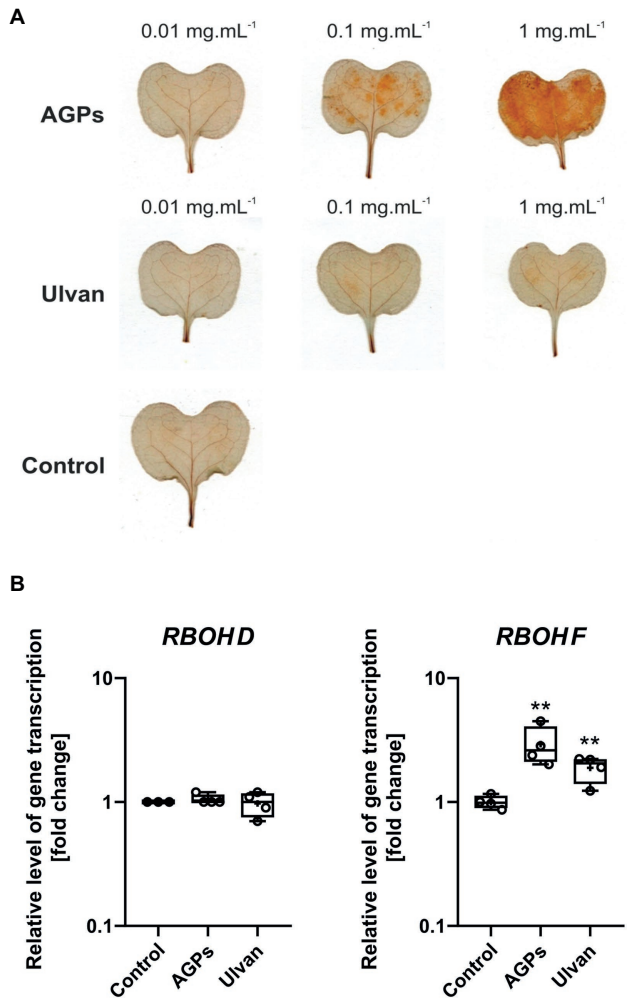

FIGURE 4 | Effect of algal elicitor treatment on accumulation of H_2O_2 and expression of *respiratory burst oxidase homologues* (*RBOHs*) in *B. napus* cotyledons. Accumulation of H_2O_2 in *B. napus* cotyledons **(A)**. Cotyledons (12-day-old) were treated with AGP-like enriched fraction (AGPs), ulvan extracted according to Yaich et al. (2013) (Ulvan), and distilled water (Control) by infiltration, the algal elicitors were tested in concentrations 0.01, 0.1, and 1 mg·ml^{-1}. H_2O_2 was detected 24 h after treatment using 3,3′-diaminobenzidine, the presence of H_2O_2 is represented by brown-red coloring. Expression of *RBOHs* in *B. napus* cotyledons **(B)**. Cotyledons were treated with AGP-like enriched fraction (AGPs), ulvan (Ulvan), and distilled water (Control) by infiltration in 0.1 mg·ml^{-1} concentration. After 24 h, gene expressions of *RBOH D* and *RBOH F* were analyzed. Data from the representative experiment are shown. Relative expression was calculated with efficiency correction and normalization to *actin*. Data are plotted at the $\log_{10}$ scale. Asterisks indicate statistically significant differences from control determined by the *t*-test $^{**}p < 0.01$.

(El Boukhari et al., 2020; Ali et al., 2021). Our results show, that even mild buffer extraction yields high amounts of proteins and saccharides with biostimulant activity within our extract. The eliciting activity of seaweed extracts is mainly attributed to the sulfated polysaccharides presented in their cell walls (Stadnik and Freitas, 2014). Nevertheless, algae contain a tremendous number of other biomolecules with potential biostimulant activity and AGPs belong to them. AGPs play a crucial role in higher plant defense responses and plant-microbe interactions (Nguema-Ona et al., 2013; Mareri et al., 2019), and their presence was confirmed also in brown and green algae (Estevez et al., 2009; Hervé et al., 2015; Ma et al., 2017; Přerovská et al., 2021). To test the ability of *U. lactuca* AGP-like glycoproteins to elicit defense responses and enhance stress resistance of higher plants, an AGP-like enriched sample containing approximately one-third of AGP-like glycoproteins was prepared by IEX chromatography. The ulvan extracted from *U. lactuca* was used for comparison. It activates plant immunity through the RBOH-dependent JA signaling pathway without inducing hypersensitive response (HR; Jaulneau et al., 2010; Freitas and Stadnik, 2015; Martin et al., 2020).

Up to now, seven studies focusing on the effects of different *Ulva* spp. extracts on plant infections with pathogens were published. Most of the studies used identical extraction protocol based on Cluzet et al. (2004), where dried *Ulva* material was autoclaved in distilled water, followed by ethanol precipitation. Some of the studies then call their product ulvan or some more generally as *Ulva* extract. In this study, ulvan was prepared according to Yaich et al. (2013) and based on excellent review of ulvan extractions done by Kidgell et al. (2019); our protocol should have high extraction yield, selectivity and low degradation. Only six studies also tried to analyze their products, mainly by means of spectrophotometric analyses, monosaccharide composition, and FT-IR analyses (Cluzet et al., 2004; Paulert et al., 2009, 2010; Jaulneau et al., 2011; Hernández-Herrera et al., 2014; Borba et al., 2019). Ulvan is mainly composed of rhamnose and glucuronic acid with the main repeating disaccharide unit (→4)-β-D-GlcA*p*-(1→4)-α-L-Rha*p*-(1→, in which glucuronic acid can be replaced to a certain extent by iduronic acid or xylose). Sulfation occurs mainly on C3 of the rhamnose and also C2 of the xylose or glucuronic acid (Lahaye and Robic, 2007; Kidgell et al., 2019). Although our results of ulvan analyses agrees with previously published data, outstanding is the presence of 3-*O*-methyl-hexose and unidentified saccharides, which possibly comes from contaminating glycoproteins. The most intriguing is the nature of negatively charged monosaccharide with retention time 36.47 min. Nevertheless, based on the knowledge of ulvan composition and the separation principle of the HPAEC/PAD technique, its long elution time indicates a strongly polar nature suggesting that we are dealing with a sulfated monosaccharide such as rhamnose-3-sulfate, which would correspond to its high content in ulvan (Templeton et al., 2012; Yaich et al., 2013). The composition of AGP-like enriched samples differs greatly from ulvan containing greater variety of monosaccharides and even more unidentified ones including rhamnose-3-sulfate. If true, the origin of this sulfated monosaccharide in the sample purified by ion-exchange chromatography, which should not contain ulvan, remains unknown. However, the correlation between sulfation and salt tolerance was previously proven (Aquino et al., 2011). Thus, the hypothetical presence of sulfated monosaccharide within AGP-like glycoproteins might be an adaptation to the marine environment. The other unidentified negatively charged monosaccharide with retention time 25.15 min is most probably

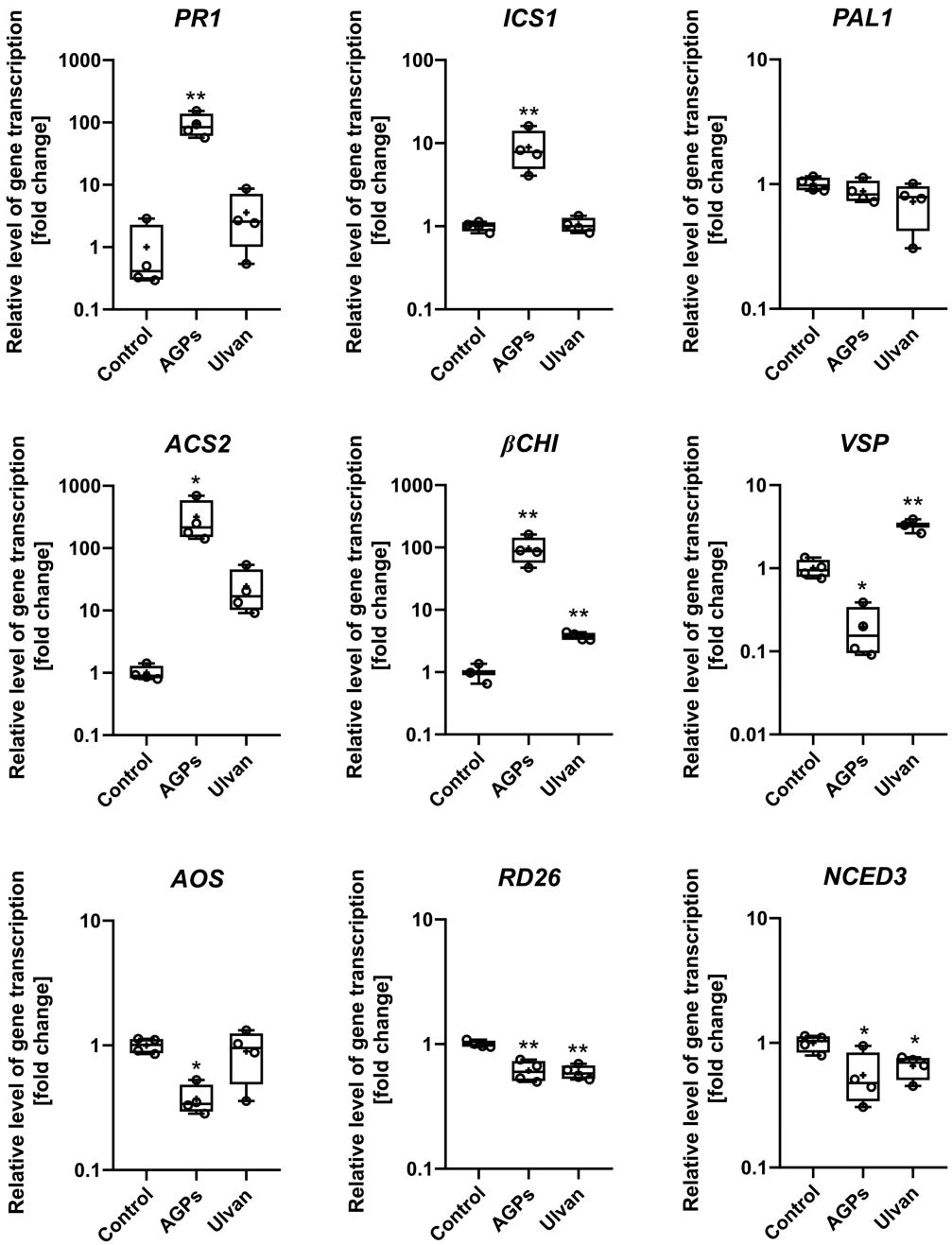

FIGURE 5 | Effect of algal elicitor treatment on activation of plant defense pathways in *B. napus* cotyledons. Cotyledons were treated with AGP-like enriched fraction (AGPs), ulvan extracted according to Yaich et al. (2013) (Ulvan) and distilled water (Control) by infiltration in 0.1 mg·mL^{-1} concentration. After 24 h, gene expressions of marker genes of salicylic acid pathway (*PR1*, *ICS1*, and *PAL1*), ethylene pathway (*ACS2*), ethylene/jasmonic acid pathway (*βCHI*), jasmonic acid (*VSP* and *AOS*), and abscisic acid (*RD26*, *NCED3*) were analyzed. Data from the representative experiment are shown. Relative expression was calculated with efficiency correction and normalization to *actin*. Data are plotted at the $\log_{10}$ scale. Asterisks indicate statistically significant differences from control determined by the *t*-test $^{*}p < 0.05$ or $^{**}p < 0.01$.

4-*O*-methyl-glucuronic acid, which would be in agreement with Pfeifer et al. (2020), who found out that *Zostera marina* AGPs contained high amounts of glucuronic acid and terminal 4-*O*-methyl-glucuronic acids, rare to land plant AGPs. We hypothesize, that the presence of unusual, modified monosaccharides might play an important role in eliciting plant resistance against the pathogen. The presence of galacturonic acid is interesting since it has rarely been described as part of AGP glycans (Tan et al., 2013). Though, high content of galacturonic acid and glucuronic acid was also identified in

AGP-like glycoproteins of *Micrasterias denticulata* (Eder et al., 2008), which pointed out to the unique glycosylation of algal AGP-like glycoproteins. The high content of uronic acids was proposed as a specific adaptation to the marine environment, thanks to their calcium-binding capacity and the ability of calcium ions to protect plants from harmful effects of salt stress (Lahaye and Epstein, 1969, 1971; Cramer et al., 1985; Pfeifer et al., 2020). The ion-binding capacity of AGPs can be fine-tuned according to environmental factors (Lamport and Várnai, 2013; Pfeifer et al., 2020). Moreover, the essential role of pH-dependent periplasmic AGP–Ca^{2+} capacitor in signaling and normal plant development was reported (Lamport and Várnai, 2013; Lamport et al., 2014, 2018; Mizukami et al., 2016; Lopez-Hernandez et al., 2020). Importantly, big differences in composition can be found between the AGP-like enriched fraction prepared with the help of IEX chromatography and AGP-like glycoproteins obtained by Yariv precipitation from *U. lactuca* extract, whose composition was previously published (Přerovská et al., 2021). The discrepancies are caused most probably due to the distinct content of individual AGP-like glycoproteins, or the presence of contaminating compounds based on different purifications. For instance, the IEX purified product contained more proteins other than AGP-like glycoproteins, and possibly a large fraction of them is glycosylated making the data difficult to interpret. Moreover, Yariv precipitated AGP-like glycoproteins are highly enriched in AGP-like glycoprotein with molecular weight approximately 20 kDa compared to AGP-like enriched fraction prepared by IEX chromatography. Nevertheless, the composition of Yariv precipitated AGP-like glycoproteins still differed greatly from data known from land plant AGPs. Most importantly, the use of Yariv reagent is not suitable for large scale purification, due to the cost of Yariv reagent and mainly due to extremely low yields of the purification (Přerovská et al., 2021). Our results showed that pretreatment of *B. napus* plants with AGPs significantly reduced the development of *L. maculans* symptoms on cotyledons. To reveal the mechanism of fungus retardation induced by AGPs treatment, the direct antimicrobial activity tests of the compounds were performed in axenic cultures *in vitro*. Neither AGPs nor ulvan had any effect on the growth of *L. maculans* in this study. Unfortunately, no similar data are available for comparison. However, in the case of ulvan, various data can be found showing either no direct antifungal effect toward different pathogens (Freitas and Stadnik, 2012) or even enhancing the germination of conidia of *C. lindemuthianum* (Paulert et al., 2009). The latter corresponds to the enhanced growth of *L. maculans*, which can be explained in the same way. Simply, the polysaccharide can serve as a carbon source for the fungus. Nevertheless, since the compounds studied did not show any direct antifungal effect, but at the same time were able to reduce the severity of *L. maculans* infection at a certain concentration, it can be assumed that the protection is due to their elicitor activity. In general, elicitors trigger numerous signaling events that lead to the activation of the defense. Among the earliest is the ROS production of superoxide, hydroxyl radical and hydrogen peroxide. The latter plays a central role in biotic stress, including oxidative burst, cross-linking of cell wall proteins, callose deposition, signaling, defense gene expression, and hypersensitive response often manifested by systemic acquired resistance (Freitas and Stadnik, 2015; Waszczak et al., 2018). While AGPs caused a concentration-dependent production of H_2O_2, almost no H_2O_2 was produced after treatment with ulvan. Similar H_2O_2 accumulation was also found in *B. napus* cotyledons infiltrated with an oligosaccharide elicitor isolated from *L. maculans* mycelium (Kim et al., 2013).

These results are consistent with gene expression analysis, as ROS can potentiate the production of SA and SA-mediated signaling, leading to the expression of SA-responsive defense genes such as *PR1*. These findings agree with the proposed mode of action of *A. nodosum* extract (Stella Maris®; Cook et al., 2018). Moreover, the H_2O_2 produced could likely have direct antimicrobial activity, as the inhibitory effect of hydrogen peroxide on conidial germination and mycelial growth of *L. maculans* (Jindřichová et al., 2011) has been described previously. It is noteworthy that H_2O_2 production could be partly caused by phytotoxicity of AGPs, as necrosis formed after treatment with a high concentration (10 mg·ml^{-1}, data not shown). However, this fact is not a problem as even low concentrations lead to a significant reduction in the severity of infection without phytotoxic effects. Phytotoxicity phenomenon has already been described for other elicitors (Burketova et al., 2015; Trdá et al., 2019). Several articles describing the effect of ulvan treatment on H_2O_2 production showed a different response depending on the plants used and the priming of ROS production (Paulert et al., 2010; Abouraïcha et al., 2015; Freitas and Stadnik, 2015). Although our results seem to contradict the findings of Freitas and Stadnik (2015), where ulvan treatment resulted in higher increase of H_2O_2 production in *A. thaliana* compared to our findings, they used ulvan from *Ulva fasciata* and a different extraction methodology. Ulvan composition is highly dependent on the source species, ecophysiology, extraction, and processing procedure, which causes diverse bioactivity profiles (Kidgell et al., 2019). In order to determine the origin of the hydrogen peroxide produced, the expression of two NADPH oxidases, also called respiratory burst oxidase homologs (RBOHs), was analyzed. *RBOH D* and *RBOH F* were chosen, since they are known to be key players in stress responses in various plant pathosystems (Torres et al., 2002; Morales et al., 2016; Jasso-Robles et al., 2020). Both AGPs and ulvan caused a significant increase in the expression of *RBOH F*, but not *RBOH D*. Although these two enzymes cooperate during ROS generation, they are thought to play different roles in the regulation of hypersensitive response. While *RBOH D* is responsible for most of the ROS production during effector-triggered immunity, *RBOH F* is thought to control cell death (Torres et al., 2002). Moreover, a different expression pattern of these two NADPH oxidases has been demonstrated, with *RBOH F* being mainly expressed in leaves. Nevertheless, striking differences between their functions are evident in the literature depending on the pathosystem studied and even on the inoculation method, plant growth conditions or sampling time (Morales et al., 2016). Moreover, NADPH oxidases are not the only sources of hydrogen peroxide during defense responses. Polyamine oxidases and cell wall peroxidases also contribute (Kámán-Tóth et al., 2019; Jasso-Robles et al., 2020).

In addition to H_2O_2 accumulation, the treatment of plants with AGPs caused changes in defense genes transcription. The results suggest that increased resistance of *B. napus* against *L. maculans* elicited by AGPs is SA-dependent as indicated by elevated transcription of both SA-biosynthetic gene *ICS1* and SA-responsive gene *PR1*. Since the expression of *PAL* did not differ from the control, it is probable that SA is synthesized exclusively *via* the pathway regulated by *ICS1*. In addition to the salicylic acid signaling pathway, the AGPs induced also expression of *βCHI* gene involved in JA/ET signaling. On the other hand, the activation of *AOS* transcription, the biosynthetic gene for jasmonic acid, by AGPs, was not observed. This resembles the signaling situation reported by Šašek et al. (2012b) within *B. napus* infection with *L. maculans* who showed, that the main signaling pathways involved in this pathosystem are SA and ET signaling and that the transcription of the related genes was significantly increased 7 days after pathogen recognition. This is further supported by the strong transcription of *ACS2*, the ethylene-biosynthetic gene, elicited by AGPs treatment. Our findings indicate elicitation of both SA-dependent and ET-dependent signaling pathways. Nevertheless, the ever-increasing discoveries of crosstalks in between the signaling pathways revealed the truly complex nature of plant responses (Bürger and Chory, 2019; Yang et al., 2019), even in the plant *B. napus* (Nováková et al., 2014). Besides our results correspond to the results of Cluzet et al. (2004), who described the increased expression of *CHI*, *PR1*, and *PR10* genes after treatments with various *Ulva* extracts. The activation of *PR1* transcription was also reported in *B. napus* cotyledons after treatment with oligosaccharide elicitor isolated from *L. maculans* mycelium (Kim et al., 2013) and protein elicitor isolated from *L. maculans* cultivation medium (Nováková et al., 2016). The high production of hydrogen peroxide together with a strong induction of SA and ET signaling pathways explains significant inhibitory effects of AGPs on the infection development.

Surprisingly, ulvan caused almost no significant changes in gene expression except for slightly increased levels of *βCHI* and *VSP*, consistent with its known mode of action (Jaulneau et al., 2010; Hernández-Herrera et al., 2016; Ramkissoon et al., 2017). Based on the results, the *U. lactuca* ulvan appeared to be efficient in the pathosystems studied at higher concentrations, which was further supported by an 80% decrease in *L. maculans* infection after treatment with a concentration of 10 $mg{\cdot}ml^{-1}$ (**Supplementary Figure 3**). The variability in ulvan data may be due to the viscous nature of the concentrated samples, which causes uneven infiltration.

In addition to the major defense signaling pathways regulated by SA, JA, and ET, *B. napus* plants responded to elicitor treatment with a decrease in genes related to ABA. Both the *NCED3* biosynthetic gene and the *RD26* responsive gene were downregulated by both the AGPs and ulvan. This result is in accordance with previous findings of Jaulneau et al. (2010), who reported a transient decrease (2 days after treatment) in ABA-responsive genes in *Medicago truncatula*. On the other hand, Chen et al. (2013) found an increase in ABA in plants treated with a protein elicitor from oomycete *Phytophthora boehmeriae*, which lead to significant reduction of pathogen infection. These contrasting results indicate that the role of ABA in induced resistance by elicitors is not as straightforward as, e.g., the role of SA. The role of ABA in plant defense against pathogens is less defined and the data are less consistent compared with SA, JA, and ET signaling. Since ABA regulates stomata opening, it is suggested that ABA is an important phytohormone in protecting the host plant from pathogen penetration *via* the stomata. The possible positive role of ABA in the studied pathosystem *B. napus—L. maculans* was previously reported by Šašek et al. (2012b). Similar to ABA, several elicitors of different origins induced stomata closure and ROS production in guard cells (Allègre et al., 2009).

In conclusion, our study makes an important contribution to the understanding of the mechanisms behind the elicitor activity of *U. lactuca* extracts recently introduced in agriculture. In addition to the well-described polysaccharide ulvan, *U. lactuca* contains other compounds that elicit even stronger defenses against pathogens. We were able to prepare an AGP-like enriched fraction that efficiently induced resistance to the hemibiotrophic fungal pathogen *L. maculans* in cotyledons of *B. napus*. Examination of the signaling events revealed that the triggered defense mechanisms were regulated by H_2O_2, SA, and ET signaling. Proposed mechanisms of actions for both AGPs and ulvan are presented in the **Figure 6**. Since AGPs showed higher efficiency than ulvan, AGPs may have the potential to become a component of plant protection products in the future. Moreover, for their possible future application, our following research will be focused on increased penetration of AGPs to the plants, testing

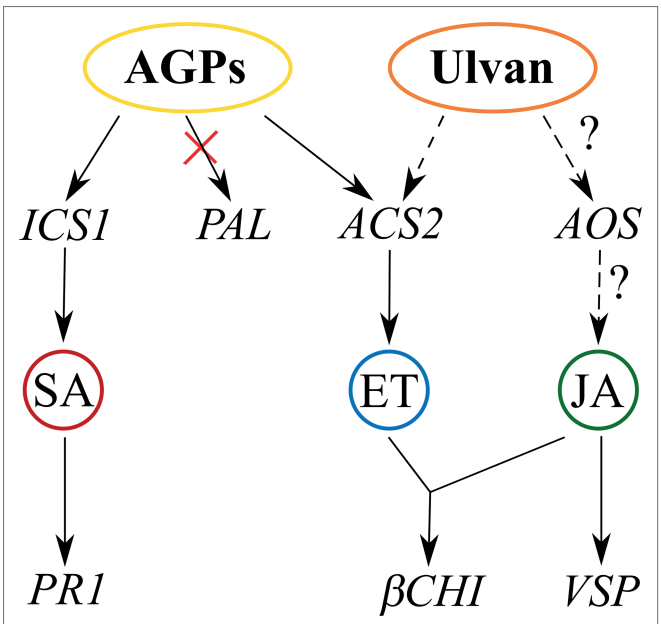

FIGURE 6 | Proposed mechanism of AGP-like enriched fraction (AGPs) and ulvan action based on transcription of signaling pathway marker genes. AGPs activate the salicylic acid signaling pathway *via isochorismate synthase 1* and the ethylene signaling pathway *via ACC synthase*. Ulvan activates the ethylene signaling pathway based on gene expression of *βCHI* and probably also jasmonic acid signaling pathway based on *VSP* expression. Full arrows indicate proven involvement of the pathways, and dashed arrows indicate likely involvement of the pathways.

oligosaccharides produced from AGPs, and assessing their effect also on other pathosystems including monocot plants, which differ in their defense signaling.

DATA AVAILABILITY STATEMENT

The original contributions presented in the study are included in the article/**Supplementary Material**; further inquiries can be directed to the corresponding author.

AUTHOR CONTRIBUTIONS

TP contributed to data collection, designing research, and analyzing the data and writing the manuscript. BJ contributed to data collection, designing plant experiments, analyzing the data, and editing the manuscript. SH contributed to data collection (saccharide analysis). J-CY and VF contributed to designing research. LB contributed to designing research and editing the manuscript. PL contributed to data collection, designing research, and editing the manuscript. All authors contributed to the article and approved the submitted version.

FUNDING

The work was supported from European Regional Development Fund-Project "Centre for Experimental Plant Biology" (no. CZ.02.1.01/0.0/0.0/16_019/0000738) and by the grant of Specific University Research (A1_FPBT_2020_001).

ACKNOWLEDGMENTS

The authors would like to thank the French Ministry of Foreign Affairs and the Agro Innovation International TIMAC AGRO for financial support. And also thank to Roman Bleha from Department of Carbohydrates and Cerials at the University of Chemistry and Technology Prague for his kind help with FT-IR analysis of ulvan.

SUPPLEMENTARY MATERIAL

The Supplementary Material for this article can be found online at: https://www.frontiersin.org/articles/10.3389/fpls.2022.893858/full#supplementary-material

REFERENCES

Abouraïcha, E., El Alaoui-Talibi, Z., El Boutachfaiti, R., Petit, E., Courtois, B., Courtois, J., et al. (2015). Induction of natural defense and protection against *Penicillium expansum* and *Botrytis cinerea* in apple fruit in response to bioelicitors isolated from green algae. *Sci. Hortic.* 181, 121–128. doi: 10.1016/j.scienta.2014.11.002

Ali, O., Ramsubhag, A., and Jayaraman, J. (2021). Biostimulant properties of seaweed extracts in plants, implications towards sustainable crop production. *Plan. Theory* 10:531. doi: 10.3390/plants10030531

Allègre, M., Héloir, M.-C., Trouvelot, S., Daire, X., Pugin, A., Wendehenne, D., et al. (2009). Are grapevine stomata involved in the elicitor-induced protection against downy mildew? *MPMI* 22, 977–986. doi: 10.1094/MPMI-22-8-0977

Aquino, R. S., Grativol, C., and Mourão, P. A. S. (2011). Rising from the sea, correlations between sulfated polysaccharides and salinity in plants. *PLoS One* 6:e18862. doi: 10.1371/journal.pone.0018862

Aziz, A., Poinssot, B., Daire, X., Adrian, M., Bézier, A., Lambert, B., et al. (2003). Laminarin elicits defense responses in grapevine and induces protection against *Botrytis cinerea* and *Plasmospara viticola*. *MPMI* 16, 1118–1128. doi: 10.1094/MPMI.2003.16.12.1118

Balesdent, M. H., Attard, A., Ansan-Melayah, D., Delourme, R., Renard, M., and Rouxel, T. (2001). Genetic control and host range of avirulence toward *Brassica napus* cultivars Quinta and jet Neuf in *Leptosphaeria maculans*. *Phytopathology* 91, 70–76. doi: 10.1094/PHYTO.2001.91.1.70

Barna, B., Fodor, J., Harrach, B. D., Pogány, M., and Király, Z. (2012). The Janus face of reactive oxygen species in resistance and susceptibility of plants to necrotrophic and biotrophic pathogens. *Plant Physiol. Biochem.* 59, 37–43. doi: 10.1016/j.plaphy.2012.01.014

Bartels, D., Baumann, A., Maeder, M., Geske, T., Heise, E. M., von Schwartzenberg, K., et al. (2017). Evolution of plant cell wall: arabinogalactan-proteins from three moss genera show structural differences compared to seed plants. *Carbohydr. Polym.* 163, 227–235. doi: 10.1016/j.carbpol.2017.01.043

Bartels, D., and Classen, B. (2017). Structural investigations on arabinogalactan-proteins from a lycophyte and different monilophytes (ferns) in the evolutionary context. *Carbohydr. Polym.* 172, 342–351. doi: 10.1016/j.carbpol.2017.05.031

Battacharyya, D., Babgohari, M. Z., Rathor, P., and Prithiviraj, B. (2015). Seaweed extracts as biostimulants in horticulture. *Sci. Hortic.* 196, 39–48. doi: 10.1016/j.scienta.2015.09.012

Becker, M. G., Zhang, X., Walker, P. L., Wan, J. C., Millar, J. L., Khan, D., et al. (2017). Transcriptome analysis of the *Brassica napus–Leptosphaeria maculans* pathosystem identifies receptor, signaling and structural genes underlying plant resistance. *Plant J.* 90, 573–586. doi: 10.1111/tpj.13514

Benedetti, M., Pontiggia, D., Raggia, S., Cheng, Z., Scalonia, F., Ferrari, S., et al. (2015). Plant immunity triggered by engineered *in vivo* releaseof oligogalacturonides, damage-associated molecular patterns. *PNAS* 112, 5533–5538. doi: 10.1073/pnas.1504154112

Bigeard, J., Colcombet, J., and Hirt, H. (2015). Signaling mechanisms in pattern-triggered immunity (PTI). *Mol. Plant* 8, 521–539. doi: 10.1016/j.molp.2014.12.022

Blumenkrantz, N., and Asboe-Hansen, G. (1973). New method for quantitative determination of uronic acids. *Anal. Biochem.* 54, 484–489. doi: 10.1016/0003-2697(73)90377-1

Boller, T., and Felix, G. (2009). A renaissance of elicitors, perception of microbe-associated molecular patterns and danger signals by pattern-recognition receptors. *Annu. Rev. Plant Biol.* 60, 379–406. doi: 10.1146/annurev.arplant.57.032905.105346

Bollig, K., Lamshöft, M., Schweimer, K., Marner, F.-J., Budzikiewicz, H., and Waffenschmidt, S. (2007). Structural analysis of linear hydroxyproline-bound *O*-glycans of *Chlamydomonas reinhardtii*—conservation of the inner core in *Chlamydomonas* and land plants. *Carbohydr. Res.* 342, 2557–2566. doi: 10.1016/j.carres.2007.08.008

Borba, M. C., Stadnik, M. B., and Stadnik, M. J. (2019). Ulvan enhances seedling emergence and reduces Fusarium wilt severity in common bean (*Phaseolus vulgaris* L.). *Crop Prot.* 118, 66–71. doi: 10.1016/j.cropro.2018.12.014

Borba, M. C., Velho, A. C., Maia-Grondard, A., Baltenweck, R., Magnin-Robert, M., Randoux, B., et al. (2021). The algal polysaccharide Ulvan induces resistance in wheat against *Zymoseptoria tritici* without major alteration of leaf Metabolome. *Front. Plant Sci.* 12:703712. doi: 10.3389/fpls.2021.703712

Bürger, M., and Chory, J. (2019). Stressed out about hormones, how plants orchestrate immunity. *Cell Host Microbe* 26, 163–172. doi: 10.1016/j.chom.2019.07.006

Burketova, L., Trda, L., Ott, P. G., and Valentova, O. (2015). Bio-based resistance inducers for sustainable plant protection against pathogens. *Biotechnol. Adv.* 33, 994–1004. doi: 10.1016/j.biotechadv.2015.01.004

Capek, P., Matulová, M., and Combourieu, B. (2008). The extracellular proteoglycan produced by *Rhodella grisea*. *Int. J. Biol. Macromol.* 43, 390–393. doi: 10.1016/j.ijbiomac.2008.07.015

Carvalho, F. P. (2006). Agriculture, pesticides, food security and food safety. *Environ. Sci. Pol.* 9, 685–692. doi: 10.1016/j.envsci.2006.08.002

Castellanos-Barriga, L. G., Santacruz-Ruvalcaba, F., Hernández-Carmona, G., Ramírez-Briones, E., and Hernández-Herrera, R. M. (2017). Effect of seaweed liquid extracts from *Ulva lactuca* on seedling growth of mung bean (*Vigna radiata*). *J. Appl. Phycol.* 29, 2479–2488. doi: 10.1007/s10811-017-1082-x

Chapman, J. M., Muhlemann, J. K., Gayomba, S. R., and Muday, G. K. (2019). RBOH-dependent ROS synthesis and ROS scavenging by plant specialized metabolites to modulate plant development and stress responses. *Chem. Res. Toxicol.* 32, 370–396. doi: 10.1021/acs.chemrestox.9b00028

Chbani, A., Majed, S., and Mawlawi, H. (2015). Mineral content of mediterranean seaweeds, *Padina pavonica* L. (Pheophytae), *Ulva lactuca* L. and *Ulva linza* L. (Chlorophytae) for biofertilizing use. *Int. J. Hortic. Sci. Technol.* 2, 133–140. doi: 10.22059/IJHST.2015.56430

Chen, Q., Chen, Z., Lu, L., Jin, H., Sun, L., Yu, Q., et al. (2013). Interaction between abscisic acid and nitric oxide in PB90-induced catharanthine biosynthesis of *catharanthus roseus* cell suspension cultures. *Biotechnol. Prog.* 29, 994–1001. doi: 10.1002/btpr.1738

Cluzet, S., Torregrosa, C., Jacquet, C., Lafitte, C., Fournier, J., Mercier, L., et al. (2004). Gene expression profiling and protection of *Medicago truncatula* against a fungal infection in response to an elicitor from green algae *Ulva* spp. *Plant Cell Environ.* 27, 917–928. doi: 10.1111/j.1365-3040.2004.01197.x

Cook, J., Zhang, J., Norrie, J., Blal, B., and Cheng, Z. (2018). Seaweed extract (Stella Maris®) activates innate immune responses in *Arabidopsis thaliana* and protects host against bacterial pathogens. *Mar. Drugs* 16:221. doi: 10.3390/md16070221

Cramer, G. R., Läuchli, A., and Polito, V. S. (1985). Displacement of Ca^{2+} by Na^{+} from the plasmalemma of root cells. *Plant Physiol.* 79, 207–211. doi: 10.1104/pp.79.1.207

Divya, K., Roja, N., and Padal, S. B. (2015). Influence of seaweed liquid fertilizer of *Ulva lactuca* on the seed germination, growth, productivity of *Abelmoschus esculentus* (L.). *Int. J. Pharmacol. Res.* 5, 344–356.

Dominguez, H., and Loret, E. P. (2019). *Ulva lactuca*, a source of troubles and potential riches. *Mar. Drugs* 17:357. doi: 10.3390/md17060357

Domozych, D., Ciancia, M., Fangel, J. U., Mikkelsen, M. D., Ulvskov, P., and Willats, W. G. T. (2012). The cell walls of green algae, a journey through evolution and diversity. *Front. Plant Sci.* 3:82. doi: 10.3389/fpls.2012.00082

Domozych, D. S., Elliott, L., Kiemle, S. N., and Gretz, M. R. (2007). *Pleurotaenium trabecula*, a desmid of wetland biofilms: the extracellular matrix and adhesion mechanisms. *J. Phycol.* 43, 1022–1038. doi: 10.1111/j.1529-8817.2007.00389.x

Domozych, D. S., Sørensen, I., Pettolino, F. A., Bacic, A., and Willats, W. G. T. (2010). The cell wall polymers of the charophycean green alga *Chara corallina*: immunobinding and biochemical screening. *Int. J. Plant Sci.* 171, 345–361. doi: 10.1086/651227

Domozych, D. S., Wilson, R., and Domozych, C. R. (2009). Photosynthetic eukaryotes of freshwater wetland biofilms: adaptations and structural characteristics of the extracellular matrix in the green alga, *Cosmarium reniforme* (Zygnematophyceae, Streptophyta). *J. Eukaryot. Microbiol.* 56, 314–322. doi: 10.1111/j.1550-7408.2009.00392.x

du Jardin, P., Xu, L., and Geelen, D. (2020). "Agricultural functions and action mechanisms of plant biostimulants (PBs)" in *The Chemical Biology of Plant Biostimulants*. eds. D. Geelen and L. Xu (Chichester, UK: John Wiley, and Sons, Ltd.), 1–30.

Eder, M., Tenhaken, R., Driouich, A., and Lütz-Meindl, U. (2008). Occurrence and characterization of arabinogalactan-like proteins and hemicelluloses in *Micrasterias* (Streptophyta). *J. Phycol.* 44, 1221–1234. doi: 10.1111/j.1529-8817.2008.00576.x

El Boukhari, M. E. M., Barakate, M., Bouhia, Y., and Lyamlouli, K. (2020). Trends in seaweed extract based biostimulants, manufacturing process and beneficial effect on soil-plant systems. *Plan. Theory* 9:359. doi: 10.3390/plants9030359

Estevez, J. M., Fernández, P. V., Kasulin, L., Dupree, P., and Ciancia, M. (2009). Chemical and in situ characterization of macromolecular components of the cell walls from the green seaweed *Codium fragile*. *Glycobiology* 19, 212–228. doi: 10.1093/glycob/cwn101

Estevez, J. M., Leonardi, P. I., and Alberghina, J. S. (2008). Cell wall carbohydrate epitopes in the green alga *Oedogonium Bharuchae* F. *Minor* (Oedogoniales, Chlorophyta)1. *J. Phycol.* 44, 1257–1268. doi: 10.1111/j.1529-8817.2008.00568.x

Fernández, P. V., Ciancia, M., Miravalles, A. B., and Estevez, J. M. (2010). Cell-wall polymer mapping in the coenocytic macroalga *Codium Vermilara* (Bryopsidales, Chlorophyta). *J. Phycol.* 46, 456–465. doi: 10.1111/j.1529-8817.2010.00821.x

Fernández, P. V., Raffo, M. P., Alberghina, J., and Ciancia, M. (2015). Polysaccharides from the green seaweed *Codium decorticatum*. Structure and cell wall distribution. *Carbohydr. Polym.* 117, 836–844. doi: 10.1016/j.carbpol.2014.10.039

Freitas, M. B., and Stadnik, M. J. (2012). Race-specific and ulvan-induced defense responses in bean (*Phaseolus vulgaris*) against *Colletotrichum lindemuthianum*. *Physiol. Mol. Plant Pathol.* 78, 8–13. doi: 10.1016/j.pmpp.2011.12.004

Freitas, M. B., and Stadnik, M. J. (2015). Ulvan-induced resistance in *Arabidopsis thaliana* against *Alternaria brassicicola* requires reactive oxygen species derived from NADPH oxidase. *Physiol. Mol. Plant Pathol.* 90, 49–56. doi: 10.1016/j.pmpp.2015.03.002

Gireesh, R., Haridevi, C. K., and Salikutty, J. (2011). Effect of *Ulva lactuca* extract on growth and proximate composition of *Vigna unguiculata* (L.) Walp. *J. Res. Biol.* 8, 624–630.

Hahn, M. G., Darvill, A. G., and Albersheim, P. (1981). Host-pathogen interactions, XIX. The endogenous elicitor, a fragment of a plant cell wall polysaccharide that elicits phytoalexin accumulation in soybeans. *Plant Physiol.* 68, 1161–1169. doi: 10.1104/pp.68.5.1161

Hahn, T., Schulz, M., Stadtmüller, R., Zayed, A., Muffler, K., Lang, S., et al. (2016). Cationic dye for the specific determination of sulfated polysaccharides. *Anal. Lett.* 49, 1948–1962. doi: 10.1080/00032719.2015.1126839

Happ, K., and Classen, B. (2019). Arabinogalactan-proteins from the liverwort *Marchantia polymorpha* L., a member of a basal land plant lineage, are structurally different to those of angiosperms. *Plan. Theory* 8:460. doi: 10.3390/plants8110460

Hardy, M. R., Townsend, R. R., and Leeab, Y. C. (1988). Monosaccharide analysis of glycoconjugates by anion exchange chromatography with pulsed amperometric detection. *Anal. Biochem.* 170, 54–62. doi: 10.1016/0003-2697(88)90089-9

Hernández-Herrera, R. M., Santacruz-Ruvalcaba, F., Ruiz-López, M. A., Norrie, J., and Hernández-Carmona, G. (2014). Effect of liquid seaweed extracts on growth of tomato seedlings (*Solanum lycopersicum* L.). *J. Appl. Phycol.* 26, 619–628. doi: 10.1007/s10811-013-0078-4

Hernández-Herrera, R. M., Santacruz-Ruvalcaba, F., Zañudo-Hernández, J., and Hernández-Carmona, G. (2016). Activity of seaweed extracts and polysaccharide-enriched extracts from *Ulva lactuca* and *Padina gymnospora* as growth promoters of tomato and mung bean plants. *J. Appl. Phycol.* 28, 2549–2560. doi: 10.1007/s10811-015-0781-4

Hervé, C., Siméon, A., Jam, M., Cassin, A., Johnson, K. L., Salmeán, A. A., et al. (2015). Arabinogalactan proteins have deep roots in eukaryotes, identification of genes and epitopes in brown algae and their role in *Fucus serratus* embryo development. *New Phytol.* 209, 1428–1441. doi: 10.1111/nph.13786

Huang, H., Ullah, F., Zhou, D.-X., Yi, M., and Zhao, Y. (2019). Mechanisms of ROS regulation of plant development and stress responses. *Front. Plant Sci.* 10:800. doi: 10.3389/fpls.2019.00800

Jamiolkowska, A. (2020). Natural compounds as elicitors of plant resistance against diseases and new biocontrol strategies. *Agronomy* 10:173. doi: 10.3390/agronomy100(2017)3

Jasso-Robles, F. I., Gonzalez, M. E., Pieckenstain, F. L., Ramírez-García, J. M., Guerrero-González, M., Jiménez-Bremont, J. F., et al. (2020). Decrease of *Arabidopsis* PAO activity entails increased RBOH activity, ROS content and altered responses to *pseudomonas*. *Plant Sci.* 292:110372. doi: 10.1016/j.plantsci.2019.110372

Jaulneau, V., Lafitte, C., Corio-Costet, M.-F., Stadnik, M. J., Salamagne, S., Briand, X., et al. (2011). An *Ulva armoricana* extract protects plants against three powdery mildew pathogens. *Eur. J. Plant Pathol.* 131, 393–401. doi: 10.1007/s10658-011-9816-0

Jaulneau, V., Lafitte, C., Jacquet, C., Fournier, S., Salamagne, S., Briand, X., et al. (2010). Ulvan, a sulfated polysaccharide from green algae, activates plant immunity through the jasmonic acid signaling pathway. *J. Biomed. Biotechnol.* 2010:525291. doi: 10.1155/2010/525291

Jindřichová, B., Burketová, L., and Novotná, Z. (2014). Novel properties of antimicrobial peptide anoplin. *Biochem. Biophys. Res. Commun.* 444, 520–524. doi: 10.1016/j.bbrc.2014.01.097

Jindřichová, B., Fodor, J., Šindelářová, M., Burketová, L., and Valentová, O. (2011). Role of hydrogen peroxide and antioxidant enzymes in the interaction between a hemibiotrophic fungal pathogen, *Leptosphaeria maculans*, and oilseed rape. *Environ. Exp. Bot.* 72, 149–156. doi: 10.1016/j.envexpbot.2011.02.018

Jones, J. D. G., and Dangl, J. L. (2006). The plant immune system. *Nature* 444, 323–329. doi: 10.1038/nature05286

Kámán-Tóth, E., Dankó, T., Gullner, G., Bozsó, Z., Palkovics, L., and Pogány, M. (2019). Contribution of cell wall peroxidase- and NADPH oxidase-derived reactive oxygen species to *Alternaria brassicicola*-induced oxidative burst in *Arabidopsis*. *Mol. Plant Pathol.* 20, 485–499. doi: 10.1111/mpp.12769

Kidgell, J. T., Magnusson, M., de Nys, R., and Glasson, C. R. K. (2019). Ulvan, a systematic review of extraction, composition and function. *Algal Res.* 39:101422. doi: 10.1016/j.algal.2019.101422

Kim, P. D., Šašek, V., Burketová, L., Čopíková, J., Synytsya, A., Jindřichová, B., et al. (2013). Cell Wall components of *Leptosphaeria maculans* enhance resistance of *Brassica napus*. *J. Agric. Food Chem.* 61, 5207–5214. doi: 10.1021/jf401221v

Klarzynski, O., Plesse, B., Joubert, J.-M., Yvin, J.-C., Kopp, M., Kloareg, B., et al. (2000). Linear b-1,3 Glucans are elicitors of defense responses in tobacco. *Plant Physiol.* 124, 1027–1038. doi: 10.1104/pp.124.3.1027

Lahaye, P. A., and Epstein, E. (1969). Salt toleration by plants, enhancement with calcium. *Science* 166, 395–396. doi: 10.1126/science.166.3903.395

Lahaye, P. A., and Epstein, E. (1971). Calcium and salt toleration by bean plants. *Physiol. Plant.* 25, 213–218. doi: 10.1111/j.1399-3054.1971.tb01430.x

Lahaye, P. A., and Robic, E. (2007). Structure and functional properties of ulvan, a polysaccharide from green seaweeds. *Biomacromolecules* 6, 1765–1774. doi: 10.1021/bm061185q

Lamport, D. T. A., Tan, L., Held, M., and Kieliszewski, M. J. (2018). The role of the primary cell wall in plant morphogenesis. *Int. J. Mol. Sci.* 19:2674. doi: 10.3390/ijms19092674

Lamport, D. T. A., and Várnai, P. (2013). Periplasmic arabinogalactan glycoproteins act as a calcium capacitor that regulates plant growth and development. *New Phytol.* 197, 58–64. doi: 10.1111/nph.12005

Lamport, D. T. A., Varnai, P., and Seal, C. E. (2014). Back to the future with the AGP–Ca^{2+} flux capacitor. *Ann. Bot.* 114, 1069–1085. doi: 10.1093/aob/mcu161

Lee, K. J. D., Sakata, Y., Mau, S. L., Pettolino, F., Bacic, A., Quatrano, R. S., et al. (2005). Arabinogalactan proteins are required for apical cell extension in the moss *Physcomitrella patens*. *Plant Cell* 17, 3051–3065. doi: 10.1105/tpc.105.034413

Levy-Ontman, O., Arad, S., Harvey, D. J., Parsons, T. B., Fairbanks, A., and Tekoah, Y. (2011). Unique *N*-glycan moieties of the 66-kDa cell wall glycoprotein from the red microalga *Porphyridium* sp. *J. Biol. Chem.* 286, 21340–21352. doi: 10.1074/jbc.M110.175042

Lin, Z., Lin, Z., Li, H., and Shen, S. (2012). Sequences analysis of ITS region and 18S rDNA of *Ulva*. *ISRN Bot.* 2012:468193. doi: 10.5402/2012/468193

Lipková, N., Medo, J., Artimová, R., Maková, J., Petrová, J., Javoreková, S., et al. (2021). Growth promotion of rapeseed (*Brassica napus* L.) and blackleg disease (*Leptosphaeria maculans*) suppression mediated by Endophytic bacteria. *Agronomy* 11:1966. doi: 10.3390/agronomy11101966

Lopez-Hernandez, F., Tryfona, T., Rizza, A., Yu, X. L., Harris, M. O. B., Webb, A. A. R., et al. (2020). Calcium binding by Arabinogalactan polysaccharides is important for normal plant development. *Plant Cell* 32, 3346–3369. doi: 10.1105/tpc.20.00027

Ma, Y., Yan, C., Li, H., Wu, W., Liu, Y., Wang, Y., et al. (2017). Bioinformatics prediction and evolution analysis of arabinogalactan proteins in the plant kingdom. *Front. Plant Sci.* 8:66. doi: 10.3389/fpls.2017.00066

Ma, Y., Zeng, W., Bacic, A., and Johnson, K. (2018). "AGPs through time and space" in *Annual plant reviews online*. ed. J. A. Roberts (Chichester, UK: John Wiley & Sons, Ltd.), 767–804.

Mareri, L., Romi, M., and Cai, G. (2019). Arabinogalactan proteins, actors or spectators during abiotic and biotic stress in plants? *Plant. Biosystems* 153, 173–185. doi: 10.1080/11263504.2018.1473525

Martin, R. L., Le Boulch, P., Clin, P., Schwarzenberg, A., Yvin, J.-C., Andrivon, D., et al. (2020). A comparison of PTI defense profiles induced in *Solanum tuberosum* by PAMP and non-PAMP elicitors shows distinct, elicitor-specific responses. *PLoS One* 15:e0236633. doi: 10.1371/journal.pone.0236633

Mathieu-Rivet, E., Kiefer-Meyer, M.-C., Vanier, G., Ovide, C., Burel, C., Lerouge, P., et al. (2014). Protein *N*-glycosylation in eukaryotic microalgae and its impact on the production of nuclear expressed biopharmaceuticals. *Front. Plant Sci.* 5:359. doi: 10.3389/fpls.2014.00359

Mercier, L., Lafitte, C., Borderies, G., Briand, X., Marie-Thérèse Esquerré-Tugayé, M.-T., and Fournier, J. (2001). The algal polysaccharide carrageenans can act as an elicitor of plant defence. *New Phytol.* 149, 43–51. doi: 10.1046/j.1469-8137.2001.00011.x

Mizukami, A. G., Inatsugi, R., Jiao, J., Kotake, T., Kuwata, K., Ootani, K., et al. (2016). The AMOR arabinogalactan sugar chain induces pollen-tube competency to respond to ovular guidance. *Curr. Biol.* 26, 1091–1097. doi: 10.1016/j.cub.2016.02.040

Mócsai, R., Figl, R., Troschl, C., Strasser, R., Svehla, E., Windwarder, M., et al. (2019). *N*-glycans of the microalga *Chlorella vulgaris* are of the oligomannosidic type but highly methylated. *Sci. Rep.* 9:331. doi: 10.1038/s41598-018-36884-1

Morales, J., Kadota, Y., Zipfel, C., Molina, A., and Torres, M.-A. (2016). The *Arabidopsis* NADPH oxidases RbohD and RbohF display differential expression patterns and contributions during plant immunity. *J. Exp. Bot.* 67, 1663–1676. doi: 10.1093/jxb/erv558

Nabti, E., Jha, B., and Hartmann, A. (2017). Impact of seaweeds on agricultural crop production as biofertilizer. *Int. J. Environ. Sci. Technol.* 14, 1119–1134. doi: 10.1007/s13762-016-1202-1

Nagel, A., Sirisakulwat, S., Carle, R., and Neidhart, S. (2014). An acetate–hydroxide gradient for the quantitation of the neutral sugar and Uronic acid profile of Pectins by HPAEC-PAD without Postcolumn pH adjustment. *J. Agric. Food Chem.* 62, 2037–2048. doi: 10.1021/jf404626d

Neik, T. X., Ama, J., Barbetti, M., Edwards, D., and Batley, J. (2020). Understanding host–pathogen interactions in *Brassica napus* in the Omics era. *Plan. Theory* 9:1336. doi: 10.3390/plants9101336

Neik, T. X., Barbetti, M., and Batley, J. (2017). Current status and challenges in identifying disease resistance genes in *Brassica napus*. *Front. Plant Sci.* 8:1788. doi: 10.3389/fpls.2017.01788

Nguema-Ona, E., Coimbra, S., Vicré-Gibouin, M., Mollet, J.-C., and Driouich, A. (2012). Arabinogalactan-proteins in root and pollen tube cells, distribution and functional properties. *Ann. Bot.* 110, 383–404. doi: 10.1093/aob/mcs143

Nguema-Ona, E., Vicré-Gibouin, M., Cannesan, M.-A., and Driouich, A. (2013). Arabinogalactan proteins in root–microbe interactions. *Trends Plant Sci.* 18, 440–449. doi: 10.1016/j.tplants.2013.03.006

Nováková, M., Kim, P. D., Šašek, V., Burketová, L., Jindřichová, B., Šantrůček, J., et al. (2016). Separation and identification of candidate protein elicitors from the cultivation medium of *Leptosphaeria maculans* inducing resistance in *Brassica napus*. *Biotechnol. Prog.* 32, 918–928. doi: 10.1002/btpr.2266

Nováková, M., Šašek, V., Dobrev, P. I., Valentová, O., and Burketová, L. (2014). Plant hormones in defense response of *Brassica napus* to *Sclerotinia sclerotiorum*—reassessing the role of salicylic acid in the interaction with a necrotroph. *Plant Physiol. Biochem.* 80, 308–317. doi: 10.1016/j.plaphy.2014.04.019

Ogawa, K., Arai, M., Naganawa, H., Ikeda, Y., and Kondo, S. (2001). A new β-D-Galactan having 3-*O*-methyl-D-galactose from *Chlorella vulgaris*. *J. Appl. Glycosci.* 48, 325–330. doi: 10.5458/jag.48.325

Palacio-López, K., Tinaz, B., Holzinger, A., and Domozych, D. S. (2019). Arabinogalactan proteins and the extracellular matrix of charophytes: a sticky business. *Front. Plant Sci.* 10:447. doi: 10.3389/fpls.2019.00447

Paulert, R., Ascrizzi, R., Malatesta, S., Berni, P., Noseda, M. D., Mazetto de Carvalho, M., et al. (2021). *Ulva intestinalis* extract acts as biostimulant and modulates metabolites and hormone balance in basil (*Ocimum basilicum* L.) and parsley (*Petroselinum crispum* L.). *Plan. Theory* 10:1391. doi: 10.3390/plants10071391

Paulert, R., Ebbinghaus, D., Urlass, C., and Moerschbacher, B. M. (2010). Priming of the oxidative burst in rice and wheat cell cultures by ulvan, a polysaccharide from green macroalgae, and enhanced resistance against powdery mildew in wheat and barley plants. *Plant Pathol.* 59, 634–642. doi: 10.1111/j.1365-3059.2010.02300.x

Paulert, R., Talamini, V., Cassolato, J. E. F., Duarte, M. E. R., Noseda, M. D., Smania, A., et al. (2009). Effects of sulfated polysaccharide and alcoholic extracts from green seaweed *Ulva fasciata* on anthracnose severity and

growth of common bean (*Phaseolus vulgaris* L). *J. Plant Dis. Prot.* 116, 263–270. doi: 10.1007/BF03356321

Pfeifer, L., and Classen, B. (2020). The cell wall of seagrasses: Fascinating, peculiar and a blank canvas for future research. *Front. Plant Sci.* 11:588754. doi: 10.3389/fpls.2020.588754

Pfeifer, L., Shafee, T., Johnson, K. L., Bacic, A., and Classen, B. (2020). Arabinogalactan-proteins of *Zostera marina* L. contain unique glycan structures and provide insight into adaption processes to saline environments. *Sci. Rep.* 10:8232. doi: 10.1038/s41598-020-65135-5

Pfeifer, L., Utermöhlen, J., Happ, K., Permann, C., Holzinger, A., Schwartzenberg, K., et al. (2021). Search for evolutionary roots of land plant arabinogalactan-proteins in charophytes: presence of a rhamnogalactan-protein in *Spirogyra pratensis* (Zygnematophyceae). *Plant J.* 109, 568–584. doi: 10.1111/tpj.15577

Přerovská, T., Henka, S., Bleha, R., Spiwok, V., Gillarová, S., Yvin, J.-C., et al. (2021). Arabinogalactan-like glycoproteins from *Ulva lactuca* (Chlorophyta) show unique features compared to land plants AGPs. *J. Phycol.* 57, 619–635. doi: 10.1111/jpy.13121

Raboanatahiry, N., Li, H., Yu, L., and Li, M. (2021). Rapeseed (*Brassica napus*), processing, utilization, and genetic improvement. *Agronomy* 11:1776. doi: 10.3390/agronomy11091776

Ramkissoon, A., Ramsubhag, A., and Jayaraman, J. (2017). Phytoelicitor activity of three Caribbean seaweed species on suppression of pathogenic infections in tomato plants. *J. Appl. Phycol.* 29, 3235–3244. doi: 10.1007/s10811-017-1160-0

Ray, D. K., Mueller, N. D., West, P. C., and Foley, J. A. (2013). Yield trends are insufficient to double global crop production by 2050. *PLoS One* 8:e66428. doi: 10.1371/journal.pone.0066428

Renzaglia, K. S., Villareal, J. C., Piatkowski, B. T., Lucas, J. R., and Merced, A. (2017). Hornwort stomata, architecture, and fate of shared with 400 million year old fossil plants without leaves. *Plant Physiol.* 174, 788–797. doi: 10.1104/pp.17.00156

Robic, A., Bertrand, D., Sassi, J.-F., Lerat, Y., and Lahaye, M. (2009). Determination of the chemical composition of ulvan, a cell wall polysaccharide from *Ulva* spp. (Ulvales, Chlorophyta) by FT-IR and chemometrics. *J. Appl. Phycol.* 21, 451–456. doi: 10.1007/s10811-008-9390-9

Rouphael, Y., and Colla, G. (2020). Editorial, biostimulants in agriculture. *Front. Plant Sci.* 11:40. doi: 10.3389/fpls.2020.00040

Šašek, V., Nováková, M., Dobrev, P. I., Valentová, O., and Burketová, L. (2012a). Beta-aminobutyric acid protects *Brassica napus* plants from infection by *Leptosphaeria maculans*. Resistance induction or a direct antifungal effect? *Eur. J. Plant Pathol.* 133, 279–289. doi: 10.1007/s10658-011-9897-9

Šašek, V., Nováková, M., Jindřichová, B., Bóka, K., Valentová, O., and Burketová, L. (2012b). Recognition of avirulence gene AvrLm1 from hemibiotrophic ascomycete *Leptosphaeria maculans* triggers salicylic acid and ethylene signaling in *Brassica napus*. *Mol. Plant-Microbe Interact.* 25, 1238–1250. doi: 10.1094/MPMI-02-12-0033-R

Seifert, G. J., and Roberts, K. (2007). The biology of arabinogalactan proteins. *Annu. Rev. Plant Biol.* 58, 137–161. doi: 10.1146/annurev.arplant.58.032806.103801

Sharma, H. S. S., Fleming, C., Selby, C., Rao, J. R., and Martin, T. (2014). Plant biostimulants, a review on the processing of macroalgae and use of extracts for crop management to reduce abiotic and biotic stresses. *J. Appl. Phycol.* 26, 465–490. doi: 10.1007/s10811-013-0101-9

Shefer, S., Lebendiker, M., Finkelshtein, A., Chamovitz, D. A., and Golberg, A. (2022). Ulvan crude extract's chemical and biophysical profile and its effect as a biostimulant on *Arabidopsis thaliana*. *Algal Res.* 62:102609. doi: 10.1016/j.algal.2021.102609

Shoubaky, G., and Salem, E. A. (2016). Effect of abiotic stress on endogenous phytohormones profile in some seaweeds. *Int. J. Pharmacogn. Phytochem. Res.* 8, 124–134.

Showalter, A. M. (2001). Arabinogalactan-proteins, structure, expression and function. *Cell. Mol. Life Sci.* 58, 1399–1417. doi: 10.1007/PL00000784

Sørensen, I., Pettolino, F. A., Bacic, A., Ralph, J., Lu, F., O'Neill, M. A., et al. (2011). The charophycean green algae provide insights into the early origins of plant cell walls. *Plant J.* 68, 201–211. doi: 10.1111/j.1365-313X.2011.04686.x

Stadnik, M. J., and Freitas, M. B. (2014). Algal polysaccharides as source of plant resistance inducers. *Trop. Plant Pathol.* 39, 111–118. doi: 10.1590/S1982-56762014000200001

Staudacher, E. (2012). Methylation—an uncommon modification of glycans. *Biol. Chem.* 393, 675–685. doi: 10.1515/hsz-2012-0132

Steiner, A. A. (1984). "The universal nutrient solution." in *The Sixth International Congress on "Soilless Culture."* Apr 29-May 5; Pudoc, Wageningen, The Netherlands, 633–650.

Tan, L., Eberhard, S., Pattathil, S., Warder, C., Glushka, J., Yuan, C., et al. (2013). An *Arabidopsis* cell wall proteoglycan consists of pectin and arabinoxylan covalently linked to an arabinogalactan protein. *Plant Cell* 25, 270–287. doi: 10.1105/tpc.112.107334

Temple, H., Mortimer, J. C., Tryfona, T., Yu, X., Lopez-Hernandez, F., Sorieul, M., et al. (2019). Two members of the DUF579 family are responsible for arabinogalactan methylation in *Arabidopsis*. *Plant Direct.* 3:e00117. doi: 10.1002/pld3.117

Templeton, D. W., Quinn, M., Van Wychen, S., Hyman, D., and Laurens, L. M. L. (2012). Separation and quantification of microalgal carbohydrates. *J. Chromatogr. A* 1270, 225–234. doi: 10.1016/j.chroma.2012.10.034

Thordal-Christensen, H., Zhang, Z., Wei, Y., and Collinge, D. B. (1997). Subcellular localization of H_2O_2 in plants. H_2O_2 accumulation in papillae and hypersensitive response during the barley—powdery mildew interaction. *Plant J.* 11, 1187–1194. doi: 10.1046/j.1365-313X.1997.11061187.x

Torres, M. A., Dangl, J. L., and Jones, D. G. (2002). Arabidopsis gp91phox homologues AtrbohD and AtrbohF are required for accumulation of reactive oxygen intermediates in the plant defense response. *PNAS* 99, 517–522. doi: 10.1073/pnas.012452499

Trdá, L., Janda, M., Macková, D., Pospíchalová, R., Dobrev, P. I., Burketová, L., et al. (2019). Dual mode of the saponin aescin in plant protection, antifungal agent and plant defense elicitor. *Front. Plant Sci.* 10:1448. doi: 10.3389/fpls.2019.01448

Van de Wouw, A. P., and Howlett, B. J. (2020). Advances in understanding the *Leptosphaeria maculans—Brassica* pathosystem and their impact on disease management. *Can. J. Plant Pathol.* 42, 149–163. doi: 10.1080/07060661.2019.1643788

Van Loon, L. C., Rep, M., and Pieterse, C. M. J. (2006). Significance of inducible defense-related proteins in infected plants. *Annu. Rev. Phytopathol.* 44, 135–162. doi: 10.1146/annurev.phyto.44.070505.143425

Vieira, H. H., Bagatini, I. L., Guinart, C. M., Vieira, A. A. H., Vieira, H. H., Bagatini, I. L., et al. (2016). tufA gene as molecular marker for freshwater Chlorophyceae. *Algae* 31, 155–165. doi: 10.4490/algae.2016.31.4.14

Villa-Rivera, M. G., Cano-Camacho, H., López-Romero, E., and Zavala-Páramo, M. G. (2021). The role of Arabinogalactan type II degradation in plant-microbe interactions. *Front. Plant Sci.* 12:730543. doi: 10.3389/fmicb.2021.730543

Waszczak, C., Carmody, M., and Kangasjärvi, J. (2018). Reactive oxygen species in plant signaling. *Annu. Rev. Plant Biol.* 69, 209–236. doi: 10.1146/annurev-arplant-042817-040322

Wichard, T., Charrier, B., Mineur, F., Bothwell, J. H., Clerck, O. D., and Coates, J. C. (2015). The green seaweed *Ulva*, a model system to study morphogenesis. *Front. Plant Sci.* 6:72. doi: 10.3389/fpls.2015.00072

Wiesel, L., Newton, A. C., Elliott, I., Booty, D., Gilroy, E. M., Birch, P. R. J., et al. (2014). Molecular effects of resistance elicitors from biological origin and their potential for crop protection. *Front. Plant Sci.* 5:655. doi: 10.3389/fpls.2014.00655

Yaich, H., Garna, H., Besbes, S., Paquot, M., Blecker, C., and Attia, H. (2013). Effect of extraction conditions on the yield and purity of ulvan extracted from *Ulva lactuca*. *Food Hydrocoll.* 31, 375–382. doi: 10.1016/j.foodhyd.2012.11.013

Yang, J., Duan, G., Li, C., Liu, L., Han, G., Zhang, Y., et al. (2019). The crosstalks between jasmonic acid and other plant hormone signaling highlight the involvement of jasmonic acid as a core component in plant response to biotic and abiotic stresses. *Front. Plant Sci.* 10:1349. doi: 10.3389/fpls.2019.01349

Yemm, E. W., and Willis, A. J. (1954). The estimation of carbohydrates in plant extracts by anthrone. *Biochem. J.* 57, 508–514. doi: 10.1042/bj0570508

Zipfel, C., Robatzek, S., Navarro, L., Oakeley, E., Jones, J. D. G., Felix, G., et al. (2004). Bacterial disease resistance through flagellin perception in *Arabidopsis*. *Nature* 428, 764–767. doi: 10.1038/nature02485

Conflict of Interest: The authors declare that the research was conducted in the absence of any commercial or financial relationships that could be construed as a potential conflict of interest.

Publisher's Note: All claims expressed in this article are solely those of the authors and do not necessarily represent those of their affiliated organizations, or those of the publisher, the editors and the reviewers. Any product that may

be evaluated in this article, or claim that may be made by its manufacturer, is not guaranteed or endorsed by the publisher.

frontiers | Frontiers in Plant Science

TYPE Original Research
PUBLISHED 26 September 2022
DOI 10.3389/fpls.2022.864086

OPEN ACCESS

EDITED BY
Essaid Ait Barka,
Université de Reims Champagne-Ardenne, France

REVIEWED BY
Hyong Woo Choi,
Andong National University, South Korea
Francesco Spinelli,
University of Bologna, Italy

*CORRESPONDENCE
Choong-Min Ryu
cmryu@kribb.re.kr

SPECIALTY SECTION
This article was submitted to Plant Pathogen Interactions, a section of the journal Frontiers in Plant Science

RECEIVED 28 January 2022
ACCEPTED 08 August 2022
PUBLISHED 26 September 2022

CITATION
Kim D, Riu M, Oh S-K and Ryu C-M (2022) Extracellular self-RNA: A danger elicitor in pepper induces immunity against bacterial and viral pathogens in the field. *Front. Plant Sci.* 13:864086. doi: 10.3389/fpls.2022.864086

Extracellular self-RNA: A danger elicitor in pepper induces immunity against bacterial and viral pathogens in the field

Doyeon Kim[1,2], Myoungjoo Riu[1,3], Sang-Keun Oh[3] and Choong-Min Ryu[1,2]*

[1]Molecular Phytobacteriology Laboratory, Infectious Disease Research Center, KRIBB, Daejeon, South Korea, [2]Department of Biosystems and Bioengineering, KRIBB School of Biotechnology, University of Science and Technology, Daejeon, South Korea, [3]Department of Applied Biology, College of Agriculture & Life Sciences, Chungnam National University, Daejeon, South Korea

Plants and animals serve as hosts for microbes. To protect themselves from microbe-induced damage, plants and animals need to differentiate self-molecules/signals from non-self, microbe-derived molecules. Damage-associated molecular patterns (DAMPs) are danger signals released from the damaged host tissue or present on the surface of stressed cells. Although a self-extracellular DNA has previously been shown to act as a DAMP in different plant species, the existence of a self-extracellular RNA (eRNA) as a danger signal in plants remains unknown. Here, we firstly evaluated the ability of a pepper self-eRNA to activate immunity against viral and bacterial pathogens under field conditions. Pepper leaves pre-infiltrated with self-eRNA exhibited reduced titer of the naturally occurring *Tomato spotted wilt virus* and diminished symptoms of *Xanthomonas axonopodis* pv. *vesicatoria* infection through eliciting defense priming of abscisic acid signaling. At the end of the growing season at 90 days after transplanting, pepper plants treated with self- and non-self-eRNAs showed no difference in fruit yield. Taken together, our discovery demonstrated that self-eRNA can successfully activate plant systemic immunity without any growth penalty, indicating its potential as a novel disease management agent against a broad range of pathogenic microbes.

KEYWORDS

DAMP, trade-off, self-eRNA, plant immunity, pepper

Introduction

Plants and animals serve as hosts for pathogenic microbes and suffer microbe-induced damage (Heil and Vega-Muñoz, 2019). In animals, the perception of and response to host-derived (self) and pathogen-derived (non-self) molecules have been investigated for a long time (Schlee and Hartmann, 2016; Barbero et al., 2021). By contrast, in plants, the perception of self- and non-self-signals and response to damage-associated molecular

patterns (DAMPs) have not received sufficient attention (Bhat and Ryu, 2016; Heil and Vega-Muñoz, 2019). In 2015, Mazzoleni and colleagues were the first to report the autotoxicity of self-extracellular DNA (self-eDNA) as a mechanism of negative plant–soil feedback (Mazzoleni et al., 2015a). Further investigation revealed that the self-inhibition of growth was not limited to plant species, and was also observed to function in other organisms including bacteria, fungi, algae, protozoa, and insects in a concentration-dependent manner (Mazzoleni et al., 2015b). Such a profound discovery led plant scientists to identify the danger signals or DAMPs released from host tissues damaged/degraded by insect and microbial attacks (Duran-Flores and Heil, 2014; Barbero et al., 2016). A recent mechanistic and cell biology study revealed that non-self-eDNA penetrates root cells, leading to limited cell permeability, chloroplast dysfunction, and reactive oxygen species (ROS) generation, while self-eDNA maintains the intercellular space and triggers hypersensitive response and systemic acquired resistance (Chiusano et al., 2021). However, most of the previous studies focused on self-eDNA-induced plant autotoxicity rather than on plant immunity activation.

Recently, the application of self-eDNA in plants revealed the existence of self-eDNA-triggered immunity against microbial pathogens. Self-eDNA fragments shorter than 700 bp in size play a critical role in the indirect activation of plant immune system against bacterial pathogens through hydrogen peroxide (H_2O_2) and mitogen-activated plant kinase (MAPK) signaling (Duran-Flores and Heil, 2018).

Like DAMP signaling in animals, infiltration of *Arabidopsis thaliana* seedling leaves with single-stranded oligodeoxynucleotides (ssODNs) elicited defense response against *Pseudomonas syringae* pv. *tomato* (*Pto*) and *Botrytis cinerea* but not against *Tobacco mosaic virus* and inhibited growth via the BAK co-receptor and ROS generation (Toum et al., 2020). Besides plant self-eDNAs, a mixture of fragmented 100 μg/ml non-self-eDNAs derived from plant pathogenic fungi including *Phytophthora capsici, Fusarium oxysporum,* and *Rhizoctonia solani* reduced the mortality of pepper (*Capsicum annuum* L.) plants by up to 40% (Serrano-Jamaica et al., 2020). Transcriptome analysis of tomato (*Solanum lycopersicum* L.) leaves treated with fragmented self-eDNA revealed the induction of plant immune-related genes including pathogenesis-related (*PR*) proteins, calcium-dependent protein kinase 1 (*CPK1*), heat shock transcription factors (*HSFs*), heat shock proteins (*HSFs*), receptor-like kinases (*RLKs*), and ethylene-responsive factors (*ERFs*; Barbero et al., 2021). Although self-eDNA-induced plant immunity has been studied extensively, the topic of extracellular RNA (eRNA)-induced plant immunity has not been intensively exploited, with the exception of *Arabidopsis* leaf infiltration with a non-self-eRNA (bacterial rRNA), which activated plant resistance against *Pseudomonas syringae* pv. tomato (Lee et al., 2016). Nonetheless, the role of self-eRNA in plant immunity remains largely unknown.

In line with our previous discovery of bacterial eRNA as a trigger of plant immunity, we evaluated whether self-eRNAs activate resistance against microbial pathogens in pepper plants. Experiments were conducted under field conditions using pepper plants challenged with eRNAs derived from pepper (self-eRNA) and *Nicotiana benthamiana* (non-self-plant-eRNA), and those derived from virulent and avirulent pathogens. Considering the growth penalty caused by self-eDNA application, we measured plant growth and yield at the end of the growing season. Intriguingly, self-eRNA-induced immunity was enough to protect pepper plants against the naturally occurring *Tomato spotted wilt virus (TSWV)*. To the best of our knowledge, this is the first report of self-eRNA-induced plant immunity against microbial pathogens under field conditions.

Materials and methods

Preparation of seedlings and bacteria

Pepper (*Capsicum annuum* L. cv. Bulkala) and *Nicotiana benthamiana* (*Nb*) seeds were sown on autoclaved soil-less potting medium (Punong Horticulture Nursery Medium Low; Punong Co. Ltd., Gyeongju, South Korea) containing zeolite, perlite, color dust, and lime (pH = 4.5 to 7.5). The seedlings of both plant species were cultivated for 6 weeks at 28°C under 12 h light/12 h dark cycle and approximately 7,000 lux light intensity using fluorescent lamps. Leaves of 6-week-old plants were harvested, immediately frozen in liquid nitrogen, and stored at −80°C until needed for RNA extraction.

Xanthomonas axonopodis pv. *vesicatoria* (*Xav*) and *Pseudomonas syringae* pv. *tomato* (*Pto*) were cultured at 30°C for 48 h in plates containing Luria-Bertani (LB; Difco Laboratories, Detroit, MI, United States) agar and King's B (KB; Difco Laboratories) agar media, respectively. Cultures of *Xav* and *Pto* were centrifuged at 16,000 × *g* for 5 min. The supernatant was discarded and the pellet containing bacterial cells was used to perform subsequent experiments.

Preparation of plant and bacterial eRNAs

Total eRNAs were isolated from pepper cultivars Bulkala (for 2020 field trial) and Asia Jumbo (for 2021 field trial), *Nb* plants, and bacterial pathogens (*Xav* and *Pto*) using TRIzol Reagent (Invitrogen, Carlsbad, CA, United States), according to the standard protocol described previously (Lee et al., 2016).

To isolate bacterial eRNAs, the centrifuged *Xav* and *Pto* cells were mixed with TRIzol Reagent and incubated at room temperature (RT) for 5 min. Then, chloroform was added to each sample, and centrifugation was performed at 10,000 × *g* for 15 min at 4°C. Subsequently, the upper phase was transferred to a new tube, and nucleic acid was precipitated by adding isopropyl alcohol. The resultant bacterial RNA pellet was resuspended in nuclease-free water.

To isolate plant eRNAs, the previously frozen leaves of 6-week-old pepper and *Nb* seedlings were ground into a fine powder using a mortar and pestle. The powdered leaf tissue (100 mg) of each plant species was mixed with 1 ml of TRIzol Reagent and incubated at RT for 5 min. Plant eRNAs were isolated as described above.

The obtained bacterial and plant eRNAs were treated with RNase and diluted to a concentration of 100 ng/μl.

Field trials

Field trials were conducted in April to August and 2021 in Nonsan, Chungcheongnam-do, South Korea (36.23577°N, 127.18946°E), where plants are occured by multiple viral diseases each year. All necessary permits were obtained from landowners to conduct these trials. Pepper seedlings were transplanted at a distance of 30 cm in furrows covered with black polyethylene film to prevent weed growth before transplanting. To test the induction of resistance under field conditions, leaves of 1-month-old pepper seedlings were infiltrated with 1 ml of 100 ng/μl plant and bacterial eRNAs. Leaves infiltrated with 1 ml of sterilized water were used as a negative control. Seedlings drenched with 1 mM benzothiadiazole (BTH; Bion 50 WG, Syngenta, Basel, Switzerland) served as a positive control. Plants roots were drenched with 50 mL of 1 mM BTH twice: first at 1 week prior to self-eRNA and non-self-eRNA infiltration, and again on the day of self-eRNA and non-self-eRNA infiltration. Each treatment was replicated four times in a completely randomized block design, with 12 plants per block in 2020 and 9 plants per block in 2021.

Bacterial Pathogen Inoculation

Plants were challenged with *Xav* as described previously (Lee et al., 2017). Briefly, at one week after self-eRNA and non-self-eRNA (*Xav*, *Pto,* and *Nb*) infiltration (which coincided with 2 -3 weeks after field transplantation), two leaves per pepper seedling were infiltrated with 500 μL of *Xav* suspension (optical density $(OD)_{600} = 0.01$); overall, five plants per block in 2020 and six plants per block in 2021 were inoculated with *Xav*. One week after pathogen inoculation, disease severity on pepper leaves was scored on a scale of 0–5, as follows: 0, no symptom; 1, mild chlorosis; 2, chlorosis; 3, severe chlorosis and mild necrosis; 4, necrosis; 5, necrosis with cell death.

Diagnosis of naturally occurring viral diseases

To evaluate virus titers in field-grown plants, qRT-PCR was performed as described previously (Kong et al., 2018). Briefly, ten leaves per replication were randomly sampled 90 days after plant and bacterial eRNA infiltration and BTH application, and immediately frozen in liquid nitrogen. Total eRNA was isolated from the frozen leaves using TRIzol Reagent (Molecular Research Inc., Cincinnati, OH, United States), according to the manufacturer's instructions and as described in our previous study (Lee et al., 2017; Kong et al., 2018). First-strand cDNA was synthesized from 2 μg of DNase-treated total eRNA using oligo dT primers and Moloney murine leukemia virus reverse transcriptase (Enzynomics, Daejeon, Korea). Then, qRT-PCR was performed using the synthesized cDNA, iQ™ SYBR® Green Supermix (Bio-Rad Inc., Hercules, CA, United States), and 10 pM primers under the following cycling conditions: initial polymerase activation for 10 min at 95°C, followed by 40 cycles of 30 s at 95°C, 60 s at 55°C, and 30 s at 72°C. Viral sequence-specific primer pairs were used to identify *Tomato yellow leaf curl virus* (*TYLCV; TYLCV*-F: 5′-CGCCCGCCTC GAAGGTTC-3′; *TYLCV*-R: 5′-TCGTCGCTTGTTTGTG CCTTG-3′) and *TSWV* (*TSWV*-F: 5′-ATGTCTAAGGTTAAGC TCAC-3′; *TSWV*-R: 5′-TCAAGCAAGTTCTGCGAGTT-3′), as described previously (Kong et al., 2018). Gene transcript levels were normalized relative to that of the pepper *ubiquitin* (*CaUBQ*) gene, which was amplified using primers *CaUBQ*-F (5′-GCACAAGCACAAGAAGGTTAAG-3′) and *CaUBQ*-R (5′-GCACCACACTCAGCATTAGGA-3′). Relative transcript levels were calculated using the $2^{-\Delta\Delta CT}$ method. Standard error of means among replicates were calculated using JMP IN ver. 4.0 (SAS Institute Inc., Cary, NC, United States) and Bio-Rad manager ver. 2.1 (Bio-Rad CFX Connect).

Expression Analysis of Defense-related genes

The expression of defense-related genes, including *Defensin (CaDEF), Chitinase type 2 (CaCHI2), 9-Lipoxygenase (CaLOX1)*, and *Pathogenesis-related 4 (CaPR4)*, was evaluated in pepper plants at the end of the growing season (i.e., at 90 days after RNA leaf-infiltration and before harvesting) by qRT-PCR. Pepper cDNA was prepared as described above, and qRT-PCR was performed using gene-specific primer pairs listed in Supplementary Table S1 (Huh et al., 2015; Kong et al., 2018), according to the same protocol as that used for virus quantification (described above).

Assessment of plant yield

To investigate whether plant and bacterial eRNAs influence plant growth, fruit number and weight per plant were recorded in plant and bacterial eRNA treatments and compared with the corresponding values obtained in water and BTH treatments. The commercially valued red pepper fruits were harvested twice from

mid- to end-August, which coincided with approximately 100 days post-treatment. Fruit number per plant was recorded at each harvest. Total fruit weight per plant was also calculated at each harvest.

Direct Effect of Pepper eRNA on *Xanthomonas axonopodis* pv. *vesicatoria'* Growth

Xav was cultured in LB agar at 30°C overnight. A single colony was then used to inoculate freshly prepared LB broth, and cultured in an incubator at 220 rpm and 30°C. 20 µl of pre-culture was added to 180 µl of fresh full-strength, 10-fold diluted (0.1), and 100-fold diluted (0.01) LB broth into a 96-well plate. To inoculate each medium with the same number of *Xav* cells, the bacterial cells were spun down by centrifugation at 8,000 rpm for 5 min at room temperature. The bacterial cell pellets were resuspended in full-strength, 10-fold dilution, and 100-fold dilution treatments, and then transferred into a 96-well plate. Then, 100 ng/µl pepper self-eRNA and *Pto* non-self-eRNA were used to inoculate each medium, which was pre-inoculated with *Xav* at (OD_{600} = 0.2). Polymyxin B (32 µg/ml), an antibiotic that kills Gram-negative bacteria, was used as a positive control. Treatment with *Xav* alone was used as a negative control. The growth of *Xav* was monitored for 45 h using Spark™ 10M multimode microplate reader (Tecan Trading AG, Switzerland).

Statistical analysis

The experimental datasets were subjected to ANOVA using JMP IN software. The statistical significance of differences among treatments was determined based on the *F*-value at $p = 0.05$. When a significant F-value was obtained for treatments, separation of means was accomplished using Fisher's protected least significant difference (LSD) test at $p = 0.05$.

Results

Self- and non-self-eRNAs induce plant immunity under field conditions

The severity of bacterial spot disease on pepper seedlings treated with self-eRNA was 2.99, which was 1.4-fold lower than that on plants treated with water (negative control; disease severity = 4.06; Figure 1). Plants treated with non-self-eRNAs, including *Xav* and *Pto* eRNAs, showed no significant difference in disease severity compared with the control. However, plants treated with BTH exhibited a 2.2-fold reduction in disease severity compared with the control.

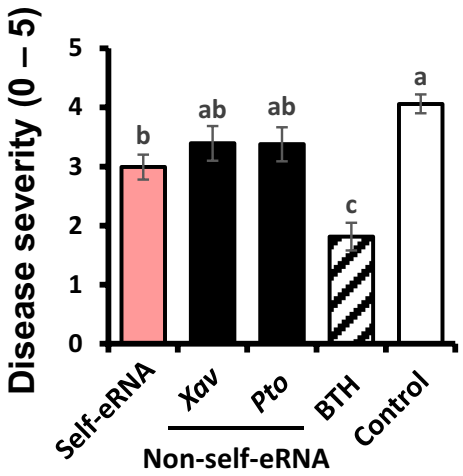

FIGURE 1
Activation of plant immunity in pepper plants treated with extracellular RNAs (eRNAs) and benzothiadiazole (BTH) under field conditions. Leaves of pepper plants were infiltrated with self-eRNA (derived from pepper plants) and non-self-bacterial eRNAs (OD_{600}=0.01; derived from virulent pathogens, *Xanthomonas axonopodis* pv. *vesicatoria* [*Xav*] and *Pseudomonas syringae* pv. *tomato* [*Pto*]), and disease severity was determined at 7 days post-infiltration. Data represent mean±standard error of mean (SEM). Different letters indicate statistically significant differences between eRNA/BTH and water (control) treatments (p=0.05; least significant difference [LSD] test).

In control plants, the titer of naturally occurring *TSWV* and *TYLCV* was 0.062 and 0.18, respectively, as shown by qRT-PCR analysis. The titer of *TSWV* in self-eRNA-treated plants was 0.04, which was 1.6-fold lower than that in control plants (Figure 2A). Non-self-eRNA treatments did not show any difference relative to the control (Figure 2A). The titer of *TYLCV* showed no significant difference among treatments (Figure 2B).

Measurement of pepper fruit yield

Fruit number and weight showed no significant difference among the various treatments, except the BTH treatment (Figures 3A,B). The number and weight of fruits in BTH-treated plants were 12.91 per plant and 270.83 g, respectively, indicating a reduction by 7.12- and 10.00-fold compared with the control (Figures 3A,B).

Upregulation of Defense-related Genes by Self-eRNA Treatment

To investigate the mechanism of immune response activation in pepper by self-eRNA treatment, the expression of defense-related genes was examined. Relative expression levels of *CaDEF* and *CaCHI2* in self-eRNA treated plants were

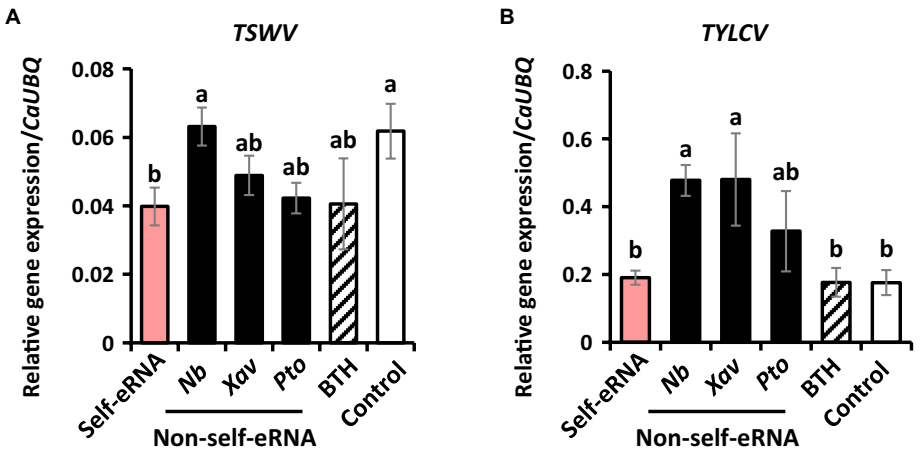

FIGURE 2
Self-eRNA treatment induces plant immunity against the naturally occurring *Tomato spotted wilt virus (TSWV)* and *Tomato yellow leaf curl virus (TYLCV)*. Induction of immunity against *TSWV* **(A)** and *TYLCV* **(B)** in pepper plants by pre-infiltration with self-eRNA (derived from pepper) and non-self-eRNA derived from *N. benthamiana (Nb)*, *X. axonopodis pv. vesicatoria (Xav)*, and *P. syringae pv. tomato (Pto)*. BTH treatment used as a positive control. The expression of immunity-related genes was evaluated by qRT-PCR at 90 days post-infiltration. The housekeeping gene *CaUBQ* was used as an internal reference. Data represent mean±SEM. Different letters indicate statistically significant differences between control and other treatments (p=0.05; LSD test).

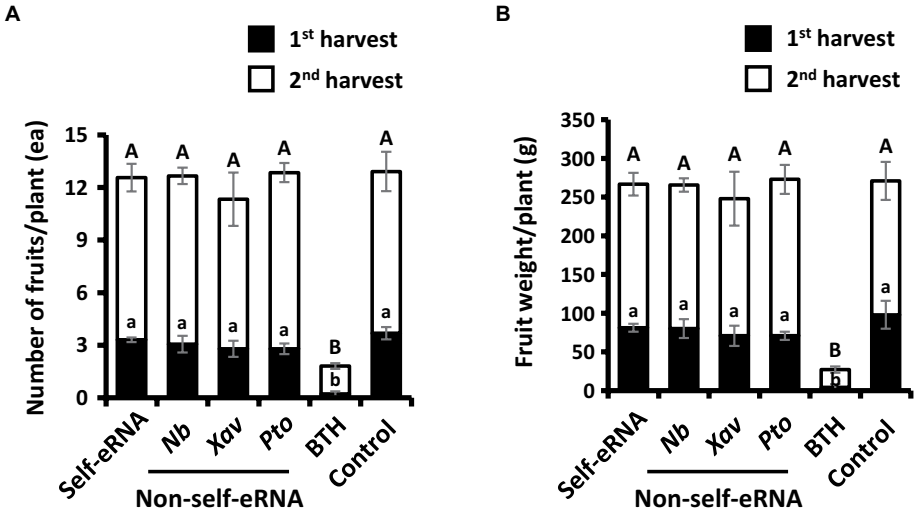

FIGURE 3
Effect of self- and non-self-eRNAs on pepper marketable yield. a, b Fruit number **(A)** and fruit weight **(B)** per plant treated with self-eRNA derived pepper and non-self-eRNA that including *N. benthamiana (Nb)*, *X. axonopodis pv. vesicatoria (Xav)*, and *P. syringae pv. tomato (Pto)*, 1 mM BTH, and control. Fruit number and weight were measured in the second round of harvest at 80 and 90 days post-infiltration, respectively. Data represent mean±SEM. Different letters indicate statistically significant differences between control and other treatments (p=0.05; LSD test).

increased by 1.43- and 1.42-fold, respectively, compared with the control (Figures 4A,B), while those of *CaLOX1* and *CaPR4* showed no significant differences relative to the control (Figures 4C,D). Both *CaDEF* and *CaCHI2* are related to ABA and JA signaling (Hong et al., 2000; Hong and Hwang, 2002; Do et al., 2004), whereas *CaPR4* and *CaLOX1* are known as SA and JA marker genes (Hwang and Hwang, 2009; Hwang et al., 2014). Together, these findings suggest that self-eRNA elicited pepper immunity through ABA signaling.

Direct Effect of Self-eRNA on *Xanthomonas axonopodis* pv. *vesicatoria'* Growth

To evaluate the direct effect of self-eRNA on the growth of *Xav*, systemic translocation of the introduced self-eRNA was monitored. The OD600 of *Xav* amended with 100 ng/μl self-eRNA and non-self-eRNA (*Pto*) was 0.37 and 0.35 respectively, while that of the polymyxin B treatment was 0.14 in full-strength LB (Figure 5 left panel). Bacterial growth in all treatments, except polymyxin B treatment, showed no significant difference compared with the control (Figure 5 left panel). In 10-fold diluted LB, the OD_{600} of self-eRNA and non-self-eRNA was 0.29 and 0.30, respectively (Figure 5 middle panel). In 100-fold diluted LB, no statistically significant differences were detected among the various treatments (Figure 5 right panel). These results indicate that self-eRNA and non-self-eRNA could not directly inhibit the growth of *Xav*.

Discussion

Our results confirmed the activation of plant systemic immunity by self-eRNA in field-grown pepper plants. Plant perception of nucleic acids (e.g., RNA and DNA) had not been intensively studied until 2015 (Mazzoleni et al., 2015a). In the field,

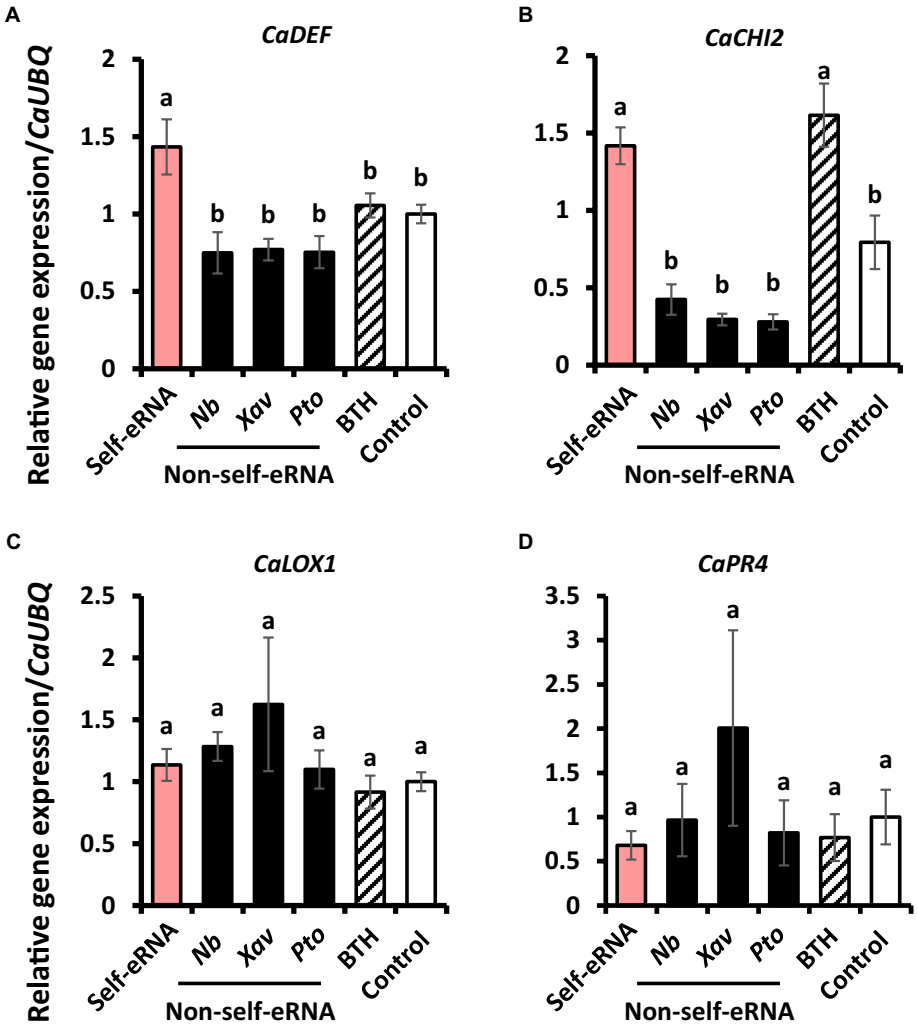

FIGURE 4
Induction of defense-related genes in pepper following self-eRNA treatment under field conditions. Quantifications of the expression of marker genes of the *CaDEF* **(A)**, *CaCHI2* **(B)**, *CaLOX1* **(C)**, and *CaPR4* **(D)**. *CaDEF* related abscisic acid, salicylic acid, and jasmonic acid signaling pathways in plants. *CaCHI2* related abscisic acid, ethylene, and jasmonic acid signaling pathways in plants. *CaLOX1* related salicylic acid and ethylene signaling pathways in plants. *CaPR4* related jasmonic acid signaling pathway in plants. Plants treated with self-eRNA and non-self-eRNA that including *N. benthamiana* (*Nb*), *X. axonopodis* pv. *vesicatoria* (*Xav*), and *P. syringae* pv. tomato (*Pto*), 1 mM BTH, and control. *CaUBQ* was used as a housekeeping gene for data normalization. Data represent mean ± SEM. Different letters indicate statistically significant differences between control and other treatments (p=0.05; LSD test).

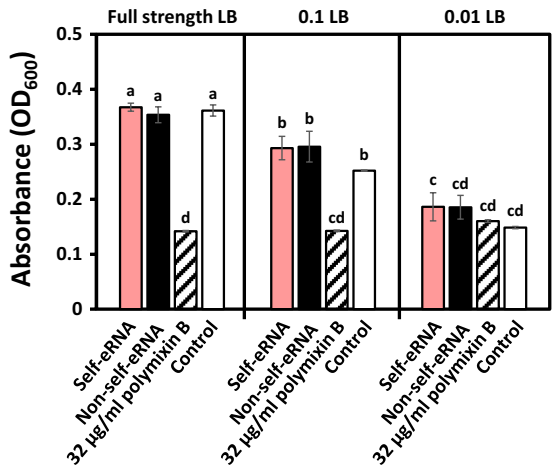

FIGURE 5
Evaluation of the direct effect of self-eRNA treatment on the growth of *X. axonopodis* pv. *vesicatoria (Xav)*. Growth of *XaV* amended with 100 ng/μl self-eRNA (pepper) and non-self-eRNA (*P. syringae* pv. *tomato*) was monitored in full-strength LB (left panel), 10-fold diluted (0.1) LB (middle panel), and 100-fold diluted (0.01) LB (right panel) for 45 h. Polymyxin B (32 μg/ml) was used as a positive control. Data represent mean ± SEM (n = 3). Different letters indicate statistically significant differences between control and other treatments (p = 0.05; LSD test).

self-eRNA clearly activated plant immunity against bacterial and viral pathogens (Figures 1, 2). The systemically translocated eRNA itself did not alter the bacterial pathogen growth (Figure 5) indicating that plants were protected by the activation of systemic immunity.

Compared with the autotoxicity induced in plants by self-eDNA application previously (Barbero et al., 2016; Duran-Flores and Heil, 2018; Serrano-Jamaica et al., 2020; Toum et al., 2020), it is noteworthy that self-eRNA-induced plant immunity was not accompanied by any growth penalty (also referred to as the allocation fitness cost; Figure 3). We cannot explain why allocation fitness cost is not required in the field trial of self-eRNA, but we have two hypotheses. Firstly, we hypothesize that self-eRNA-elicited plant immunity is not dependent on ROS and SA-mediated PR protein activation, which are strongly induced by self-eDNA treatment (Duran-Flores & Heil, 2018; Chiusano et al., 2021). Previous studies demonstrated that ROS and PR protein activation are related to the SA-dependent signaling pathway and result in a strong growth penalty (Clarke et al., 2000; Heil et al., 2000; Noutoshi et al., 2005; Walters and Heil, 2007; Kouzai et al., 2018). In the current study and many previous studies, the application of BTH (also known as acibenzolar-S-methyl) significantly reduced plant growth (Clarke et al., 2000; Heil et al., 2000; Noutoshi et al., 2005; Walters and Heil, 2007; Kouzai et al., 2018). The mode of action of BTH (as an SA analog) on the allocation fitness cost and plant immunity induction demonstrates the induction of ROS and PR proteins (Miura et al., 2013; Huot et al., 2014; Herrera-Vásquez et al., 2015; Kouzai et al., 2018; Poór, 2020). Secondly, we speculated that defense signaling can be activated independent of SA signaling, such as induced systemic resistance, by plant growth-promoting rhizobacteria (PGPR). Previous studies demonstrated that the application of PGPR and bacterial determinants on pepper and other plant species at the seedling stage successfully protected them from bacterial and viral pathogens and had no detrimental effect on plant growth; rather, plant growth was enhanced in many cases (Kong et al., 2018). Characterization of PGPR-mediated induced systemic resistance is mostly dependent on jasmonic acid (JA) and ethylene signaling rather than on SA signaling, which is activated by necrotizing pathogen-induced systemic acquired resistance (Van Der Ent et al., 2009; Beneduzi et al., 2012). Sufficient data are not yet available to determine whether JA and ethylene signaling mediate self-eRNA-induced plant immunity. Detailed mechanistic analysis of defense signaling by self-eRNA treatment under controlled conditions will enable us to understand the relationship between plant immunity and growth.

Some other questions, such as how plants recognize self-eRNA and which epitope of self-eRNA is perceived by plant receptors, remain unanswered. Despite RNA-sequencing and *Arabidopsis* mutant analysis, plant receptors potentially involved in the perception of non-self-eRNA have not been identified to date (Lee et al., 2016). However, in animal cells, the mechanism of self-eRNA perception has been proposed and confirmed (Schlee and Hartmann, 2016; Heil and Vega-Muñoz, 2019). For example, in the mammalian system, Toll-like receptors (3, 7, 8, and 10), RIG-like receptors, and protein kinase R (PKR) have been reported to function as mammalian RNA sensors (Alexopoulou et al., 2001; Kato et al., 2006; Mancuso et al., 2009; Mayo and Cole, 2017; Heil and Vega-Muñoz, 2019). Further molecular and biochemical evaluation is needed to identify potential plant receptor(s) using *Arabidopsis* as a model plant species. It would be interesting to determine the eRNA epitope that directly binds to a plant receptor. Similar to the case study of non-self-eRNA in *Arabidopsis*, differential fractionation of eRNA could be conducted in pepper to identify the eRNA determinant by screening for the activation of plant immunity and the biochemical response, such as callose deposition, to microbe-associated molecular pattern (MAMP) recognition by self-eRNA (Lee et al., 2016). Based on the previous studies of pattern recognition, rRNA, tRNA, small RNA, and each fragmented product are good candidates for MAMPs. The self-eRNA, as an example of DAMP and MAMP, must be conserved within and variable between plant species.

ABA signaling is widely regarded as an important player in plant immunity as well as in critical abiotic stress responses (Lievens et al., 2017). ABA signaling is involved in plant defense against insect pests including thrips, which is a well-known vector of plant DNA viruses (Geminivirus) such as *TSWV* (Bedford et al., 1994; Escobar-Bravo et al., 2018; Guo et al., 2020). We speculate that the lower level of TSWV in self-eRNA-pretreated pepper plants is the result of reduced virus-vector infestation through plant immune activation *via* ABA signaling (Figures 2, 4A,B). Moreover, the long-lasting immune memory conferred by self-eRNA suggests its potential for field applications.

In conclusion, we report, for the first time, self-eRNA-induced plant immunity against bacterial and viral pathogens in pepper. Our results were obtained from field trials, indicating that

self-eRNA can potentially be applied to plants in the agricultural field in the near future. Moreover, self-eRNA-induced immune activation is advantageous, since it is not compromised by a growth penalty. However, the concept of self-eRNA-induced plant immunity is in its infancy, and intensive investigation is required to understand why and how plants manipulate the balance between immunity and growth.

Data availability statement

The original contributions presented in the study are included in the article/Supplementary material, further inquiries can be directed to the corresponding author.

Author contributions

DK conducted the field trial, performed viral diagnosis. MR examined the expression of defense-related genes and participated in the field trial. DK and MR created the figures and wrote the manuscript. S-KO reviewed the manuscript. C-MR conceived the study, participated in its design and coordination, and wrote the manuscript.

Funding

This research was supported by grants from the Rural Development Administration (RDA), Strategic Initiative for Microbiomes in Agriculture and Food, Ministry of Agriculture, Food and Rural Affairs, Republic of Korea (as part of the multi-ministerial Genome Technology to Business Translation Program; 918017-4), Center for Agricultural Microorganism and Enzyme (Project No. PJ015049) of RDA, and the KRIBB Initiative Program, South Korea.

Conflict of interest

DK, MR, and CM-R were employed by the company KRIBB.

The remaining author declares that the research was conducted in the absence of any commercial or financial relationships that could be construed as a potential conflict of interest.

Publisher's note

All claims expressed in this article are solely those of the authors and do not necessarily represent those of their affiliated organizations, or those of the publisher, the editors and the reviewers. Any product that may be evaluated in this article, or claim that may be made by its manufacturer, is not guaranteed or endorsed by the publisher.

Supplementary material

The Supplementary material for this article can be found online at: https://www.frontiersin.org/articles/10.3389/fpls.2022.864086/full#supplementary-material

References

Alexopoulou, L., Holt, A. C., Medzhitov, R., and Flavell, R. A. (2001). Recognition of double-stranded RNA and activation of NF-kappaB by toll-like receptor 3. *Nature* 413, 732–738. doi: 10.1038/35099560

Barbero, F., Guglielmotto, M., Capuzzo, A., and Maffei, M. E. (2016). Extracellular self-DNA (esDNA), but not heterologous plant or insect DNA (etDNA), induces plasma membrane depolarization and calcium signaling in Lima bean (*Phaseolus lunatus*) and maize (*Zea mays*). *Int. J. Mol. Sci.* 17:1659. doi: 10.3390/ijms17101659

Barbero, F., Guglielmotto, M., Islam, M., and Maffei, M. E. (2021). Extracellular fragmented self-DNA is involved in plant responses to biotic stress. *Front. Plant Sci.* 12:686121. doi: 10.3389/fpls.2021.686121

Bedford, I. D., Briddon, R. W., Brown, J. K., Rosell, R. C., and Markham, P. G. (1994). Geminivirus transmission and biological characterisation of *Bemisia tabaci* (Gennadius) biotypes from different geographic regions. *Ann. Appl. Biol.* 125, 311–325. doi: 10.1111/j.1744-7348.1994.tb04972.x

Beneduzi, A., Ambrosini, A., and Passaglia, L. M. (2012). Plant growth-promoting rhizobacteria (PGPR): their potential as antagonists and biocontrol agents. *Genet. Mol. Biol.* 35, 1044–1051. doi: 10.1590/S1415-47572012000600020

Bhat, A., and Ryu, C.-M. (2016). Plant perceptions of extracellular DNA and RNA. *Mol. Plant* 9, 956–958. doi: 10.1016/j.molp.2016.05.014

Chiusano, M. L., Incerti, G., Colantuono, C., Termolino, P., Palomba, E., Monticolo, F., et al. (2021). *Arabidopsis thaliana* response to extracellular DNA: self versus nonself exposure. *Plan. Theory* 10:1744. doi: 10.3390/plants10081744

Clarke, J. D., Volko, S. M., Ledford, H., Ausubel, F. M., and Dong, X. (2000). Roles of salicylic acid, jasmonic acid, and ethylene in *cpr*-induced resistance in. *Arabidopsis Plant Cell* 12, 2175–2190. doi: 10.1105/tpc.12.11.2175

Do, H. M., Lee, S. C., Jung, H. W., Sohn, K. H., and Hwang, B. K. (2004). Differential expression and *in situ* localization of a pepper defensin (CADEF1) gene in response to pathogen infection, abiotic elicitors and environmental stresses in *Capsicum annuum*. *Plant Sci.* 166, 1297–1305. doi: 10.1016/j.plantsci.2004.01.008

Duran-Flores, D., and Heil, M. (2014). Damaged-self recognition in common bean (*Phaseolus vulgaris*) shows taxonomic specificity and triggers signaling via reactive oxygen species (ROS). *Front. Plant Sci.* 5:585. doi: 10.3389/fpls.2014.00585

Duran-Flores, D., and Heil, M. (2018). Extracellular self-DNA as a damage-associated molecular pattern (DAMP) that triggers self-specific immunity induction in plants. *Brain Behav. Immun.* 72, 78–88. doi: 10.1016/j.bbi.2017.10.010

Escobar-Bravo, R., Ruijgrok, J., Kim, H. K., Grosser, K., van Dam, N., Klinkhamer, P. G. L., et al. (2018). Light intensity-mediated induction of trichome-associated allelochemicals increases resistance against thrips in tomato. *Plant Cell Physiol.* 59, 2462–2475. doi: 10.1093/pcp/pcy166

Guo, H., Sun, Y., Yan, H., Li, C., and Ge, F. (2020). O_3-induced priming defense associated with the abscisic acid signaling pathway enhances plant resistance to Bemisia tabaci. *Front. Plant Sci.* 11:93. doi: 10.3389/fpls.2020.00093

Heil, M., Hilpert, A., Kaiser, W., and Linsenmair, K. E. (2000). Reduced growth and seed set following chemical induction of pathogen defence: does systemic acquired resistance (SAR) incur allocation costs? *J. Ecol.* 88, 645–654. doi: 10.1046/j.1365-2745.2000.00479.x

Heil, M., and Vega-Muñoz, I. (2019). Nucleic acid sensing in mammals and plants: facts and caveats. *Int. Rev. Cell Mol. Biol.* 345, 225–285. doi: 10.1016/bs.ircmb.2018.10.003

Herrera-Vásquez, A., Salinas, P., and Holuigue, L. (2015). Salicylic acid and reactive oxygen species interplay in the transcriptional control of defense genes expression. *Front. Plant Sci.* 6:171. doi: 10.3389/fpls.2015.00171

Hong, J. K., and Hwang, B. K. (2002). Induction by pathogen, salt and drought of a basic class II chitinase mRNA and its in situ localization in pepper (Capsicum annuum). *Physiol. Plant.* 114, 549–558. doi: 10.1034/j.1399-3054.2002.1140407.x

Hong, J. K., Jung, H. W., Kim, Y. J., and Hwang, B. K. (2000). Pepper gene encoding a basic class II chitinase is inducible by pathogen and ethephon. *Plant Sci.* 159, 39–49. doi: 10.1016/S0168-9452(00)00312-5

Huh, S. U., Lee, G. J., Jung, J. H., Kim, Y., Kim, Y. J., and Paek, K. H. (2015). *Capsicum annuum* transcription factor WRKYa positively regulates defense response upon TMV infection and is a substrate of CaMK1 and CaMK2. *Sci. Rep.* 5:7981. doi: 10.1038/srep07981

Huot, B., Yao, J., Montgomery, B. L., and He, S. Y. (2014). Growth–defense tradeoffs in plants: A balancing act to optimize fitness. *Mol. Plant* 7, 1267–1287. doi: 10.1093/mp/ssu049

Hwang, I. S., Choi, D. S., Kim, N. H., Kim, D. S., and Hwang, B. K. (2014). Pathogenesis-related protein 4b interacts with leucine-rich repeat protein 1 to suppress PR4b-triggered cell death and defense response in pepper. *Plant J.* 77, 521–533. doi: 10.1111/tpj.12400

Hwang, I. S., and Hwang, B. K. (2009). The pepper 9-Lipoxygenase gene *CaLOX1* functions in defense and cell death responses to microbial pathogens. *Plant Physiol.* 152, 948–967. doi: 10.1104/pp.109.147827

Kato, H., Takeuchi, O., Sato, S., Yoneyama, M., Yamamoto, M., Matsui, K., et al. (2006). Differential roles of MDA5 and RIG-I helicases in the recognition of RNA viruses. *Nature* 441, 101–105. doi: 10.1038/nature04734

Kong, H. G., Shin, T. S., Kim, T. H., and Ryu, C.-M. (2018). Stereoisomers of the bacterial volatile compound 2,3-butanediol differently elicit systemic defense responses of pepper against multiple viruses in the field. *Front. Plant Sci.* 9:90. doi: 10.3389/fpls.2018.00090

Kouzai, Y., Noutoshi, Y., Inoue, K., Shimizu, M., Onda, Y., and Mochida, K. (2018). Benzothiadiazole, a plant defense inducer, negatively regulates sheath blight resistance in *Brachypodium distachyon*. *Sci. Rep.* 8:17358. doi: 10.1038/s41598-018-35790-w

Lee, G., Lee, S.-H., Kim, K. M., and Ryu, C.-M. (2017). Foliar application of the leaf-colonizing yeast *Pseudozyma churashimaensis* elicits systemic defense of pepper against bacterial and viral pathogens. *Sci. Rep.* 7:39432. doi: 10.1038/srep39432

Lee, B., Park, Y.-S., Lee, S., Song, G. C., and Ryu, C.-M. (2016). Bacterial RNAs activate innate immunity in *Arabidopsis*. *New Phytol.* 209, 785–797. doi: 10.1111/nph.13717

Lievens, L., Pollier, J., Goossens, A., Beyaert, R., and Staal, J. (2017). Abscisic acid as pathogen effector and immune regulator. *Front. Plant Sci.* 8:587. doi: 10.3389/fpls.2017.00587

Mancuso, G., Gambuzza, M., Midiri, A., Biondo, C., Papasergi, S., Akira, S., et al. (2009). Bacterial recognition by TLR7 in the lysosomes of conventional dendritic cells. *Nat. Immunol.* 10, 587–594. doi: 10.1038/ni.1733

Mayo, C. B., and Cole, J. L. (2017). Interaction of PKR with single-stranded RNA. *Sci. Rep.* 7:3335. doi: 10.1038/s41598-017-03047-7

Mazzoleni, S., Bonanomi, G., Incerti, G., Chiusano, M. L., Termolino, P., Mingo, A., et al. (2015a). Inhibitory and toxic effects of extracellular self-DNA in litter: a mechanism for negative plant-soil feedbacks? *New Phytol.* 205, 1195–1210. doi: 10.1111/nph.13121

Mazzoleni, S., Cartenì, F., Bonanomi, G., Senatore, M., Termolino, P., Giannino, F., et al. (2015b). Inhibitory effects of extracellular self-DNA: a general biological process? *New Phytol.* 206, 127–132. doi: 10.1111/nph.13306

Miura, K., Okamoto, H., Okuma, E., Shiba, H., Kamada, H., Hasegawa, P. M., et al. (2013). SIZ1 deficiency causes reduced stomatal aperture and enhanced drought tolerance via controlling salicylic acid-induced accumulation of reactive oxygen species in *Arabidopsis*. *Plant J.* 73, 91–104. doi: 10.1111/tpj.12014

Noutoshi, Y., Ito, T., Seki, M., Nakashita, H., Yoshida, S., Marco, Y., et al. (2005). A single amino acid insertion in the WRKY domain of the Arabidopsis TIR-NBS-LRR-WRKY-type disease resistance protein SLH1 (sensitive to low humidity 1) causes activation of defense responses and hypersensitive cell death. *Plant J.* 43, 873–888. doi: 10.1111/j.1365-313X.2005.02500.x

Poór, P. (2020). Effects of salicylic acid on the metabolism of mitochondrial reactive oxygen species in plants. *Biomol. Ther.* 10:341. doi: 10.3390/biom10020341

Schlee, M., and Hartmann, G. (2016). Discriminating self from non-self in nucleic acid sensing. *Nat. Rev. Immunol.* 16, 566–580. doi: 10.1038/nri.2016.78

Serrano-Jamaica, L. M., Villordo-Pineda, E., González-Chavira, M. M., Guevara-González, R. G., and Medina-Ramos, G. (2020). Effect of fragmented DNA From plant pathogens on the protection Against wilt and root rot of Capsicum annuum L. Plant. *Front. Plant Sci.* 11:581891. doi: 10.3389/fpls.2020.581891

Toum, L., Conti, G., Guerriero, F. C., Conforte, V. P., Garolla, F. A., Asurmendi, S., et al. (2020). Single-stranded oligodeoxynucleotides induce plant defence in Arabidopsis thaliana. *Ann. Bot.* 126, 413–422. doi: 10.1093/aob/mcaa061

Van Der Ent, S., Van Wees, S. C. M., and Pieterse, C. M. J. (2009). Jasmonate signaling in plant interactions with resistance-inducing beneficial microbes. *Phytochemistry* 70, 1581–1588. doi: 10.1016/j.phytochem.2009.06.009

Walters, D., and Heil, M. (2007). Costs and trade-offs associated with induced resistance. *Physiol. Mol. Plant Pathol.* 71, 3–17. doi: 10.1016/j.pmpp.2007.09.008

Advantages of publishing in Frontiers

OPEN ACCESS
Articles are free to read for greatest visibility and readership

FAST PUBLICATION
Around 90 days from submission to decision

HIGH QUALITY PEER-REVIEW
Rigorous, collaborative, and constructive peer-review

TRANSPARENT PEER-REVIEW
Editors and reviewers acknowledged by name on published articles

Frontiers
Avenue du Tribunal-Fédéral 34
1005 Lausanne | Switzerland

Visit us: www.frontiersin.org
Contact us: frontiersin.org/about/contact

REPRODUCIBILITY OF RESEARCH
Support open data and methods to enhance research reproducibility

DIGITAL PUBLISHING
Articles designed for optimal readership across devices

FOLLOW US
@frontiersin

IMPACT METRICS
Advanced article metrics track visibility across digital media

EXTENSIVE PROMOTION
Marketing and promotion of impactful research

LOOP RESEARCH NETWORK
Our network increases your article's readership